Dissertation zur Erlangung des Doktorgrades
der Fakultät Chemie und Pharmazie
der Ludwig-Maximilians-Universität München

γ-substituted *N*-acylated-*N*-aminoethyl peptide mimetics of mucin MUC1 B-cell epitopes and photoswitchable peptide hormones for photopharmacology

Manuel Tobias Gailer

aus

München, Deutschland

2024

Erklärung

Diese Dissertation wurde im Sinne von § 7 der Promotionsordnung vom 28. November 2011 von Frau Prof. Dr. Anja Hoffmann-Röder betreut.

Eidesstattliche Versicherung

Diese Promotion wurde eigenständig und ohne unerlaubte Hilfe erarbeitet.

München, 24.04.2024

Manuel Gailer

Dissertation eingereicht am: 30.04.2024

Erstgutachter: Prof. Dr. Anja Hoffmann-Röder

Zweitgutachter: Prof. Dr. Oliver Trapp

Tag der mündlichen Prüfung: 11.10.2024

Die Welt ist nur eine Schule der Erkenntnis.

Michel de Montaigne

List of publication

T. Podewin, J. Ast, J. Broichhagen, N. H. F. Fine, D. Nasteska, P. Leippe, M. Gailer, T. Buenaventura, N. Kanda, B. J. Jones, C. M'Kadmi, J.-L. Baneres, J. Marie, A. Tomas, D. Trauner, A. Hoffmann-Röder, D. J. Hodson, Conditional and Reversible Activation of Class A and B G Protein-Coupled Receptors Using Tethered Pharmacology, *ACS Central Science*, **2018**, *4*, 166-179.[1]

S. M. Hofmann, C. V. Frost, T. Podewin, M. Gailer, E. Weber, M. Zacharias, W. Zinth, A. Hoffmann-Röder, Folding and Unfolding of the Short Light-Triggered β-Hairpin Peptide AzoChignolin Occurs within 100 ns, *The Journal of Physical Chemistry B*, **2020**, *124*, 5113-5121.[2]

S. Gutenthaler, S. Tsushima, R. Steudtner, M. Gailer, A. Hoffmann-Röder, B. Drobot, L. Daumann, Lanmodulin peptides – unravelling the binding of the EF-Hand loop sequences stripped from the structural corset, *Inorganic Chemistry Frontiers*, **2022**, *9*, 4009-4021.[3]

Danksagung

Nachdem ich ein Drittel meines Lebens an der LMU verbracht habe, möchte ich mich bei all jenen bedanken, die mich in dieser langen und oft auch schwierigen Zeit begleitet und unterstützt haben.

Größter Dank gebührt meiner Familie. Meiner Frau Vanessa und meinem Sohn Mattis danke ich für die moralische Unterstützung, die Geborgenheit und den Halt, den sie mir gegeben haben. Diese viereinhalb Jahre waren von Entbehrungen, Frustration und regelmäßig langen Arbeitszeiten gekennzeichnet, welche wir als junge Familie gemeinsam geschultert haben. Danke auch dir, Vanessa, für das Verständnis, dass du für mich, meine Arbeit und die damit verbundene finanzielle Situation aufgebracht hast. Großer Dank gilt auch meinen Eltern, die mich im Studium jederzeit unterstützt haben und während der Promotion des Öfteren finanziell ausgeholfen haben. Ohne dies wäre ein schuldenfreier Start in das Berufsleben nicht möglich gewesen. Großer Dank geht auch an meine beiden Brüder und meine Großeltern, die jederzeit ein offenes Ohr für mich hatten, sich meine Sorgen angehört haben und mir jederzeit Unterstützung angeboten haben.

Dank möchte ich auch meiner Doktormutter Frau Prof. Dr. Anja Hoffmann-Röder aussprechen. Sie war stets offen für meine Ideen und ließ mir bei der Gestaltung der Themen freie Hand. Dadurch war es mir möglich, mich in viele Themen und Methoden selbstständig einzuarbeiten. Frau Prof. Dr. Anja Hoffmann-Röder gab mir regelmäßig die Möglichkeit, meine Arbeit auf Symposien zu präsentieren und mich mit anderen Wissenschaftlern aus aller Welt auszutauschen.

Herrn Prof. Dr. Oliver Trapp möchte ich für die Übernahme des Zweitgutachtens danken.

Auch möchte ich mich bei meinem Arbeitskreis bedanken. Die Promotionszeit war für alle von uns ein Ausnahmezustand. Dennoch haben wir immer versucht, das Beste daraus zu machen und uns gegenseitig moralisch als auch fachlich zu unterstützen. Leider haben einige nicht bis zum Schluss durchgehalten. Ebenso möchte ich mich bei meinen Praktikanten bedanken, insbesondere Johanna Pröll, Phoebe Foster und Jonathan Tietze. Großen Dank geht auch an Ulla Hülsmann, die immer ein offenes Ohr und eine helfende Hand hatte.

Table of Contents

Index of abbreviations

ACBT	Azo-Carbetocin
Acm	acetamidomethyl
AMPP	3-[3-(aminomethyl)phenylazo]-phenylacetic acid
ANP	Atrial natriuretic peptide
ARC	Arcuate nucleus
ASD	Autism spectrum disorder
AVP	Arginine Vasopressin
AzoPhe	Phenylazophenylalanine
BMPP	3-[3-(bromomethyl)phenylazo]-phenylacetic acid
Boc	Butyloxycarbonyl
cAMP	cyclic Adenosine monophosphate
CBT	Carbetocin
Cbz	Benzyl chloroformate
CD	Circular dichroism
^{c}Hex	Cyclohexane
CIS	Chemical induces shift
CNS	Central nervous system
CPP	Cell penetrating peptide
Cys	Cysteine
DAG	Diacylglycerol
DBU	1,8-Diazabicyclo[5.4.0]undec-7-ene
DCC	*N,N'*-Dicyclohexylcarbodiimide
DCM	Dichloromethane
DIC	*N,N'*-Diisopropylcarbodiimide
DMAP	*N*,*N*'-Dimethylaminopyridine
DMF	*N*,*N*'-Dimethylformamide
DNA	Deoxyribonucleic acid
DPC	Dodecylphosphocholine
EDC	1-Ethyl-3-(3-dimethylaminopropyl)carbodiimide
ER	Endoplasmic reticulum
EtOAc	Ethyl acetate
Fmoc	Fluorenylmethoxycarbonyl

FSH	Follicle-stimulating hormone
γ-AApeptide	*N*-acylated-*N*-aminoethyl amino acid
GIRK	G protein-coupled inwardly-rectifying potassium channels
Gly	Glycine
GnIH	Gonadotropin-inhibitory hormone
GnRH	Gonadotropin-releasing hormone
GPCR	G protein-coupled receptor
GTP	Guanosine-5'-triphosphate
h	hours
HATU	*O*-(7-Azabenzotriazol-1-yl)-*N,N,N',N'*-tetramethyluronium-hexafluorphosphat
HBTU	*O*-(Benzotriazol-1-yl)-*N,N,N',N'*-tetramethyluronium-hexafluorphosphat
His	Histidine
HOAt	1-Hydroxy-7-azabenzotriazol
HOBt	1-Hydroxybenzotriazol
HPG	hypothalamic–pituitary–gonadal
IP3	inositol 1,4,5-trisphosphate
KP	Kisspeptin
LH	Luteinizing Hormone
Lys	Lysine
MD	molecular dynamics
Met	Methonine
min	minutes
Mmt	Monomethoxytrityl
MOR	μ-opioid receptor
NBS	*N*-Bromosuccinimide
NMP	*N*-Methyl-2-pyrrolidone
NMR	Nuclear magnetic resonance
NPFFR1	Neuropeptide FF receptor 1
NRSP	Non-ribosomal synthesised peptides
OD	Optical density
OT	Oxytocin
OXTR	Oxytocin-receptor
Pbf	2,2,4,6,7-Pentamethyl-dihydrobenzofuran-5-sulfonyl protecting group

PBS	Phosphate buffered saline
PCPP	Photoswitchable cell penetrating peptide
PG	Protecting group
PKC	Proteinkinase C
PLC	Phopsholipase C
PNA	Peptide nucleic acid
PSS	Photostationary state
Py	Pyridine
PyBOP	Benzotriazol-1-yl-oxytripyrrolidinophosphonium-hexafluorophosphat
r.t.	Room temperature
RAM	Rink amide
SDS	Sodium dodecyl sulfate
Ser	Serine
SPPS	Solid phase peptide synthesis
TACA	Tumor-associated carbohydrate antigene
t-Bu	*tert*-Butyl
TEA	Triethylamine
TFA	Trifluoro acetic acid
TFE	Trifluoroethanol
THF	Tetrahydro furane
Thr	Threonine
TIPS	Triisopropylsilane
Trp	Tryptophane
TRPC	Transient receptor potential channel
Trt	Triphenylmethyl
Tyr	Tyrosine
UV	Ultraviolet
VT	Vasotocine

Abstract

Teil 1

Aufgrund der stetigen Zunahme der Krebserkrankungen in allen Bevölkerungsgruppen ist das Interesse der Forschung an neuen Behandlungsmöglichkeiten groß. Behandlungen mit herkömmlichen Therapien, wie die Chemo- oder Strahlentherapie, gehen mit schweren Nebenwirkungen und Verminderung der Lebensqualität des Patienten einher. Daher rückt die Immuntherapie als Alternative in den Blickpunkt der aktuellen Forschung. Von Bedeutung sind in dieser Therapie die Oberflächenproteine der malignen Zellen. Diese oftmals überexprimierten Glycoproteine[4] sind zum Beispiel Ausgangspunkt für die Entwicklung therapeutischer Vakzine. Der in den malignen Zellen veränderte Stoffwechsel, der mit einer Herunterregulierung der Glycosyltransferasen einhergeht, ist die Ursache für das Auftreten verkürzter Glycane.[5] Diese werden als tumorassoziierte Antigene bezeichnet. Zwei wichtige tumorassiziierte Antigene sind das T_N- und das T-Antigen der tandem repeat sequenz des Mucins MUC1, einem Oberflächenprotein epithelialer Zellen.[6]

Während die Peptideptiope in gesunden Zellen durch die langen Kohlenhydratketten abgeschirmt sind, liegen sie in Tumorzellen frei und sind für das Immunsystem zugänglich.[7] Dieser Unterschied ermöglicht es, die tumor-assoziierten Glycopeptide zur Entwicklung von Vakzinen zur Erforschung der Krebsimmunotherapie zu entwickeln. Dabei muss jedoch eine Toleranz des Immunsystems gegenüber den tumorassoziierten Antigenen und somit den Tumorzellen verhindert werden. Eine Verknüpfung der Vakzine mit Immunostimmulanzien, wie Carrier-Proteinen, zur Steigerung der Immunogenität der Glycoproteine ist eine bewährte Strategie. Dabei werden die Glycoproteine über einen Spacer mit Tetanus-Toxoid (TTox) oder KRN7000 verbunden.[7, 8]

Ein Problem stellt die geringe Bioverfügbarkeit von Glycopeptiden dar, da diese von Proteasen und Glycosidasen im Körper abgebaut werden.[9] Um eine hohe Wirksamkeit der Vakzine zu erzielen, muss daher deren Stabilität erhöht werden. Einflussnahme ist beispielsweise unter Einsatz von Peptidmimetika möglich. Diese imitieren mit Hilfe eines unnatürlichen Rückgrats Primär- und Sekundärstrukturen natürlicher Peptide und können als Pharmakophore eingesetzt werden.[10] Der Einsatz solcher Verbindungen führt in der Regel zu einer höheren metabolischen Stabilität und folglich höheren Bioverfügbarkeit.

Die in dieser Arbeit verwendeten Peptidmimetika, die von *Niu et. al.*[11] entwickelten sogenannten AA-Peptide (N-acylierte-N-Aminoethyl-Aminosäuren), wurden ursprünglich von chiralen PNAs (Peptidnukleinsäuren) abgeleitet. AA-Peptide stimmen in der Anzahl an Seitenketten und funktionellen Gruppen mit natürlichen Peptiden überein. Im Peptidrückgrat alternieren natürliche sekundäre Amide mit tertiären Amiden. Hieraus ergibt sich auch eine Alternierung der natürlichen Seitenketten mit der *N*-acyl-Seitenkette. Die Position der natürlichen Seitenkette unterteilt die AAPeptide in die zwei Formen: das α-AAPeptid mit der natürlichen Seitenkette in α-Position und das γ-AAPeptid mit der Seitenketten in γ-Position. Die tertiären *N*-acyl-Amide erhöhen die Flexibilität des Peptides und verändern inner- und intramolekularen Wechselwirkungen, wodurch die Eigenschaften des AAPeptids modifiziert werden.[11]

In dieser Arbeit wurden die γ-AAPeptid-Mimetika-Strukturen des T_N- und des T-Antigens synthetisiert. Die Synthese der Zuckers und des γ-AAPeptids wurde in meiner Masterarbeit erarbeitet.[12] Nach Aufbau des tertiären Amids durch Kupplung des γ-AAPeptids mit dem T_N-Antigen, respektive dem T-Antigen wurden die beiden Festphasenbausteine **2.9** und **2.12** gewonnen. Diese wurden in in die *tandem repeat*-Sequenz des epithelialen Mucins MUC1 mit Hilfe der mikrowellenunterstützten Festphasenpeptidsynthese eingebaut.

Teil 2

Die Kontrolle biologischer Prozesse stand schon immer im Fokus naturwissenschaftlicher Forschung. Die Kontrolle oder Manipulation solcher Prozesse ermöglicht einen Einblick in die Funktion, wie auch in übergeordnete oder untergeordnete Systeme. Um diese Prozesse besser verstehen zu können, ist geeignetes Werkzeug notwendig. Dieses muss jedoch einigen Anforderungen entsprechen, um eine Verfälschung der Ergebnisse durch äußere Einwirkung zu verhinden. Auf zellulärer Ebene finden Prozesse auf spatiotemporale Weise statt. Licht, als nicht-invasives Instrument mit spatiotemporaler Präzission bietet die Möglichkeit, solche Prozesse zu steuern.[13]

Notwendig sind hierfür lichtempfindliche Moleküle, sogenannte Photoschalter, die durch Einwirkung von Licht Veränderungen in der Konformation und/oder der Polarität eingehen. Azobenzole, welche durch Belichtung mit bestimmten Wellenlängen zwischen der E (*trans*) und Z (*cis*) Konformation in Pikosekunden isomerisieren[14], zeichnen sich durch ihre

synthetisch zugängliche Variabilität aus. Durch Einbau von Photoschaltern in Peptide kann die Sekundärstruktur des Peptids durch Isomerisierung beeinflusst werden.[13, 15] In dieser Arbeit wurde eine Reihe von Photoschaltern synthestisiert, um diese an verschiedenen Positionen kurzer linearer und cyclischer Peptide einzubauen.

Des Weiteren wurden die Festphasenbausteine der Photoschalter AzoPhe und AMPP, sowie Derivate von AzoPhe und AMPP synthetisiert und in folgende Peptide eingebaut.

Azo-Carbetocin

Carbetocin ist ein Mimetikum des Hormons Oxytocin. Oxytocin (griechich: schnelle Geburt) ist ein cyclisches Peptid bestehend aus neun Aminosäuren, welches bei der Geburt die Kontraktion der Gebärmuttermuskulatur anregt und die Abstoßung der Plazenta erleichtert.[16] Im zentralen Nervensystem dient Oxytocin vor allem als Neurotransmitter und beeinflusst das soziale Verhalten, unter anderem Angst, Stress, Lern- und Erinnerungsprozesse.[17] Oxytocin unterscheidet sich in nur zwei Aminosäuren von den Vasopressinen, was in einer geringen Selektivität gegenüber den Vasopressin-Rezeptoren resultiert. Des Weiteren besitzt Oxytocin eine sehr kurze Halbwertszeit und daher eine niedrige Bioverfügbarkeit. Aus diesem Grund wurde Carbetocin entwickelt[18], welches eine deutlich höhere Halbwertszeit und eine höhere Bioverfügbarkeit aufweist.[19] Des Weiteren besitzt Oxytocin eine hohe Selektivität gegenüber dem Oxytocin-Rezeptor.[20] Dennoch handelt es sich bei Carbetocin um einen partiellen Agonisten mit Unterschieden in der Signaltransduktion.[20, 21] Um diese Unterschiede zu untersuchen, eignen sich photoschaltbare Carbetocin Derivate.

Hierfür wurden sechs Carbetocin Derivate synthetisiert, wobei die Photoschalter entweder als Seitenkette oder in das Peptid-Rückgrat mit Hilfe der Festphasen-Peptidsynthese eingebaut wurden. Je nach Position und Art des Photoschalters unterschieden sich die Azo-Carbetocine (ACBT) in der Selektivität und der Stärke der agonistischen oder antagonistischen Eigenschaften. Diese Eigenschaften wurden mit Hilfe von Calcium imaging getestet (Dr. Iuliia Karpenko; Faculty of Pharmacy, University of Strasbourg). Während **ACBT2** der einzige OXTR-Agonist ist, stellte sich **ACBT6** als der stärkste OXTR-Antagonist heraus. Die Internalisierung des Oxytocinrezeptors wurde mittels konfokaler Mikroskopie untersucht. Während der schwache Agonist **ACBT2** keine Internalisierung des Rezeptors einleitete, bewies sich *cis*-**ACBT6** als starker Antagonist für den Oxytocinrezeptor.

Azo-Kisspeptin

Kisspeptin wurde 1996 als Metastasesuppressor entdeckt[22], weshalb es zunächst den Namen Metastatin trug. Erst fünf Jahre später wurde Kisspeptin als Ligand für den Rezeptor GPR54 entdeckt. Die Bindung von Kisspeptin an GPR54 führt zur Ausschüttung von Gonadotropin-Releasing-Hormon, ein Hormon, das für die Freisetzung von luteinisierendem Hormon (LH) und follikelstimulierendem Hormon (FSH) verantwortlich ist.[23]

Mutationen im GPR54-kodierenden Genabschnitt führen zu autosomal rezessivem iodopathischem hypogonadotropischem Hypogonadismus[24, 25], einer Erkrankung mit unvollständiger oder ausbleibender Pubertät.

Unter den Kisspeptinliganden (KP-13, KP-14, KP-54) ist KP-10 das kürzeste natürliche Peptid.[26] Anhand von Alaninscans konnten die für die Bindung und Rezeptoraktivierung essentiellen Aminosäuren analysiert werden. Zwei aromatische Aminosäuren Phe6 und Phe10 bilden einen Cluster, der für die Bindung an GPR54 wichtig ist. Dadurch ergaben sich drei Substitutionsmöglichkeiten mit Photoschaltern. In AzoKP-1 (NS6AMPP) sollte AMPP neben Phe6 einen möglichst großen Einfluss auf Rezeptor-Bindung haben. In AzoKP-2 (F10AzoPhe) und AzoKP-3 (F6AzoPhe) wurden die essentiellen Phenylalanine gegen AzoPhe substituiert, um einen Einfluss auf die Clusterbildung zu gewinnen.[27]

Die photoschaltbaren Kisspeptin-Analoga wurden mittels Patch clamp (Dr. Jian Qiu; Group of Prof. Dr. Martin J. Kelly, Oregon Health and Science University) und *in vitro* Zellstudien (Dr. Jan-Erik Hoffmann; Group of Prof. Dr. Carsten Schulz, Oregon Health and Science University) untersucht. Das mit AMPP substituierte AzoKP-1 zeigte keine Bindung an den untersuchten Rezeptoren. Das AzoPhe-Analogon AzoKP-2 hingegen zeigte eine deutliche Aktivierung von GPR54 nach Belichtung, jedoch etwas schwächer als das natürliche KP-10. Die Belichtung von AzoKP-3 führte hingegen zu einer Hypopolarisierung durch Bindung an NPFFR1, was durch die *in vitro* Zellstudien bestätigt werden konnte.

1 Microwave-assisted solid-phase peptide synthesis

1.1 Introduction

For the treatment of diseases, peptides have been in the shadow of small molecules for a long time. This is mainly due to their major drawbacks. These drawbacks are their *in vivo* instability due to enzymatic degradation, their size-dependent low ability for membrane diffusion and their incapacity to cross the blood-brain barrier.[28] Whereas the high instability towards proteases and peptidases is an essential characteristic for peptides, these characteristics hinder the oral delivery of peptides. But peptides also have several advantages. With an infinite way of combining their building blocks, it is possible to develop a great variety of different structures and therefore peptides have the highest ability to fulfil any biological demand as potency, specificity, selectivity and target affinity.[29] While hepatic metabolism of small molecules with its non-mechanistic based toxicity is a challenging problem, these problems are rarely observed with peptide drugs.[30]

But most important in the last two decades, there was extensive progress in solid-phase peptide synthesis (SPPS) which not only shortened the coupling and deprotection steps with the help of microwave-assisted synthesis and thus reduced time consumption from one hour per amino acid to a minimum of 2 − 4 minutes allowing the formation of libraries.[31] The combination of SPPS with Native Chemical Ligation (NCL) enables the synthesis of functional proteins such as bacterial polymerases.[32, 33]

One of the major advances of SPPS, especially in the field of pharmacological science, is the possibility of post-translational modification (PTM) of peptides. PTMs can be selectively introduced in two different ways. First, modified SPPS-building blocks can be synthesised and second, with the use of different protecting groups, modifications can be introduced on the side-chains and *C*- and *N*-termini after assembly of the peptide bonds. Examples for these post-translational modifications are the cyclization of Oxytocin[34], the formation of disulfid-bridges of Insulin[35] or the huge variety of MUC-1 glycopeptides.[7]

But from the very beginning of the first synthesized peptides to the micro-wave assisted SPPS using *Fmoc*-Strategy has been a long way. The very first peptide was synthesised by T. Curtius in 1882, using the silver salt of glycine and benzoylchloride, resulting in an *N*-protected Gly-Gly dipeptide. Later, E. Fourneau and E. Fischer were able to synthesise and publish the first free Gly-Gly dipeptide by hydrolysis of diketopiperazine.[36] Emil Fischer, also introduced the

terminology “peptide” in 1902 and synthesised an 18 amino acid long peptide using an acyl chloride coupling method in 1907.[37] Since easily removable protecting groups were not available, the peptide synthesis was severly limited. The development of the carbobenzoxy group (Cbz or Z) by Bergmann and Zervas in 1932, an amino protecting group cleavable by catalytic hydrogenation, paved the way for the next step.[38] Modern peptide chemistry started with the elongation at the *N*-terminus and the use of temporary protecting groups. The first natural hormone, oxytocin, was synthesised by du *Vigneaud et al.* in 1953[34], earning him the Nobel Prize in Chemistry in 1955. Some years later, the orthogonality of protection groups for peptide synthesis was developed by introducing the acid-labile *tert*-butoxycarbonyl (Boc) group by Albertson and McKay[39], which is still one of the principles of peptide synthesis today. Whereas the early peptides were synthesised in solution, R. B. Merrifield published the first solid phase peptide synthesis (SPPS) in 1963 using a chloromethylated nitropolystyrene resin.[40] Later, he improved the procedure by using a chloromethylcopolystyrene-divinylbenzene resin and *N*-Boc-protected amino acids.[41] Merrifield also received the Nobel Prize for his work on solid matrix in 1984. The use of 9-fluorenylmethoxycarbonyl group (*Fmoc*) by Han and Carpino in 1970[42], perfected the orthogonal synthetic strategy and established the nowadays mainly used *Fmoc*/*t*-Bu approach. Since then, new protecting groups, technical inventions like automated SPPS machines and the use of microwave-assisted synthesis has pushed the field of peptide chemistry into new areas.

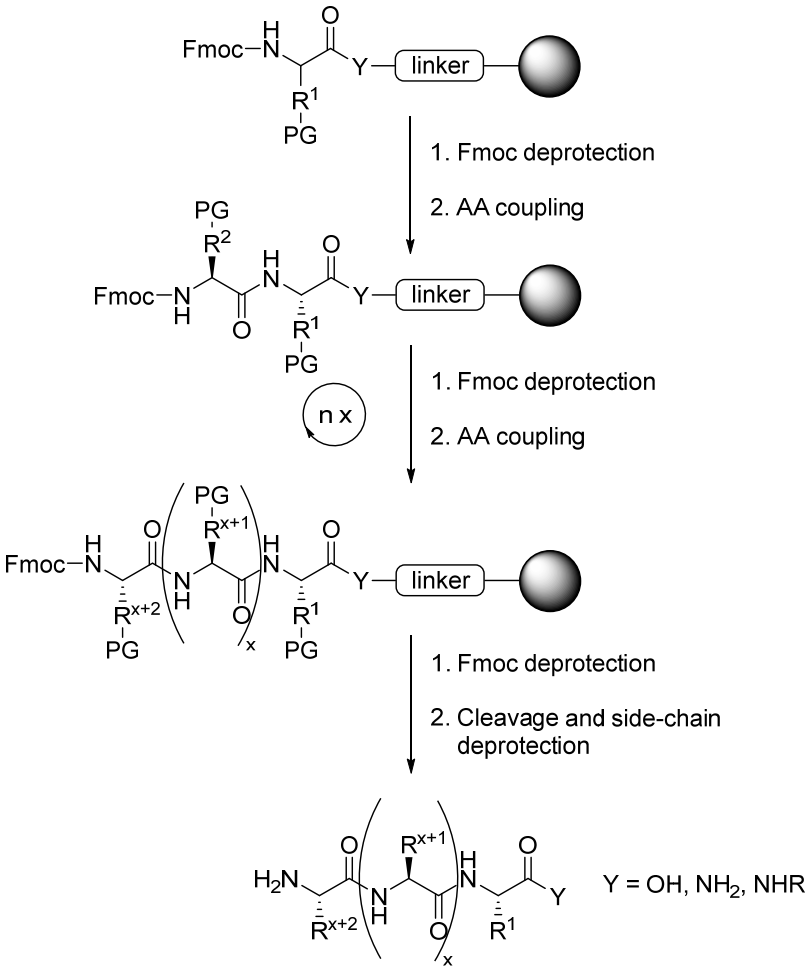

Scheme 1.1: General synthetic strategy of solid phase peptide synthesis.[43]

Today, a typical synthetic strategy for SPPS is described as schown in Scheme 1.1. On a commercially available preloaded resin, the first amino acid is detached to the resin by a linker molecule. In the first step, the *Fmoc*-protected amine is deprotected under basic conditions, while the side-chain protecting groups remain due to their orthogonality. The cycle ends with the coupling of the second amino acid. After the coupling of the last amino acid, the peptide can be cleaved from the resin and the side-chain protecting groups under acidic conditions, resulting in fully unprotected peptide.[44] Each of these steps is described in detail below.

.

1.2 Synthesis of pharmacologically active peptides

1.2.1 The resin

Planning a SPPS starts with the right choice of the solid support, or the solid phase, the resin. The polymeric solid support consists of small beads, mostly derived from polystyrene cross-linked with 1-2% divinylbenzene. Further solid supports consist of polyethylene glycol (PEG) or polyethylene glycol-acrylamide (PEGA) copolymers, for example.[45, 46] Commercial ones are usually available in two different particle sizes; 100-200 mesh (75-150 µm) or 200-400 mesh (35-75 µm). The mesh size is defined in the number of openings per square inch, which are the entry to the polymer network inside the beads where the elongation of the peptide takes place. Diffusion into the 3D polymer network is one of the most important factors for coupling reactions and the diffusion rates affect the reaction kinetics dramatically.[40, 47] Resins swell in aprotic solutions like *N*,*N*-dimethylformamide (DMF), *N*-Methyl-2-pyrrolidon (NMP) or dichloromethane (DCM) up to a multiple of their size and thus swelling properties influence the diffusion rate.[48] The connection between a growing peptide chain and the solid support is the linker, which should be stable to all chemicals used in SPPS and easily (and sometimes orthogonally) detachable without the formation of by-products. There are a number of different linkers which all fulfil their special requirements, and the resin is usually named after the linker. However, one the most frequently used solid supports is the Wang resin,[49] which is stable under basic conditions and weak acids. Detachment of the resin needs a treatment of 90-95% TFA for 1-2 h, which allows selective deprotection of strongly acid labile side-chain protection groups. *C*-terminal proline attached to a Wang resin or other sterically unhindered linker molecules lead to diketopiperazine formation after *Fmoc*-deprotection.[50] For this purpose, sterically hindered resins like the 2-chlorotrityl resin are used preferably.[51] Furthermore, 2-chlorotrityl resins allow the detachment of the fully protected peptide by treatment with 1-5% TFA in DCM 1-20 min, without affecting the side-chain protecting groups. This procedure allows selective *N*- to *C*-terminal cyclisation. Moreover, with the choice of the right resin *C*-terminal amides, esters, alcohols etc. can be furnished after global deprotection.[52] *C*-terminal amides, which may reduce the overall solubility of the peptide on one hand, can on the other hand increase the biological activity and stability against enzymatic degradation on the other.[53] Therefore, Rink amide resins are used and peptides can be detached by 50% TFA in 1 h.

1.2.2 The side-chain protection groups

The synthesis of peptides is based on the principle of the orthogonality of the protecting groups.[54, 55] In *Fmoc*-chemistry[56], acid labile side-chain protecting groups are chosen and called permanent protecting groups (Figure 1.1). For the *N*-terminus, *Fmoc* is used as a base labile temporary protecting group. This protecting group strategy prevents side reactions of the side-chains, which would result in branched peptides, complicating purification of the desdired product.

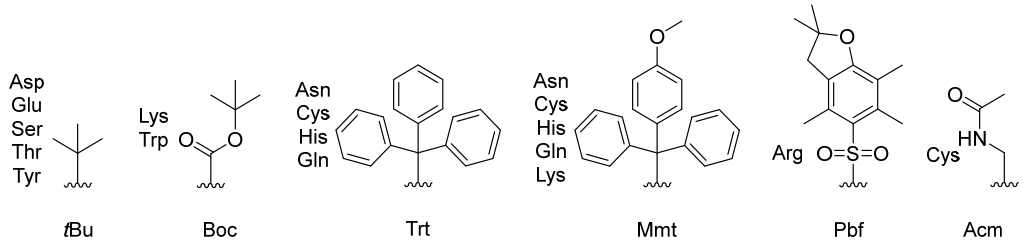

Figure 1.1: Common side-chain protecting groups used in SPPS.[45, 57]

For arginine, 2,2,4,6,7-pentamethyldihydrobenzofuran-5-sulfonyl (Pbf) is the most common side-chain PG, cleavable with 90% TFA in 1 h. For peptides containing multiple Arg, longer treatment with TFA is recommended. Aspartic and glutamic acid are usually protected with *tert*-butyl ester (O^{t}Bu), which can be also cleaved with 90% TFA in about 30 min. Asparagine, glutamine, cysteine and histidine are protected with triphenylmethyl (Trt) and deprotection with 90% TFA gives free side-chains in 30-60 min. Ser, Thr (90% TFA, 30 min) and Tyr (35% TFA) are usually available as ^{t}Bu-protected SPPS building blocks and Trp and Lys normally used as Boc-protected amino acids, cleavable with 90-95% TFA for 1 h. For selective deprotection of single side-chains without affecting the attachment on the resin, a number of PGs are available. In this manner, Lys and Cys side-chains can be selectively deprotected for cyclisation or formation of disulfide-bridges. For Lys, the most common PGs are *p*-methyltrityl, (Mtt, 1% TFA, 30 min) or 1-(4,4-dimethyl-2,6-dioxocyclohexylidene)ethyl (ivDde, $NH_2OH{\cdot}HCl$, imidazole). For Cys side-chains, *p*-methoxytrityl (Mmt, 1% TFA) or acetamidomethyl (Acm, stable to TFA, selective deprotection and simultaneous disulfide-bond formation with I_2) are available.[45, 58]

1.2.3 Coupling reagents

The backbone of peptides consists of iterative amide linkages, the peptide bonds, and their formation is the crucial step of any peptide synthesis. Since, ammonium salts would be the

result of a direct treatment of an amine with a carboxylic acid, a number of different coupling reagents have been developed for smooth formation of peptide bonds.[59] Coupling reagents activate the carboxylic acid by transforming the OH-group in to a good leaving group. The peptide bond is formed by a nucleophilic attack of the amino group of another amino acid. Three classes of coupling reagents are basically used, Carbodiimids, Phosphonium salts and Uronium salts, but active esters, anhydrides, acyl azides and many others are also suitable in some cases. Side reactions in the formation of peptide bonds can be problematic and each activation strategy has its advantages and disadvantages.[59] Up to a ten-fold excess of coupling reagent and amino acids are used to guarantee complete coupling.[43]

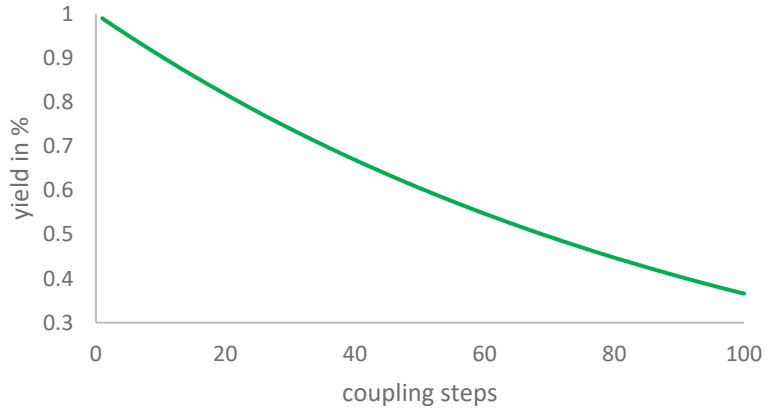

Figure 1.2: Theoretical yield by 99 % coupling efficacy each step.[60]

Mathemathically, the coupling 19 amino acids with a 99% yield each step would result in an overall yield of 83% for a 20 amino acid peptide (Figure 1.2).[60] Capping with acetic anhydride after crucial steps[45] is the one way to avoid peptide chains with a single deletion, which impedes purification due to similar polarity.

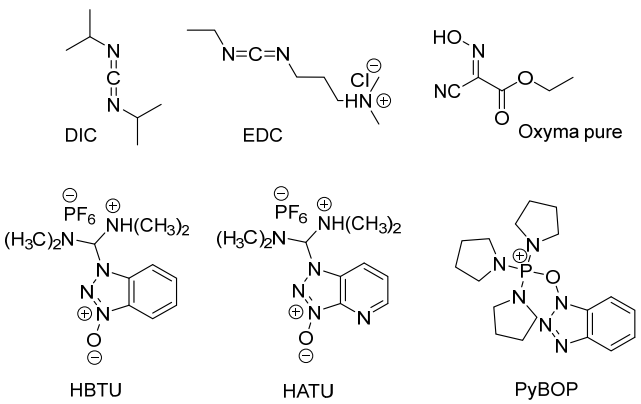

Figure 1.3: Common coupling reagents in SPPS.[61]

N,*N*'-Dicyclohexylcarbodiimide (DCC)[62] is a coupling reagent frequently used in the formation of ester and amides. The formation of insoluble urea byproducts as major drawback led to the invention of *N*,*N*'-diisopropylcarbodiimide (DIC) and 1-ethyl-3-(3-dimethylaminopropyl) carbodiimide (EDC).[63] In SPPS, DCC is replaced by DIC, which is used in combination with Oxyma pure®[64], 1-Hydroxy-7-azabenzotriazol (HOAt) or 1-Hydroxybenzotriazol (HOBt) to form the corresponding active esters (Figure 1.3). Carbodiimides react with carboxylic acids to acylisourea, an intermediate which is too reactive for the direct conversion into amides. Racemisation and the slow [1,3]-acyl shift under formation of *N*-acylurea are undesired reactions, which should be avoided. Therefore, the addition of activation bases like HOBt, HOAt or Oxyma pure® are necessary.[59]

For the solution phase peptide synthesis, EDC is widely used, valued for its good water solubility and easy removal of excess EDC or its corresponding urea in the work up. (2-(1*H*-benzotriazol-1-yl)-1,1,3,3-tetramethyluronium hexafluorophosphate (HBTU)[65] and (1-[Bis(dimethylamino)methylene]-1H-1,2,3-triazolo[4,5-b]pyridinium 3-oxide hexafluorophosphate (HATU)[66] are the most popular representatives of uronium salt reagents. Moreover, HATU/HOAt gives better coupling yields with less racemisation then HBTU/HOBt or Benzotriazol-1-yl-oxytripyrrolidinophosphonium-hexafluorophosphat (PyBOP).[67, 68] The nitrogen in position 7 of HOAt stabilises a seven-membered transition state with its directing properties, which fastens the reaction and minimises racemisation.[69]

A drawback of uronium salts, is the need of pre-activation in order to prevent a reaction with the free N^{α}-amino group, leading to truncated peptides with *N*-terminal guanidino or carbodiimide groups. In contrast, *in situ*-activation is possible with phosphonium salts like PyBOP, as they do not react with N^{α}-amines.[68] Phosphonium and uronium salt reagents need an excess of tertiary bases in order to form carboxylate ions. Typically, two equivalents of *N*,*N*'-diisopropylethyl amine or *N*-methyl pyrrolidine are used.[70]

1.2.4 Cleavage and deprotection

The cleavage strategy depends strongly on the peptide sequence and can vary in cocktail composition, reaction time or the need of inert gas.[71] For cleavage, TFA is used in high concentrations. The treatment of the resin bound peptide with TFA leads to the formation of cations. These more or less stable cations have to be quenched by scavenger reagents in order to prevent the alkylation of unprotected side-chains. Two cleavage cocktails, TFA/phenol/water/TIPS (eq.: 88/5/5/2) and TFA/phenol/water/TIPS (eq.: 88/5/5/2) are widely

used, as they are compatible with any sequences.[57] Whereas most amino acid side-chains can be deprotected under air, Cys, Trp and Met containing peptides should be treated maximal for 2 h under inert gas and light exclusion to avoid oxidation under acidic conditions.[71]

1.2.5 SPPS of the long peptide Ghrelin

Ghrelin is the endogenous ligand for the growth hormone secretagogue receptor GHSR-1a.[72] Synthesised on membrane-bound ribosomes, the 117-residue pre-proghrelin is translocated into the lumen of the rough endoplasmic reticulum.[73] After cleavage by peptidases, 94-residues long proghrelin undergoes post-translational *O*-*n*-octanoylation at Ser3 by the ghrelin *O*-acyltransferase (GOAT) in the endoplasmic reticulum,[74, 75] which is essential for ghrelin's effects on systemic metabolism. During the vectoral transport of acylated proghrelin to the Golgi complex, cleavage at the C-terminal Pro-Arg site results in the formation of the 28-aa long ghrelin.[76] Ghrelin has a number of functions and by binding to GHS-R1a, ghrelin activates orexigenic neural circuits[77], stimulation of gut motility and gastric acid secretion[78], as well as modulation of sleep[79], regulation of glucose metabolism, stress and anxiety. The importance of acylation is shown by the inability of Des-acyl-ghrelin to bind to GHS-R1a at physiological concentrations.[80]

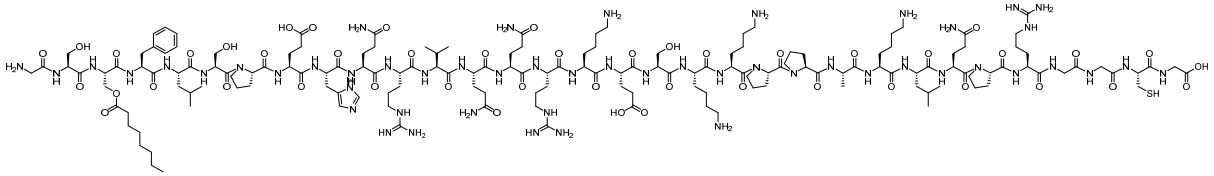

Figure 1.4: Ghrelin-GGCG-OH (**1.1**) with its acylated Ser3.[1]

1.2.5.1 Results and Discussion

In order to investigate activation and internalisation of G protein coupled receptors, tethered pharmacology is a very successful tool. Therefore, a benzyl guanine-linked Ghrelin which allows a SNAP-tag directed activation of its receptor GHS-R1a was developed by Podewin. et. al.[1]

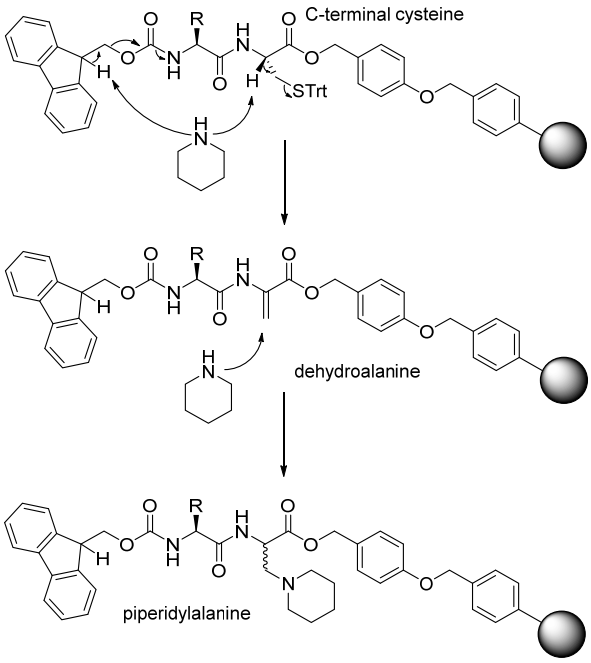

Scheme 1.2: Side reaction during each deprotection step in SPPS with *C*-terminal Cysteine under formation of piperidyl alanine.[81]

For the coupling of BG-amine, a C-terminal Cysteine containing GGC linker was needed. A challenging side-chain reaction of C-terminal Cysteines in SPPS however, is the formation of piperidinyl alanine under basic conditions. During each deprotection cycle of the *Fmoc*-protected amines, β-elimination takes place followed by the addition of piperidine, leading to the formation of *C*-terminal piperidinyl alanine. The elimination step is strongly dependent on the side-chain protecting group used, with the protecting group *t*Bu tend to be most fragile to this side reaction, followed by Acm and Trt.[81] Therefore, we used a GGCG-linker with a C-terminal glycine to avoid side reactions. For the introduction of the side-chain modified Ser3, the SPPS building block *Fmoc*-Ser-(*n*-octanoyl)-OH (**1.2**) was synthesised.[82, 83] L-Serin (**1.3**) was protected with *Fmoc*-OSu and subsequently acylated with octanoyl chloride in TFA, providing 87% of the product over two steps. The SPPS building block **1.2** was then used for the synthesis of Ghrelin-GGCG (**1.1**)

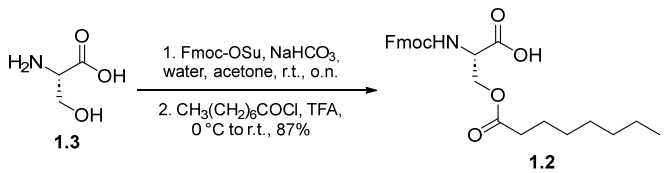

Scheme 1.3: Synthesis of Ser3 SPPS building block.[82, 83]

For peptides of this length, resins with lower loadings usually promise better yields[84], and consequently a 0.23 mmol/g Gly-wang resin was used. Coupling conditions for the SPPS are showed in table 3.1. Double coupling of position 21-32 was used to guarantee attachement of the amino acids. Otherwise coupling might be impaired by extended aggregation of the longer peptide chains. After global deprotection with TFA/phenol/water/TIPS (8.8/0.5/0.5 /0.2) for 2 h at room temperature, the crude peptide was precipitated in cold diethyl ether. After centrifugation, the residue was washed with diethyl ether for 5 times, diluted in 10 mL acetonitrile/water (1:1) and lyophilised. The crude product was then purified by reversed-phase HPLC (H_2O/MeCN 95/5 → 20/80 in 40 min) to receive the peptide as a white fluffy powder.

1.3 Overview of peptide mimetics

In medicine, but especially in neurology, endocrinology, immunology and hematology, peptides are of great interest. In 2019, 25% of the global pharmaceutical market were based on peptides, proteins or antibodies.[85] However, medicinal use is severely limited due to proteolytic and enzymatic degradation, the associated poor general and oral bioavailability, problematic transport through cell membranes (hydrophilicity), and the non-selective binding behavior (conformational flexibility) to receptors.[86] This is mainly due to the physiochemical properties of the peptides, such as water solubility, lipophilicity, formation of hydrogen bonds, chemical and metabolic stability, and rapid elimination through the liver and kidneys.[87, 88]

Efforts were made in the last decades to address the limitations of peptide-based drugs, however, today a hugh variety of peptidomimetics have been developed. While maintaining the biological activity, funciontal modifications can be introduced into peptide and thus science is able to overcome the intrinsic drawbacks of peptides.[88]

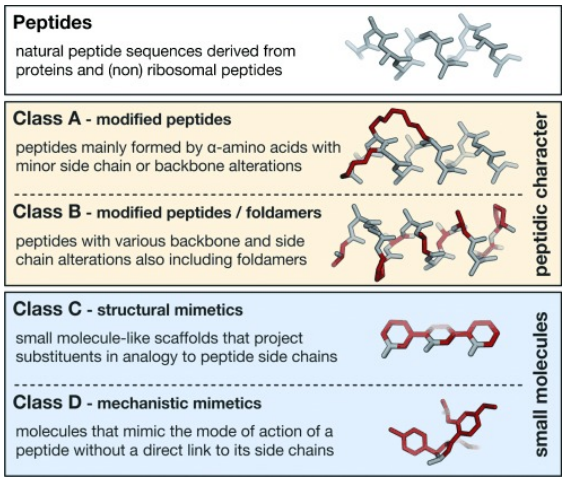

Figure 1.5: Classification of peptidomimetics by *Grossmann and coworkers*.[89]

From the late 90s on, peptidomimetics have been categorized by their similarity with the parent peptide, especially the spatial orientation of their functionalities.[90] A modern classification, suggested by Pelay-Gimeno et. al.[89] is based on the degree of their similarity to the natural peptide precursor, or respectively, their degree of peptide character (Fig.: 1.5). The peptides synthesized in this work belong to Class A, due to minor side chain and backbone alterations.

There are few different possibilities for the modification, base on the structural features of pepties. A widely used strategy is the replacement of an amide bond, enhancing the stability against enzymatic degradation. Examples are azapeptides[91, 92], thioamides[93] or α-aminoxy-peptides[94]. α-aminooxypeptides, the oxo analogues of α-aminopeptides, have a high tendency to form rigid peptide structures. This is due to the repulsion of the lone pair of electrons of the oxygen atom in the vicinity of the nitrogen atom. This results in a higher nucleophilicity of the nitrogen, a change in the torsional properties of the bonds and the hydrogen bonds.[95-97] Aza-peptides are obtained by replacing a rotatable Cα-C(O) bond with a rigid Nα-C(O) bond.[98] The resulting change in geometry at the α-position from tetrahedral to trigonal results in the loss of chiral information. Furthermore, the the carbonyl group of azapeptides have a reduced electrophilicity.[99] However, these changes improve the stabilization against enzymatic hydrolysis.[91, 100-102]

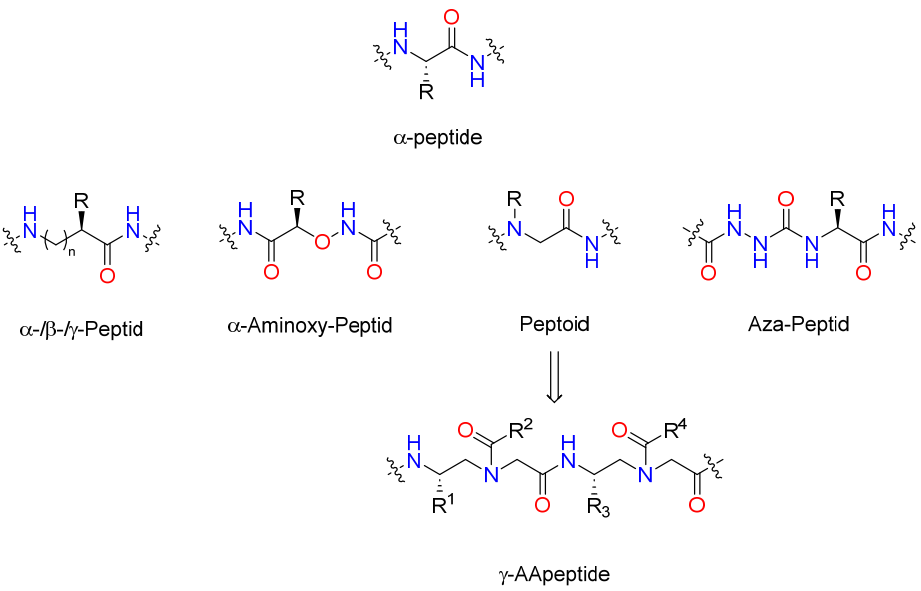

Figure 1.6: Structures of different peptidomimetics.

Side chain modifications enable the introduction of non-natural amino acids. The hydrophobicity, polarity and acidity/basicity of the parent peptide can be altered by introducing relevant side chains. Larger aromatic side chains improve π-stacking, whereas the introduction of β-peptides[103-105] enhance the proteolytic stability and stabilize helical structures[106]. An example for the improvement of the chemical and metabolic stability is the β^3-homo-threonine-conjugate of the T_N-antigene, synthesized by Hoffmann-Röder and co-workers.[107]

The introduction of photoswitchable side chain modifications should be mentioned at this point, but will be discussed later.

At least, mimetics of the secondary structure of binding epitopes can be used to alter protein-protein interactions. Chemistry provides a number of mimetics for α-helices, β-turn, β-hairpin and β-sheet structures to improve their stability and therapeutic potential.[88] An important mimetic of the α-helix are peptoids. Peptoids[108] are α-peptide mimetics, with the side chain attached to the nitrogen atom, resulting in a tertiary amide. This modification provides a stable secondary structure of chiral helices, which is stable in different solvents and pH values. While the tertiary amine improves proteolytic stability, the lack of chiral centers and hydrogen-bond donors makes folding of these peptides difficult. The results are *cis*- and *trans*-conformers. Additionally, tight turns facilitate intramolecular interactions.[88] A further development of peptoids are AA-peptides described be Cai and co-workers[11, 109], which will be discussed in the next chapter.

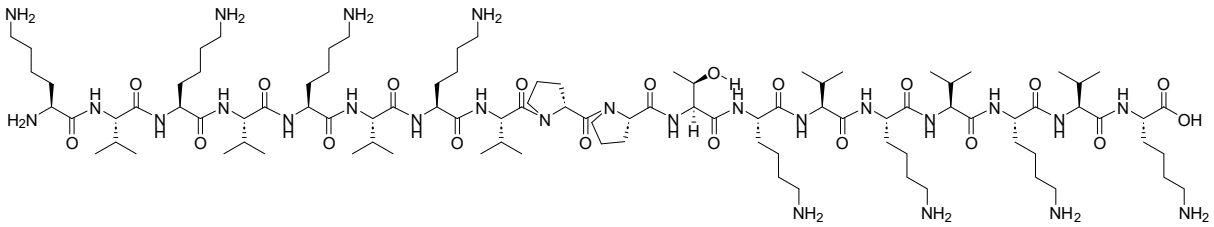

Figure 1.7: Structure of SVS-1.[110]

The structure of β-hairpins is stabilized by an extend of hydrogen-bonds but also by turn-inducing amino acid sequences like D-Pro-L-Pro. This effect was demonstrated in the D-Pro-L-Pro containing anti-cancer peptide SVS-1, which shows membrane induced folding of β-haiprins in the presence the negatively charged membrane surface of cancer cells. In contrast, the L-Pro-L-Pro containing analogous peptide was incapable of β-haiprin formation. [110, 111]

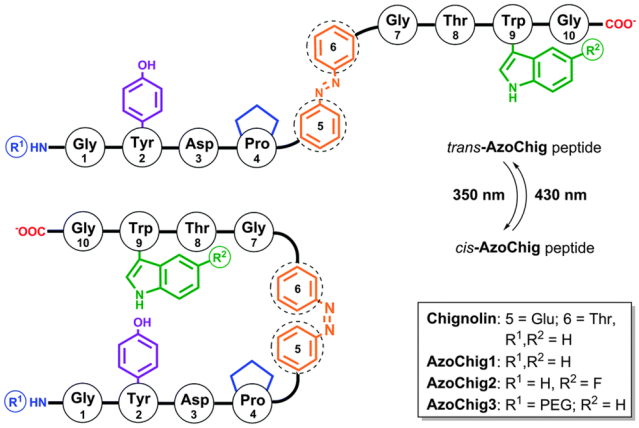

Figure 1.8: Switching of AzoChignolin by the light of different wavelengths.[112]

While SVS-1 only forms β-hairpin structure in presence of negatively charged membranes, the photoswitchable azobenzene amino acid AMPP allows β-hairpin formation of Azochignolin triggered by light. Azochignolin is a short nine amino acid long peptide, derived from the model-peptide chignolin. The backbone mimtic AMPP starts nucleation of the β-hairpin formation by light-triggered switching of its conformation from E → Z. By introducing AMPP into the peptide chignolin, β-hairpin formation can be studied by time-resolved infrared-spectroscopy.[2, 112-118]

1.4 Analtical Data of Ghrelin-GGCG

***Fmoc*-Ser(*n*-Octanoyl)-OH (1.2)[119]**

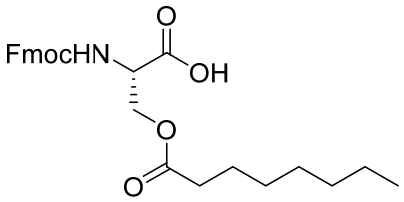

Compound **3.11** was synthesized in accordance to literature known protocols.[82, 83]

To a solution of 500 mg (4.76 mmol, 1.0 eq.) of L-Serin in 40 mL acetone/water (1:1), 800 mg, (9.52 mmol, 2.0 eq.) $NaHCO_3$ and 1.60 g (4.76 mmol, 1.0 eq.) *Fmoc-O*Su was added. The solution was stirred at room temperature overnight. After acidification to pH = 2 with 1 N HCl, the solution was extracted with EtOAc (3 x 100 mL) and dried over $MgSO_4$. The crude product was solved in 20 mL TFA, cooled to 0°C and 2.03 mL (11.9 mmol, 2.5 eq.) octanoyl chloride were added dropwise. After stirring at room temperature overnight, the solvent was removed under reduced pressure and the residue was co-evaporated with toluene (5 x 20 mL), and dichloromethane (2 x 20 mL). The crude product was purified by flash-chromatography on silica (^{C}Hex/EtOAc 8:1 → 4:1) to give 1.88 g (4.14 mmol, 87%) of the product as an amorphous white solid.

HR EI-MS (positiv), m/z: 454.2228 ($[M+H]^+$, calc.: 454.2224)

HR EI-MS (positiv), m/z: 471.3490 ($[M+NH]^+$, calc.: 471.2489)

^{1}H-NMR (400 MHz, $CDCl_3$) δ = 9.56 (s, 1H, COO***H***), 7.77 (d, *J* = 7.5 Hz, 2H, ***H***4-, ***H***5-*Fmoc*), 7.65 – 7.50 (m, 2H, ***H***1-, ***H***8-*Fmoc*), 7.41 (t, *J* = 7.5 Hz, 2H, ***H***3-, ***H***6-*Fmoc*), 7.36 – 7.28 (m, 2H, ***H***2-, ***H***7-*Fmoc*), 6.52 (d, *J* = 5.6 Hz, 1H, N***H***-*Fmoc*, K2), 5.72 (d, *J* = 8.2 Hz, 1H, N***H***-*Fmoc*, K1), 4.72 (dt, *J* = 8.0 Hz, *J* = 3.9 Hz, 1H, $\boldsymbol{H}_\alpha$, K1), 4.54 (d, *J* = 4.2 Hz, 2H, C$\boldsymbol{H}_2$-*Fmoc*, K2), 4.49 (dd, *J* = 16.3 Hz, *J* = 3.9 Hz, 2H, $\boldsymbol{H}_\beta$), 4.44 (d, *J* = 7.1 Hz, 2H, C$\boldsymbol{H}_2$-*Fmoc*, K1), 4.34 – 4.27 (m, 1H, $\boldsymbol{H}_\alpha$, K2), 4.24 (t, *J* = 6.8 Hz, 1H, ***H***9-*Fmoc*), 2.33 (t, *J* = 7.6 Hz, 2H, $\boldsymbol{H}2_{Oct}$), 1.68 – 1.58 (m, 2H, $\boldsymbol{H}3_{Oct}$), 1.27 (bs, 8H, $\boldsymbol{H}4_{Oct}$, $\boldsymbol{H}5_{Oct}$, $\boldsymbol{H}6_{Oct}$, $\boldsymbol{H}7_{Oct}$), 0.88 (t, *J* = 6.7 Hz, H3, $\boldsymbol{H}8_{Oct}$) ppm.

^{13}C-NMR (100 MHz, $CDCl_3$) δ = 173.8 (***C***1_{Oct}), 173.6 (***C***OOH), 156.6 (***C***=O-*Fmoc*, K2), 156.2 (***C***=O-*Fmoc*, K1), 143.7, 143.6 (***C***1a-, ***H***8a-*Fmoc*, K1), 143.5(***C***1a-, ***H***8a-*Fmoc*, K2), 141.4

(***C***4a-, ***C***5a-*Fmoc*), 127.9 (***C***3-, ***C***6-*Fmoc*), 127.2 (***C***2-, ***C***7-*Fmoc*), 125.1 (***C***1-, ***C***8-*Fmoc*, K1), 124.8 (***C***1-, ***C***8-*Fmoc*, K2), 120.1 (***C***4-, ***C***5-*Fmoc*), 68.0 (***C***H_2-*Fmoc*, K2), 67.6(***C***H_2-*Fmoc*, K1), 63.7 (***C***β, K1), 63.3 (***C***β, K2), 53.7 (***C***α, K2), 53.4(***C***α, K1), 47.1 (***C***9-*Fmoc*), 34.0 (***C***1_{Oct}), 31.7 (***C***4-***C***7_{Oct}), 29.1 (***C***4-***C***7_{Oct}), 29.0 (***C***4-***C***7_{Oct}), 24.8 (***C***3_{Oct}), 22.7 (***C***4-***C***7_{Oct}), 14.1 (***C***8_{Oct}) ppm.

Ghrelin-GGCG (1.1)[1]

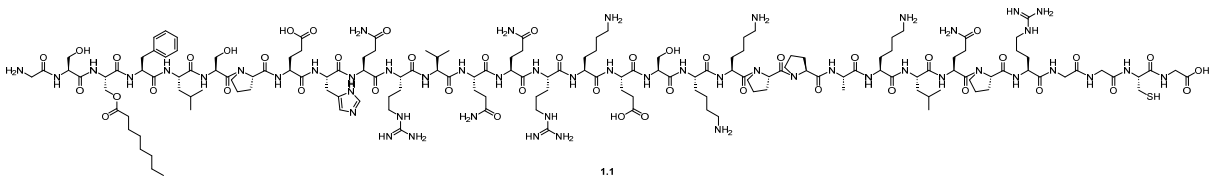

1.1

Synthesis was carried out on a preloaded Fmoc-Gly-Wang (0.23 mmol/g) low loading resin using DIC/Oxyma® as coupling reagents. Coupling conditions are shown in table 3.1. SPPS building block *Fmoc*-HisTrt-OH was first coupled at 25°C without microwave for 120 s before heating to 50°C. *Fmoc*-deprotection was achieved by treatment with 20% piperidine in DMF. After automated SPPS, the resin was transferred into a Merrifield reactor and the resin was freed from DMF by washing with DCM several times and global deprotection of the peptide was done with TFA/TIPS/phenol/water (88/0.2/0.5/0.5) for 2 h at room temperature. The peptide was precipitated in cold diethyl ether, centrifuged and washed with Et_2O for five times. The crude peptide was diluted in 10 mL acetonitrile/water (1:1), lyophilised and purified by reverse-phase HPLC (MeCN/water, 95/5 → 70/30 in 40 min) to furnish Ghrelin-GGCG (**3.3**) in high purity with a mass error of 2.61 ppm of the theoretical mass (Figure 3.2).

Table 1.1: Coupling conditions of microwave assisted SPPS of **1.1**

Compound	step	**1.1**		
		t [s]	p [W]	T [°C]
Fmoc-Cys*t*Bu-OH	1	120	30	90
Fmoc-Gly-OH	1	120	30	90
Fmoc-Gly-OH	1	120	30	90
Fmoc-ArgPBf-OH	2	120	30	90
Fmoc-Pro-OH	1	120	30	90
Fmoc-GlnTrt-OH	1	120	30	90
Fmoc-Leu-OH	1	120	30	90
Fmoc-Lys*t*Bu-OH	1	120	30	90
Fmoc-Ala-OH	1	120	30	90
Fmoc-Pro-OH	2	120	30	90
Fmoc-Pro-OH	1	120	30	90
Fmoc-Lys*t*Bu-OH	1	120	30	90
Fmoc-Lys*t*Bu-OH	1	120	30	90
Fmoc-Ser*t*BU-OH	1	120	30	90
Fmoc-Glu*t*Bu-OH	1	120	30	90
Fmoc-Lys*t*Bu-OH	1	120	0	90
Fmoc-ArgPbf-OH	2	120	30	90
Fmoc-GlnTrt-OH	2	120	30	90
Fmoc-GlnTrt-OH	2	120	30	90
Fmoc-Val-OH	2	120	30	90
Fmoc-ArgPbf-OH	2	120	30	90
Fmoc-GlnTrt-OH	2	120	30	90
Fmoc-HisTrt-OH	2	50	35	480
Fmoc-GlnTrt-OH	2	120	30	90
Fmoc-Pro-OH	2	120	30	90
Fmoc-Ser*t*Bu	2	120	30	90
Fmoc-Leu-OH	2	120	30	90
Fmoc-Phe-OH	2	120	30	90
Fmoc-Ser*n*Otc-OH	2	120	30	90
Fmoc-Ser*t*Bu-OH	2	120	30	90
Fmoc-Gly-OH	2	120	30	90

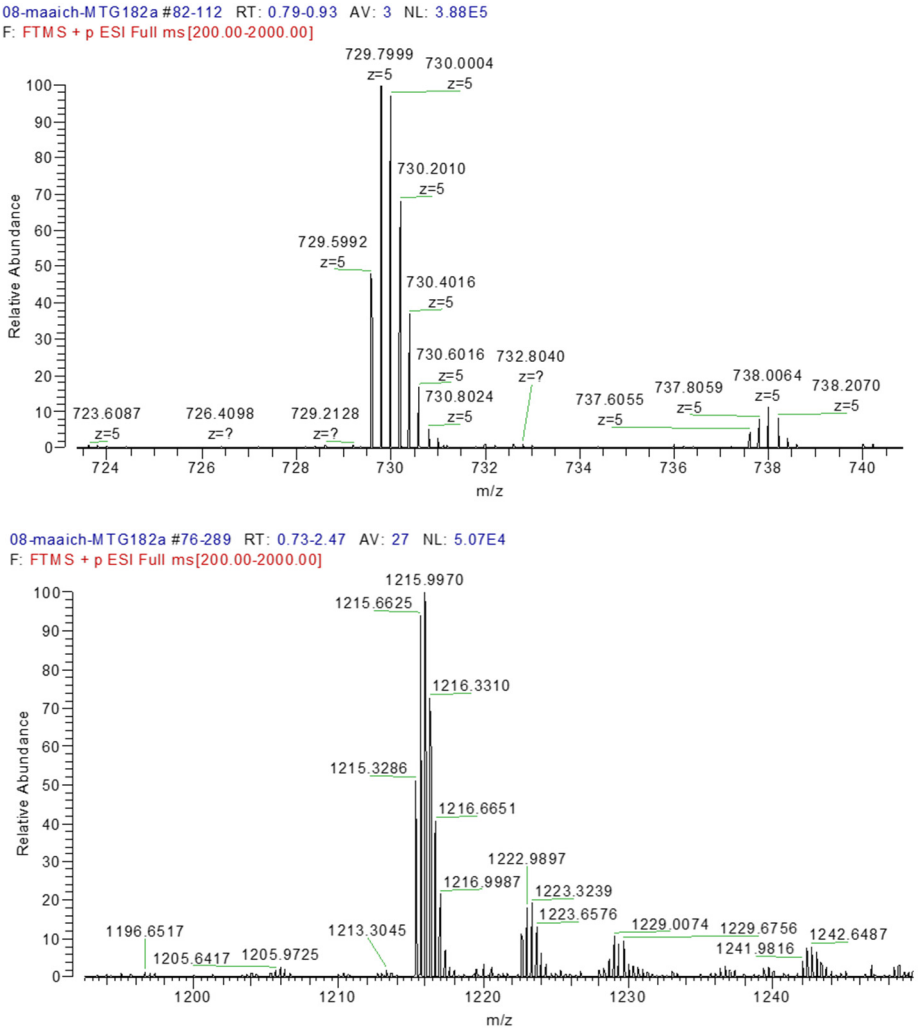

Figure 1.9: HRMS spectrum of Ghrelin-GGCG (**1.1**): HRMS (+ESI) m/z calc. for $C_{158}H_{266}N_{51}O_{46}S^{3+}$ $[M + 3H]^{+}$: 1215.6594; found: 1215.6625, m/z calc. for $C_{158}H_{268}N_{51}O_{46}S^{5+}$ $[M + 5H]^{+}$: 729.7985; found: 729.7999.

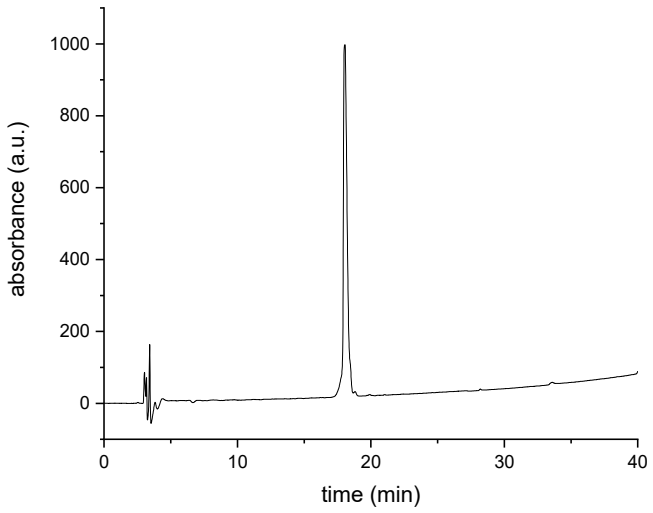

Figure1.10: Reversed-phase HPLC run (MeCN/water 95/5 → 20/80 in 40 min) with a retention time of 18.0 min.

2 MUC1-γ-AApeptide mimetics

2.1 γ-AA-peptides

In this work, the used a monomeric building block of the peptidomimetic structure called γ-AA-peptides[11], which are oligomers of γ-substituted *N*-acylated-*N*-aminoethyl amino acid.[120] They are derived from chiral peptide nucleic acids (PNA)[121, 122], where a pseudopeptide backbone mimics the ribose phosphate backbone.[123] PNAs hybridize with high affinity and sequenz specifity and are used as antisense and antigene agents.[124] Introducing linear[109] and cyclic[125] γ-AApeptides, sulfono-γ-AApeptides[126] and α/sulfono-γ-AApeptides[127], Cai and coworkers transferred the principle of PNAs onto peptides.

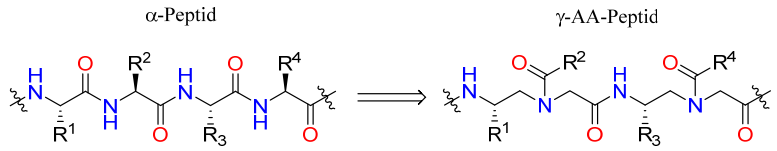

Figure 2.1: Structure of α-peptide and γ-AApeptide.[11]

With the same chain length, γ-AApeptides have the same number of side chains and functional groups as natural peptides, but unlike the natural peptide, they have alternating secondary and tertiary amides in the peptide backbone. Furthermore, only one side chain of two contiguous amino acids corresponds to the natural side chain, while the other side chain arises from the residue of a carboxylic acid and is attached to the tertiary amide. The tertiary amide causes a higher flexibility of the peptide backbone. Each tertiary amide bond can switch between its *cis* and *trans* conformation, which can lead to a change in structure and resulting properties. In comparison to its natural structures, the γ-AApeptide building block lacks of one hydrogen-bond donor and one chirality center. However, the relative distances and positions of the side chains are preserved. (Figure 2.1).[11, 109]

The synthesis can be done by several strategies either in liquid phase or on solid support. In liquid phase, two different protection group strategies can be used, depending on the side-chain protecting group R (Scheme 2.1). If the side-chain carries an acid-labile protecting group, the carboxylic acid should be protected by a benzylic ester. If not, acid-labile *tert*-butyl esters can be used. For the synthesis of huge libraries, the preparation of monomeric SPPS building blocks by direct acylation of the secondary amine is not feasible because of the synthetic effort in preparation of all different building blocks. A submonomeric approach, where the secondary

amine is acylated with allyloxycarbonyl chloride (Alloc-Cl), each building block can be acylated individually during SPPS.[128]

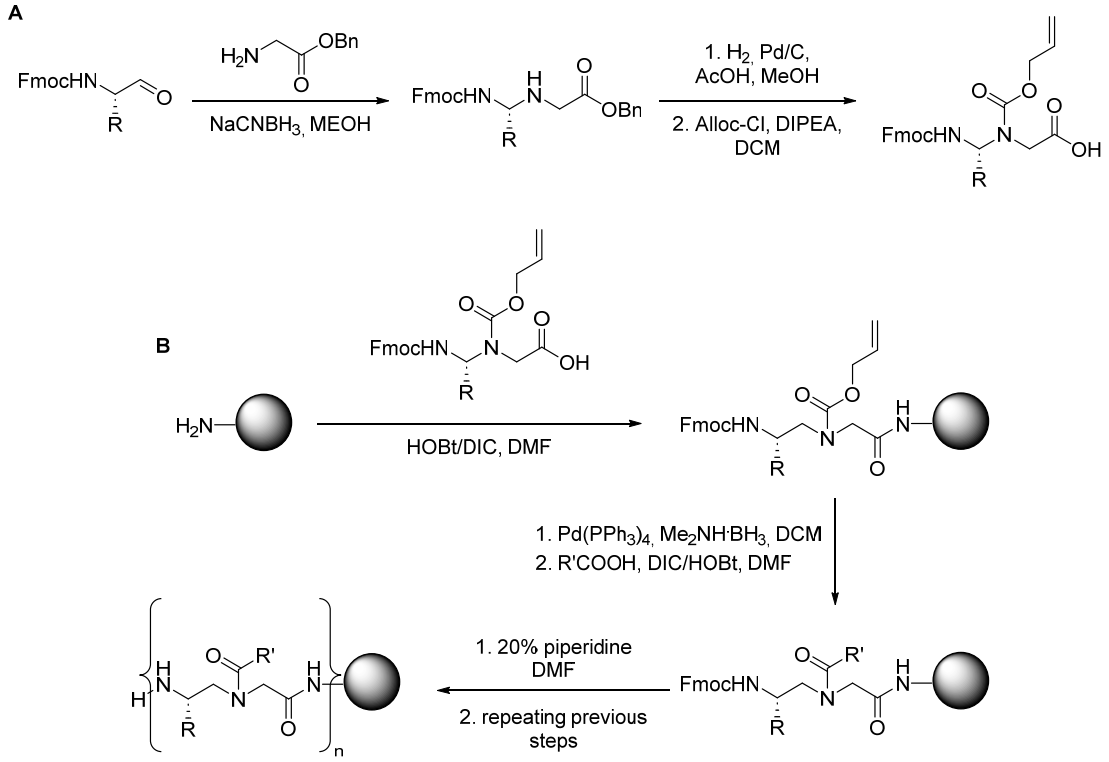

Scheme 2.1: A) Synthetesis of submonomeric γ-AA peptide building blocks. B) SPPS-strategy for the synthesis of γ-AAPeptide liberaries.[128]

CAI and his group tested the use of γ-AApeptides for different classes of peptides and their therapeutic applications. The stability against proteolytic degradation was tested by treating a γ-AApeptide with chymotrypsin, thermolysin, and pronase for 24 h and no degradation was observed.[11] For therapeutic applications, Cai and coworkers developed several γ-AApeptides with anti-cancer properties, antimicrobial acitivies, TAT peptide mimetics and $A\beta_{40}$ aggregation disrupting peptides for Alzheimer's disease.[129]

The transcription factor p53, a tumor suppressor protein, can initiate the expression of proteins responsible for repairing DNA, arresting cell growth in the G1/S phase of the cell cycle, or initiating apoptosis. The murine double minute 2 protein (MDM2) inhibits p53 binding to DNA and also promotes p53 proteolysis. Overexpression of MDM2 in tumor cells prevents activation of p53 and leads to uncontrolled cell growth. For instance, the interaction of MDM2 and the transactivation domain of p53 could be disrupted by new γ-AA peptide mimetic, bearing Phe, Trp and Leu side-chains, which are important for the perturbation of the interaction of the

transcription factor 53 and murine double minute 2 protein (MDM2) and thus the cell growth of tumor cells could be prevented.[11]

A further example is the γ-AAPeptide mimetic of Tat 48-57, which binds RNA and promotes uptake by cells. In contrast to native Tat protein, the mimetic was less toxic and more stable towards enzymatic degradation, both important properties for a cell penetrating peptide (CPP).[130]

Besides conventional antibiotics, nature provides a second strategy to fight bacterial infections, called host defense peptide (HDPs) or antimicorbial peptides (AMP). With their amphiphatic structures, HDPs penetrate the cell surface causing membrane disruption and cell death.[131] Cai and coworkers developed linear helical[132], cyclic[125] and lipo γ-AApeptides[133, 134], with high antimicrobial activity. Furthermore, resisting enzymatic degradation these HDP-γ-AApeptide mimetics overcome the intrinsic drawbacks of natural peptides.[129]

2.2 MUC1-γ-AApeptide mimetic

Today, in the context of an ageing society, cancer is still one of the main causes of death. Next to surgery, radiotherapy or chemotherapy, cancer immunotherapy became a promising complementary or even alternative treatment. Membrane proteins, usually important for cell recognition, signaling or transport of ions and small molecules, are given a key role in immunotherapy. Changes in the cell metabolism of cancer cells are responsible for altered glycosylation patterns of cell surface glycoproteins, so called tumor-associated carbohydrate antigens (TACA).[7, 135] These TACA can be used for distinction between healthy and malignant cells, which helps to address the immune response solely to malignant tissues.[7] A family of cell surface proteins are called mucins, which are heavily *O*-glycolylated polymorphic proteins on epithelial cells.[6] As a protective biochemical layer and as transmitters of cell-cell interaction during cell adhesion or signal transduction, mucins are expressed by many different tissues in the digestive system, respiratory system and eyes.[6]

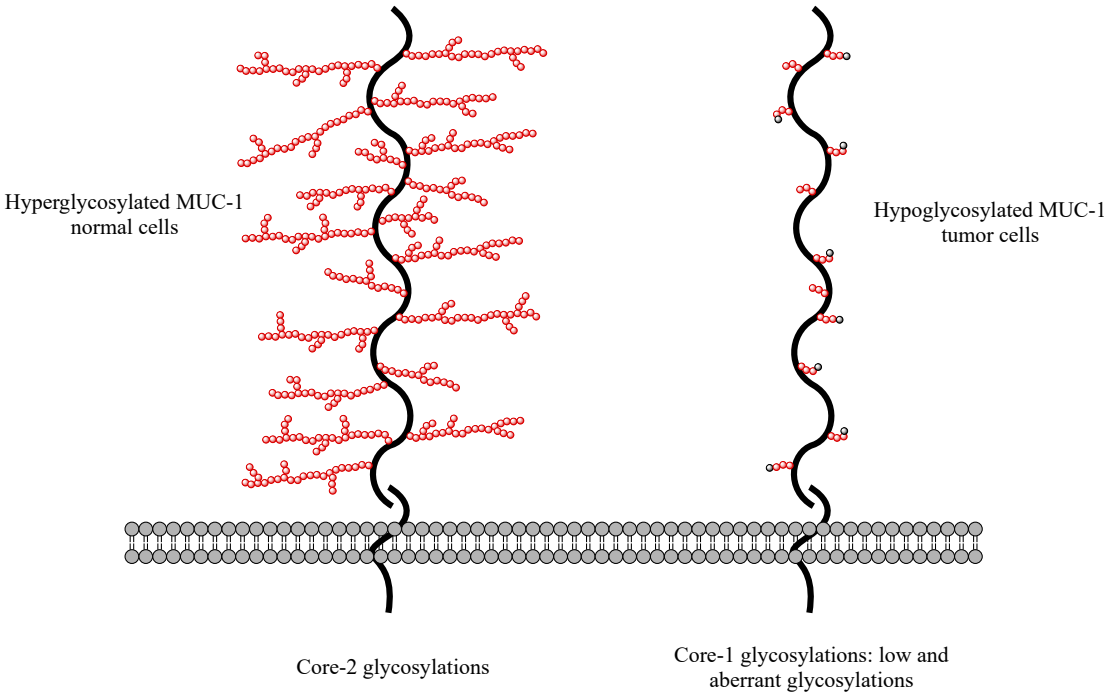

Figure 2.2: Structure of MUC1: unglycosylated (left), in healthy cells (middle) and in tumor cells (right).[136]

One important mucin is the membrane bound MUC1[137], consisting of 20-125 tandem repeats of the sequence AHGVTSAPDTRPAPGSTAPPA, which is heavily glycosylated on its Ser and Thr side-chains. During normal biosynthesis, the first is the glycosylation of the tandem repeat with α-*N*-acetylgalactosamin by the polypeptidyl-GalNAc-transferase (ppGalNAcTs)[138] in the Golgi apparatus. The activity of the ppGalNAcTs is enhanced, if Proline residues are nearby

(+1, +3, −1, −3).[139-141] The resulting T_N-antigen can be glycosylated by three different transferases. First, core 1 structure or Thomsen-Friedenreich-antigen (T-antigen) is synthesiszed by core 1 β1,3-galactosyltransferase (T-synthase) which is the most regular modification.[142, 143] Core 3 is synthesized by core 3 β1,3-*N*-acetyglucosaminyltransferase (core 3 β3GlcNAcT) and at least the sialyltransferase St6GalNAc-I synthesizes the sialyl-T_N antigen. The T-antigen or core 1 structure can be further branched or elongated by several enzymes. While core 2 β6-GlcNAcT transfers an acetylglucosaminyl-residue forming the branched core 2 structure, the core 1 β3-GlcNAcT elongates the T-antigen to the extendes core 1 structure.[144] Furthermore, the core 1 structure can be sialylted either by ST6GalNAc-II to the branched Sia6Core 1 strcuture[145] or elongated by ST3Gal-I to the Sia3Core 1 structure, which can be branched by ST6GalNAc-III and ST6GalNAc-IV.[146] The donors for these reactions is uridine diphosphate galactose (UDP-Gal), uridine diphosphate *N*-acetylglucosamine (UDP-GlcNAc) or cytidine-5-monophospho-*N*-acetyleuraminic acid (CMP-NeuAc) respectively.[145, 146]

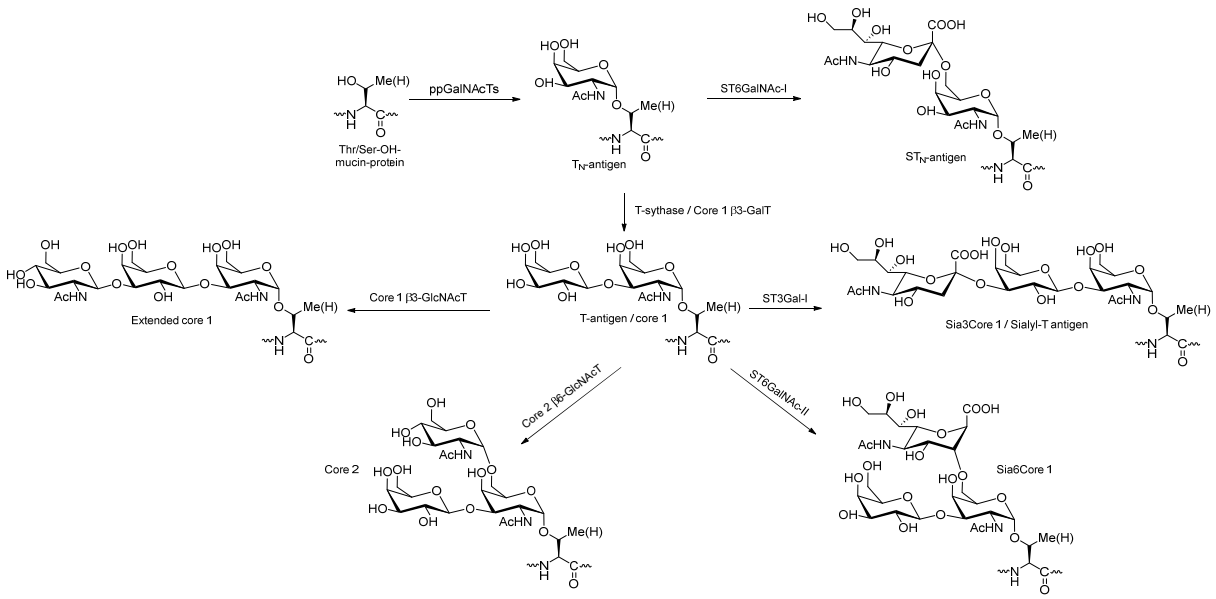

Scheme 2.2: Biosynthesis of tumor associated antigens of MUC1.[7, 135]

In malignant tissues, aberrant glycosylation leads to truncated glycan structures, so-called tumor associated antigens composed of *O*-glycosylated mono- (Tn antigen), di- (T- and STn-antigen) and tri-saccharides (ST-antigen).[147] A changed metabolism causes down-regulation of β-1,2-galactosyltransferase and thus, the transfer of the Core1-structure to Core2-structure is reduced.[147, 148] However, the change in glycosyltransferase-activity is responsible for the presentation of immature structures like T_N- and T-antigen on the surface of cancer cells.[149, 150] Furthermore, sialylation of T_N- and T-antigens by upregulated sialyltransferases terminates

the growth of the glycosyl chain.[151, 152] While the long natural polysaccharide sterically shield the peptide epitopes, the truncated glycosyl patterns in malignant cells make peptide epitopes accessible to the immune system. In MUC1, the *O*-glycosylated peptide motifs, PDTR, GVTS and GSTA exists, and upon glycosylation of these domains, the β-turn conformation of the backbone is stabilised in these sequences. This effect is strongest for the PDTR domain.[153]

Tumor-associated MUC1 occurs in 80% of human cancer, especially in carcinomas of the blood, breast, colon, liver, prostate, ovarian and stomach. Therefore in 2009, the *National Cancer Institute of the USA* declared MUC1 second important tumor antigens.[137] Used as markers for prognosis estimation, cancer detection or therapy monitoring, TACAs can also trigger strong humoral immune response when presented to the immune system in combination with immunostimulants.[154] But in addition to TA-MUC1, malignant tissues also express MUC1 polysaccharide peptide chains typical for healthy tissues. This biological microheterogeneity of the glycan-structure of cancer cells makes the isolation of pure TA-MUC1 impossible.[7] With the help of chemical synthesis, the combination of specific and pure TA-MUC1 with Toll-like receptor ligands, T-cell epitope peptides or other immunostimulants can be used in vaccine development. The combination with immunostimulants is crucial for avoiding immune tolerance. The activation of the T-cell dependent pathway results in an immune response towards the cancer cells. There are three different strategies to combine MUC1 with immunostimulating components, which are shown in Figure 2.3. The glycosylated MUC1-B-cell epitope is connected with the immunostimulant through a non-immunogenic spacer, which also prevent the vaccine components from influencing each other.[7]

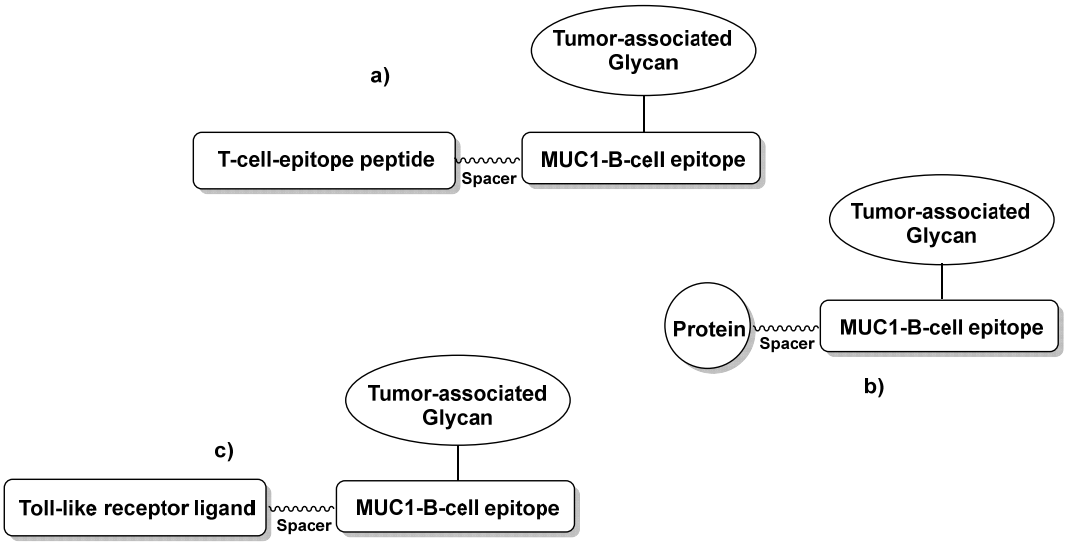

Figure 2.3: Three different strategies to synthesise a vaccine by combining MUC1 with immunostimulating components.[7]

While the long-branched glycosylation of the extracellular domain of healthy cells protect the peptide backbone from proteases[153], the backbone of the 20-mer of TA-MUC1 with its short glycosyl chains is exposed to enzymatic degradation. A strong immune response with a high efficacy is crucial for vaccination, since it minimises the possibility of immune escape mechanisms by the tumor which could lead to increased tolerance to the presented antigens.[155] Enzymatic degradation of the peptidic vaccine as a main drawback can reduce the immune response and thus trigger an immune escape mechanism.

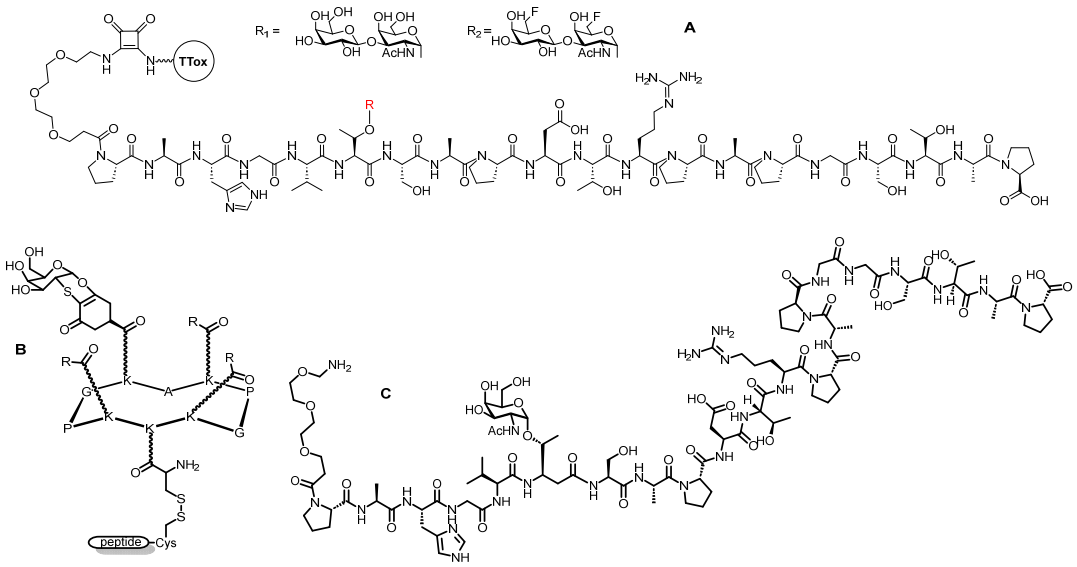

Figure 2.4: A) Fully synthesised difluoro-T-antigen-MUC1-TTox vaccine;[156] B) T-cell epitope OvaPadre linked to a monosaccharide through RAFT;[157] C) unnatural amino acid used for the T_N-antigen building block.[107]

Therefore, various strategies have been pursued in recent years to improve the enzymatic stability of MUC1 antigens while maintaining immunological efficiency. Modifications of the saccharide structure improve stability against glycosidases, while the use of peptide mimetics reduces enzymatic degradation by peptidases. Hoffmann-Röder et al. synthesised a difluoro-T-antigen-MUC1-TTox vaccine, which was used in combination with Freund's adjuvant to immunise mice to get extraordinarily strong immune reactions.[158] An example, in which only the saccharide epitope is used, is a mimetic developed by RICHICHI. The bioactive saccharide epitopes 2-deoxy-2-thio-α-*O*-galactosid are linked to a RAFT (regioselectively addressable functionalized template), which also contains a T-cell peptide epitope OvaPadre. This T_N-mimetic has the same $^4C_1$-conformation as its natural version and elicits a long-lasting IgG/IgM antibody response.[157] For the stabilisation of the peptide backbone, unnatural amino acids

have been introduced into the glycosylation side like the T_N-antigen analogue *Fmoc*-β3hThr(αACBT3GalNac)-OH[107] or the fluorinated prolines (4S)-4-fluoro-L-proline 4,4-difluoro-L-proline.[159] While the introduction of β-amino acids improve, enzymatic stability, fluorinated prolines additionally enhance the key CH/π interaction in the β-hairpin and therefore binding of antibodies to the MUC1.[159]

2.3 Objective

The aim of this project was the synthesis of γ-substituted *N*-acylated-*N*-minoethyl peptide mimetics of the mucin MUC1 B-cell epitope to improve enzymatic stability as well as immunogenicity. Since the efficacy of peptide-based vaccines can be reduced by enzymatic degradation, the use of such a mimetic is of interest. Furthermore, the flexibility of the γ-AApeptide allows β-hairpin formation of MUC1-mimetics, which is essential for antigen recognition.[153] The antigen mimetics synthesised in this thesis are a combination of AApeptides with the MUC1 B-cell epitopes.[160] The synthesis of the mono- and disaccharide mimetics was performed according to the T_N- and T-antigen synthesis[158, 160-165] and the γ-AApeptide monomers were synthesised according the work of CAI and coworkers under use of the *tert*-butyl ester protection groups.[11] The synthesised γ-AApeptide glycan structure mimics the Val-Thr(glycan) sequence in the glycosylation domain GVTS.[160] All three antigens were sythesized in the previous master's thesis.[12]

2.4 Synthesis of the γ-AApeptide

The synthesis of the γ-AApeptide followed the synthesis strategy of *Niu et. al.*[11]

The γ-AApeptide moiety was synthesized in four steps, starting with L-valine (**2.1**) and glycine. The reduction of L-valine to L-valinol was carried out with BH_3:THF complex.[166] After protection of the amine, L-valinol was oxidized under SWERN-conditions to L-valinal (**2.2**).[167] The reductive amination[11] of the aldehyde with *t*Bu-protected glycine (**2.3)** led to the formation of the secondary amine **2.4**.

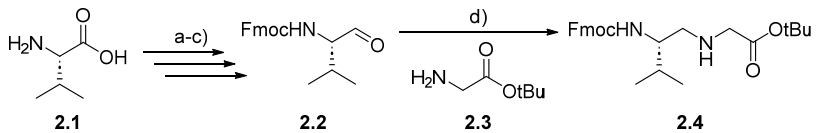

Scheme 2.3.: Sythesis of the dipeptide of γ-AApeptide: a) 1) $NaBH_4$, I_2, THF, 66 °C, 22 h, 2) KOH, R.T., 4 h, 82%.[166] b) Fmoc-OSu, $NaHCO_3$, R.T., 23 h, 98%. c) DMSO, Oxyallylchloride, Et_3N, DCM, -78 °C, 17 h, 94%.[167] d) $NaBH_3CN$, MeOH, AcOH, 0 °C → R.T., 85%.[12]

2.5 Synthesis of the T_N-mimetic

The synthesis of the T-antigen and T_N-antigen analogues followed the synthesis strategy of the natural antigens.[158, 160-165] Starting from D-galactose (**2.5**), the glycosyl-donor 2-azido-2-deoxy-3,4,6-tri-*O*-acetyl-α-D-galactopyranoside (**2.6**) was synthesized with a yield of 29% over four steps. The KOENIGS-KNORR[168] glycosylation of D-lactic acid with **2.6** was carried out with a satisfactory yield of 64%. This step (Scheme 2.4) required the pre-drying of all reagents and the use of an activated molecular sieve (4 Å) to prevent the addition of water to the oxocarbenium ion and the formation of hydrolysis products. Azido chloride **2.6** was added to a suspension of D-lactic acid, silver carbonate and silver perchlorate and stirred in the absence of light for four days. After reduction and acetylation of the azid, the D-lactic acid moiety was deprotected with TFA to get the free 2-(R)-hydroxypropionic acid **2.7**. For the coupling of **2.7** to the γ-AApeptide HATU/HOAt was used. The coupling product *O*-(2-acetamido-3,4,6-tri-*O*-acetyl-2-desoxy-α-D-galactopyranosyl)-2-(R)-hydroxypropionamido-*N*-[2'-*N*'-*Fmoc*-3'-methylbutyl]-glycine-*tert*-butylester (**2.8**) could be obtained with a yield of 95%.

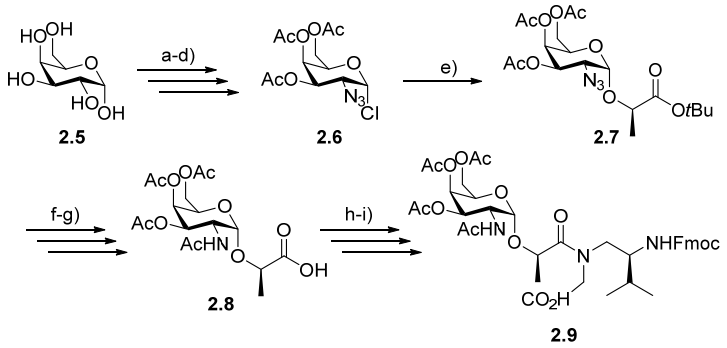

Scheme 2.4.: Synthesis of the TN-γ-AApeptide-mimetic: a) NaOAc, Ac_2O, refluc → r.t., 66%. b) HBr. Ac_2O, DCM, 0 °C, 1h, 79%. c) Zn*, N-methylimidazole, EtOAc, 1.5. h 82%. d) NaN_3, $FeCl_3 \cdot 6\ H_2O$, 30% H_2O_2, MeCN, −30 °C, 1 d, 70%. e) D-lactic acid-OtBu, Ag_2CO_3, $AgClO_4$, DCM, toluene, 4 d, r.t., dark, 64%. f) Zn*, THF, Ac_2O, AcOH 24 h, r.t. 83%; g) TFA/water (10:1), r.t., 2 h, quant. h) γ-AA-peptide-OtBu, HATU, HOAt, Pyridin, 6d, 94%. i) TFA/water (10:1), r.t., 2 h, quant.[12]After further deprotection of the carboxylic acid with 80% TFA, the SPPS building block *O*-(2-acetamido-3,4,6-tri-*O*-acetyl-2-desoxy-α-D-galactopyranosyl)-2-(R)-hydroxypropionamido-*N*-[2'-*N*'-*Fmoc*-3'-methylbutyl]-glycine (**2.9**), the γ-AApeptide mimetic of the T_N antigen, is obtained in quantitative yield. The resulting tertiary amide can be present in both *cis* and *trans* conformation and additional rotamers may occur due to the free rotatability of the bonds.

2.6 Synthesis of γ-AApeptide T-antigen

The T-antigen analogue was synthesised in seven steps followed the synthesis strategy of the natural antigens[158, 160-165] starting with the *t*Bu-protected T_N antigen analogue **2.10** (Scheme 2.5). The alcohol protecting groups of the sugar moiety were modified to get a free glycosyl-acceptor on C3. The following glycosylation[165] is performed according the HELFERICH-method by reaction of acceptor with donor α/β-Ac_5GalBr and mercury(II) cyanide, whereby *O*-(2-acetamido-2-desoxy-4,6-*O*-benzyliden-3-*O*-[2,3,4,6-tetra-*O*-acetyl-β-D-galactopyranosyl]-α-D-galactopyranosyl)-2-(R)-hydroxypropionic acid-*tert*-butylester (**2.11**) was obtained with a yield of 87%. After glycosylation, the benzylidene proting group was removed and the unprotected alcohols were acetylated. The carboxyl function was deprotected with TFA in order to use the T-antigen building block for the coupling to γ-AApeptide building block **2.4**.

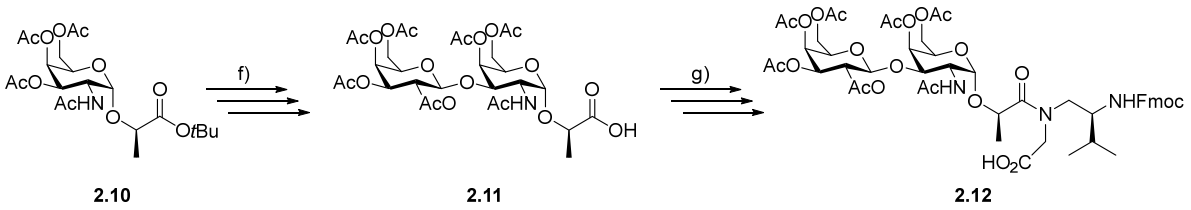

Scheme 2.5: Synthesis of the T-γ-AApeptide-mimetic: a) NaOMe-solution (1%ig), MeOH, pH = 8.5, 24 h, r.t, 97%.; b) BADA,CSA, MeCN, 650 mbar, 68 °C, 4 h, 86%; c) α/β-Ac_5GalBr, $Hg(CN)_2$, NO_2Me/DCM, 30 h, R.T, 87% d) AcOH/water (4:1), 4 h, 80 °C; pyridine/AC_2O (2:1), 18 h, r.t, 74%; e) TFA, water (10:1), 0 °C, 2 h, quant.; f) γ-AApeptide-OtBu, HATU/HOAt, 6 d, 52%), g) TFA/water (10:1), r.t., 2 h, quant.[12]

Analogues to the T_N antigen mimetic, coupling of the T-antigen mimetic to **2.4** was performed with HATU/HOAt with a yield of 62%. By deprotecting the carboxylic acid function of the peptide moiety with TFA, the γ-AApeptide T-antigen mimetic **2.12** could be obtained in a quantitative yield for solid phase synthesis.

2.7 Synthesis of MUC1-mimetics

The glycopeptide building blocks were finally incorporated into the MUC1 sequence by SPPS. The tandem repeat sequence chosen by *Martínez-Sáez et al.* and a low loading Rink amide (RAM) resin as solid support were used.[169] In contrast to Wang resins, the RAM linker allows facile cleavage of the acetic protecting groups of the sugar moiety with hydrazine. For the

formation of a strong immune response, the combination of the antigen with an immunostimulant is necessary. Hence, a PEG_3-azid spacer was coupled at the N-terminus of the peptide to allow for the formation of a fully synthetic vaccine, e.g. by click-chemistry.

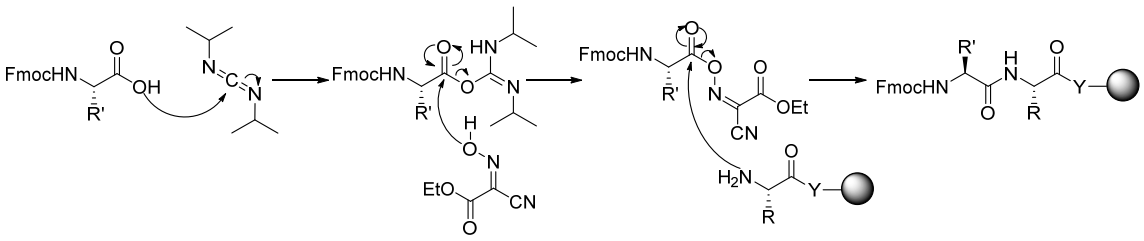

Scheme 2.6: Mechanism of amide bond formation with DIC/OxymaPure®.

For the coupling of all amino acids except synthetic antigens, DIC as an activator and OxymaPure® buffered with a 0.1 equivalent DIPEA were used as coupling reagents. The coupling conditions are shown in table 2.1. Using DIC/OxymaPure® for coupling has several advantages. First of all, it is a very cheap combination, with low racemisation properties and a greater thermal stability then common coupling reagents.[64, 170] Since hydroxybenzotriazole-based reagents are proven to have explosive properties, DIC/OxymaPure® is the preferred coupling reagent nowadays. Coupling at high temperatures of 70 – 90 °C in the microwave assisted synthesis shortens expenditure of time, which is helpful in the synthesis of longer peptides. By raising the temperature from ambient conditions to 86 °C, a 50-fold increase in reaction rate for both, the coupling and the deprotection step is gained, based on the Arrhenius equation.[171] But higher temperatures are not feasible with every kind of amino acid. Therefore, cysteine, arginine and histidine are coupled at adjusted temperatures to minimize side reactions.

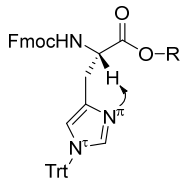

Figure 2.5: Mechanism of racemisation of Histidine in basic media.

For example, the π-nitrogen in Histidine is sufficient basic to abstract the α-proton, hence higher temperatures promotes racemisation during activation.[172] Therefore, Histidine is coupled at 50 °C but with an increased reaction time of up to 10 min.

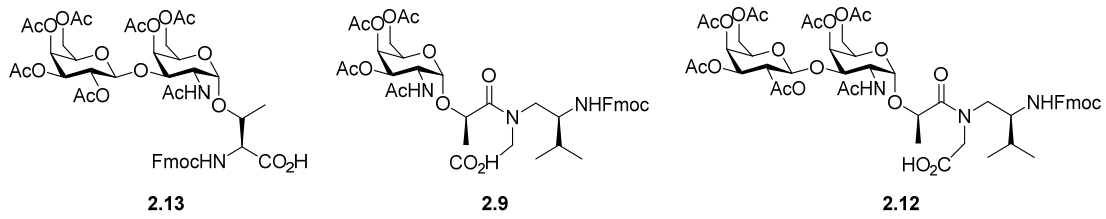

Figure 2.6: Synthesized antigens: T-antigen (**2.13**), T_N-antigen-γ-AAmimetic (**2.9**), T-antigen-γ-AAmimetic (**2.12**).[12]

Next to antigens **2.13** and **2.9**, the natural T-antigen (**2.12**) was synthesised according to the same procedure.[12, 158, 161-164] All three antigens (Figure 2.6) were coupled at room temperature over a period of one hour using HBTU/HOBt (Scheme 2.7) for activation according to the procedure of *Martínez-Sáez et al*.[169] In order to furnish fully synthetic vaccines, an *N*-terminal azid-containing PEG-linker was introduced. The PEG-linker was synthesised by Sebastian Neidig and Phoebe Foster (Hoffmann-Röder group).

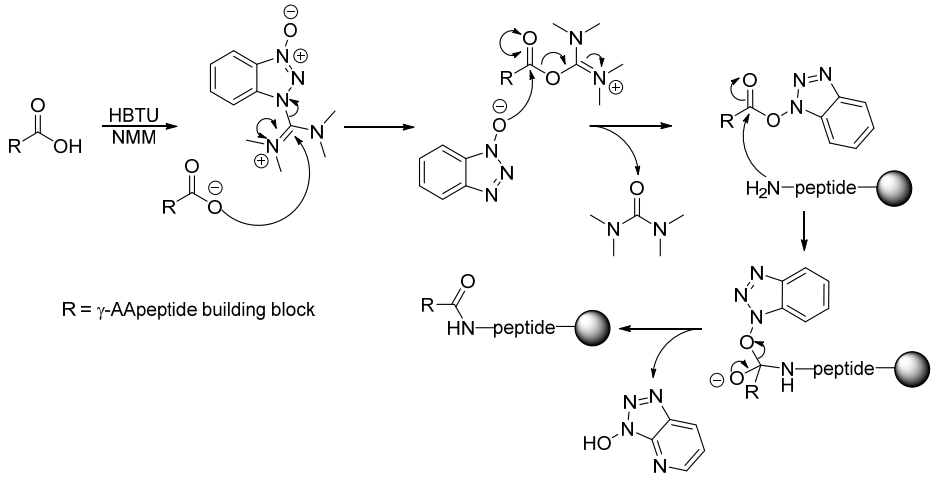

Scheme 2.7: Coupling of the γ-AApeptide T- and T_N-antigen building blocks.

After completion of the SPPS, the *O*-acetyl groups of the sugar moieties were cleaved with 5% hydrazine in DMF overnight.[173] Global deprotection and the removal from solid support took place with reagent-B[71] (TFA/TIPS/phenole/water; 88/0.2/0.5/0.5) shaking the resin in a Merriefield reactor for 2 h. After precipitation in cold diethyl ether and purification by reversed phase HPLC, the peptides could be furnished in high purity.

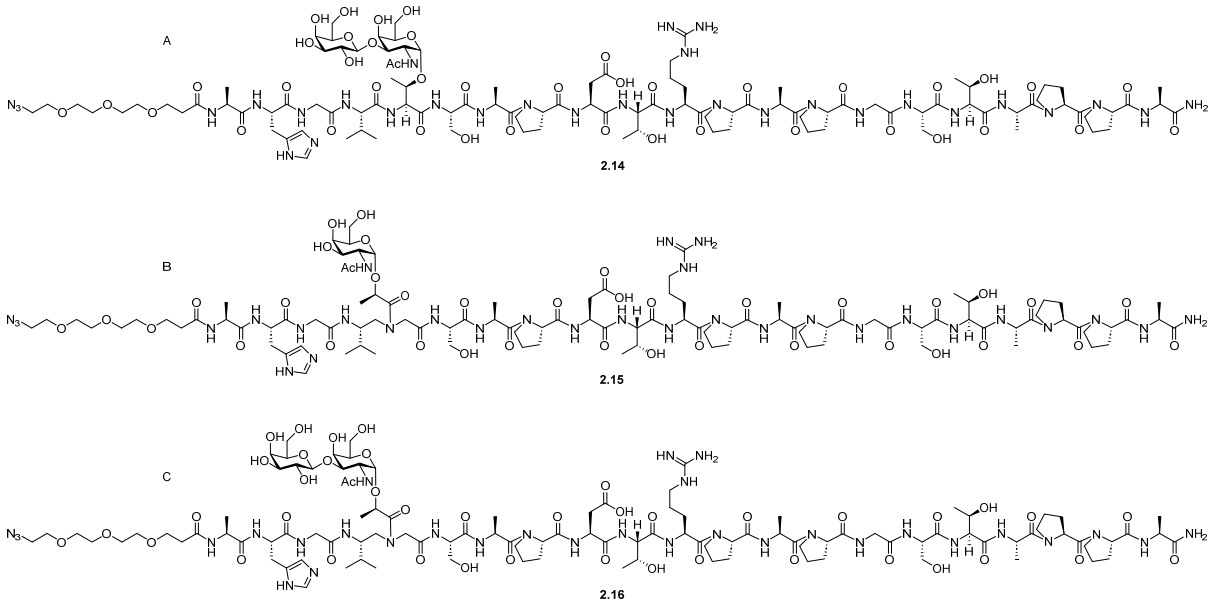

Figure 2.7: A) MUC1 containing the T-antigen; B) MUC1-T_N antigen mimetic; C) MUC1-T antigen mimetic.

Due to the high number of around 100 protons, the analysis and assignment of the NMR-signals of these peptides is difficult. Nevertheless, an important characteristic signal is provided by cross-peaks of the anomeric saccharidic centre in the HSQC-NMR, which can be easily identified. While α-anomeric cross-peaks (GalNac) of natural peptide appear around 4.80 – 4.50/98.4 – 96.2 ppm, the β-anomeric cross peak (Gal) is shifted to lower ppm in the ^{1}H-spectrum and to higher ppm in the ^{13}C-spectrum at around 4.30 – 4.20/104.5 – 103.9 ppm. In natural peptides, for both anomeric positions, single cross-peaks should appear which can be seen in Figure 2.7 A of the natural MUC1 glycosylation domain in **2.14**. In contrast, the HSQC-spectra of mimetic **2.15** shows four cross-peaks for the α-anomeric centre. While **2.14** is largely build up by *trans*-amide bonds, the tertiary amide of the γ-AApeptide building block in **2.15** causes a mixture of *cis*/*trans*-amide bonds, but also allows rotational freedom due to the adjacent CH_2-groups.

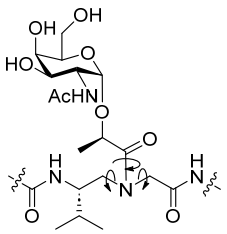

Figure 2.8: Rotational freedom of the γ-AApeptide.

This flexibility is reduced by the more sterically demanding disaccharide in **2.16**. Mimetic **2.16** shows only two crosspeaks of the α-anomeric centre and one cross-peak for the β-anomeric

centre. Future investigations should be done to analyse the origin of these multiple crosspeaks. The multiple cross-peaks can be derived from either rotamers or from anomerization during the synthesis.

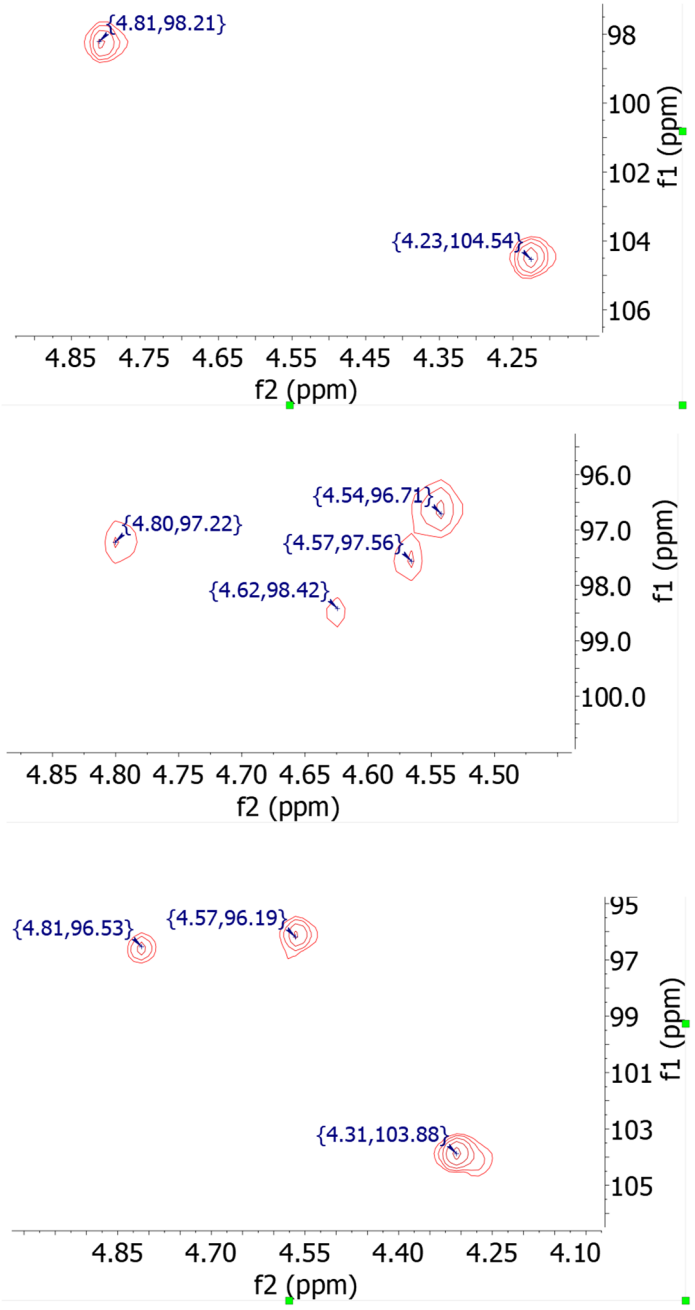

Figure 2.9: HSQC-cross peaks of the peptides **2.14** (top), **2.15** (middle) and **2.16** (below). The NMR-spectra show a higher conformational flexibility caused by the tertiary amide in **2.15** and **2.16**.

In future work, the peptides should be coupled by click-chemistry to KRN7000 (or α-GalCer) to obtain fully synthetic vaccines. KRN7000 is a potent immunostimulant, which contains an

α-galactosylceramide structure.[8] This glycolipid activates invariant natural killer T cells.[174] Using this glycolipid vaccine approach circumvents disadvantages in conventionally vaccination, especially the need of external adjuvants.[175] A two component vaccine consisting of the α-GalCer and T_N-antigen was already formulated into liposomes and immunisation of mice generated an immune response with high-affinity antibodies.[175]

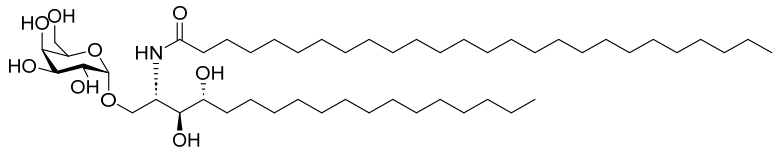

Figure 2.10: Structure of KRN7000.[176]

The combination of the synthesized MUC1-mimetics with the highly immunogenic glycolipid KRN7000 should be stable against proteolytic degradation. The higher stability along with the highly immunogenicity of the the glycolipid should lead to a strong and sustaining immune response.

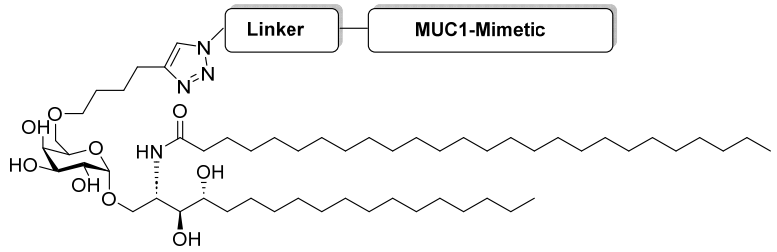

Figure 2.11: Future work: fully synthesized vaccine attached KRN7000.

2.8 Analytical Data MUC1-mimetics

Peptide Synthesis

Synthesis was carried out on a preloaded Fmoc Ala TentaGel® S RAM low loading resin using DIC/Oxyma® and HBTU/HOBt as coupling reagents. Coupling conditions are shown in table 1. For standard coupling an upstream ramp heating (75°C, 170 W, 15 s) was used. *Fmoc*-HisTrt-OH was first coupled at 25°C without a microwave for 120 s before heating. *Fmoc*-deprotection was achieved by treatment with 20% piperidine in DMF. After automated SPPS, the resin was transferred into a Merrifield reactor and the *O*-acetyl groups of the sugar moieties were cleaved with 5% hydrazine in DMF overnight.[173] Afterwards, the resin was freed from DMF by washing with DCM several times and global deprotection of the peptide was done with TFA/TIPS/phenol/water (88/0.2/0.5/0.5) for 2 h. Peptides were precipitated in cold diethyl ether, centrifuged and washed with Et_2O for five times. After purification by reverse-phase HPLC (MeCN/water, 95/5 → 70/30 in 40 min), peptides **2.14**, **2.15** and **2.16** could be furnished in high purity.

Table 2.1: Coupling conditions of microwave assisted SPPS of peptides **2.14**, **2.15** and **2.16.**

Compound	step	**2.14**			**2.15**			**2.16**		
		t [s]	p [W]	T [°C]	t [s]	p [W]	T [°C]	t [s]	p [W]	T [°C]
Fmoc-Pro-OH	1	120	30	90	120	30	90	120	30	90
Fmoc-Pro-OH	1	120	30	90	120	30	90	120	30	90
Fmoc-Ala-OH	1	120	30	90	120	30	90	120	30	90
Fmoc-Thr*t*Bu-OH	1	120	30	90	120	30	90	120	30	90
Fmoc-Ser*t*Bu-OH	1	120	30	90	120	30	90	120	30	90
Fmoc-Gly-OH	1	120	30	90	120	30	90	120	30	90
Fmoc-Pro-OH	1	120	30	90	120	30	90	120	30	90
Fmoc-Ala-OH	1	120	30	90	120	30	90	120	30	90
Fmoc-Pro-OH	1	120	30	90	120	30	90	120	30	90
Fmoc-ArgPbf-OH	2	120	30	90	120	30	90	120	30	90
Fmoc-Thr*t*Bu-OH	1	120	30	90	120	30	90	120	30	90
Fmoc-ApsTrtOH	1	120	30	90	120	30	90	120	30	90
Fmoc-Pro-OH	1	120	30	90	120	30	90	120	30	90
Fmoc-Ala-OH	1	120	30	90	120	30	90	120	30	90
Fmoc-Ser*t*Bu-OH	1	120	30	90	120	30	90	120	30	90
2.13, 2.9, **2.12**	1	3600	0	25	3600	0	25	3600	0	25
Fmoc-Val-OH	2	120	30	90						
Fmoc-Gly-OH	2				120	30	90	120	30	90
Fmoc-Gly-OH	1	120	30	90						
Fmoc-HisTrt-OH	1	50	35	480	50	35	480	50	35	480
Fmoc-Ala-OH	1	120	30	90	120	30	90	120	30	90
Fmoc-Peg_3-N_3	1	120	30	90	120	30	90	120	30	90

Azido-4,7,10-trioxadodecanylamido-*N*-L-alanyl-L-histidyl-L-glycyl-L-valyl-*O*-{2-acetamido-2-desoxy-3-*O*-[β-D-galactopyranosyl]-α-D-galactopyranosyl)}-L-threonyl-L-seryl-L-alanyl-L-prolyl-L-aspartyl-L-threonyl-L-arginyl-L-prolyl-L-alanyl-L-prolyl-L-glycyl-L-seryl-L-threonyl-L-alanyl-L-prolyl-L-prolyl- L-alanine (**2.14)**

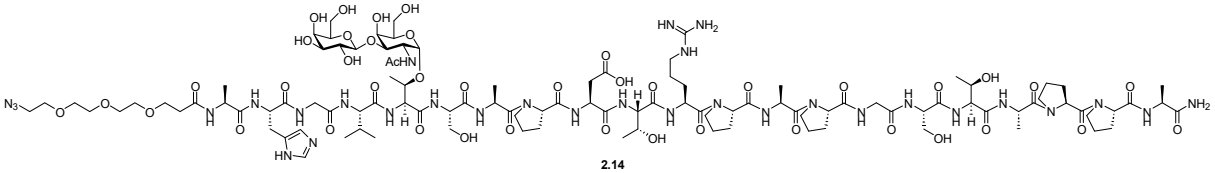

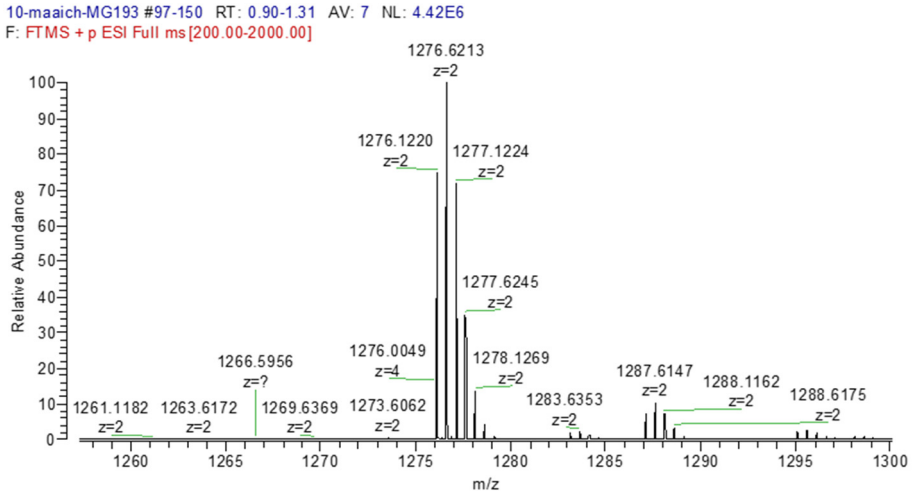

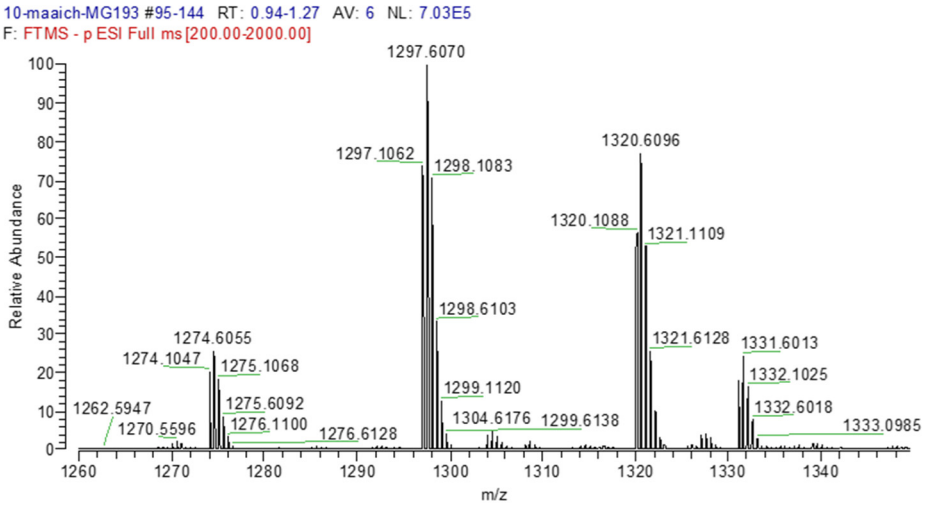

Figure 2.12: HRMS spectrum of T-MUC1-mimetic **2.14**: HRMS (+ESI) m/z calc. for $C_{106}H_{173}N_{31}O_{42}^{2+}$ $[M + H]^{2+}$: 1276.6189; found: 1276.6213. HRMS (−ESI) m/z calc. for $C_{107}H_{11}N_{31}O_{44}^{2-}$ $[M+ FA – H]^{2-}$: 1297.6070; found: 1297.6070.

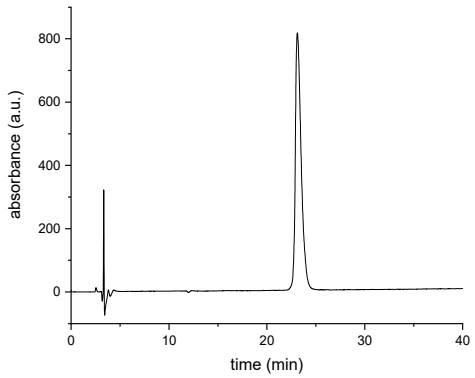

Figure 2.13: Reversed-phase HPLC run of **2.14** (MeCN/water 95/5 → 70/30 in 40 min) with a retention time of 23.1 min.

Azido-4,7,10-trioxadodecanylamido-*N*-L-alanyl-L-histidyl-L-glycyl-*O*-(2-acetamido-3,4,6-tri-*O*-acetyl-2-desoxy-α-D-galactopyranosyl)-2-(R)-hydroxypropionamido-*N*-[2'-amido-3'-methylbutyl]-glycyl-L-seryl-L-alanyl-L-prolyl-L-aspartyl-L-threonyl-L-arginyl-L-prolyl-L-alanyl-L-prolyl-L-glycyl-L-seryl-L-threonyl-L-alanyl-L-prolyl-L-prolyl- L-alanine (**2.15)**

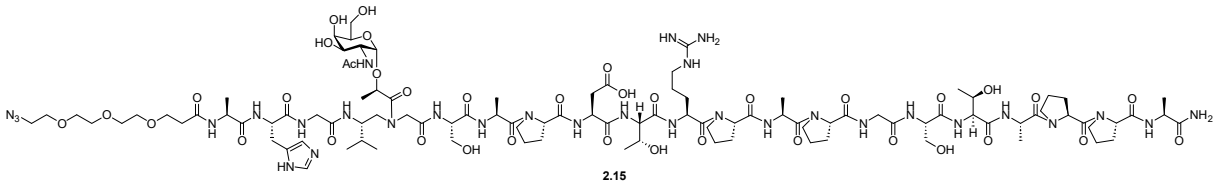

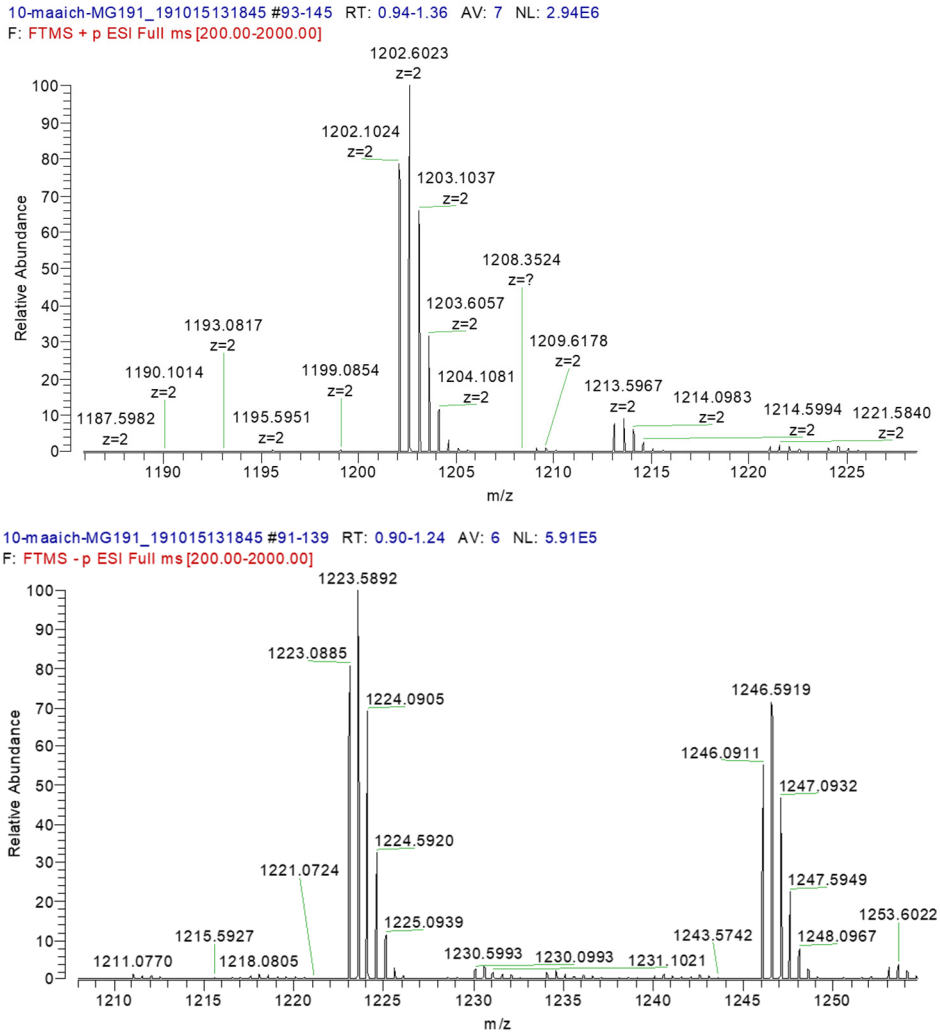

Figure 2.14: HRMS spectrum of T-MUC1-mimetic **2.15**: HRMS (+ESI) m/z calc. for $C_{101}H_{165}N_{31}O_{37}^{2+}$ $[M + H]^{2+}$: 1202.6003; found: 1202.6023. HRMS (−ESI) m/z calc. for $C_{102}H_{163}N_{31}O_{39}^{2-}$ $[M+ FA – H]^{2-}$: 1223.5884; found: 1223.5892.

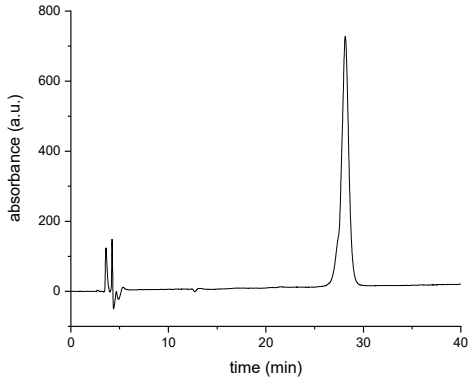

Figure 2.15: Reversed-phase HPLC run of **2.15** (MeCN/water 95/5 → 70/30 in 40 min) with a retention time of 28.1 min.

Azido-4,7,10-trioxadodecanylamido-*N*-L-alanyl-L-histidyl-L-glycyl-*O*-{2-acetamido-2-desoxy-3-*O*-[β-D-galactopyranosyl]-α-D-galactopyranosyl)}-2-(R)-hydroxypropionamido-*N*-[2'-amido-3'-methylbutyl]-glycyl-L-seryl-L-alanyl-L-prolyl-L-aspartyl-L-threonyl-L-arginyl-L-prolyl-L-alanyl-L-prolyl-L-glycyl-L-seryl-L-threonyl-L-alanyl-L-prolyl-L-prolyl- L-alanine (**2.16)**

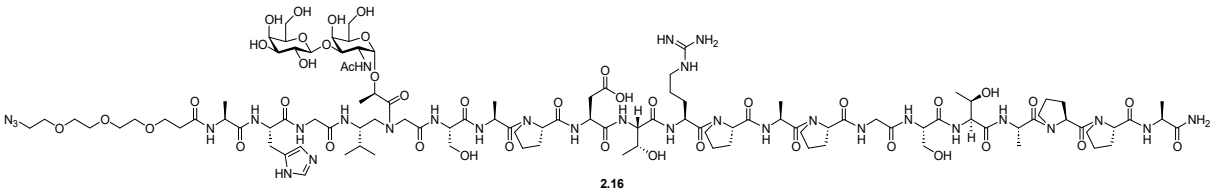

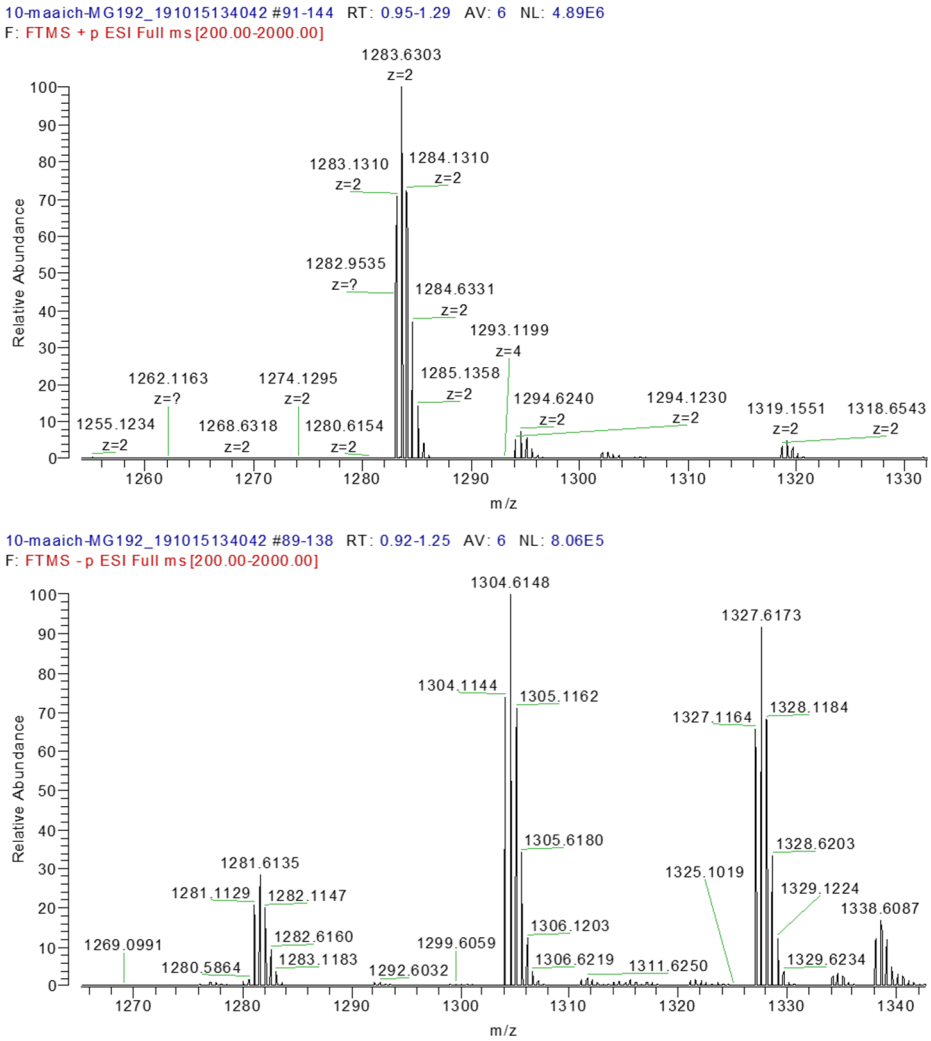

Figure 2.16: HRMS spectrum of T-MUC1-mimetic **2.16**: HRMS (+ESI) m/z calc. for $C_{107}H_{175}N_{31}O_{42}^{2+}$ [M + H]$^{2+}$: 1283.6267; found: 1283.6303. HRMS (−ESI) m/z calc. for $C_{108}H_{173}N_{31}O_{44}^{2-}$ [M+ FA – H] $^{2-}$: 1304.6148; found: 1304.6148.

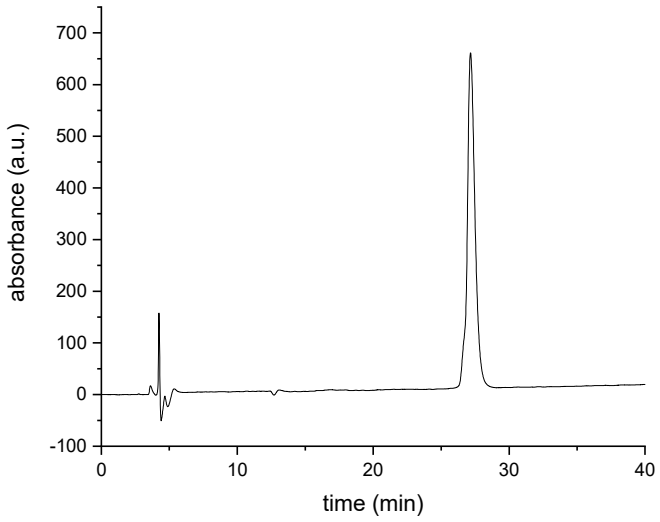

Figure 2.17: Reversed-phase HPLC run of **2.16** (MeCN/water 95/5 → 70/30 in 40 min) with a retention time of 27.1 min.

3 Photopharmacology

3.1 Introduction into Photopharmacology

Taking control over biological processes is a challenging task and tools to achieve control are an ongoing research area. Biological processes on the cellular level takes place in a spatiotemporal fashion, which sets the requirement for the development of suitable tools.[177] Furthermore, taking control must happen in orthogonality to cellular processes, otherwise results could be falsified. However, light provides a non-invasive way with high spatiotemporal precision[178] to control small molecules, peptides, proteins and receptors. Control by light requires photo-responsible elements, which undergo predictable changes in conformation and polarity upon illumination. These elements are called photoswitches, due to their ability to respond to light with a change in geometry. Out of a number of photochromic molecules, which interconvert between open and closed forms (spiropyrans, diarylethylens thiophenfulgides) and those switching between *E* (*trans*) and *Z* (*cis*) double bonds (azobenzenes, stilbenes, hemithioindigos), azobenzenes (AB) are the most frequently used chromophores in biological applications[13] for several reasons. Azobenzenes reversibly isomerise nearly solvent-independent on the picosecond timescale with a low rate of photobleaching and high photostationary states and quantum yields.[179] At least, their simple synthesis and modification offers a number of azobenzene derivatives with a wide range of absorption wave lengths from UV to the near infra-red area and photoactivated state stabilities from seconds to years.[13] Next to their predictable distance change, the molecular dipole moment shifts upon isomerisation (Scheme 3.1).[14]

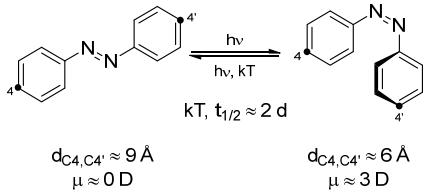

Scheme 3.1: Switching of trans- and cis-azobenzene.[14]

The thermodynamically more stable *trans*-azobenzene has a planar structure with C_{2h} symmetry[180], while the non-planar *cis*-isomer adopts a C_2 symmetry[181]. The absorption spectrum of azobenzenes shows two characteristic transitions, which are slightly overlapping. *Trans*-azobenzene has a strong π→π* transition in the UV (320 nm) and a formally symmetry forbidden and therefore weak n→π* transition in the blue-light (440 nm). In contrast, *cis*-

azobenzene has a weak π→π* absorption band around 280 nm and a n→π* transition around 440 nm which is slightly stronger than the *trans*-azobenzene transition.[13] Illumination with UV light of 320 nm induces E → Z isomerisation, while Z → E isomerisation takes place upon illumination with 450 nm or by thermal relaxation. While the π→π* transition is much smaller for the *trans*-AB, the n→π* transitions are very similar for both isomers (Figure 3.1). However, the predominant excitation of the Z-isomer (Z → E isomerisation) is enabled by the higher absorption coefficient of *cis*-AB.[182, 183] The absorption coefficient for the *trans*-isomer (25°C, MeOH) at 313 nm is 22447.4 ± 1.0 L mol^{-1} cm^{-1} and at 436 nm 486.2 ± 0.3 L mol^{-1} cm^{-1}. In contrast, the absorption coefficient for the *cis*-isomer is significantly smaller at 313 nm (35°C, MeOH; 2016 ± 37 L mol^{-1} cm^{-1}) and somewhat higher at 436 nm (35°C, MeOH; 1402 ± 23 L mol^{-1} cm^{-1}).[183] Whereas thermal relaxation yields in over 99.99 % *trans*-AB, the overlapping absorption bands results in a photostationary state (PSS) of 80% *cis*-AB or ~95% *trans*-AB upon light-induced isomerisation.[13]

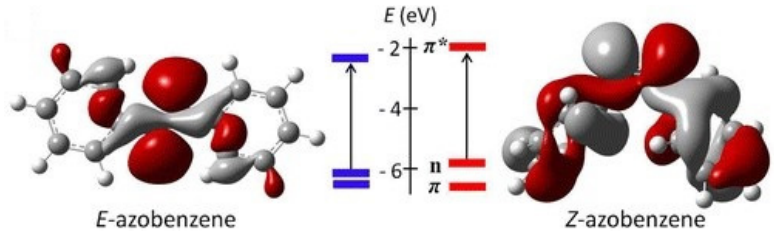

Figure 3.1: HOMO of E-AB and Z-AB including the energetic diagram of the π, n and π* orbitals. Reprinted with permission from David Bléger, Jutta Schwarz, Albert M. Brouwer, and Stefan Hecht; *Journal of the American Chemical Society*, **2012**, *134* (51), 20597-20600.[182] Copyright 2025 American Chemical Society.

For isomerisation, four mechanisms have been proposed, including inversion, concerted inversion, rotation and inversion-assisted rotation, which are shown in Scheme 3.2. The predominant mechanism depends on the substitution pattern (steric and electronic effects) of the AB, excitation energy (wavelength) and the solvent (temperature, polarity and viscosity), but most theoretical and experimental studies explain AB-isomerisation by rotation mechanism and thermal relaxation of *cis*-AB by inversion mechanism.[184]

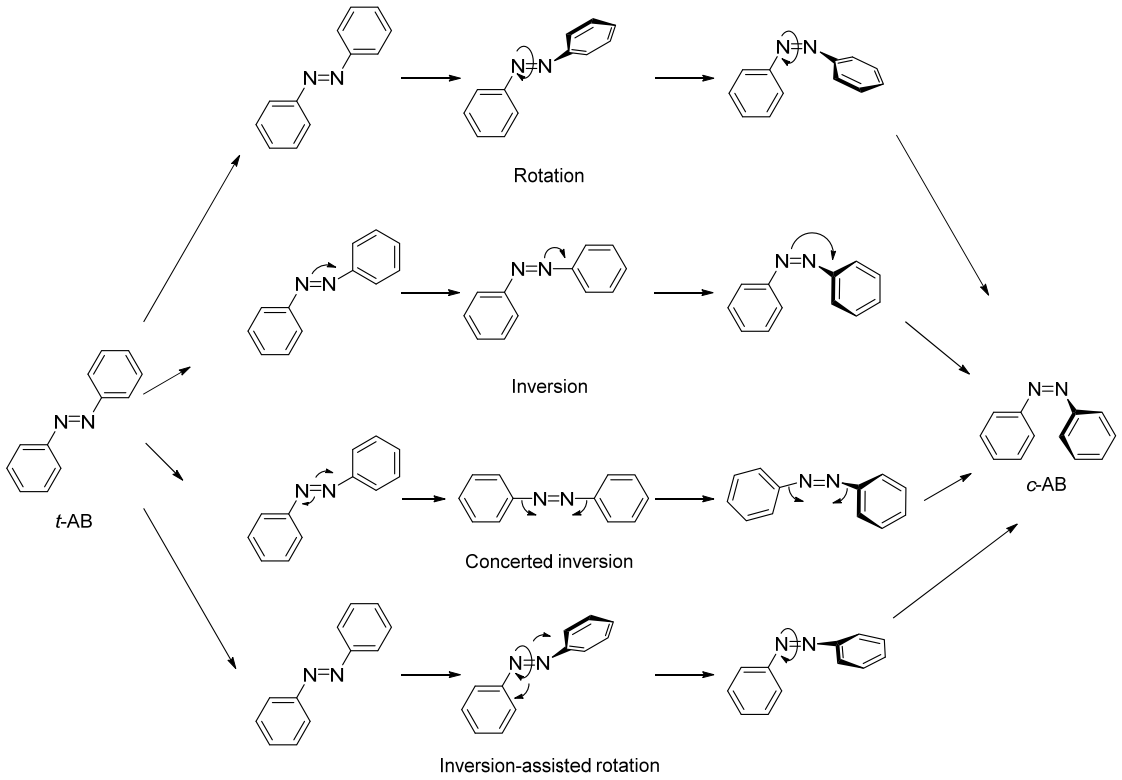

Scheme 3.2: Mechanism of trans-to-cis isomerisation of azobenzene.[184]

The change in geometry and dipole upon light-driven isomerisation of azobenzenes influences the secondary structure of a peptide[185] and therefore its pharmacological properties.[177] Incorporation of photoswitches should ideally result in a high affinity state and a low affinity state or in general in one isomer with high potency and one isomer with a low potency.[186] However, the photoswitchable unit with its absorbance spectrum and its isomeric stability should be carefully adapted to different biological applications or therapeutic scenarios. The bistability of both isomers is of importance and a high population of the thermodynamically less stable *cis*-state guarantees a bigger effect upon isomerisation. Nevertheless, the nature of sigmoidal dose-response curves principally enables a complete on-off control in pharmacological approaches even with a low population of the active state by choosing the right concentration.[187] Absorbance spectrum, bistability, solubility and the resistance to reduction can be modified by substitution of the azobenzene. The position of substitution is crucial, as para- and ortho-substitutions have a much higher influence on the electronic properties then meta-substitutions. While push-pull systems result in redshifted absorption bands, their bistability is reduced by the high single bond character of the azo bond. The same applies to electron donating substituents in *ortho*-position, which cause a bathochromic shift of the π-π^* transition, but reduce the half-life of the *cis*-isomer in water by stabilising the formation of azonium ions.[188] In contrast, electron withdrawing substituents (Cl, F) in *ortho*-position

also provide red-shifted absorption spectra and additionally stabilise the *cis*-isomer. Furthermore, *ortho*-halogination results in separated absorption bands. FERINGA and co-workers[189] synthesised antibiotics, which can be controlled by visible light. Whereas tetra-*ortho*-chlorination yielded in a PSS *cis*:*trans* ratio of 87:13 upon illumination with 652 nm, irradiation times up to 3 h where necessary. Using wavelengths of higher energy shortened the irradiation times, but also lowered the PSS to *cis*:*trans* of 1:1 at 527 nm. Better results could be obtained with tetra-*ortho*-fluorinated azobenzene moieties. Irradiation with 527 nm resulted in a PSS of *cis*:*trans* of 89:11.[189]

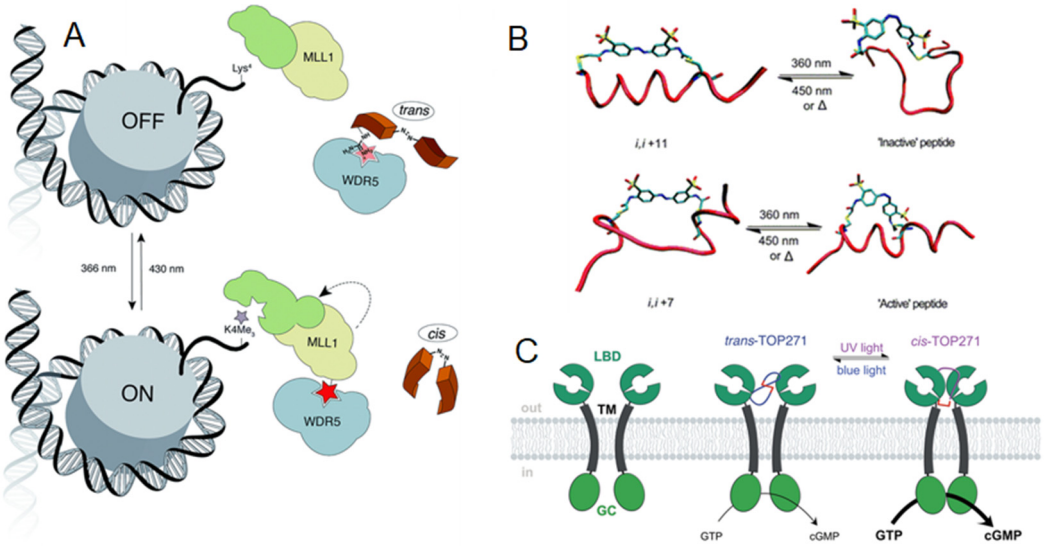

Figure 3.2: Examples of photoswitchable pepides: a) truncated AMBP-containg WIN sequence for control of histone methyl transferase MILL1[190]; b) α-helix formation induced by a bridging azobenzene for cytochrome c release;[191] c) AMPP-containing NMP for the control of the NPR-A/cGMP signaling pathway.[192]

For the introduction of chromophoric units into peptides, a number of *Fmoc*-protected photoswitchable SPPS building blocks have been synthesised.[193] But also, haloacetamido containing azobenzene for the selective reaction with cysteine side-chains have been used to gain influence on the secondary structures.[194] In this case, the secondary structure could be influenced by the use of different wavelengths. Therefore, photoswitches have been used in a wide range of biological applications. For the photocontrolled uptake by cells, an oligo-arginine chain was connected over sterically hindered push-pull azobenzene to an equally long oligo-glutamate chain. While in the *cis*-isoform of the photoswitchable cell penetrating peptide (PCPP), the oligoarginine was masked by the oligo-glutamate chain, the cellular uptake by HeLa cells hand in 10-fold increase upon photoconversion into the *trans*-PCPP.[195] Another important chromophore is 3-[3-(aminomethyl)phenylazo]-phenylacetic acid (AMPP, **3.1**),

which has been used for the investigation of β-hairpin formation of small model peptides[112-118, 196] or β-turn nucleation of amyloid-β.[197] Furthermore, with an AMPP-containing ANP, the selective and reversible control of the NPR-A/cGMP signaling pathway was possible (Figure 3.2: C).[192] Next to β-hairpins, the formation of α-helices can be controlled by light using bridging azobenzene. DNA binding motifs usually contain a high α-helical content, whereas secondary structure formation occurs by interaction with other structural motifs like DNA. Haloacetamid containing azobenzene coupled to two i,i +7 or i,i+11 spaced cysteine side-chains were able to trigger α-helix formation and DNA strand binding.[198-200] The same light-induced manipulation of α-helix formation was used to stimulate mitochondrial membrane depolarisation and cytochrome c release, resulting in cell apoptosis (Figure 4.2: B).[191] Another frequently used chromophore is (4-aminomethyl)phenylazobenzoic acid (AMPB, **3.2**). Epigenetic control of the histone methyltransferase MLL1 by introducing AMPB into a truncation-sequence of the WDR5-Interacting peptide (WIN-peptide) enables the manipulation of the Deptor gene transcription and thus the control leukemia cell growth by light (Figure 4.2: A).[190] In summary, photositchable units are excellent building blocks for the manipulation and control of biological target structures.

3.2 Objective

Taking control over biological processes is a field of ongoing research. Spatiotemporal precission and orthogonality to the cellular processes is important to avoid falsification of the experiments. In accordance to these conditions, photoresponsible elements like azobenzene-photoswitches undergo changes in conformation and polarity upon illumination.[14] Incorperation of azobenzene-photoswitches in peptides enables influence the secondary structure[185] and therefore their binding affinity towards receptors. In addition to their simple synthesis and their photochemical advantages, there are already several photoswitchable azobenzene SPPS building blocks discribed in the literature.

Carbetocin is a mimetic of the hormone oxytocin. As the endogenous ligand of OXTR, it plays an important role in labour[16] and social behaviour[17]. The short half-life of oxytocin[201] led to the development of Carbetocin, which has an improved enzymatic stability[19] and receptor selectivity[20]. Nevertheless, carbetocin is a partial agonist with differences in signal transduction.[20, 21] Photoswitchable carbetocin derivatives are suitable for the investigation of the OXTR. The aim of this project was the synthesis of a small library of photoswitchable

AzoCarbetocins (**ACBT**). For this reason, azobenzene photoswitches were introduced into the backbone of the ring, as well as amino acid side-chains. Last but not least, an azobenzene photoswitch should be introduced by *N*-alkylation in exchange of the amino acid proline. The biological evalution of the synthesized ACBTs should be carried out by Dr. Iuliia Karpenko, Faculty of Pharmacy, University of Strasbourg.

Kisspeptin-54, first discovered as a metastasesuppresor[22], is crucial for the sexual maturation in mammals. Next to KP-54, severl short kisspeptins excist, whereas kp-10 is the shortest and most active one.[202] Its binding to the kisspeptin receptor Kiss1R (GPR54) results in the release of gonadotropin-releasing-hormon (GnRH), which itself triggers the release of the gonadotropins LH and FSH.[23] Mutation in the GPR54-encoding gene results in iodopatic hypogonadotropic hypogonadism.[24, 25] The aim of the project is the synthesis of photoswitchable kisspeptin mimetics, Azo-KPs. The incorporation of azobenzene-photoswitches into the hydrophobic cluster[27] of kp-10 should enable control over the secondary structure and thus the receptor affinity. The photoswitchable kisspeptin analogues should be investigated using patch clamp (Dr. Jian Qiu; Group of Prof. Dr. Martin J. Kelly, Oregon Health and Science University) and in vitro cell studies (Dr. Jan-Erik Hoffmann; Group of Prof. Dr. Carsten Schulz, Oregon Health and Science University).

Several azobenzenes known from the literature are to be synthesized as photoswitches, which can be incorporated into the peptides as SPPS building blocks. Furthermore, based on these syntheses, photoswitches should be synthesized that can be incorporated via *N*-alkylation or aromatic substitution.

3.3 Synthesis of photoswitchable building blocks

The synthesis of the azobenzene photoswitches used in the projects 3.4, 3.5 and 3.6 is described in the following part.

3.3.1 AzoPhe[203]

The chromophore phenylazophenylalanine (formerly Pap, in recent publications AzoPhe, **3.3**) acts as photoswitchable side-chain which is derived from the canonical amino acid phenylalanine **3.4**. A single CH_2-spacer between the Cα-carbon atom and the azobenzene side-chain guarantees a minimum number of conformational isomers of the side chain. The reduced flexibility should result in a higher effect between *cis*- and *trans*-AzoPhe.[204] In contrast to bridging or backbone photoswitches, the side-chain of AzoPhe causes only local perturbation and sterical rearrangements[205], which qualifies this chromophore for the use in small peptides. AzoPhe was first used by Goodman *et. al.*, to demonstrate the effects of photoisomerisation onto structural changes of peptide derivatives using copolymers of AzoPhe and γ-benzyl-gluatmic acid.[203, 206] Later, Woolley used phenylazophenylalanine for the switching of Ion-Dipole interactions in a gramicidin channel analogue.[207] Besides its use in SPPS, Bose *et. al.* introduced AzoPhe into the transcription factor CAP of E.Coli by an orthogonal tRNA-aminoacyl tRNA synthase pair, showing the ability of AzoPhe to control bigger structures.[204] At least, small peptides containing several AzoPhe units, were able to form hydrogels[208] and nanofibers[209] upon *cis* to *trans* isomerisation.

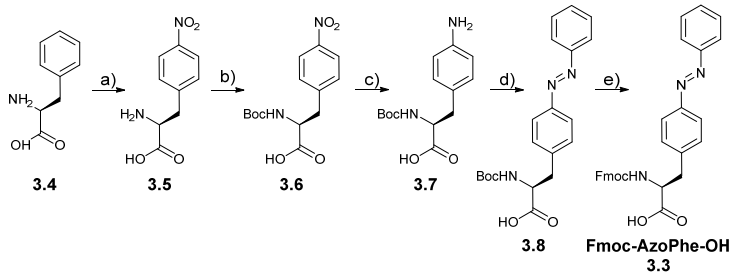

Scheme 3.3: Synthesis of Fmoc-AzoPhe-OH (**3.3**): a) H_2SO_4, HNO_3, 0 °C, 2 h, 94%; b) 1 M NaOH, Boc_2O, dioxane/water, r.t., 5 h, 94%; c) Pd/C 10%, MeOH, r.t., o.n. 86%; d) nitroso-benzene, AcOH, r.t., 2 h, 85%; e) 1. TFA/water (9:1), r.t., 2 h; 2. $NaHCO_3$, Fmoc-OSu, acetone/water, r.t., 18 h, 91%.[204, 208, 210-212]

The *Fmoc*-AzoPhe-OH **3.3** SPPS building block can be synthesised based on a modified procedure of *Goodman et al.*[203] and *Bose et. al.*[204], starting from commercially available L-Phenylalanine **3.4** using *tert*-Butyl protecting group to enhance solubility (Scheme 3.3). Nitration of **3.4** using a mixture of fuming nitric acid and concentrated sulphuric acid yielded

in 4-nitrophenylalanine (**3.5**). After Boc-protection of the α-amino group using di-*tert*-butyl dicarbonate, *N*-Boc-4-nitro-phenylalanine (**3.6**) could be furnished in an excellent yield. The nitro group was then reduced by hydrogenation with Pd/C in a very good yield to obtained *N*-Boc-4-nitro-phenylalanine (**3.7**). The following azo-coupling under Mills condition with commercially available nitrosobenzene resulted in Boc-AzoPhe-OH (**3.8**) in a very good yield. After removal of the Boc-protecting group with TFA/water (9:1) and subsequent protection with *Fmoc-O*Su afforded the SPPS building block *Fmoc*-AzoPhe-OH (**3.3**) in excellent yield. Spectral and photophysical properties are described by Bose et. al.[204]

3.3.2 *t*Bu$_2$AzoPhe

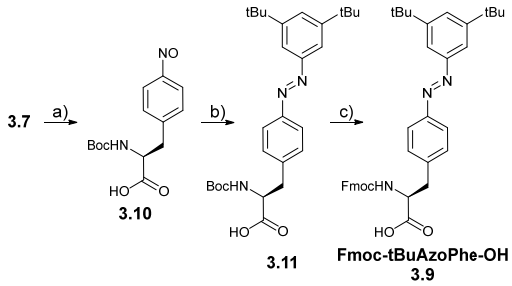

Scheme 3.4: Synthesis of *Fmoc-t*BuAzoPhe-OH: a) Oxon®, DCM/water (1:1), r.t., 4 h, b) 3,5-di-*tert*-butylaniline, AcOH, r.t., o.n., 24% over two steps; c) 1. TFA/water (9:1), r.t., 2 h; 2. $NaHCO_3$, Fmoc-OSu, r.t., o.n. 81%.[118, 208]

While the aromatic rings of AzoPhe are able to interact with aromatic side-chains by π-π stacking interactions, a bulkier version with a reduced ability for π-stacking was synthesised. This photoswitch should also have a greater sterically difference upon *cis-trans* isomerisation. The bulky *Fmoc-t*Bu$_2$AzoPhe-OH (**3.9**) was synthesised in three steps starting from aniline **3.7**. Oxidation of **3.7** with Oxon® and subsequent azo-coupling of the *N*-Boc-4-nitroso-phenylalanine (**3.10)** with 3,5-di-*tert*-butylaniline under Mills-conditions afforded Boc-*t*BuAzoPhe-OH (**3.11**) in a poor yield of 24% over two steps. After deprotection with TFA/water (9:1) followed by *Fmoc*-protection of the α-amino group, **3.9** could be furnished in a very good yield (Scheme 3.4).

3.3.3 AMPP[112, 118, 179, 192, 193, 197, 213, 214]

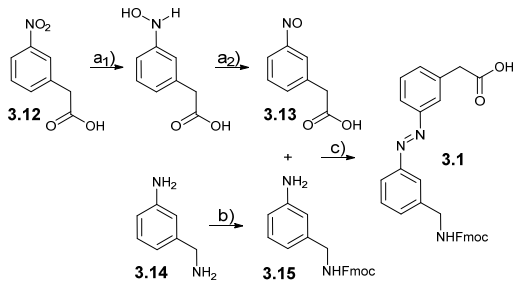

Scheme 3.5: Synthesis of AMPP: a) 1. NH_4Cl, zinc, 2-methoxyethanol, 0 °C → r.t., 2 h; 2. $FeCl_3 \cdot 6\,H_2O$, EtOH/H_2O (2:1), 0 °C → r.t., 2 h; b) Fmoc-OSu, Et_3N, DMF/MeCN (1:10), r.t. 2 h, 48%; c) AcOH, r.t. o.n., 67%.[118]

Besides photoswitchable side-chains like AzoPhe, a number of backbone photoswitches have been published in the last decades. One example, which is often used as β-turn motif is 3-[3-(aminomethyl)phenylazo]-phenylacetic acid (**AMPP**, **3.1**).[112, 118, 179, 192, 193, 197, 213, 214] The additional methylene spacers between the carboxyl/amino group and the aromatic ring guarantee a reduced rigidity, which enables an easier adoption of native structures. While photoswitchable side-chains usually substitute a single amino acid, AMPP can replace up to four amino acids.[192] Furthermore, in contrast to AzoPhe, the incorporation of **3.1** results in large structural shifts like β-hairpin formation upon isomerisation.

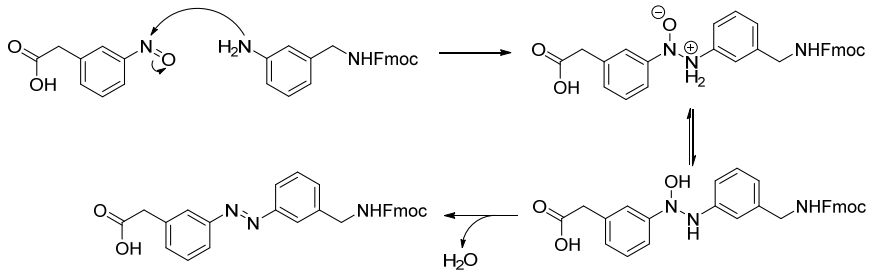

Scheme 3.6: Mechanism of the Baeyer-Mills reaction.[215]

The photophysical and spectral data as well as the synthesis of AMPP is described in the literature using Mills reaction, which is a typical procedure for the formation of asymmetric azobenzenes, using the condensation of a nitroso and an amino benzene.[112, 118, 193, 215, 216] The crucial step is the formation of the instable nitrosobenzene (Scheme 3.6). Therefore, in a first step 2-(3-nitrophenyl)acetic acid (**3.12**) was reduced to the corresponding hydroxylamine by zinc in slightly acidic solution (Scheme 3.5). The ensuing oxidation with $FeCl_3$ formed 2-(3-nitrosophenyl)acetic acid (**3.13**) which was subsequently used for the Mill's reaction on the

same day. The nitrosobenzene **3.13** and Fmoc-protected 3-aminobenzylamine **3.15** were solved in acetic acid and stirred over night to form *Fmoc*-AMPP-OH **3.1** in a fair yield.

3.3.4 BMPP

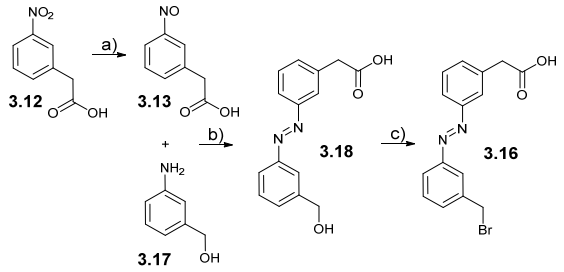

Scheme 3.7: Synthesis of BMPP: a) 1. NH_4Cl, zinc, 2-methoxyethanol, 0 °C → r.t., 2 h; 2. $FeCl_3 \cdot 6\,H_2O$, EtOH/H_2O (2:1), 0 °C → r.t., 2 h; b) b) AcOH, r.t. o.n., 67%; c) PPh_3, NBS, THF (absol.), 0 °C, 15 min, 84%.[118]

In order to afford an AMPP derivative, which can be coupled to an amine by SPPS standard coupling procedure and attached to a thiol under basic conditions on the other side, 3-[3-(bromomethyl)phenylazo]-phenylacetic acid (**BMPP**, 3.**16**) was synthesised (Scheme 3.7). The first step, the reduction of the Nitrobenzene **3.12** to the Nitrosobenzene **3.13** was performed under the same conditions as further explained above. For Mill's reaction, Nitrosobenzene **3.13** and 3-aminobenzyl alcohol (**3.17**) were solved in acetic acid and stirred overnight to furnish 3-[3-(hydroxymethyl)phenylazo]-phenylacetic acid (**3.18**) in a fair yield. At least, the bromination of the alcohol **3.18** under Appel conditions using triphenylphosphine and *N*-Bromosuccinimide[217, 218] afforded BMPP **3.16** in a very good yield (Scheme 3.8).

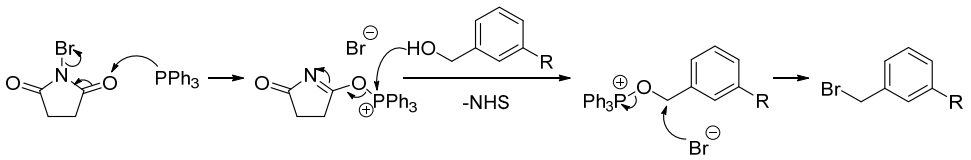

Scheme 3.8: Bromination by Appel reaction using triphenylphosphine and N-Bromosuccinimide as bromine source.[217]

3.3.5 2-[3-(perfluorophenyl)phenylazo]-phenylacetic acid

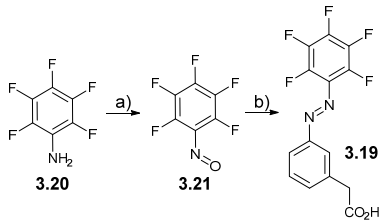

Scheme 3.9: Synthesis of PFAPP **3.19**: a) Oxone®, DCM/water (1:1), r.t., 12 h; b) 3-amino phenylacetic acid, AcOH, 6 h, 7.5% over two steps.[219]

While AMPP has methylene-spacer between the amino/carboxyl group and the benzene, 2-[3-(perfluorophenyl)phenylazo]-phenylacetic acid (**3.19**), possess only one methylene group on the carboxylic side. The perfluorinated exo-ring is electron-deficient enough, to be substituted by thiols in *para*-position to the azobridge. [219, 220] Perfluorinated AzoPhe was genetically encoded by Hoppmann *et. al.*[219] and incoperated into Ca^{2+}-saturated Calmodulin (CaM). After cyclisation with a nearby cysteine residue, the binding affinity of CaM towards the CaM binding domain of the neuronal nitric oxide synthase (NOS-I) could be reduced upon switching from *trans* to *cis*. Furthermore, perfluorination resulted in a n-π* band separation, sufficient for bidirectional switching with 540 nm (*trans* → *cis*) and 405 nm (*cis* → *trans*). At least, the small difference in size between a proton and fluorine does not significantly influence the ring-bulkiness and thus, the geometry of the azobenzene moiety.[205] The first step of the synthesis[219] of **3.19** is the oxidation of pentafluoro aniline **3.20** with Oxone® to pentafluoro nitroso benzene (**3.21**) and subsequently use in Mill's reaction (Scheme 3.9) with 3-amino phenylacetic acid afforded PFAPP **3.19**. Reaction of 3-nitroso phenylacetic acid **3.13** with pentafluoro aniline **3.20**, only provided traces of **3.19**.

3.3.6 4-(phenylazo)benzylamine[221]

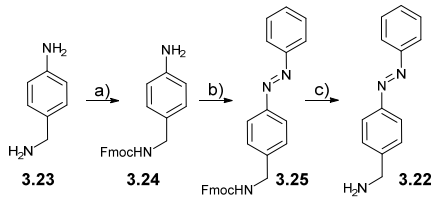

Scheme 3.10: Synthesis of 4-(phenylazo)benzylamine: a) Fmoc-OSu, Et_3N, DMF/MeCN (1:10), r.t., 4 h, 61%; b) nitrosobenzene, AcOH, r.t., o.n., 87%; c) piperidine, DCM, r.t., 20 min, 97%.[118, 221]

Next to side-chain or backbone incorporation of chromophores by SPPS building blocks, *N*-alkylation can be used to introduce photoswitches into a peptide. After coupling of bromoacetic acid, the photoswitch can be attached by nucleophile substitution in basic solution. Therefore, 4-(phenylazo)benzylamine[221] **3.22** was synthesised in three steps, starting from 4-aminobenzyl amine **3.23** following a modified protocol of *Fillafer et. al.*[221]. *Fmoc*-protection of the benzylic amine afforded (9H-fluoren-9-yl)methyl (4-aminobenzyl)carbamate (**3.24**) and azo-coupling under Mill's condition with commercially available nitrosobenzene resulted in (9H-fluoren-9-yl)methyl (E)-(4-(phenyldiazenyl)benzyl)carbamate (**3.25**). Deprotection with 20% peperidine in DCM resulted in the 4-(phenylazo)benzylamine **3.22** with 51% yield over three steps (Scheme 3.10).

3.3.7 Analytica Data of the photoswitches

(S)-2-amino-3-(4-nitrophenyl)propanoic acid 3.5[210]

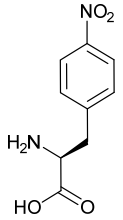

To a solution of L-phenylalanine (3.50 g, 21.2 mmol, 1.0 eq) in conc. sulphuric acid (10 mL) at 0°C, fuming nitric acid (1.05 mL, 25.1 mmol and 1.2eq) was added over a period of 30 min. After 1.5 h, the reaction mixture was poured on ice (35 mL) and neutralised with 37% aqueous ammonium hydroxide. The precipitate was filtered off and washed with cold water. After crystallisation from water, 4.18 g the product (19.9 mmol, 94%) was obtained as yellow solid.

HRMS (ESI): m/z calcd. for ($[M+H]^+$) 210.0641, found 210.0625.

^{1}H-NMR (400 MHz, D_2O): δ = 8.28 (d, *J* = 8.7 Hz, 2H, ***H***ε), 7.53 (d, *J* = 8.7 Hz, 2H, ***H***δ), 4.04 (dd, *J* = 7.6 Hz, *J* = 5.5 Hz, 1H, ***H***α), 3.38 (dd, *J* = 14.4 Hz, *J* = 5.8 Hz, 1H, ***H***β_1), 3.27(dd, *J* = 14.4 Hz, *J* = 7.6 Hz, 1H, ***H***β_1) ppm.

^{13}C-NMR (100 MHz, D_2O): δ = 173.4 (***C***OOH), 147.1 (***C***ζ), 143.4 (***C***γ), 130.4 (***C***δ), 124.1 (***C***ε), 55.6 (***C***α), 36.3 (***C***β) ppm.

(2S)-2-[(*tert*-butoxycarbonyl)-amino]-3-(4-nitrophenyl) propanoic acid 3.6[211]

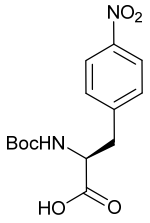

To a solution of 1.27 g of 4-Nitro-L-phenylalanine (6.04 mmol, 1.0 eq.) in 50 mL of a mixture of dioxane/water (3:2), 14 mL of 1 M aqueous NaOH and 1.45 g Di-*tert*-butyl dicarbonate (6.65 mmol, 1.1 eq.) were added. After 5 h at room temperature, additional 1.00 g Di-tert-butyl (4.58 mmol, 0.8 eq.) was added. After completion, the reaction was acidified to pH = 2.0 with 1 M HCl and extracted three times with 80 mL EtOAc. The combined organic phases were dried over Magnesium sulphate and the solvent was removed under reduced pressure. The crude

product was then purified by flash chromatography on silica (^{c}Hex/EtOAc, 3:1 + 1% AcOH) to furnish 1.76 g of the product (5.68 mmol, 94%) as a colourless solid.

R_f (^{C}Hex/EtOAc, 3:1 + 1% AcOH): 0.3
HRMS (ESI): m/z calcd. for ([M+NH_4]$^+$) 328.1503, found 328.1504.

^{1}H-NMR (400 MHz, DMSO-d_6): δ = 8.15 (d, *J* = 8.6 Hz, 2H, ***H***ε), 7.53 (d, *J* = 8.6 Hz, 2H, ***H***δ), 7.20 (d, *J* = 8.6 Hz, 1H, N***H***-*Boc*), 4.24 – 4.14 (ddd, *J* = 13.6 Hz, 8.6 Hz, 4.5 Hz, 1H, ***H***α), 3.18 (dd, *J* = 13.7 Hz, 4.6 Hz, 1H, ***H***β$_1$), 2.96 (dd, *J* = 13.7 Hz, 10.6 Hz, 1H, ***H***β$_2$) 1.29 (s, 9H, C(C***H***$_3$)$_3$) ppm.

^{13}C-NMR (100 MHz, DMSO-d_6): δ = 173.1 (***C***OOH), 155.4 (***C***=O-*Boc*), 146.5 (***C***γ), 146.3 (***C***ζ), 130.5 (***C***δ), 123.2 (***C***ε), 78.2 (***C***(CH$_3$)$_3$), 54.5 (***C***α), 36.3 (***C***β), 28.1 (C(***C***H$_3$)$_3$) ppm.

(2S)-2-[(*tert*-butoxycarbonyl)-amino]-3-(4-aminophenyl)-propanoic acid 3.7[212]

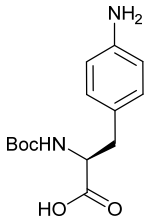

In an argon-filled Schlenk-flask 1.73 g *N*-Boc-4-Nitro-L-phenylalanin (5.58 mmol, 1.0 eq) were dissolved in 120 mL Methanol and 0.23 g Pd on activated coal (10%) were added. The flask was evaporated and purged with H_2 for three times. After 3 d, the solution was filtrated through Hyflo® and the solvent was removed in vacuo furnish 1.35 g of the product (4.80 mmol, 86%) as a colourless solid.

HRMS (ESI): m/z calcd. for ([M]) 280.1423, found 280.1428.
^{1}H-NMR (400 MHz, DMSO-d_6): δ = 7.39 (bs, 1H, COO***H***), 6.88 (d, *J* = 8.2 Hz, 2H, ***H***δ), 6.48 (d, *J* = 8.3 Hz, 2H, ***H***ε), 3.98 (td, *J* = 9.3 Hz, 4.8 Hz, 1H, ***H***α), 2.83 (dd, *J* = 13.8 Hz, 4.6 Hz, 1H, ***H***β$_1$), 2.66 (dd, *J* = 13.8 Hz, 9.8 Hz, 1H, ***H***β$_2$), 1.34 (s, 9H, C(C***H***$_3$)$_3$) ppm.

^{13}C-NMR (100 MHz, DMSO-d_6): δ = 174.3 (***C***OOH), 155.9 (***C***=O-*Boc*), 147.4 (***C***ζ), 130.0 (***C***δ), 125.2 (***C***γ), 114.3 (***C***ε), 78.5 (***C***(CH$_3$)$_3$), 56.1 (***C***α), 36.3 (***C***β), 28.7 (C(***C***H$_3$)$_3$) ppm.

(S,E)-2-((*tert*-butoxycarbonyl)amino)-3-(4-(phenyldiazenyl)phenyl)propanoic acid 3.8[204]

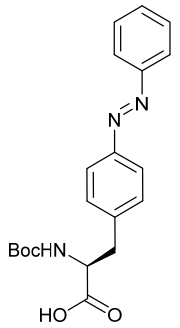

To a stirred solution of 3.00 g (10.7 mmol, 1.0 eq.) *N*-Boc-4-Amino-L-phenylalanin in 30 mL conc. acetic acid were added 1.15 g (10.7 mmol, 1.0 eq.) of Nitrosobenzene. The reaction mixture was stirred for 2 h at room temperature and the solvent was removed under reduced pressure. The residue was then co-evaporated with toluene (5 x 30 mL) and Dichlormethane (2 x 50 mL). The crude product was purified by flash-chromatography on silica (DCM → DCM/MeOH 99:1) to give 3.35 g (9.08 mmol, 85%) of the product as an amorphous orange solid.

R_f (DCM/MeOH, 9:1): 0.45

HRMS (ESI): m/z calcd. for ($[M+H]^+$) 370.1761, found 370.1764.

^{1}H-NMR (400 MHz, DMSO-d_6): δ = 7.86 (dd, *J* = 8.1 Hz, *J* = 1.4 Hz, 2H, ***H***θ), 7.81 (d, *J* = 8.3 Hz, 2H, ***H***ε), 7.61 – 7.51 (m, 3H, ***H***ι, ***H***κ), 7.47 (d, *J* = 8.3 Hz, 2H, ***H***δ), 7.02 (d, *J* = 7.7 Hz, 1H, N***H***-*Boc*), 4.30 – 4.15 (m, 1H, ***H***α), 3.15 (dd, *J* = 13.8 Hz, *J* = 4.6 Hz, 1H, ***H***β_1), 2.97 (dd, *J* = 13.9 Hz, *J* = 10.0 Hz, 1H, ***H***β_2), 1.32 (s, 9H, C(C***H***$_3$)$_3$) ppm.

^{13}C-NMR (100 MHz, DMSO-d_6): δ = 173.1 (***C***OOH), 155.3 (***C***=O-*Boc*), 152.0 (***C***η), 150.6 (***C***ζ), 141.9 (***C***γ), 131.1(***C***ι, ***C***κ), 130.0 (***C***δ), 129.2 (***C***ι, ***C***κ), 122.3 (***C***θ), 122.2 (***C***ε), 78.0 (***C***(CH3)3), 54.7 (***C***α), 36.4 (***C***β), 28.0 (C(***C***H$_3$)$_3$) ppm.

(S,E)-2-((((9H-fluoren-9-yl)methoxy)carbonyl)amino)-3-(4-(phenyldiazenyl)phenyl)-propanoic acid (Fmoc-AzoPhe-OH, 3.3)[208]

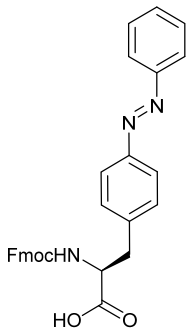

Compound **3.3** was synthesized in accordance to literature known protocols.[118, 208]

In an ice-bath, 3.29 g (8.66 mmol) *N*-Boc-phenylalanine-4‘-azobenzene was dissolved in 30 mL TFA/H_2O (9:1) and stirred at room temperature for one hour. The solvent was removed under reduced pressure and the residue was co-evaporated with toluene (5 x 50 mL) and Dichlormethane (2 x 50 mL). The residue was dissolved in 250 mL water/acetone (1:1) and 2.18 g (25.9 mmol, 3.0 eq.) $NaHCO_3$ and 2.92 g (8.66 mmol, 1.0 eq) Fmoc-*O*Su were added. After 18 h stirring at room temperature, the solution was acidified to pH = 2 with 1 M chloric acid. The aqueous phase was extracted with 3 x 100 mL Ethyl acetate and dried over magnesium sulphate. The crude product was purified by flash-chromatography on silica (DCM → DCM/MeOH 98:2) to furnish 3.87 g (7.88 mmol, 91%) of an orange product.

R_f (DCM/MeOH, 9:1): 0.5
HRMS (ESI): m/z calcd for ($[M+H]^+$) 492.1918, found 492.1921.

^{1}H-NMR (400 MHz, DMSO-d_6): δ = 7.91 – 7.84 (m, 4H, ***H***4-, ***H***5-*Fmoc*, ***H***θ), 7.81 (d, *J* = 8.3 Hz, 2H, ***H***ε), 7.78 (d, *J* = 8.6 Hz, 1H, N***H***-*Fmoc*), 7.68 – 7.53 (m, 5H, ***H***1-, ***H***8-*Fmoc,* ***H***ι, ***H***κ), 7.50 (d, *J* = 8.3 Hz, 2H, ***H***δ) 7.38 (q, *J* = 7.1 Hz, 2H, ***H***3-, ***H***6-*Fmoc*), 7.32 – 7.24 (m, 2H, ***H***2-, ***H***7-*Fmoc*), 4.33 – 4.24 (m, 1H, ***H***α), 4.24 – 4.13 (m, 3H, ***H***9-*Fmoc*, C***H***$_2$-*Fmoc*), 3.22 (dd, *J* = 13.7 Hz, *J* = 4.3 Hz, 1H, ***H***β_1), 2.99 (dd, *J* = 13.7 Hz, *J* = 10.7 Hz, 1H, ***H***β_2) ppm.

^{13}C-NMR (100 MHz, DMSO-d_6): δ = 173.1 (***C***OOH), 155.9 (***C***=O-*Fmoc*), 152.0 (***C***η), 150.6 (***C***ζ), 143.8 (***C***1a-, ***C***8a-*Fmoc*), 143.7 (***C***1a-, ***C***8a-*Fmoc*), 142.1 (***C***γ), 140.7 (***C***4a-, ***C***5a-*Fmoc*), 131.3 (***C***ι, ***C***κ), 130.2 (***C***δ), 129.4 (***C***ι, ***C***κ), 127.6 (***C***3-, ***C***6-*Fmoc*), 127.0 (***C***2-, ***C***7-*Fmoc*) 125.2 (***C***1-, ***C***8-*Fmoc*), 122.4 (***C***θ), 120.1 (***C***4-, ***C***5-*Fmoc*), 65.6 (***C***H_2-*Fmoc*), 55.3 (***C***α), 46.6 (***C***9-*Fmoc*), 36.4 (***C***β) ppm.

(S,E)-2-((*tert*-butoxycarbonyl)amino)-3-(4-((3,5-di-*tert*-butylphenyl)diazenyl)phenyl)-propanoic acid 3.11

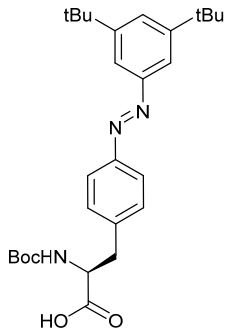

Compound **3.11** was synthesized in accordance to literature known protocols.[204]

To a solution of 1.0 g (3.57 mmol, 1.0 eq.) *N*-Boc-4-Amino-L-phenylalanin dissolved in 30 mL DCM a solution of 2.19 g (7.13 mmol, 2 eq.) Oxon® dissolved in 30 mL water were added. After stirring for 4 h at room temperature, the organic phase was separated and the aqueous phase was extracted 2 times with 30 mL DCM. The combined organic phases were dried over $MgSO_4$ and purification by flash chromatography on silica (DCM → DCM/MeOH 99.5/0.5) 423 mg of (S)-2-((*tert*-butoxycarbonyl)amino)-3-(4-nitrosophenyl)propanoic acid could be furnished.

The Nitrosyl was directly dissolved in 30 mL conc. acetic acid and 295 mg (1.43 mmol) 3,5-Di-*tert*-butylanilin were added. After stirring over-night at room temperature, the solvent was removed under reduced pressure and the crude product was co-evaporated for five times with toluene and two times with DCM. After purification by flash chromatography on silica (DCM→DCM/MeOH, 9:1) 420 mg (0.87 mmol, 24% over two steps) of the product could be furnished as orange solid.

R_f (DCM/MeOH, 9:1): 0.48
HRMS (ESI): m/z calcd for ($[M+H]^+$) 482.3013, found 482.3011.

^{1}H-NMR (400 MHz, DMSO-d_6): δ = 8.34 (bs, 1H, COO***H***), 7.86 (d, *J* = 8.4 Hz, 2H, ***H***ε), K2), 7.81 (d, *J* = 8.4 Hz, 2H, ***H***ε, K1), 7.71 (d, *J* = 1.8 Hz, 2H, ***H***θ, K1), 7.70 (d, *J* = 1.8 Hz, 2H, ***H***θ, K2), 7.62 (t, *J* = 1.8 Hz, 1H, ***H***κ, K2), 7.61 (t, *J* = 1.8 Hz, 1H, ***H***κ, K1), 7.49 (d, *J* = 8.4 Hz, 2 H, ***H***δ, K1), 7.45 (d, *J* = 8.3 Hz, 2H, ***H***δ, K2), 7.01 (d, *J* = 6.7 Hz, 1H, N***H***-*Boc*), 4.26 (t, *J* = 6.6 Hz, 1H, ***H***α, K1), 4.21 (s, 1H, ***H***α, K2), 3.22 (dd, *J* = 6.5 Hz, *J* = 2.9 Hz, 1H, ***H***β_1, K1), 3.14 (dd, *J* = 14.1, *J* = 4.4, 1H, ***H***β_1, K2), 2.96 (dd, *J* = 14.2 Hz, *J* = 10.0 Hz, 1H, ***H***β_2, K2), 1.36 (s, 27H, C(C***H***$_3$)$_{3,ar}$ K1, K2, C(C***H***$_3$)$_3$-*Boc*, K1), 1.32 (s, 9H, C(C***H***$_3$)$_3$-*Boc*), K2) ppm.

^{13}C-NMR (100 MHz, DMSO-d$_6$): δ = 173.0 (***C***OOH), 170.0 (***C***=O-Boc), 151.9 (***C***η, K1), 151.9 (***C***η, K2), 151.6 (***C***ι, K2), 151.6 (***C***ι, K1), 151.3 (***C***ζ, K1), 150.7 (***C***ζ, K2), 141.5 (***C***γ, K1), 138.2 (***C***γ, K2), 130.3 (***C***δ, K1), 129.9 (***C***δ, K2), 125.2 (***C***κ, K2), 125.0 (***C***κ, K1), 122.5 (***C***ε, K2), 122.1 (***C***ε, K1), 116.5 (***C***θ), 116.4 (***C***θ), 78.0 (***C***(CH$_3$)$_3$-Boc), 54.7 (***C***α, K2), 53.0 (***C***α, K1), 36.3 (***C***β, K1), 35.6 (***C***β, K2), 34.6 (2 x ***C***(CH$_3$)$_3$), 31.0 (2 x C(***C***H$_3$)$_3$), 28.0 (C(***C***H$_3$)$_3$-Boc) ppm.

(S,E)-2-((((9H-fluoren-9-yl)methoxy)carbonyl)amino-3-(4-((3,5-di-*tert*-butylphenyl)diazenyl)phenyl)propanoic acid (Fmoc-*t*BuAzoPhe-OH, 3.9)

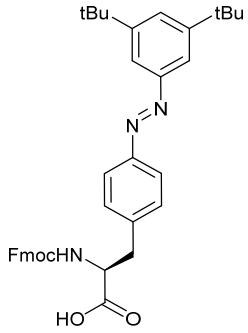

Compound **3.9** was synthesized in accordance to literature known protocols.[118, 208]

To a solution of 333 mg (0.69 mmol, 1.0 eq.) **3.11** in 1 mL water at 0°C, 9 mL TFA was added. After stirring for 2 h at room temperature, the solvent was removed under reduced pressure and the free amino acid was co-evaporated five times with toluene and two times with DCM. The free amine was then solved in 30 mL acetone/water (1:1) and 116 mg (1.38 mg, 2.0 eq.) $NaHCO_3$ and 233 mg (0.69 mmol, 1.0 eq.) Fmoc-OSu was added. After 18 h stirring at room temperature, the solution was acidified to pH = 2 with 1 M Chloric acid. The aqueous phase was extracted with 3 x 100 mL ethyl acetate and dried over magnesium sulphate. The crude product was purified by flash-chromatography on silica (DCM → DCM/MeOH, 99.5:0.5) to furnish 338 mg (0.56 mmol, 81% over two steps) of an orange product.

R_f (DCM/MeOH, 9:1): 0.50
HRMS (ESI): m/z calcd for ([M+H]$^+$) 604.3170, found 604.3172.

^{1}H-NMR (400 MHz, DMSO-d$_6$): δ = 7.86 (d, *J* = 7.6 Hz, 2H, ***H***4-, ***H***5-*Fmoc*), 7.82 (d, *J* = 8.3 Hz, 2H, ***H***ε), 7.81 (d, *J* = 8.8 Hz, 1H, N***H***-*Fmoc*), 7.70 (d, *J* 1.7 Hz, 2H, ***H***θ), 7.66 – 7.59 (m, 3 H, ***H***κ, ***H***1-, ***H***8-*Fmoc*), 7.49 (d, *J* = 8.4 Hz, 2H, ***H***δ), 7.38 (q, *J* = 7.8 Hz, 2H, ***H***3-, ***H***6-*Fmoc*), 7.33 – 7.20 (m, 2H, ***H***2-, ***H***7-*Fmoc*), 4.27 (ddd, *J* = 10.6 Hz, *J* = 8.7 Hz, *J* = 4.5 Hz, 1H,

Hα), 4.23 – 4.11 (m, *J* = 3H, ***H***9-*Fmoc*, C***H***$_2$-*Fmoc*), 3.21 (dd, *J* = 13.8 Hz, *J* = 4.3 Hz, 1H, ***H***β_1), 2.98 (dd, *J* = 13.7 Hz, *J* = 10.8 Hz, 1H, ***H***β_2), 1.36 (s, 18H, 2 x C(C***H***$_3$)$_3$) ppm.

^{13}C-NMR (100 MHz, DMSO-d$_6$): δ = 173.1 (***C***OOH), 155.9 (***C***=O-*Fmoc*), 151.9 (***C***η, ***C***ι), 151.7 (***C***η, ***C***ι), 150.7 (***C***ζ), 143.8 (***C***1a-, ***C***8a-*Fmoc*), 143.7 (***C***1a-, ***C***8a-*Fmoc*), 141.7 (***C***γ), 140.7 (***C***4a-, ***C***5a-*Fmoc*), 140.7 (***C***4a-, ***C***5a-*Fmoc*), 130.1 (***C***δ), 127.6 (***C***3-, ***C***6-*Fmoc*), 127.5 (***C***3-, ***C***6-*Fmoc*), 127.0 (***C***2-, ***C***7-*Fmoc*), 125.2 (***C***κ, ***C***1-, ***C***8-*Fmoc*), 125.2 (***C***κ, ***C***1-, ***C***8-*Fmoc*), 122.4 (***C***ε), 120.1 (***C***4-, ***C***5-*Fmoc*), 116.6 (***C***θ), 65.6 (***C***H$_2$-*Fmoc*), 55.2 (***C***α), 46.5 (***C***9-*Fmoc*), 36.3 (***C***β), 34.7 (2 x (***C***(CH$_3$)$_3$), 31.1 (2 x (C(***C***H$_3$)$_3$) ppm.

(E)-2-(3-((3-(hydroxymethyl)phenyl)diazenyl)phenyl)acetic acid 3.18

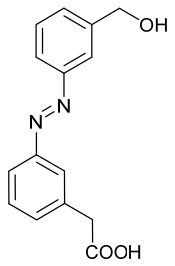

Compound **3.18** was synthesized in accordance to literature known protocols.[118]

A solution of 2.17 g (12.0 mmol, 1.0 eq.) 2-(3-nitrophenyl)acetic acid in 30 mL 2-methoxyethanol in an argon atmosphere was stirred for 10 min at room temperature, before a solution of 963 mg (18.0 mmol, 1.5 eq.) NH_4Cl in 20 mL H_2O was added. The reaction mixture was cooled to 0°C and 1.96 (32.3 mmol, 2.5 eq.) zinc was added. After 1 h, the reaction solution was filtered with Hyflo® and the filtrate was added within 30 min to a 0°C cold solution of 9.73 g (36.0 mmol, 3.0 eq.) $FeCl_3 \cdot 6\ H_2O$ in 50 mL EtOH/H_2O (2:1). After stirring for 2 h, the solution was diluted with 50 mL water and extracted 4 times with 200 mL Et_2O. The combined organic layers were dried with $MgSO_4$ and after removal of the solvent, the crude product was purified by column chromatography on silica gel (^{C}Hex/EtOAc 9:1 + 1% AcOH). The product **3.18** was furnished as green-turquoise oil in 89% (1.77 g, 10.7 mmol) yield.

To a solution of 1.36 mg, (8.23 mmol, 1 eq.) of 2-(3-nitrosophenyl)acetic acid in 30 mL concentrated acetic acid, 1.02 g (8.23 mmol, 1 eq.) 3-aminobenzyl alcohol were added and the reaction mixture was stirred over-night at room temperature. After removal of the solvent under reduced pressure, the residue was coevaporated 5 times with toluene and 2 times with dichloromethane. After purification by flash chromatography on silica (^{C}Hex/EtOAc, 5:1+ 1%

AcOH → 2:1 + 1% AcOH) to furnish 1.30 mg of the product (4.81 mmol, 58%) as an orange solid.

R_f (^{C}Hex/EtOAc, 1:1 + 1% AcOH): 0.27
HRMS (ESI): m/z calcd for ([M+H]$^+$) 271.1077, found 271.1076.

^{1}H-NMR (400 MHz, DMSO-d$_6$): δ = 7.86 (s, 1H, ***H***12), 7.84 – 7.77 (m, 3H, ***H***4, ***H***6, ***H***16), 7.60 – 7.44 (m, 4H, ***H***7, ***H***8, ***H***14, ***H***15), 4.63 (s, 2H, ***H***17), 3.74 (s, 2H, ***H***2), 3.36 (bs, 1H, O***H***) ppm.

^{13}C-NMR (150 MHz, DMSO-d$_6$): δ = 172.5 (***C***OOH), 152.0 (***C***5, ***C***11), 144.2 (***C***4), 136.6 (***C***3), 132.6 (***C***7, ***C***8, ***C***14, ***C***15), 129.4 (***C***7, ***C***8, ***C***14, ***C***15), 129.3 (***C***7, ***C***8, ***C***14, ***C***15), 129.2 (***C***7, ***C***8, ***C***14, ***C***15), 123.1 (***C***4, ***C***6, ***C***16), 121.7 (***C***4, ***C***6, ***C***16), 121.4 (***C***4, ***C***6, ***C***16), 119.6 (***C***12), 62.5 (***C***17), 40.3 (***C***2) ppm.

(E)-2-(3-((3-(bromomethyl)phenyl)diazenyl)phenyl)acetic acid 3.16

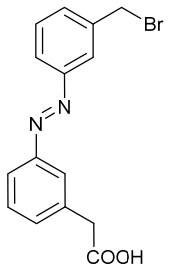

Compound **3.16** was synthesized in accordance to literature known protocols.[217, 218]

To a solution of 1.00 g (3.69 mmol, 1 eq.) 3-(3-hydroxymethylphenylazo)phenyl acetic acid in 30 mL absol. THF at 0 °C, 1.45 g (5.55 mmol, 1.5 eq.) PPh_3 were added. In small portions, 988 mg (5.55 mmol, 1.5 eq.) NBS were added and the solution was stirred for 15 min. The solution was diluted with 100 mL EtOAc and the organic phase was washed with 100 mL H_2O and 100 mL brine. After drying over $MgSO_4$, the crude product was purified by flash-chromatography on silica (^{C}Hex/EtOAc 4:1 and 1% AcOH) to furnish 1.03 g (3.09 mmol, 84%) of the product as yellow solid.

R_f (^{C}Hex/EtOAc, 1:1 + 1% AcOH): 0.43
HRMS (ESI): m/z calcd for ([M−H]$^-$) 331.0088, found 331.0088.

^{1}H-NMR (400 MHz, $CDCl_3$): δ = 12.49 (bs, 1H, COO***H***), 7.97 (s, 1H, ***H***11), 7.86 (d, *J* = 7.7 Hz, 1H ***H***15), 7.83 – 7.78 (m, 2H, ***H***3, ***H***5), 7.66 (d, *J* = 7.3 Hz, 1H, ***H***13), 7.60 (d, *J* = 7.7 Hz, 1H,

H14), 7.56 (t, *J* = 8.1 Hz, 1H, ***H***6), 7.48 (d, *J* = 7.4 Hz, 1H, ***H***7), 5.43 (s, ***H***16$_{cis}$), 4.85 (s, 2H, ***H***16$_{trans}$), 3.89 (s, ***H***2$_{cis}$), 3.74 (s, 2H, ***H***2$_{trans}$) ppm.

^{13}C-NMR (150 MHz, $CDCl_3$): δ = 172.5 (***C***OOH), 152.1 (***C***5, ***C***11), 151.8 (***C***5, ***C***11), 139.7 (***C***3, ***C***13), 136.6 (***C***3, ***C***13), 132.9 (***C***7), 132.3 (***C***13), 130.0 (***C***6, ***C***14), 129.4 (***C***6, ***C***14), 123.2 (***C***3, ***C***5, ***C***15), 123.1 (***C***3, ***C***5, ***C***15), 122.6 (***C***11), 121.5 (***C***3, ***C***5), 41.2 (***C***2) 33.7 (***C***16).

(9*H*-Fluoren-9-yl)methyl (3-aminobeznyl)carbamate 3.15[118]

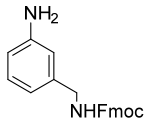

To a solution of 5.0 g (40.9 mmol, 1.0 eq) 3-aminobenzylamin in 50 mL MeCN/DMF (10:1) 5.70 mL (40.9 mmol, 1.0 eq) TEA and 13.8 g (40.9 mmol, 1.0 eq) Fmoc-OSu solved in 70 mL MeCN were added. After stirring for 2 h at room temperature, the reaction was quenched with 30 mL water and the precipitated product was filtered off and washed with 50 mL Trifluorethanol/Methoxyethanol (1:1). After drying at reduced pressure, 1.71 g (4.97 mmol, 61%) of the product (**3.15**) was furnished as a white solid. The product was used for the next reaction without purification.

R_f (DCM/MeOH, 95:5): 0.4
HRMS (ESI): m/z calcd for ([M+H]$^+$) 345.1597, found 345.1599.

^{1}H-NMR (400 MHz, $CDCl_3$): δ = 7.89 (d, *J* = 7.5 Hz, 2 H, ***C***4-, ***C***5-*Fmoc*), 7.79 (t, *J* = 6.1 Hz, 1 H, N***H***-*Fmoc*), 7.73 (d, *J* = 7.4 Hz, 2 H, ***C***1-, ***C***8-*Fmoc*), 7.42 (t, *J* = 7.4 Hz, 2 H, ***H***3-, ***H***6-*Fmoc*), 7.33 (t, *J* = 7.4 Hz, 2 H, ***H***2-, ***H***7-*Fmoc*), 6.96 (t, *J* = 7.7 Hz, 1 H, ***H***5), 6.50 (s, 1 H, ***H***2), 6.46 (d, *J* = 7.9 Hz, 1 H, ***H***6), 6.41 (d, *J* = 7.5 Hz, 1 H, ***H***4), 5.04 (s, 2 H, N***H***$_2$), 4.33 (d, *J* = 7.0 Hz, 2 H, C***H***$_2$-*Fmoc*), 4.24 (t, *J* = 6.9 Hz, 1 H, ***H***9-*Fmoc*), 4.08 (d, *J* 6.1 Hz, 2 H, ***H***7) ppm.

^{13}C-NMR (100 MHz, $CDCl_3$): δ = 156. 3 (***C***=O-*Fmoc*), 148.6 (***C***1), 143.9 (***C***1a-, ***C***8a-*Fmoc*), 140.7 (***C***4a-, ***C***5a-*Fmoc*), 140.3 (***C***3), 128.7 (***C***5), 127.6 (***C***3-, ***C***6-*Fmoc*), 127.08 (***C***2-, ***C***7-*Fmoc*), 125.2 (***C***1-, ***C***8-*Fmoc*), 120.1 ***C***4-, ***C***5-*Fmoc*), 114.6 (***C***4), 112.6 (***C***2, ***C***6), 112.5 (***C***2, ***C***6), 65.4 (***C***H$_2$-*Fmoc*), 46.8 (***C***9-*Fmoc*), 44.0 (***C***7).

3-[3-(aminomethyl)phenylazo]phenylacetic acid 3.1[118]

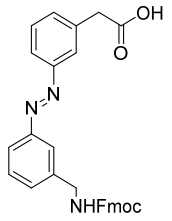

A solution of 403 g (2-44 mmol, 1.0 eq.) freshly prepared 2-nitrosophenylacetic acid and 840 mg (9*H*-fluoren-9-yl)methyl (3-aminobenzyl)carbamate (2.44 mmol, 1.0 eq.) were solved in 15 mL glacial acetic acid and the solution was stirred at room temperature overnight. The solvent was evaporated and the crude product was co-evaporated five times with toluene and two times with DCM. The crude product was then purified by flash-chromatography on silica (^{C}Hex/EtOAc 3:1 and 1% AcOH → ^{C}Hex/EtOAc 1:1 and 1% AcOH) to furnish 804 mg (1.63mmol, 67% over two steps) of the product as an orange solid.

R_f (^{C}Hex/EtOAc, 1:1 + 1% AcOH): 0.4
HRMS (ESI): m/z calcd for ([M+H]$^+$) 492.1918, found 492.1916.

^{1}H-NMR (400 MHz, $CDCl_3$): δ = 8.04 (t, *J* = 6.1 Hz, 1 H, N***H***-*Fmoc*), 7.88 (d, *J* = 7.5 Hz, 2 H, ***H***4-, ***H***5-*Fmoc*), 7.85 – 7.76 (m, 4 H, ***H***16 {7.84}, ***H***4 {7.83}, ***H***6 {7.80}, ***H***12 {7.80}), 7.73 (d, *J* = 7.4 Hz, 2 H, ***H***1-, ***H***8-*Fmoc*), 7.55 (t, *J* = 7.7 Hz, 2 H, ***H***7, ***H***15), 7.49 (d, *J* = 7.7 Hz, 1 H, ***H***8), 7.45 (d, *J* = 7.4 Hz, 1 H, ***H***14), 7.40 (t, *J* = 7.4 Hz, 2 H, ***H***3-, ***H***6-*Fmoc*), 7.32 (t, *J* = 7.1 Hz, 2 H, ***H***2-, ***H***7-*Fmoc*), 4.40 (d, *J* = 6.9 Hz, 2 H, C***H***$_2$-*Fmoc*), 4.35 (d, *J* = 6.1 Hz, 2 H, ***H***17), 4.26 (t, *J* = 8.04 Hz, 1 H, ***H***9-*Fmoc*), 3.76 (s, 2 H, ***H***2) ppm.

^{13}C-NMR (150 MHz, $CDCl_3$): δ = 172.6 (***C***1), 156.5 (***C***=O-*Fmoc*), 152.1 (***C***5, ***C***11), 152.0 (***C***5, ***C***11), 143.9 (***C***1a-, ***C***8a-*Fmoc*), 141.5 (***C***13), 140.8 (***C***4a-, ***C***5a-*Fmoc*), 136.6 (***C***3), 132.7 (***C***8), 130.2 (***C***14), 129.4 (***C***7, ***C***15), 129.3 (***C***7, ***C***15), 127.6 (***C***3-, ***C***6-*Fmoc*), 127.1 (***C***2-, ***C***7-*Fmoc*), 125.2 (***C***1-, ***C***8-*Fmoc*), 123.2 (***C***4), 121.6 (***C***6, ***C***12), 121.4 (***C***6, ***C***12), 120.6 (***C***16), 120.1 (***C***4-, ***C***5-*Fmoc*), 65.5 (***C***H_2-*Fmoc*), 46.8 (***C***9-*Fmoc*), 43.6 (***C***17), 40.4 (***C***2) ppm.

(E)-2-(3-((perfluorophenyl)diazenyl)phenyl)acetic acid 3.19

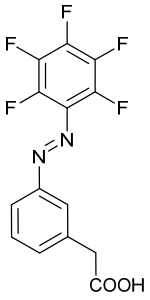

Compound **3.19** was synthesized in accordance to literature known protocols.[219]

To a solution of 2.00 g (10.9 mmol, 1.0 eq.) 2,3,4,5,6-pentafluoroaniline in 60 mL dichloromethane, a 125 mL solution of Oxone® (6.72g, 21.8 mmol, 2.0 eq.) in water was added under argon atmosphere. The reaction mixture was stirred for 12 h at room temperature. The organic layer was extracted with dichloromethane (2 × 100 mL) then washed with 0.1 M HCl (100 mL) and brine (100 mL). The organic phase was dried over $MgSO_4$ and the solvent was removed at room temperature under reduced pressure. The crude product was then dissolved in 12 mL conc. acetic acid and 1.65 g (10.9 mmol, 1.0eq.) 3-aminophenyl acetic acid was added. The reaction mixture was stirred in the absence of light for 6h under argon atmosphere before co-evaporation with toluene (5 × 20 mL) and dichloromethane (3 × 50 mL). The crude product was purified by flash-chromatography on silica (^{C}Hex/EtOAc 9:1 and 1% AcOH) to furnish 268 mg (0.812 mmol, 7.5% over two steps) of the product as an orange solid.

R_f (^{C}Hex/EtOAc, 1:1 + 1% AcOH): 0.37
HRMS (ESI): m/z calcd for ([M−H]$^-$) 329.03549, found 329.03555.

^{1}H-NMR (400 MHz, $CDCl_3$): δ = 12.46 (s, 1 H, COO***H***), 7.85 – 7.79 (m, 2 H, ***H***$_{ar,trans}$), 7.64 – 7.56 (m, 2 H, ***H***$_{ar,trans}$), 7.44 (t, *J* = 7.8 Hz, 1 H, ***H***7_{cis}), 7.29 (d, *J* = 7.7 Hz, 1 H, ***H***8_{cis}), 7.15 (d, *J* = 8.0 Hz, 1 H, ***H***6_{cis}), 6.85 (s, 1 H, ***H***4_{cis}), 3.77 (s, 2 H, C***H***$_{2,trans}$), 3.59 (s, 2 H, C***H***$_{2,cis}$) ppm.

^{13}C-NMR (150 MHz, $CDCl_3$): δ = 172.4 (***C***OOH), 152.3 (***C***$_{ar}$), 137.0 (***C***$_{ar}$), 134.7 (***C***$_{ar}$), 129.6 (***C***$_{ar}$), 123.6 (***C***$_{ar}$), 121.6 (***C***$_{ar}$), 40.0 (***C***H_2) ppm.

^{19}F-NMR (150 MHz, $CDCl_3$): δ = -147.66 – 147.86 (m, 2 F, ***F***$_{ar,cis}$), -150.86 – -151.52 (m, 2 F, ***F***$_{ar,trans}$), -152.43 – -152.82 (m, 1 F, ***F***$_{ar,trans}$), -155.93 (t, *J* = 22.7 Hz, 1 F, ***F***$_{ar,cis}$), -160.98 – -161.21 (m, 1 F, ***F***$_{ar,cis}$), -162.10 – -162.70 (m, 2 F, ***F***$_{ar,trans}$) ppm.

(9H-fluoren-9-yl)methyl (E)-(4-(phenyldiazenyl)benzyl)carbamate 3.25[221]

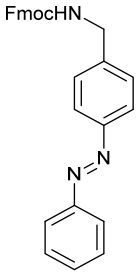

Compound **3.25** was synthesized in accordance to literature known protocols.[118]

To a solution of 1.0 g (8.18 mmol, 1.0 eq) 4-aminobenzylamin in 50 mL MeCN/DMF (10:1) 1.14 mL (8.18 mmol, 1.0 eq) TEA and 2.76 g (8.18 mmol, 1.0 eq) Fmoc-OSu were added. After stirring for 4 h at room temperature, the reaction was quenched with 10 mL water and the precipitated product was filtered off and washed with 20 mL Trifluorethanol/Methoxyethanol (1:1). After drying at reduced pressure, 1.71 g (4.97 mmol, 61%) of the product (**18**) was furnished as a white solid. The product was used for the next reaction without purification. To a solution of 1.38 g (4.0 mmol, 1.0 eq.) 4-(*N*-Fmoc-aminomethyl)aniline in 30 mL conc. acetic acid 389 mg (3.64 mmol, 0.91 eq.) Nitrosobenzene were added. After stirring over night at room temperature, the solvent was removed under reduced pressure and the residue was coevaporated five times with toluene and two times with DCM. After purification by flash chromatography on silica (cHex/EtOAc 8:1→4:1→2:1→1:1) to furnish 1.36 mg of the product (4.14 mmol, 87%) as an orange solid.

HRMS (ESI): m/z calcd for ($[M+H]^+$) 434.1863, found 434.1864.

^{1}H-NMR (400 MHz, $CDCl_3$): δ = 7.93 (d, *J* = 7.1 Hz, 2H, ***H***11, ***H***15), 7.89 (d, *J* = 8.2 Hz, 2H, ***H***4, ***H***6), 7.78 (d, *J* = 7.5 Hz, 2 H, ***H***4-, ***H***5-*Fmoc*), 7.61 (d, *J* = 7.4 Hz, 2H, ***H***1-, ***H***8-*Fmoc*), 7.56 – 7.45 (m, 3H, ***H***12, ***H***13, ***H***14) 7.45 – 7.36 (m, 4H, ***H***3-, ***H***6-*Fmoc*, ***H***3, ***H***7), 7.33 (t, *J* = 7.4 Hz, 2H, ***H***2-, ***H***7-*Fmoc*), 5.19 – 5.11 (m, 1H, N***H***-*Fmoc*), 4.51 (d, *J* = 6.7 Hz, 2H, C$\boldsymbol{H}_2$-*Fmoc*), 4.46 (d, *J* = 6.0 Hz, 2 H, ***H***1, K_1), 4.37 – 4.29 (m, 2 H, ***H***1, K_2), 4.25 (t, *J* = 6.6 Hz, 1 H, H9-*Fmoc*) ppm.

^{13}C NMR (101 MHz, $CDCl_3$): δ = 156.6 (***C***=O-*Fmoc*), 152.8 (***C***10), 152.2 (***C***5), 144.0 (***C***1a-, ***C***8a-*Fmoc*), 141.6 (***C***2, ***C***4a-, ***C***5a-*Fmoc*), 141.5 (***C***2, ***C***4a-, ***C***5a-*Fmoc*), 131.2(***C***12, ***C***13, ***C***14), 129.2 (***C***12, ***C***13, ***C***14), 128.2 (***C***3-, ***C***6-*Fmoc*, ***C***3, ***C***7), 127.8 (***C***3-, ***C***6-*Fmoc*, ***C***3, ***C***7), 127.2 (***C***2-, ***C***7-*Fmoc*), 125.1 (***C***1-, ***C***8-*Fmoc*), 123.3 (***C***4, ***C***6), 123.0 (***C***11, ***C***15), 120.1 (***C***4-, ***C***5-*Fmoc*), 66.8 (***C***H_2-*Fmoc*), 47.5 (***C***9-*Fmoc*), 44.9 (***C***1) ppm.

(E)-(4-(phenyldiazenyl)phenyl)methanamine 3.22[221]

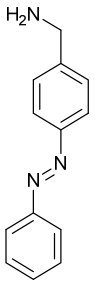

To a solution of 1.06 g (2.44 mmol) of *Fmoc-N*-4-(phenylazo)benzylamine in 16 mL DCM at 0°C, 4 mL piperidine were added and the solution was stirred at room temperature for 20 min. The solvent was removed under reduced pressure and the crude product was purified by flash chromatography on silica (ᶜHex/EtOAc, 1:1 -> DCM/MeOH 9:1) to furnish 500 mg of the product (2.37 mmol, 97%) as an orange solid.

MS (EI): m/z calcd for ([M−NH_2]⁻) 195.0927, found 195.0916.

^{1}H-NMR (600 MHz, DMSO-d_6): δ = 8.36 (bs, 2 H, N***H***$_2$), 7.95 – 7.93 (m, 2 H, ***H***4, ***H***6), 7.92 – 7.90 (m, 2 H, ***H***11, ***H***15), 7.69 – 7.67 (m, 2 H, ***H***3, ***H***7), 7.63 – 7.58 (m, 3 H, ***H***12, ***H***13, ***H***14), 4.16 (s, 2H, ***H***1) ppm.^{13}C-NMR (150 MHz, DMSO-d_6): δ = 151.9 (***C***10), 151.8 (***C***5), 137.4 (***C***2), 131.9 (***C***13), 130.0 (***C***3, ***C***7), 129.6 (***C***12, ***C***14), 122.7 (***C***4, ***C***6, ***C***11, ***C***15), 42.0 (***C***1) ppm.

NMR-Spectra

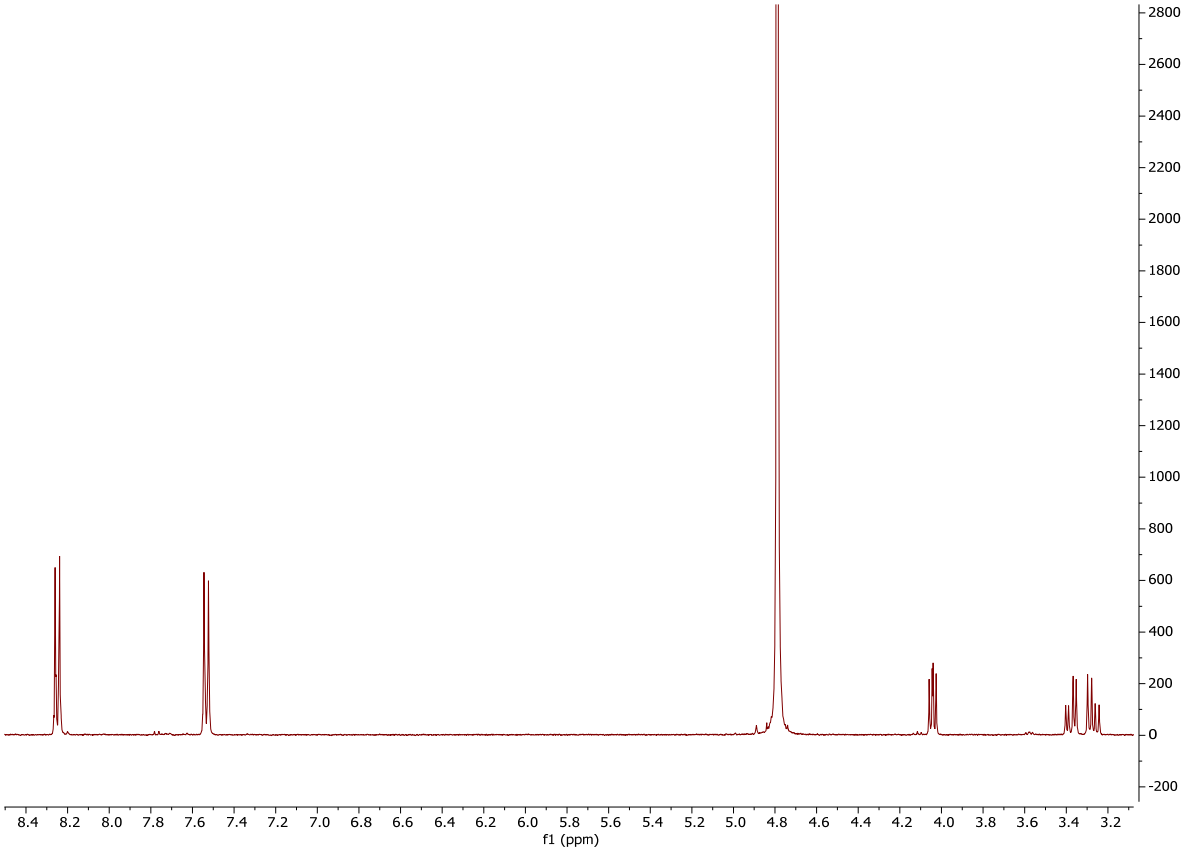

Figure 3.3: ^{1}H-NMR of **3.5**

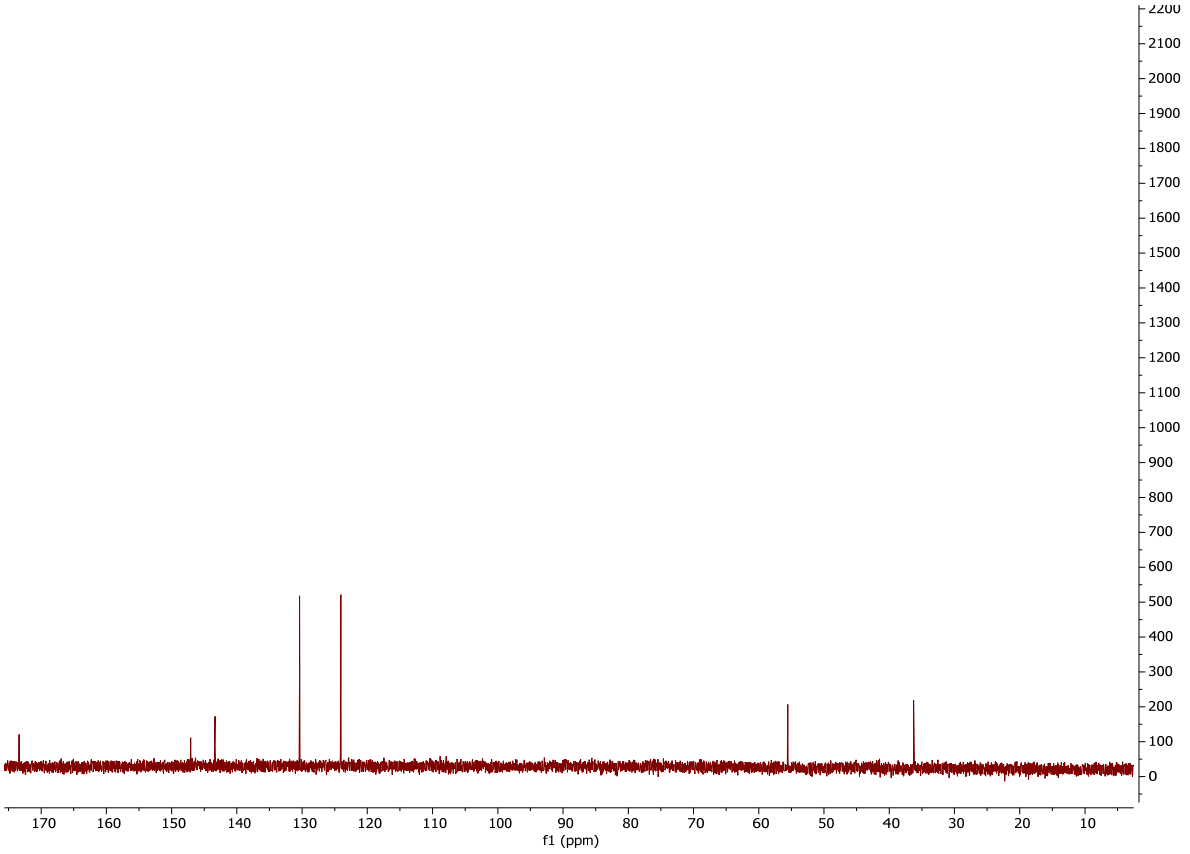

Figure 3.4: ^{13}C-NMR of **3.5**

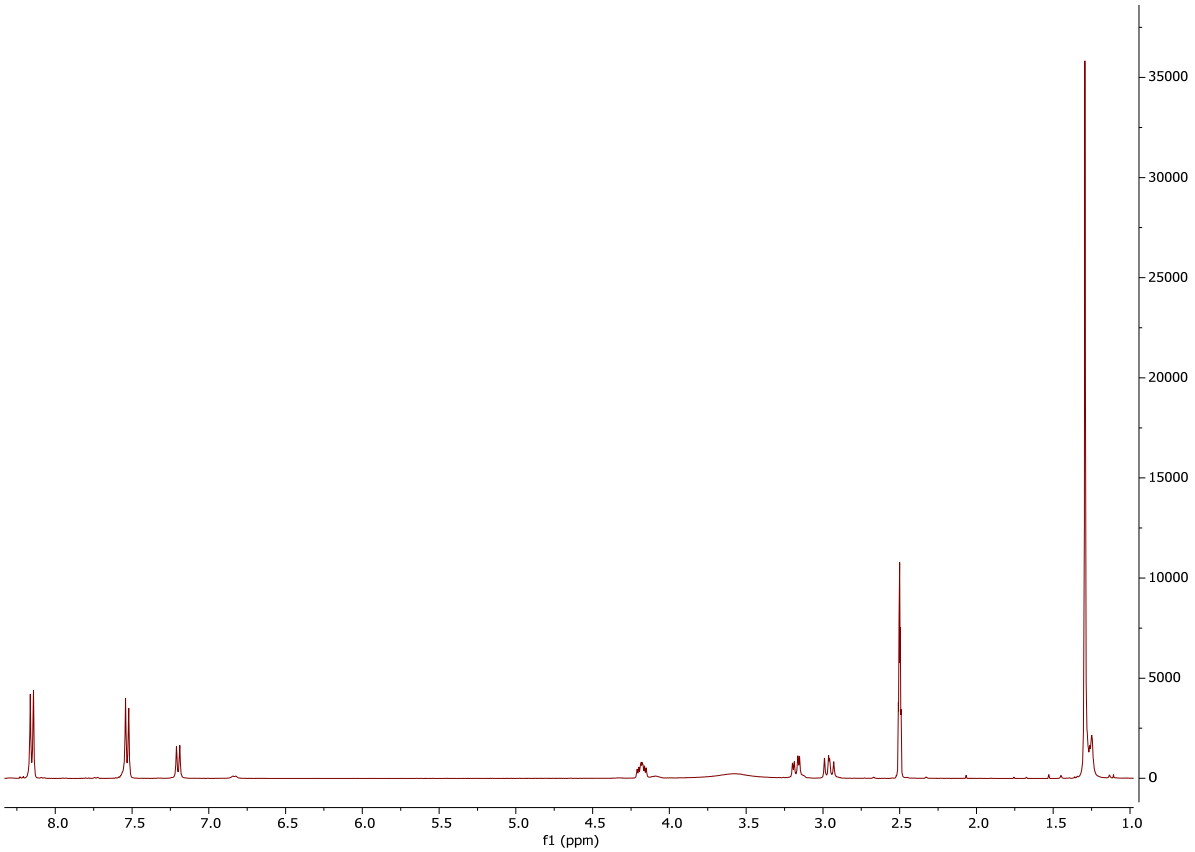

Figure 3.5: ^{1}H-NMR of **3.6**

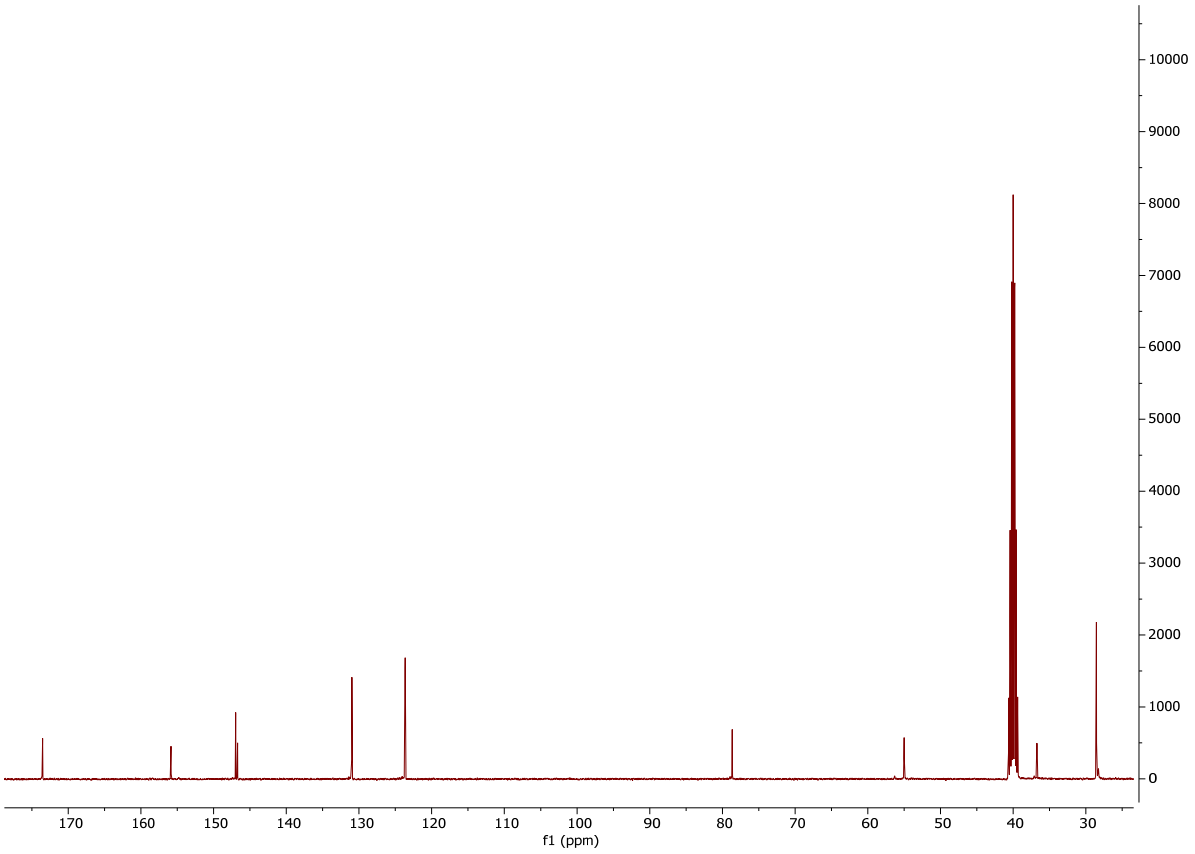

Figure 3.6: ^{13}C-NMR of **3.6**

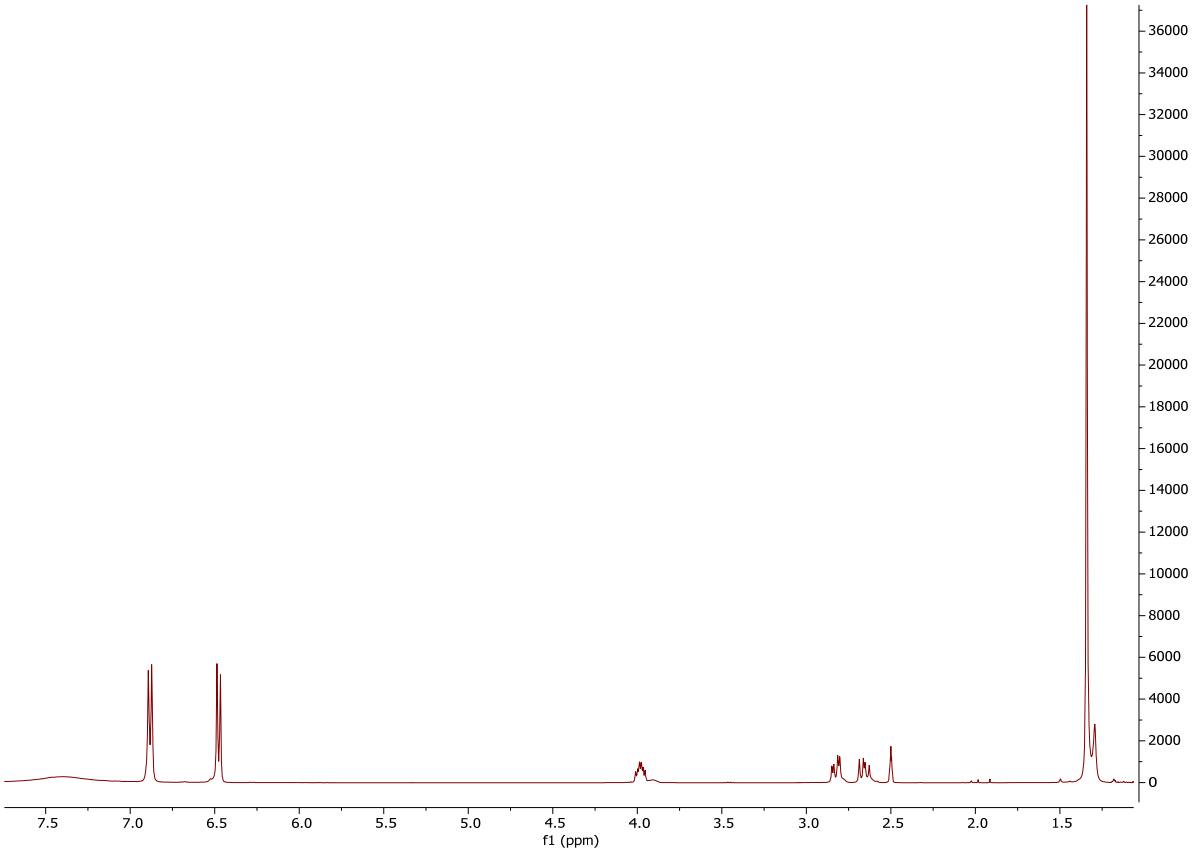

Figure 3.7: ^{1}H-NMR of **3.7**

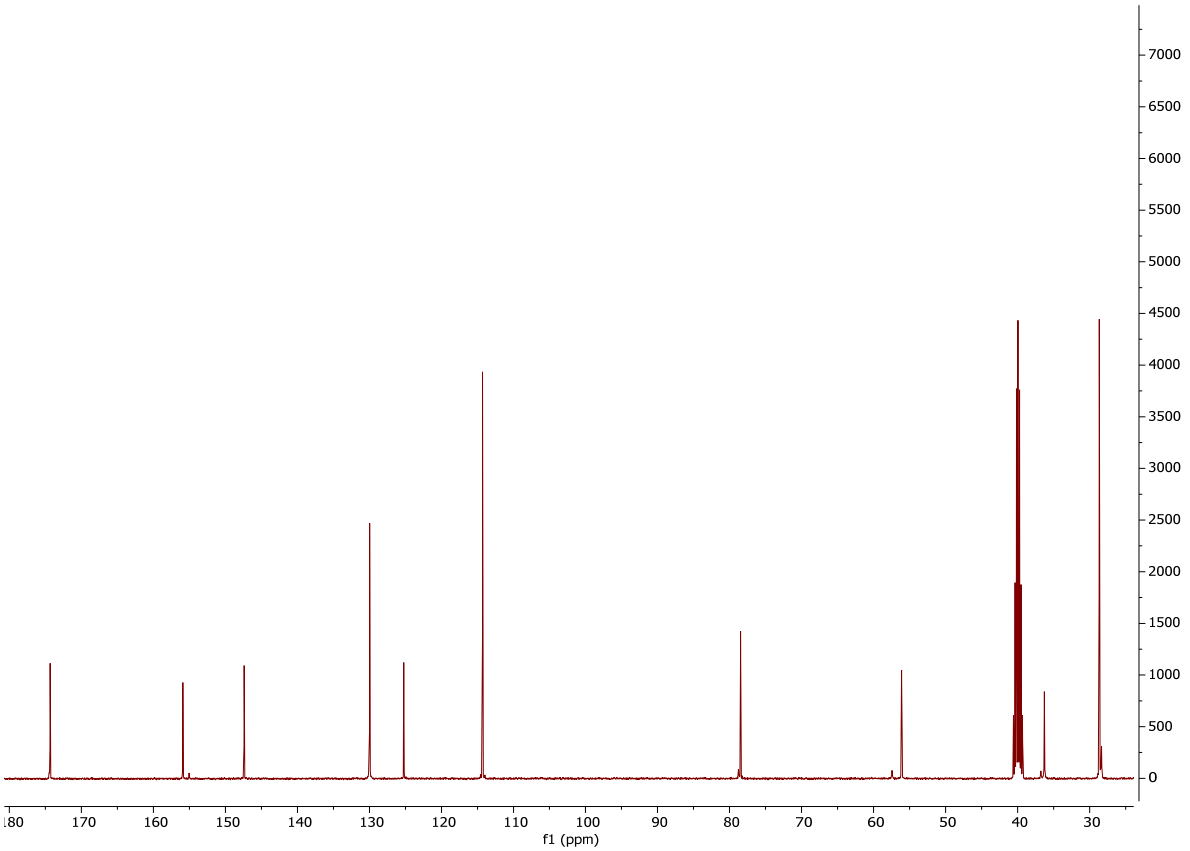

Figure 3.8: ^{13}C-NMR of **3.7**

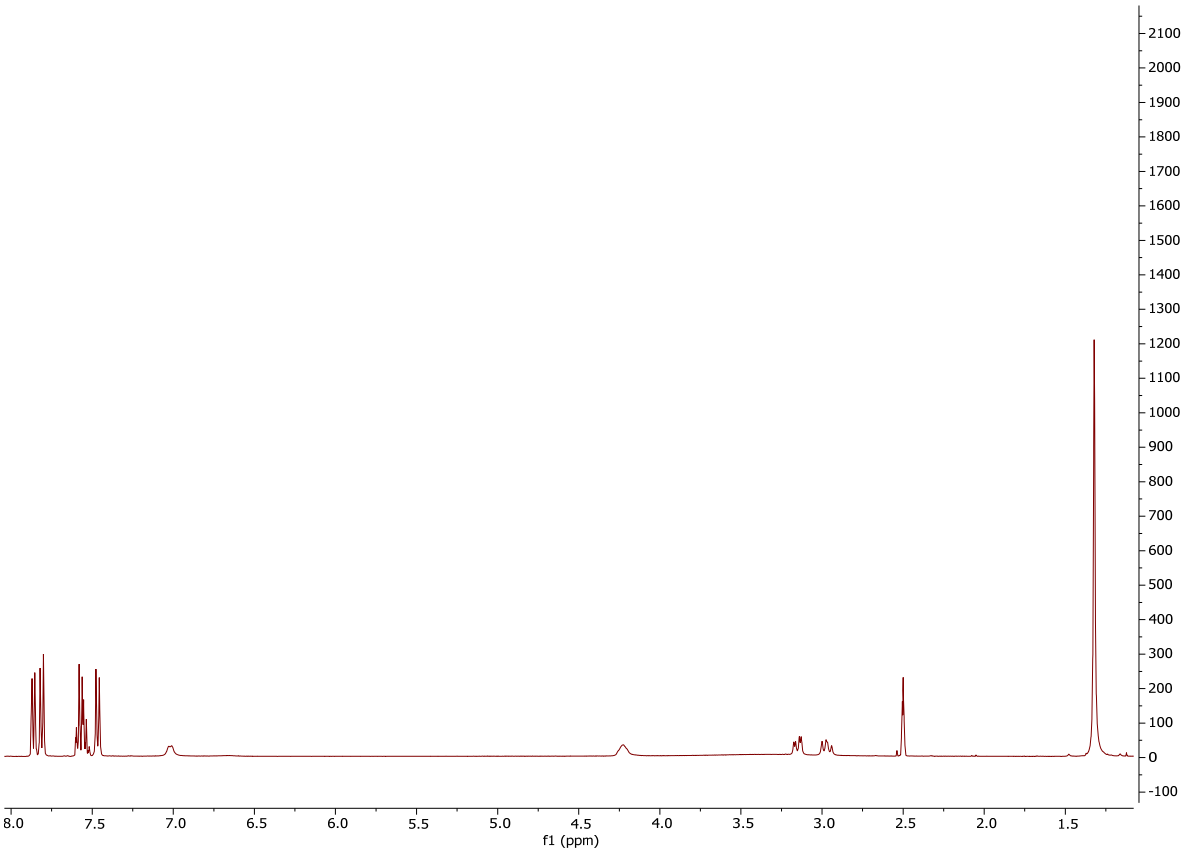

Figure 3.9: ^{1}H-NMR of **3.8**

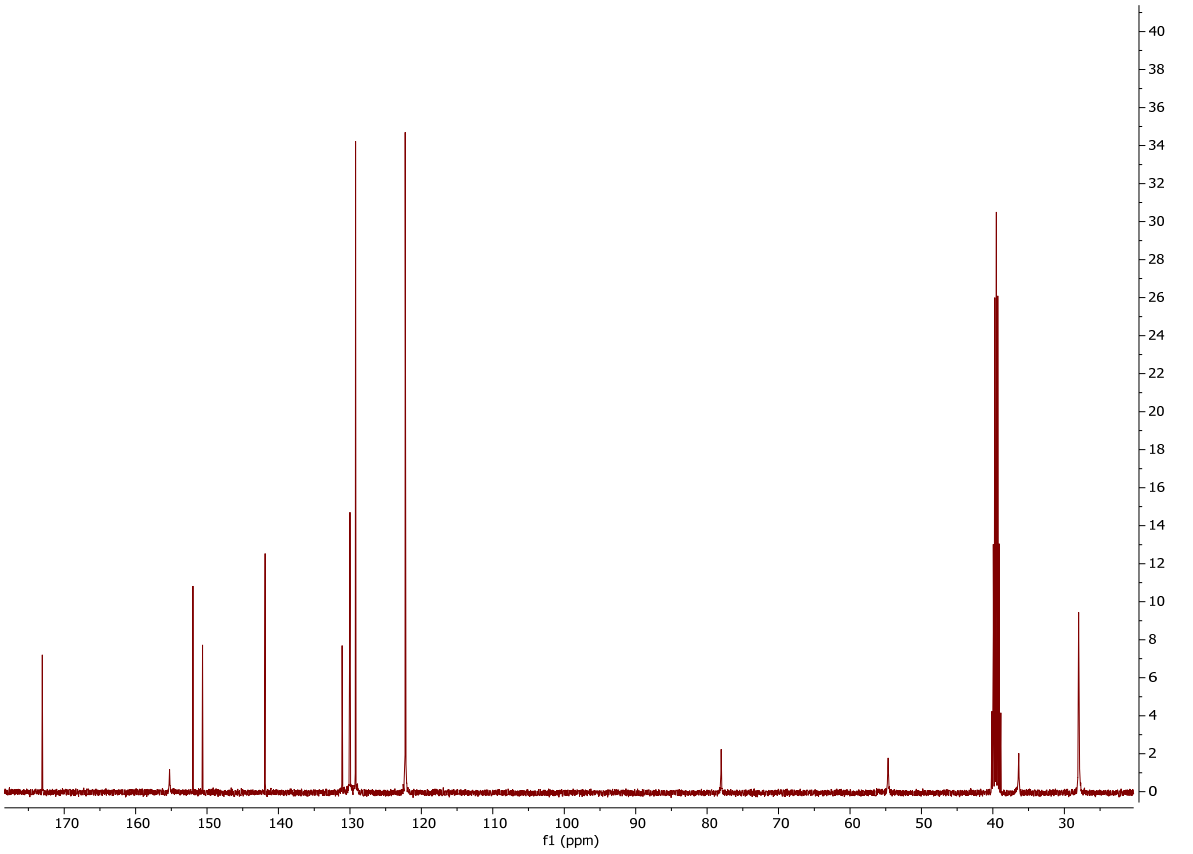

Figure 3.10: ^{13}C-NMR of **3.8**

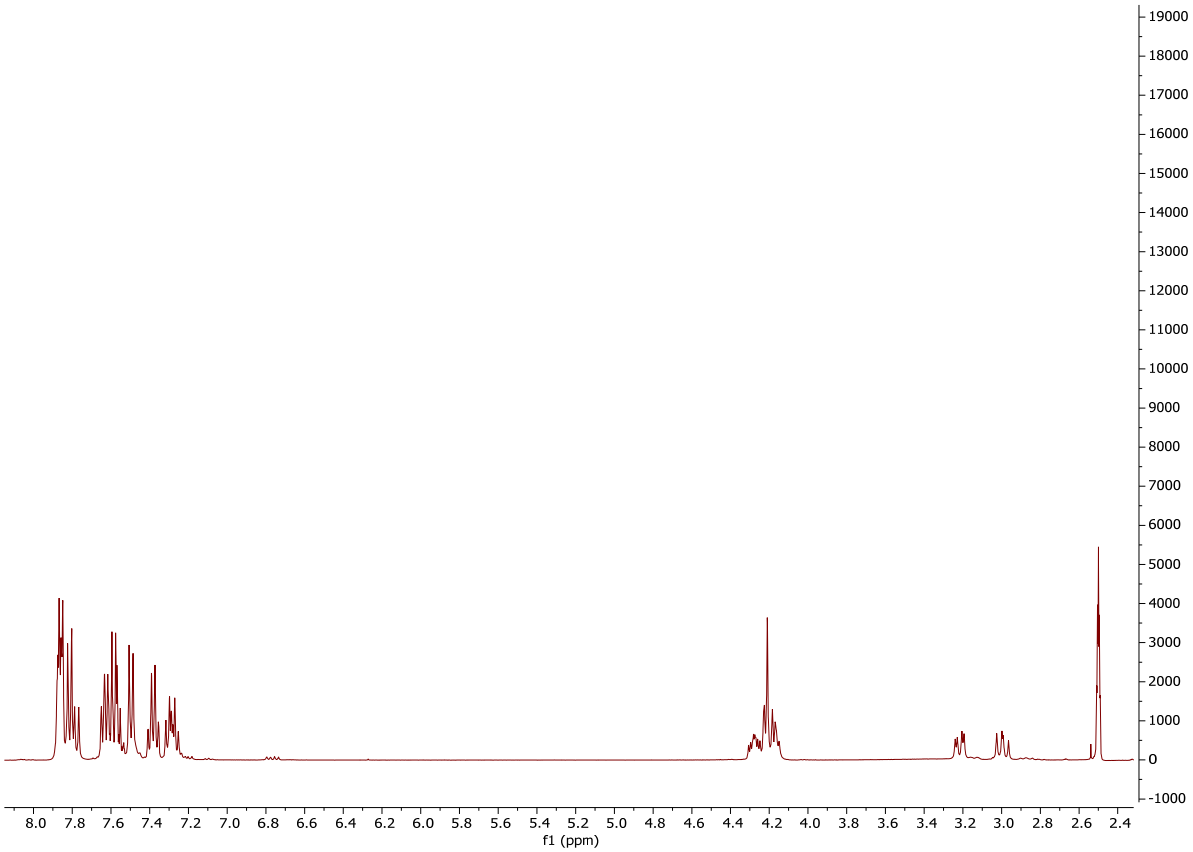

Figure 3.11: ^{1}H-NMR of **3.3**

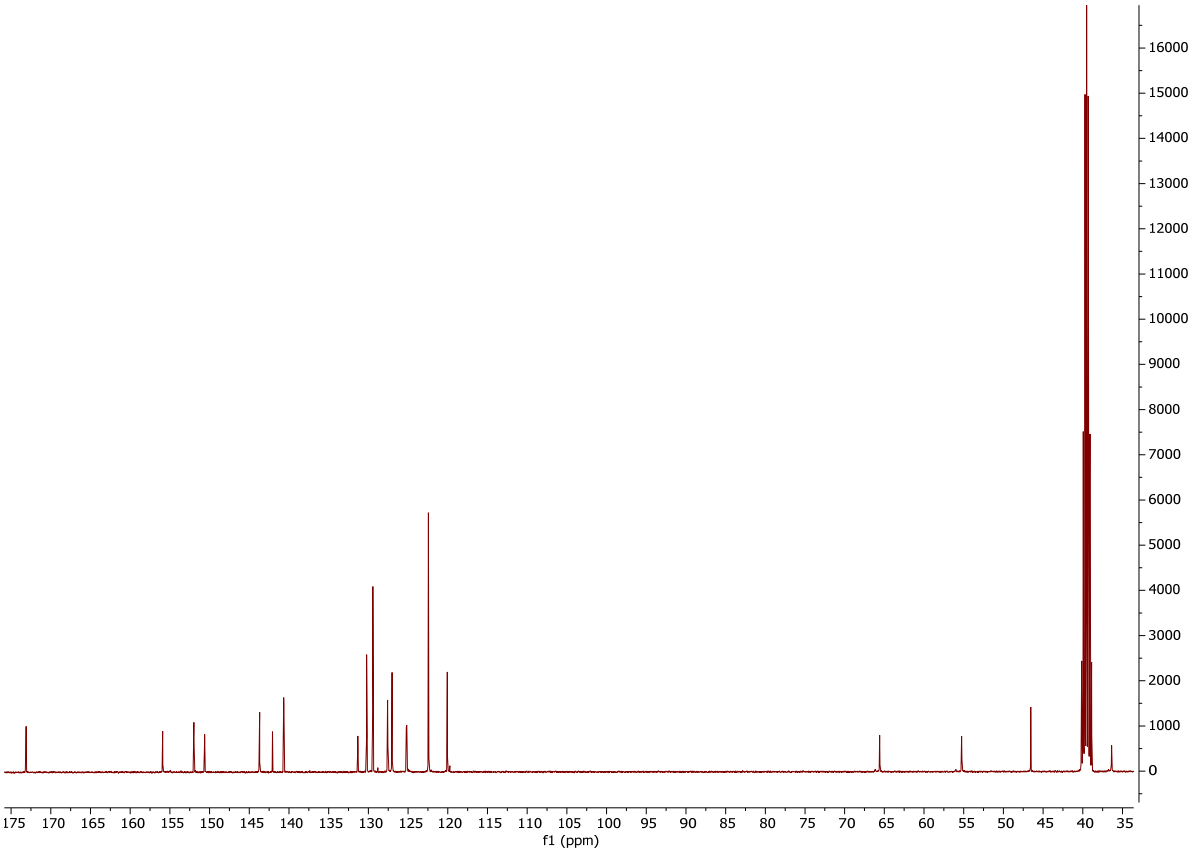

Figure 3.12: ^{13}C-NMR of **3.3**

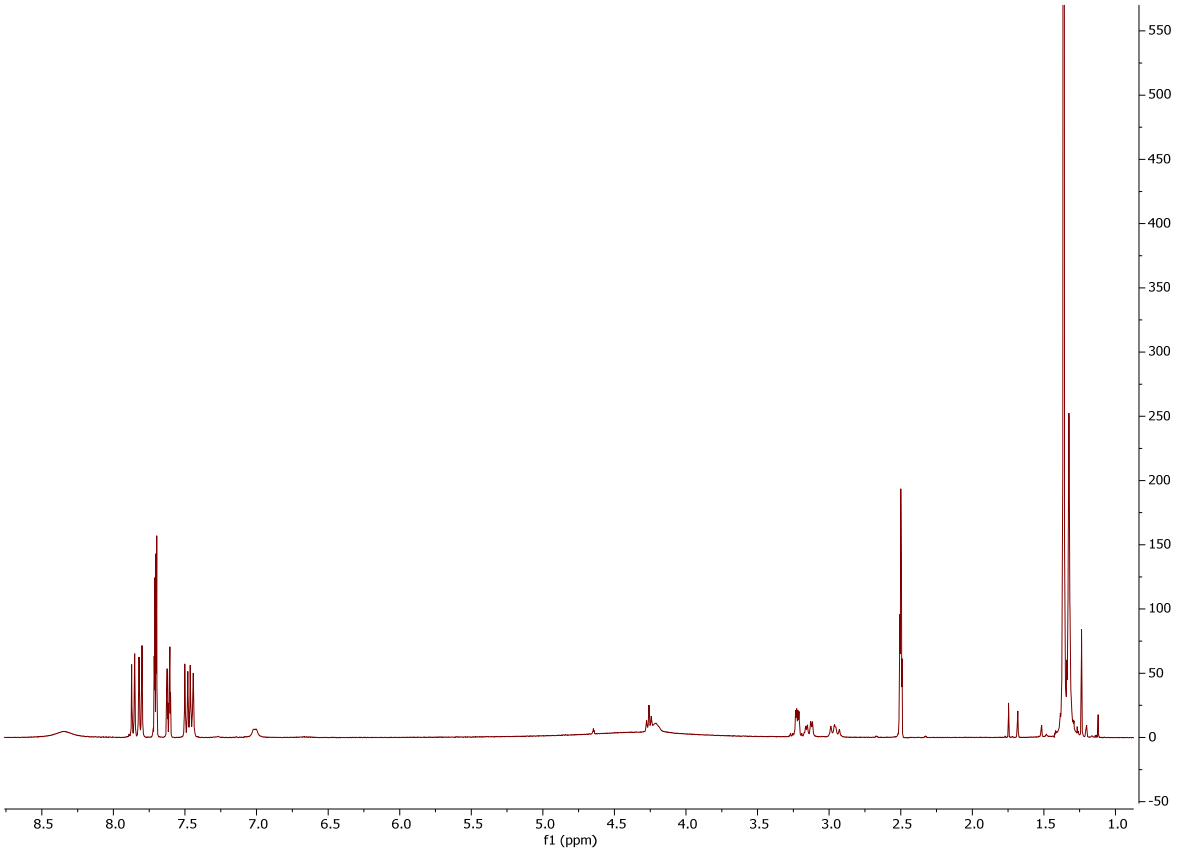

Figure 3.13: ^{1}H-NMR of **3.11**

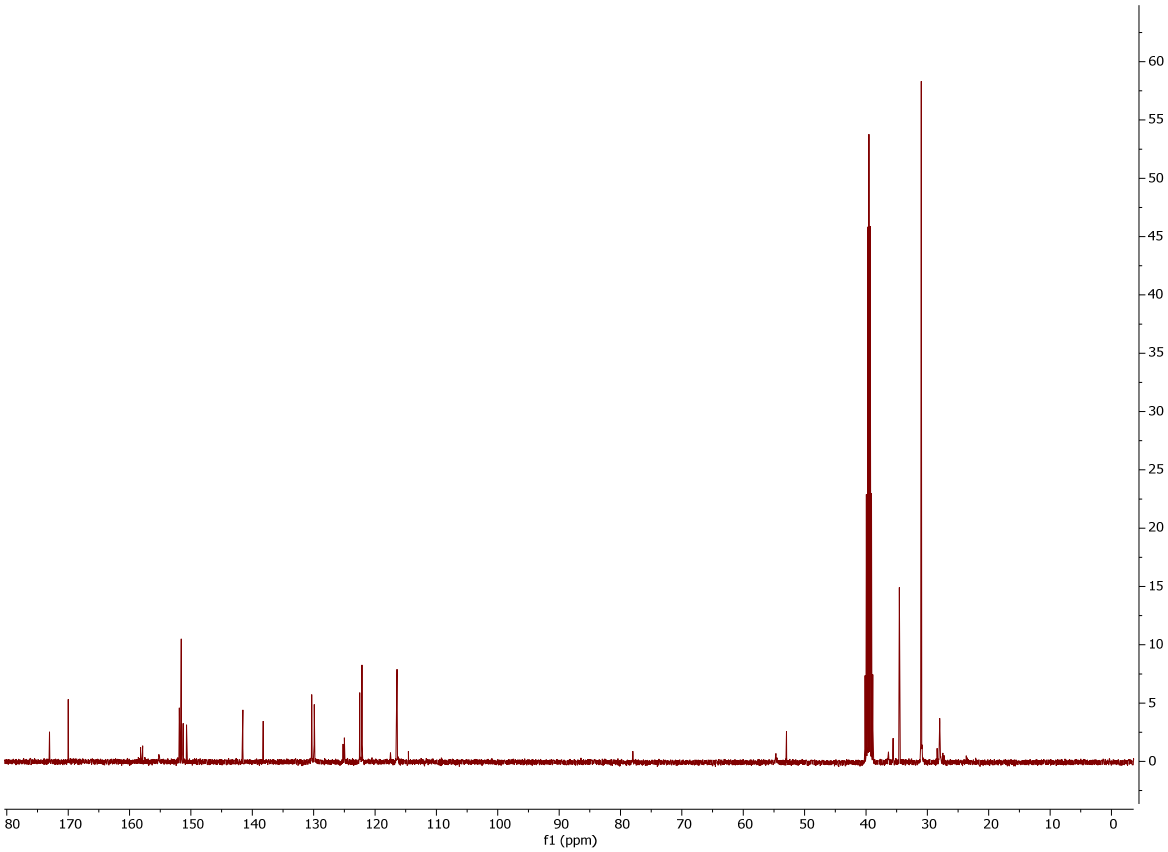

Figure 3.14: ^{13}C-NMR of **3.11**

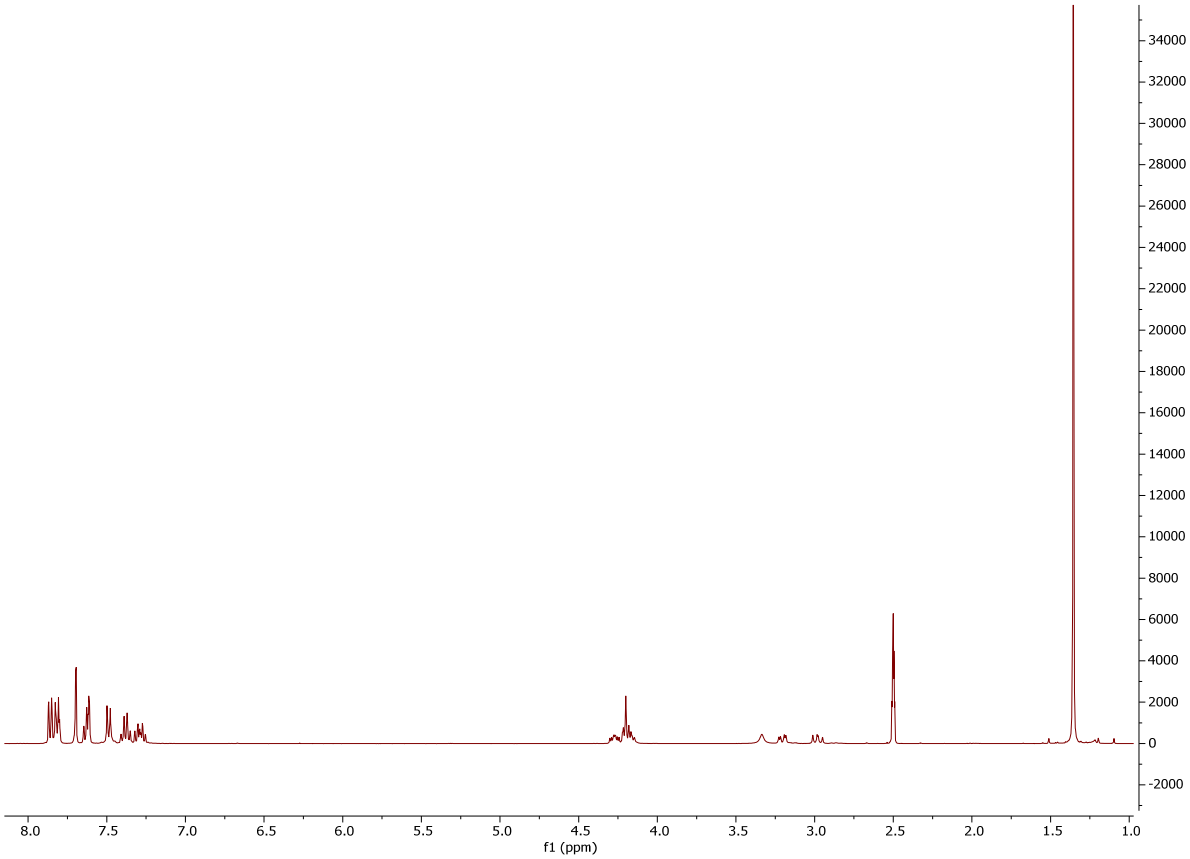

Figure 3.15: ^{1}H-NMR of **3.9**

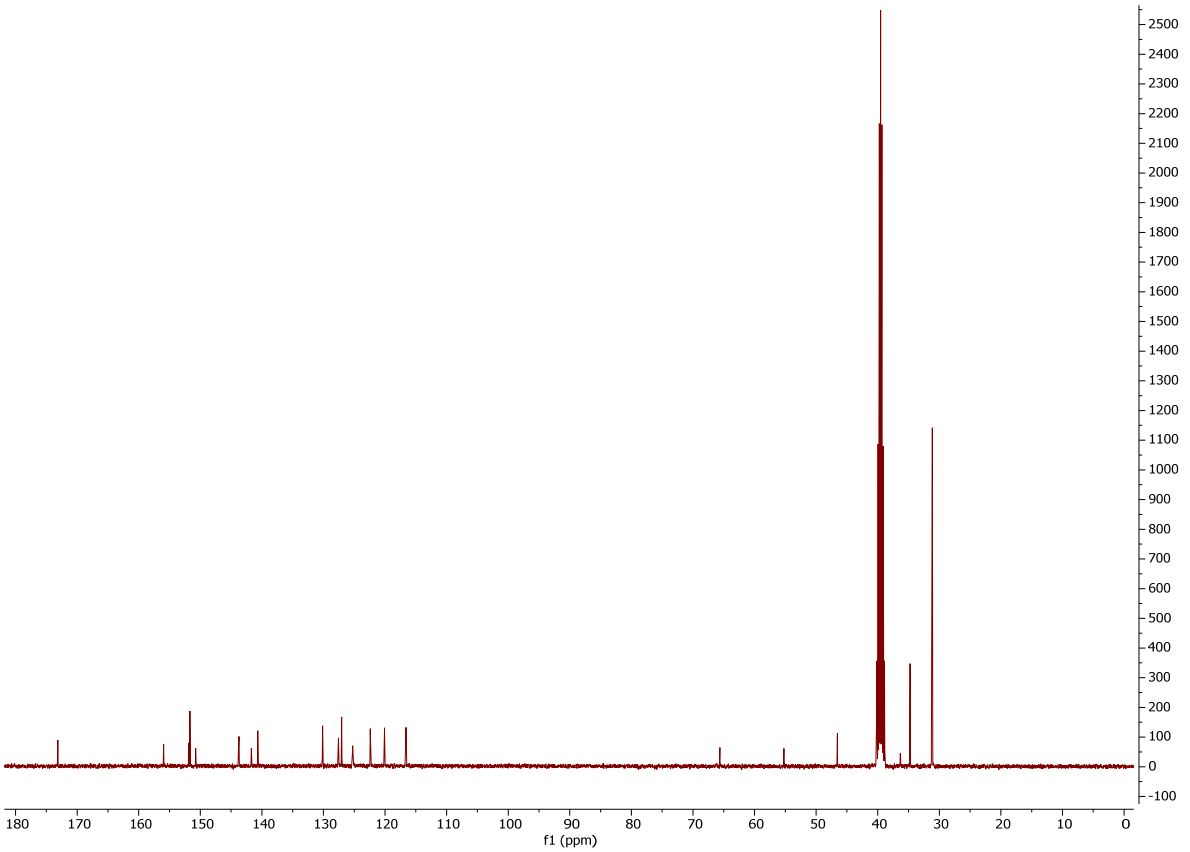

Figure 3.16: ^{13}C-NMR of **3.9**

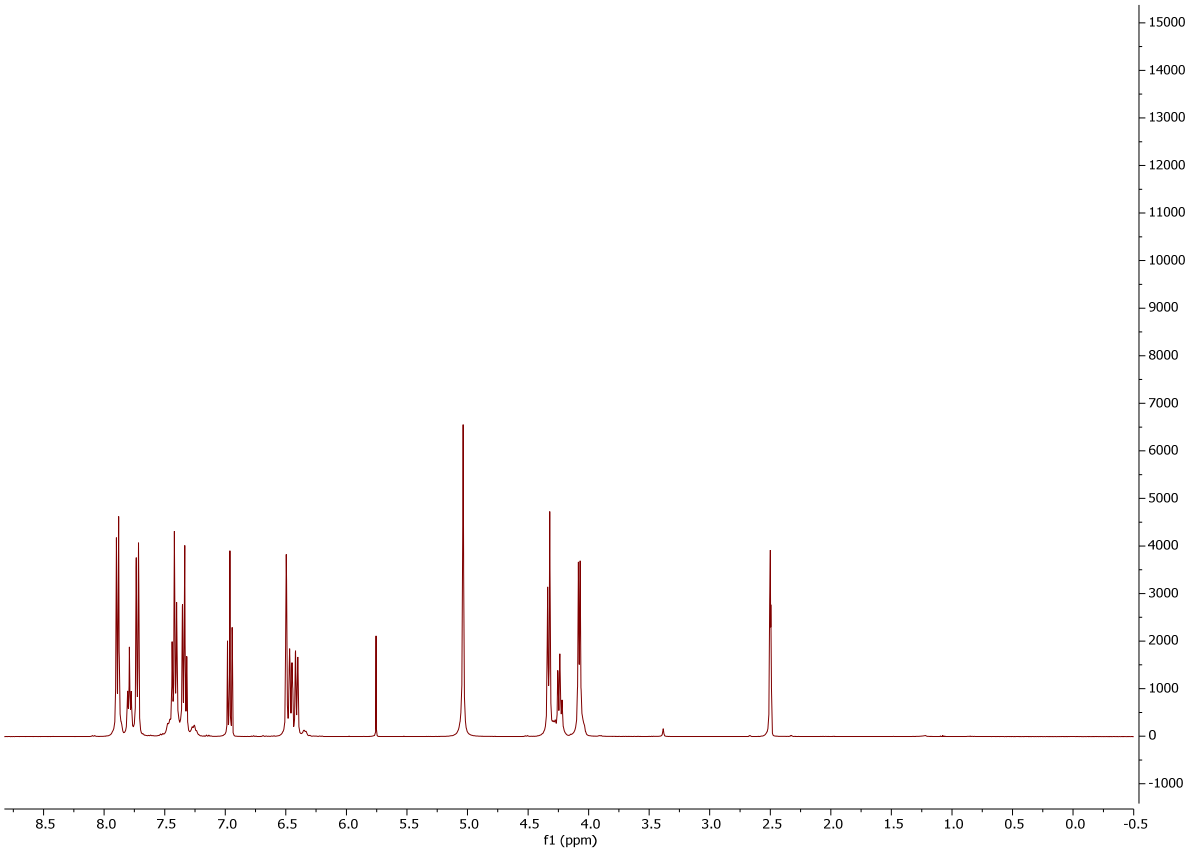

Figure 3.17: ^{1}H-NMR of **3.15**

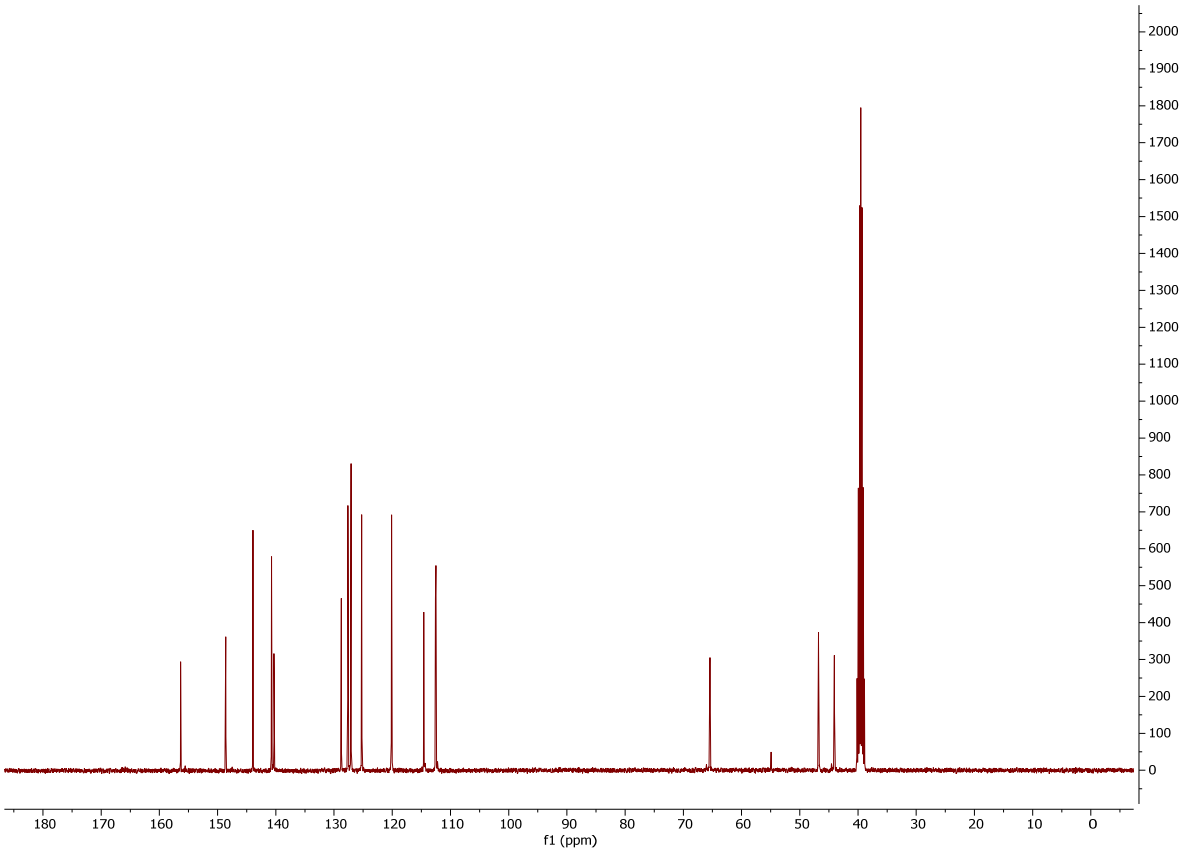

Figure 3.18: ^{13}C-NMR of **3.15**

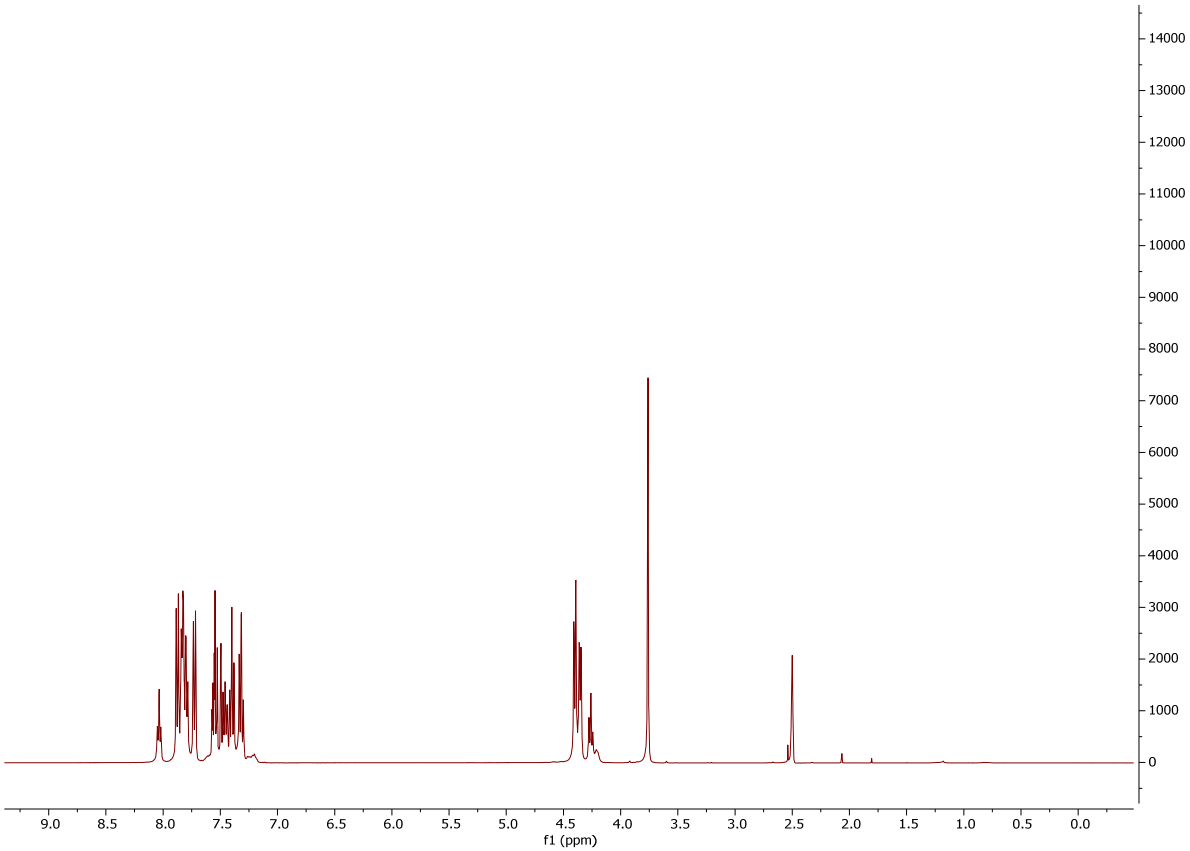

Figure 3.19: ^{1}H-NMR of **3.1**

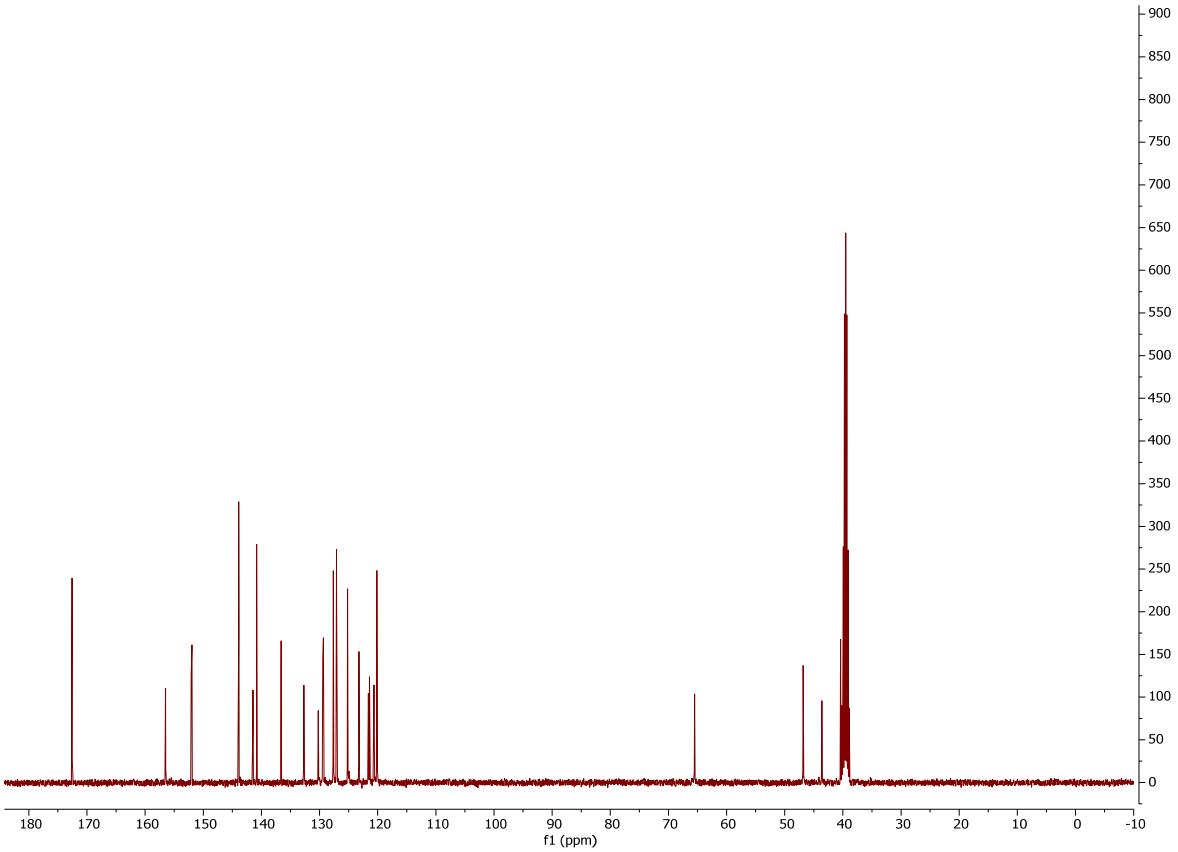

Figure 3.20: ^{13}C-NMR of **3.1**

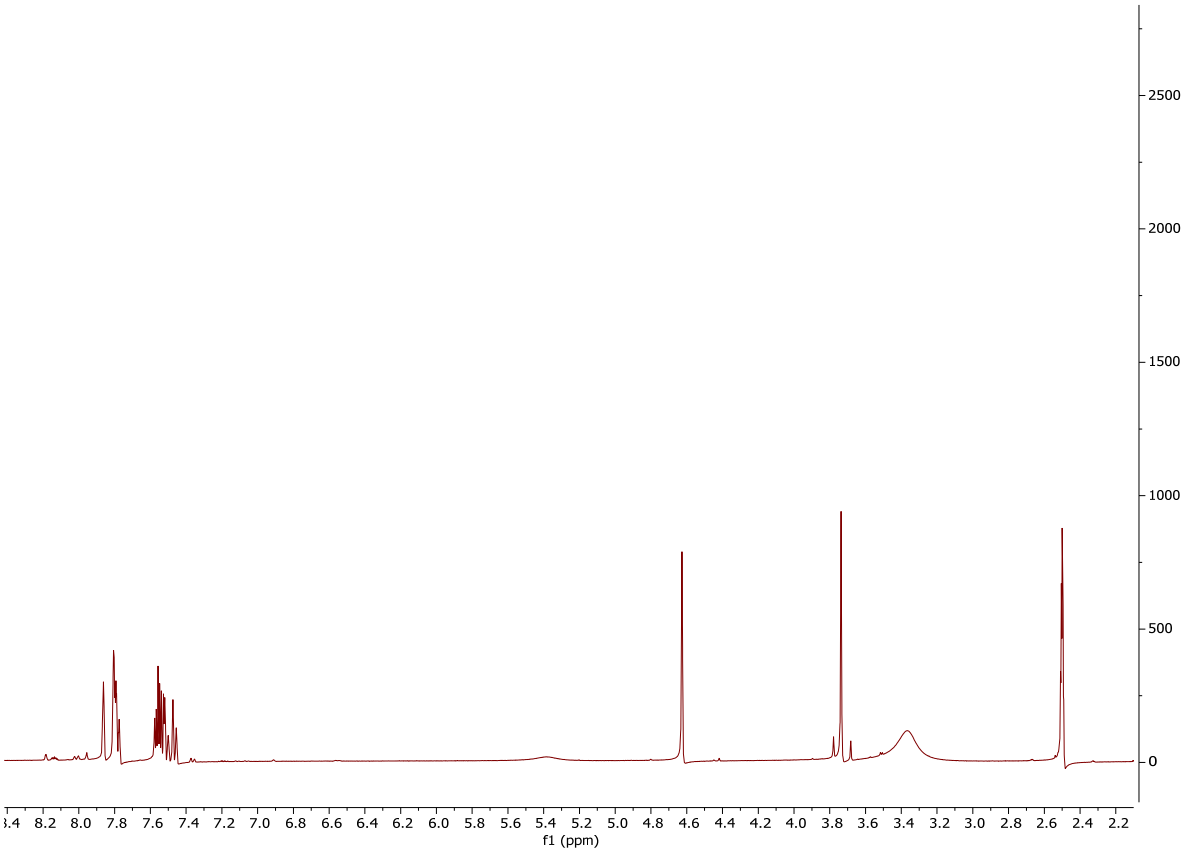

Figure 3.21: ^{1}H-NMR of **3.18**

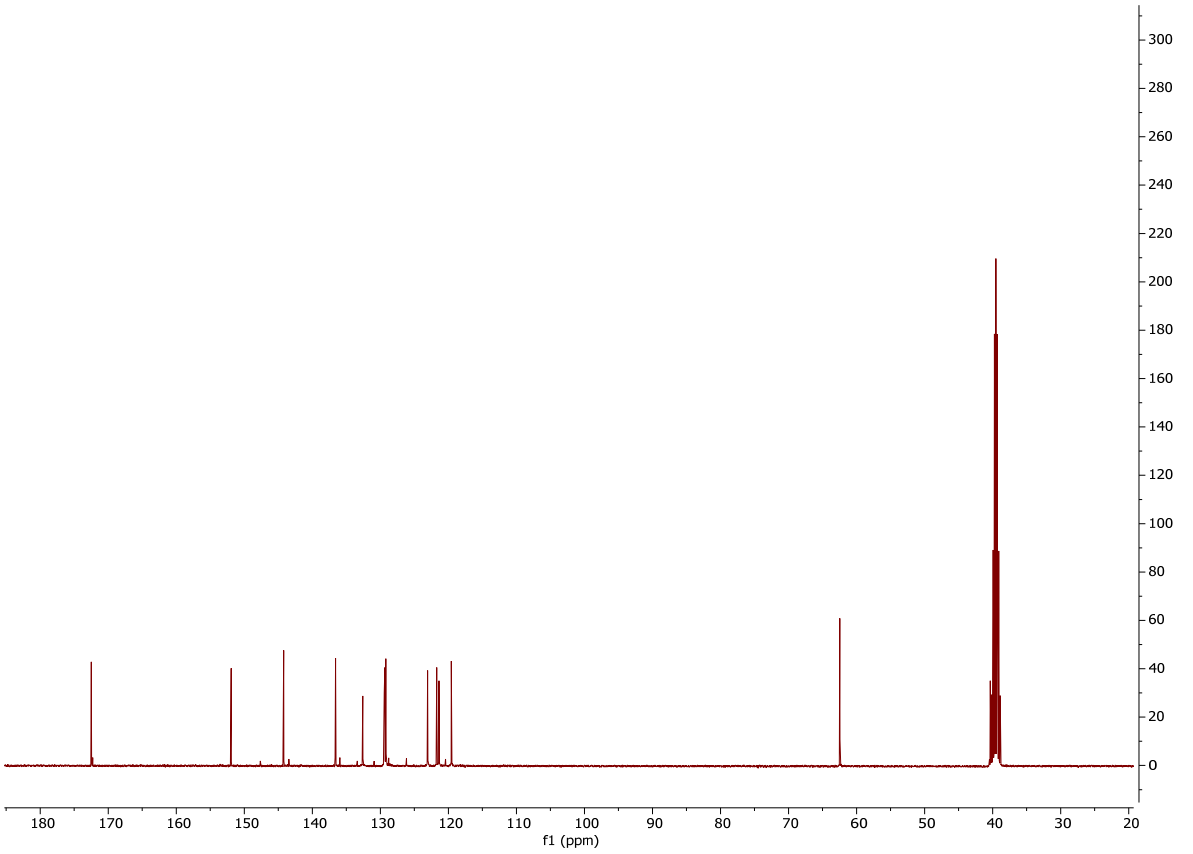

Figure 3.22: ^{13}C-NMR of **3.18**

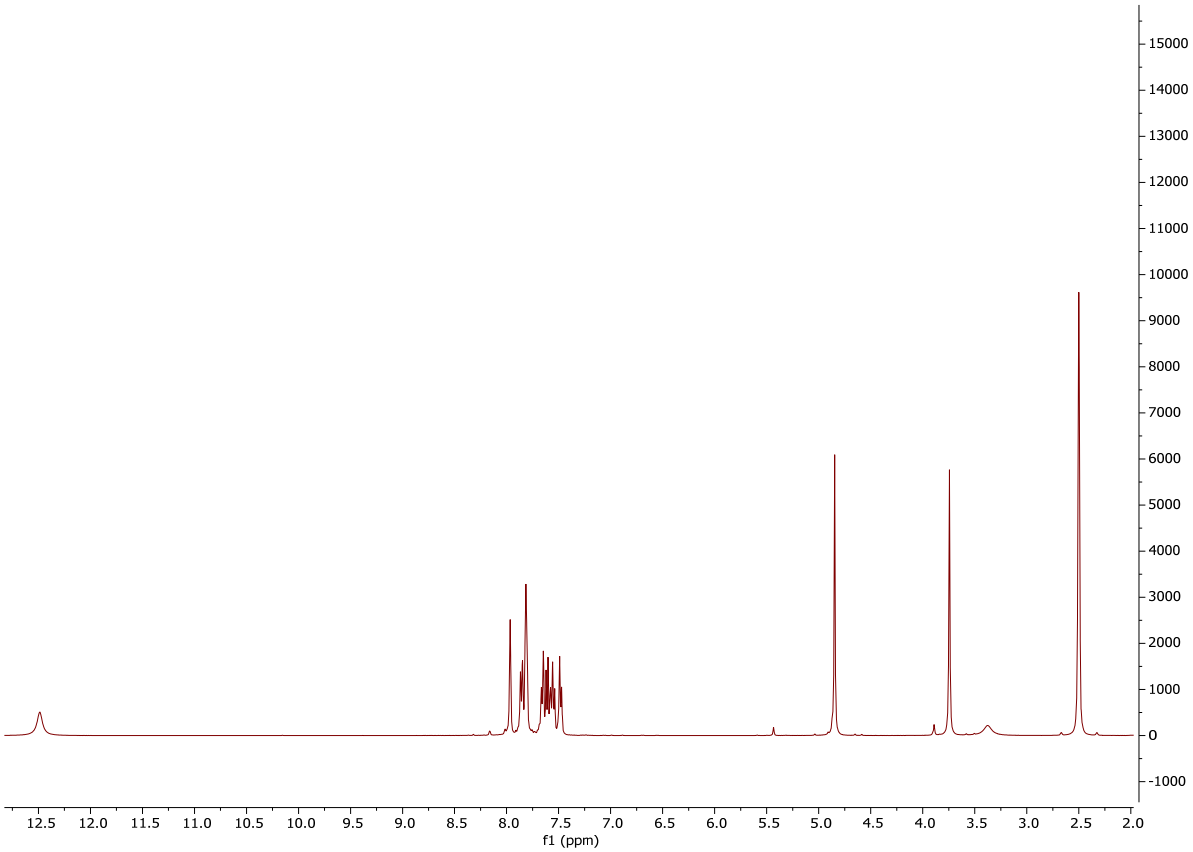

Figure 3.23: ^{1}H-NMR of **3.16**

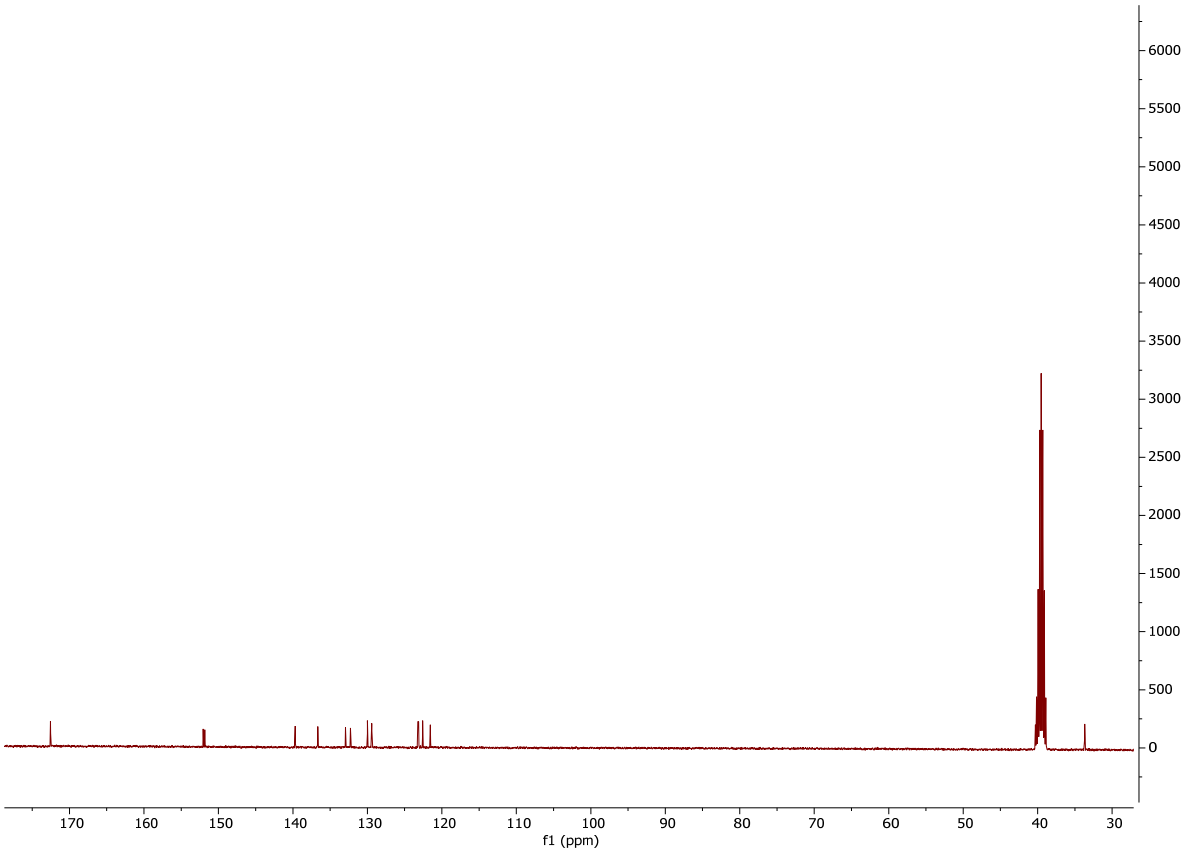

Figure 3.24: ^{13}C-NMR of **3.16**

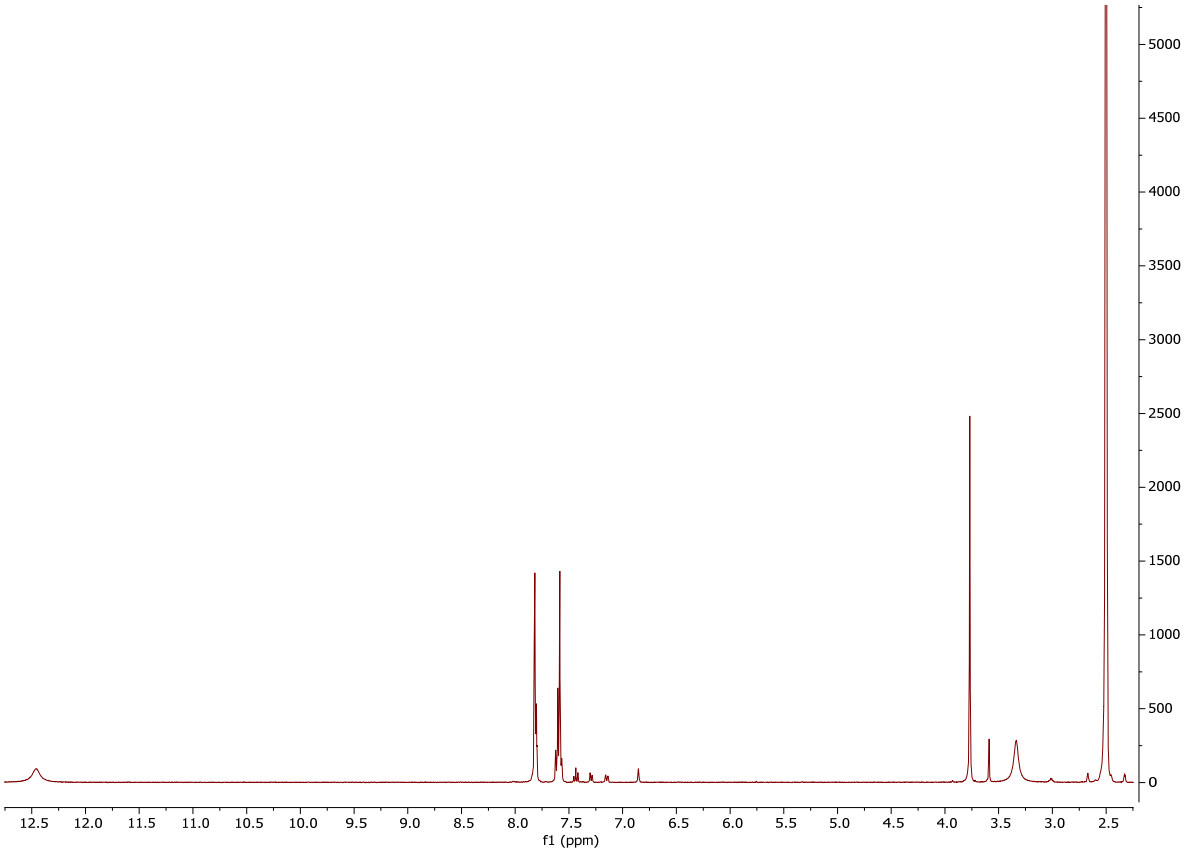

Figure 3.25: ^{1}H-NMR of **3.19**

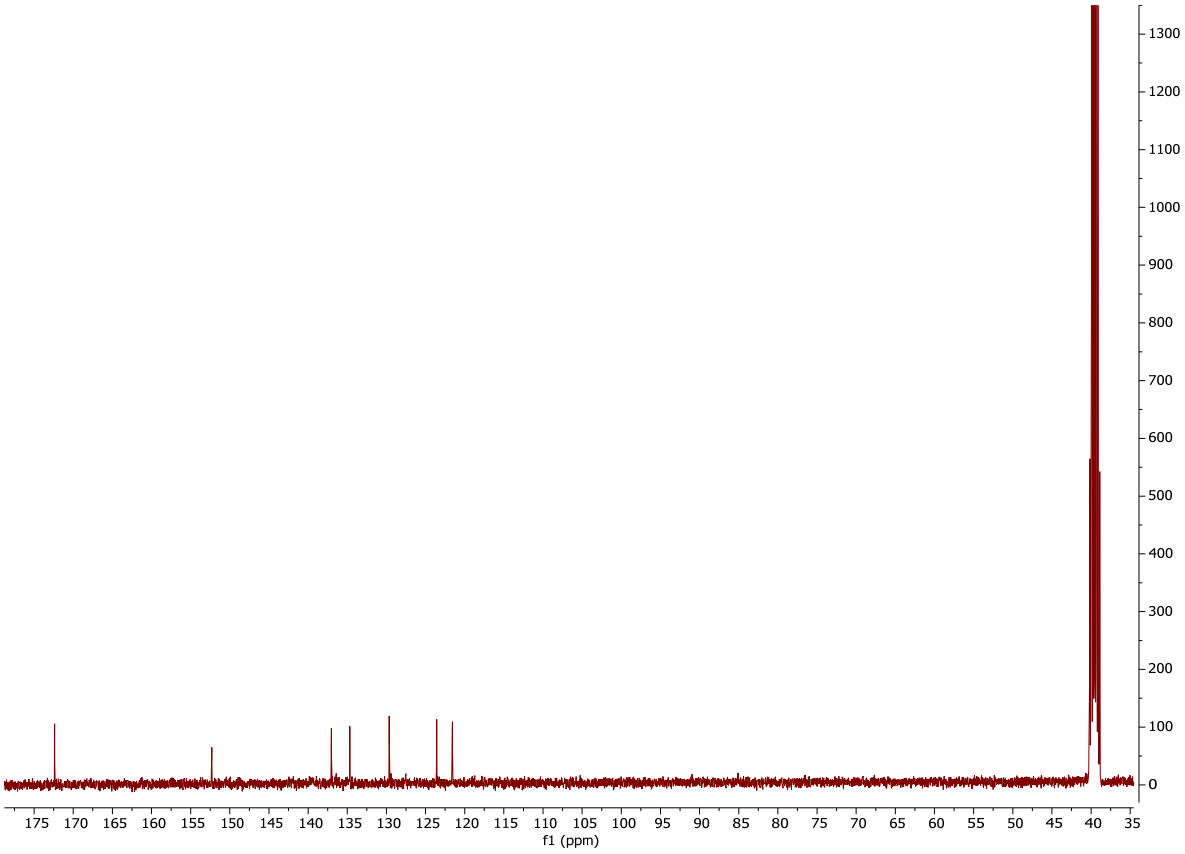

Figure 3.26: ^{13}C-NMR of **3.19**

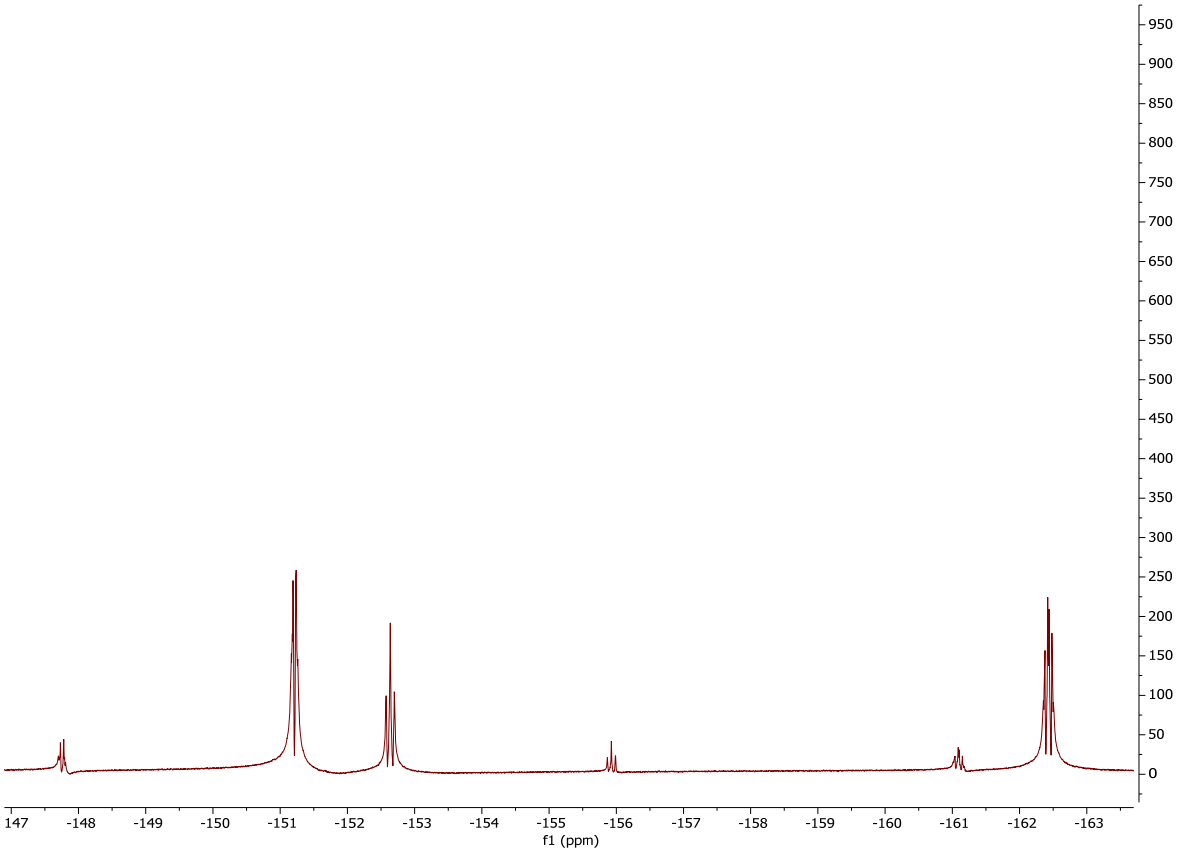

Figure 3.27: ^{19}F-NMR of **3.19**

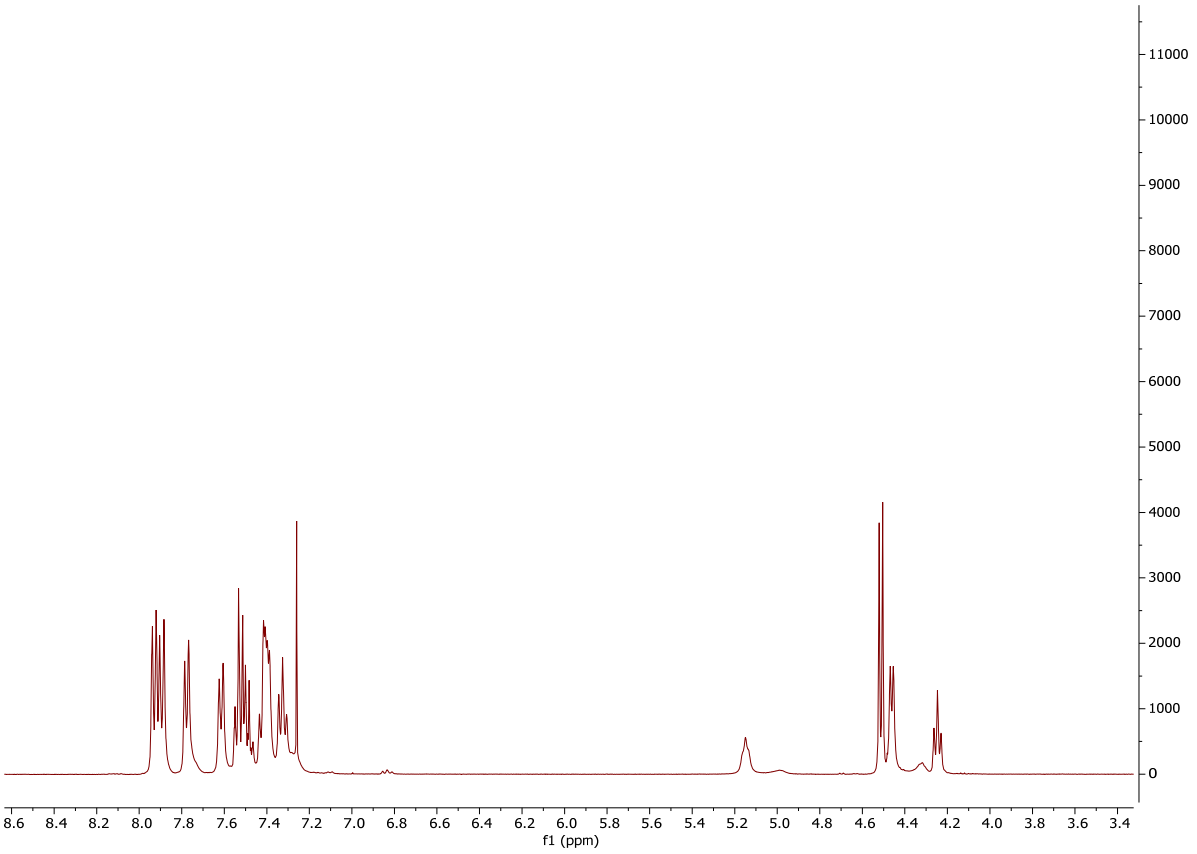

Figure 3.28: ^{1}H-NMR of **3.25**

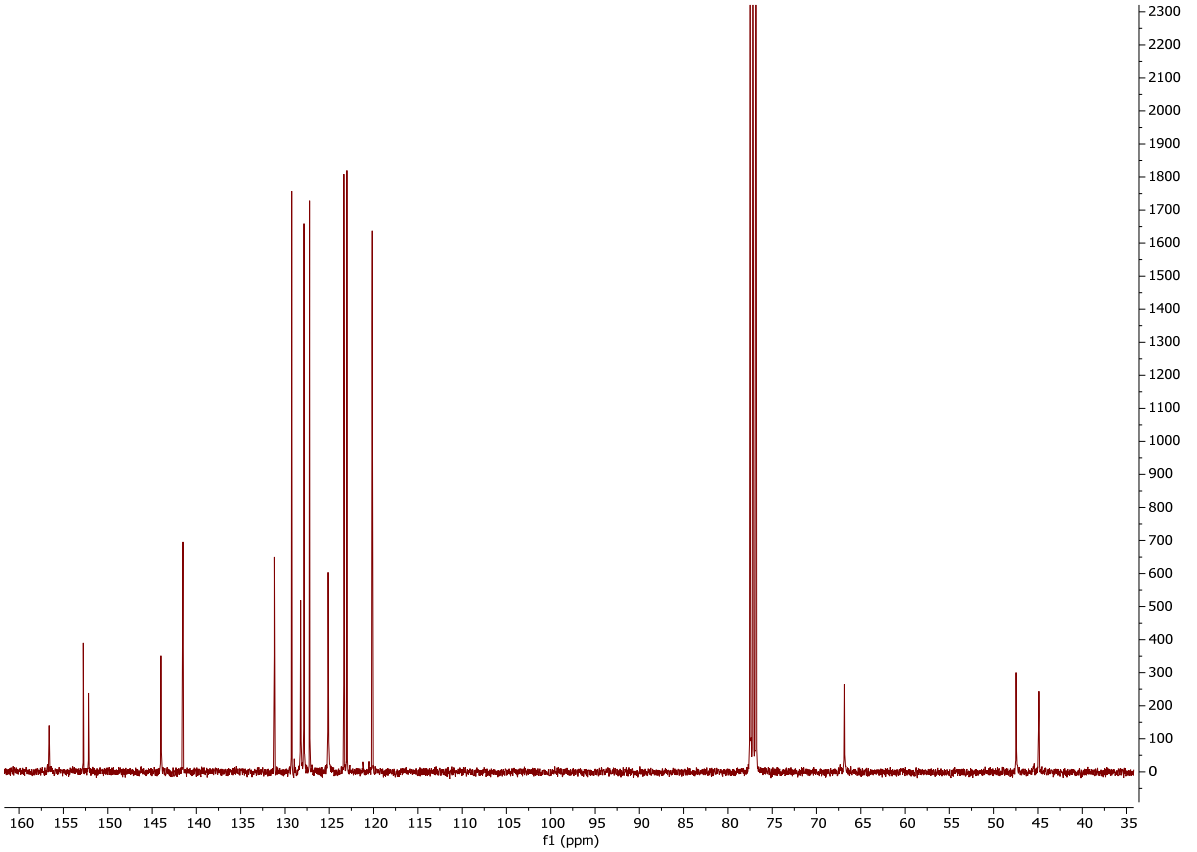

Figure 3.29: ^{13}C-NMR of **3.25**

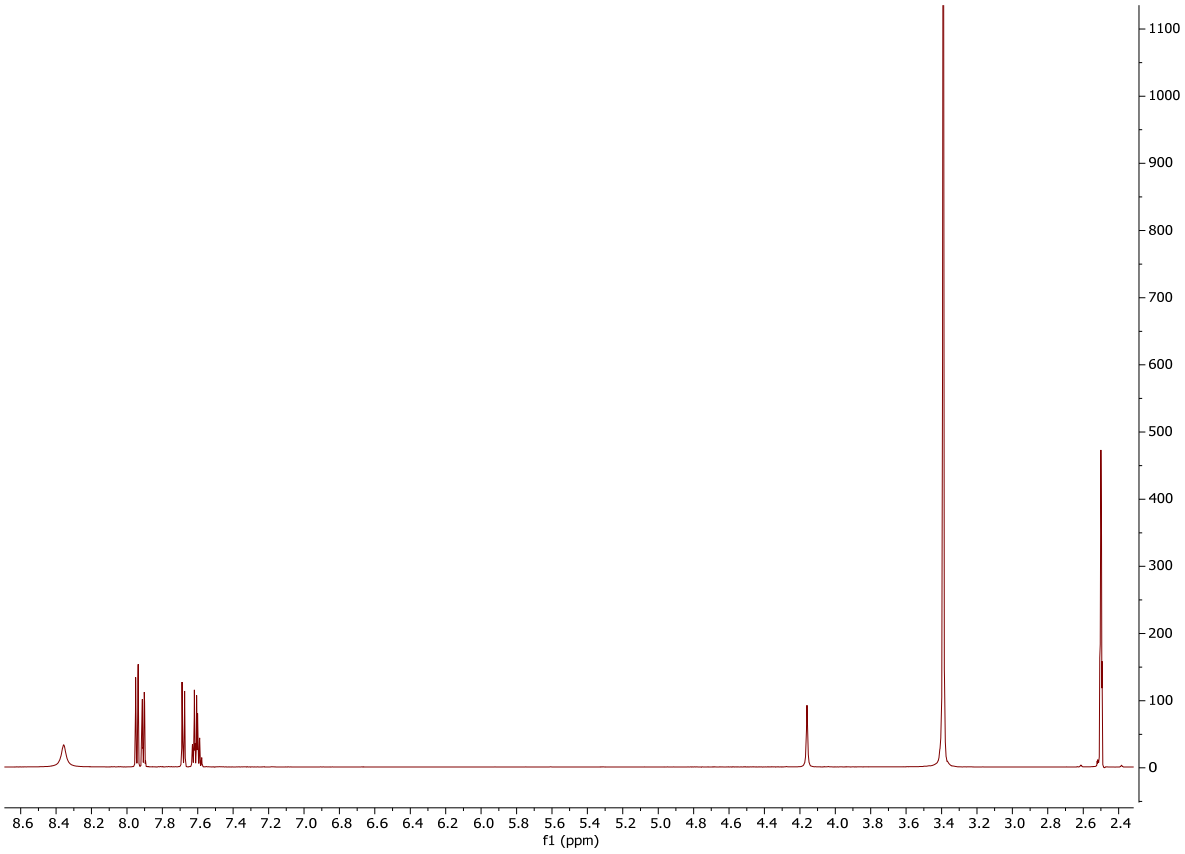

Figure 3.30: ^{1}H-NMR of **3.22**

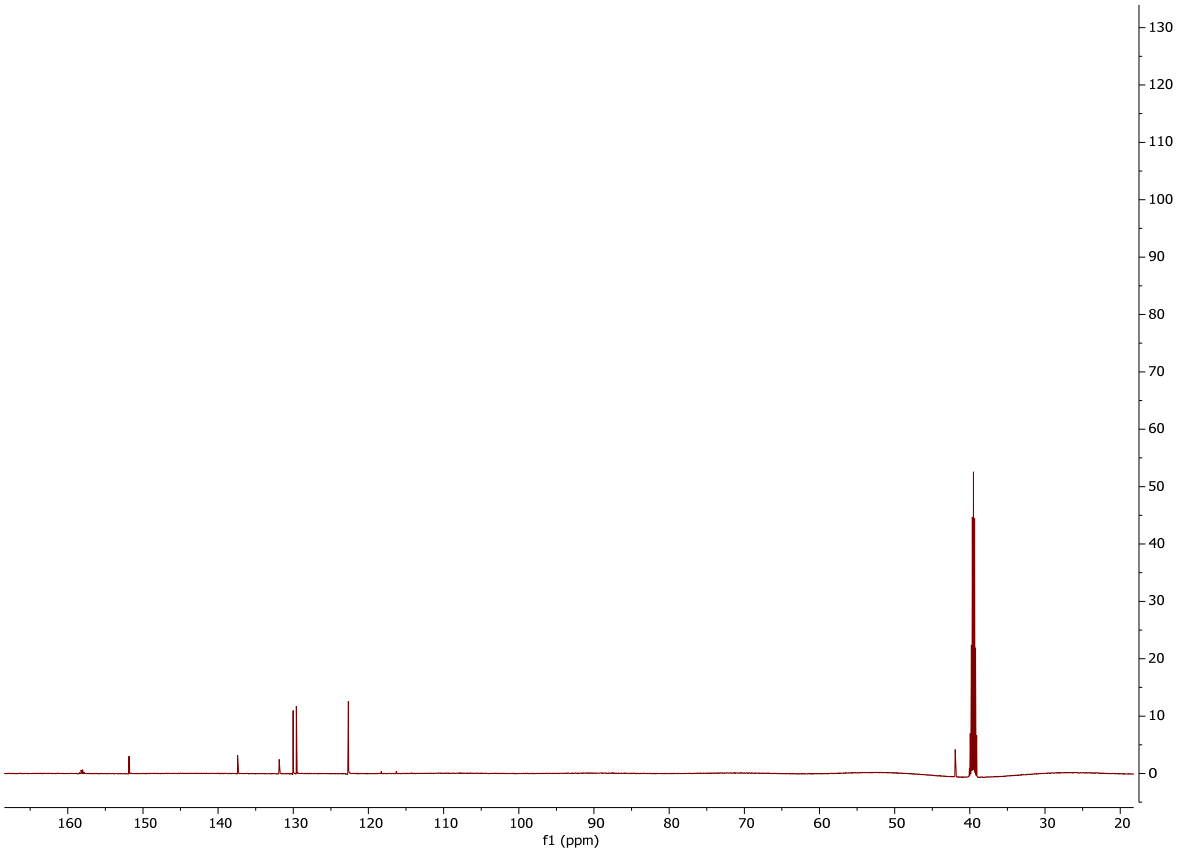

Figure 3.31: ^{13}C-NMR of **3.22**

3.4 Photoswitchable Ligands for the Oxytocin receptor

3.4.1 Short introduction

In 1955 Vincent du Vigneaud received the Nobel Prize for the isolation and synthesis of the hormones Oxytocin (OT) and Vasopressin (AVP). Over 65 years later, the Oxytocin receptor is still subject of ongoing research on a wide area of disciplines. Synthesized in the magnocellular neurons of the hypothalamus, Oxytocin is directly secreted into the brain and it is delivered over the posterior pituitary gland into the blood.[222-224] Due to the coupling of the Oxytocin receptor (OXTR) to different G protein subtypes (G_q, G_i and G_o)[225], ligand binding can have diverse effects on the excitability of cells via activation or inhibition of ion channels.[226] During labour it causes contraction of the uterine smooth muscles,[16] giving it the name Oxytocin (Greek for "quick birth"), and later, triggered by suckling of the newborn, contraction of the mammary myoepithelium takes place during lactation.[227] As a neurotransmitter, it plays an important role any many kinds of social behaviour. Social bonding and anxiety, social memory, trust and affiliation in connection with oxytocin have been in the focus of behavioral research for more than twenty years.[17, 228] Besides its use in labour and especially in case of postpartum haemorrhage, medication of neurodevelopmental and psychiatric disorders like schizophrenia and autism with this hormone is in research[229]; however there are several drawbacks with this form of treatment. Oxytocin has a short half-life ($3 - 6$ min)[201], intravenous administration for the treatment of neurodevelopmental and psychiatric disorders fails as it does not cross the blood brain barrier in a significant amount[230] and third, it shows a low selectivity towards the OXTR vs. the related Vasopressin receptors (V1aR, V1bR and V2R) at higher concentrations[231].

3.4.2 G protein coupled receptors

The G protein coupled receptors (GPCR) are the largest receptor family in eukaryotes.[232, 233] Next to hormones, neurotransmitters and drugs, GPCRs can be stimulated by light and odours and thus they are responsible for intracellular communication and processing environmental influences.[234, 235] They are divided into five classes: the adhesion family, the frizzled family, the secretin family, the glutamate family and the rhodopsin family which is the largest one.[236] Consisting of seven transmembrane helices, GPCRs build up a system of three intracellular loops with the *N*-terminus, a transmembrane hydrophobic region and three extracellular loops with the *C*-terminus.[237, 238] Next to the intracellular part, a heterotrimeric G protein, responsible for the downstream signalling process, is attached to the plasma membrane by lipid anchors.[239]

The G protein is built up by an α-, a β- and a γ-subunit, while the last two form a stable dimer. These subunits convey the downstream signaling process in the intracellular space. GPCRs are not typical on-off switches; hence, there is an equilibrium of both states. This basal activity can be shifted upon binding of ligands, to the active state by full or partial agonists, or to the inactive state by inverse agonists (Figure 3.32). In contrast, neutral antagonists preserve the equilibrium and hinder the receptor binding site to bind endogenous ligands and inverse agonists shifts the activity below the basal state.[237, 240]

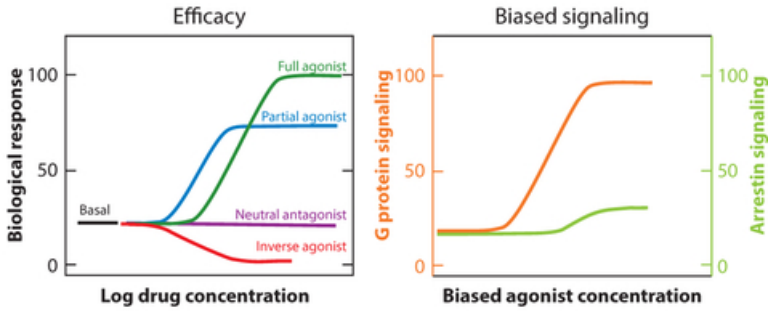

Figure 3.32: Efficacy of different ligands (left) and biased signaling of agonists (right).[240]

There are four different Gα subclasses, $G\alpha_s$, $G\alpha_{i/o}$, $G\alpha_{(11/12)}$ and $G\alpha_{(q/11)}$ and each of them activates a different downstream process.[241] OXTR is mainly bound by $G\alpha_{(q/11)}$[242], why this signalling process is discussed in more detail.

Binding of an agonist causes a structural shift of the transmembrane helices. In consequence, guanosine diphosphate (GDP) is released from the α-subunit and binding of guanosine triphosphate (GTP) results in the dissociation of the βγ-heterodimer. Both parts of the G protein take part in the following downstream processes. While βγ-heterodimer activates ion channels, the α-subunit activates the phospholipase C (PLC) which cleaves phosphatidylinositol 4,5-bisphosphate into diacylglycerol (DAG) and inositoltriphosphate (IP_3). DAG then activates proteinkinase C (PKC), which in turn leads to contraction or cell adhesion (vie Rho-mediated Rho kinase) or cell growth (via eukaryotic elongation factor, eEF2). IP_3 binds to the inositoltriphosphate receptor ($InsP_3R$) causing Ca^{2+}-release from the endoplasmic reticulum (RER). Ca^{2+} binds to Calmodulin and the Ca^{2+}-complex activates three different enzymes. First, the myosin light-chain kinase (MLCK), resulting in a contraction of the muscle in the uterus or of mammary myoepithelial cells. Second, MLCK activates the phosphoinoitide-3-kinase (PI3K) which improves both, cell survival and migration and influences bone trophic effects.

At least, MLCK activates the nitric oxide synthase (NOS) linked to vasodilation (Figure 3.33).[243-245]

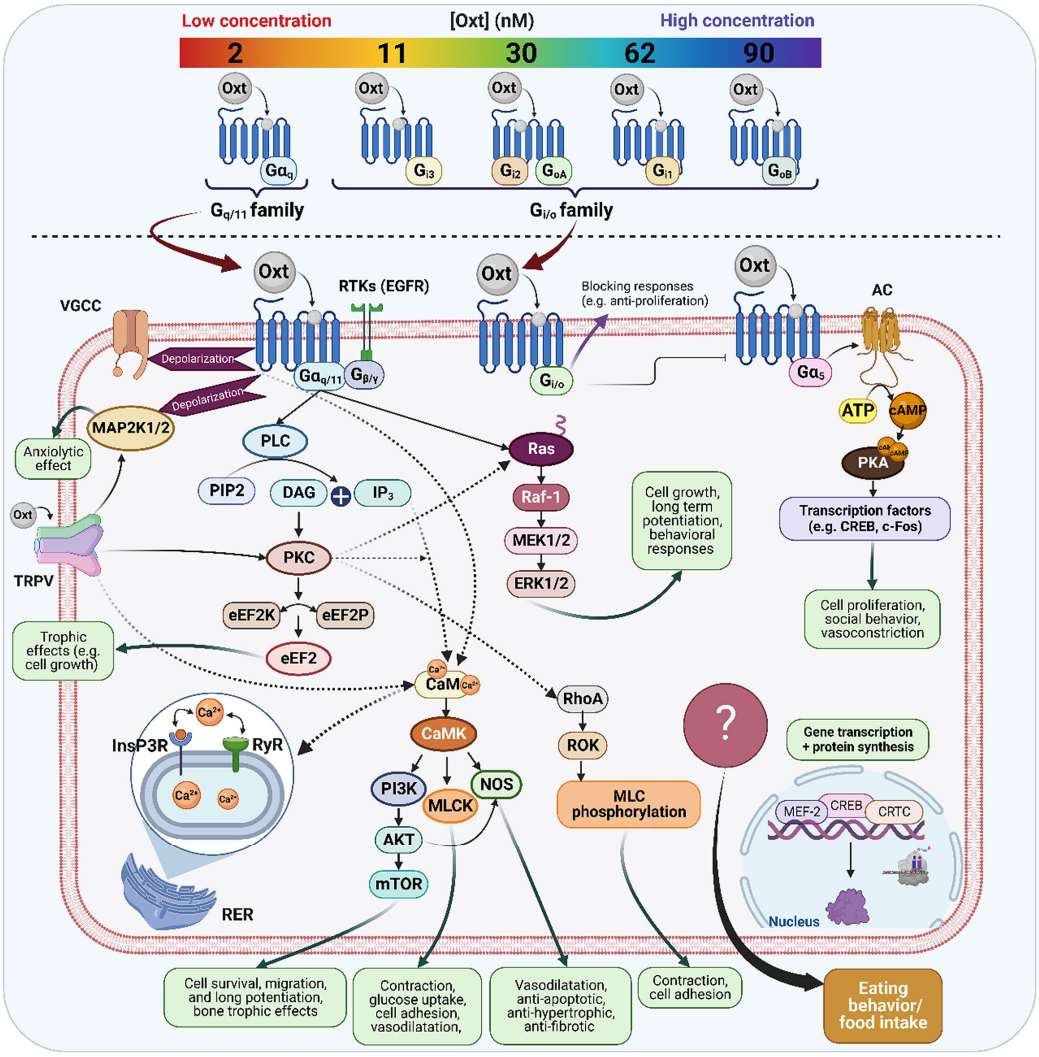

Figure 3.33: Cellular response upon ligand binding of OXTR.[246]

Although $G\alpha_{(q/11)}$ is the OXTR-coupled G protein found in most areas of the brain, some $G\alpha_{i/o}$-isoforms coupled to OXTR are also found in CNS in high concentrations. The signalling pathway of the $G\alpha_{i/o}$ family is different. While $G\alpha_{o}$-isoforms are directly involved in the regulation of ion channels, the $G\alpha_{i}$ isoforms inhibit the adenylate cyclase which results in a decrease of the cAMP concentration. Furthermore, they activate the phosphatidylinositol-4,5-bisphosphate 3-kinase (PI3K) and the mitogen-activated protein kinase (MAPK) pathways.[243, 247]

Nevertheless, next to the ubiquitous expression of $G\alpha_{(q/11)}$, the oxytocin ligand also discriminates strongly between G protein subtypes.[247] The EC_{50} of oxytocin rises from G_q = 2.16 nM, G_{i3} = 11.5 nM, G_{oA} = 29.8 nM; G_{i2} = 32.27 nM; G_{i1} = 62.63 nM to G_{oB} = 91.8 nM.[225]

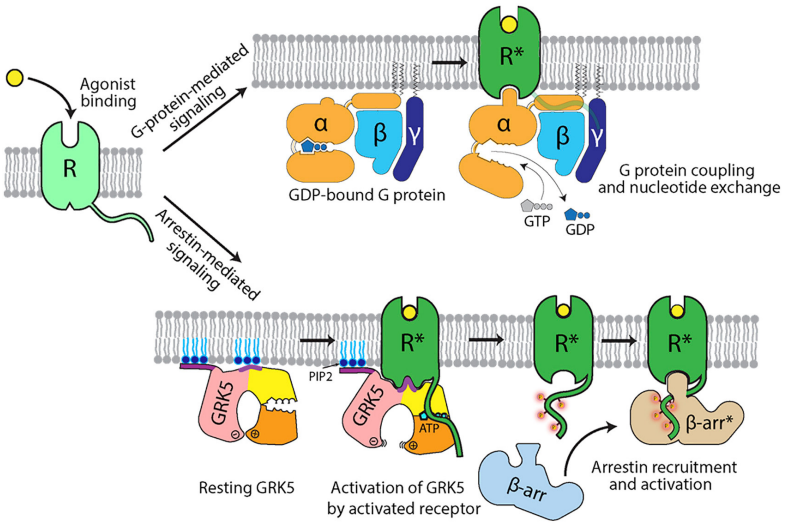

Figure 3.34: Comparison of the classical G-protein pathway and arrestin-mediated signaling.[248]

Besides signalling by G proteins, down-stream signalling can be mediated also by β-arrestins (Figure 3.34).[249] Phosphorylation of the intracellular *C*-tail by GPCR-kinase[250, 251] uncouples the receptor from G proteins, followed by β-arrestin binding[252]. Finally, endocytosis of the receptor leads to dephosphorylation and receptor recycling or degradation.[253] Furthermore, β-arrestins are involved in the desensitisation of the OXTR.[249, 254, 255]

3.4.3 Selectivity of the Oxytocin ligands

OXTR and the Vasopressin receptors (AVPRs) are both seven transmembrane domain G protein coupled receptors of the rhodopsin family. Whereas only one oxytocin receptor exists, three different Vasopressin receptors, V1aR, V1bR and V2R, are known. Their natural ligand vasopressin is involved in antidiuretic actions, regulation of blood pressure and behavior.[256]

Similarities in signalling pathways exist between OXTR and V1aR/V1bR, as they couple to $G\alpha_q$ and $G\alpha_{i/o}$. Additionally $G\alpha_q$ and $G\alpha_{i/o}$, V1bR signaling is also mediated via $G\alpha_s$ signaling pathway.In contrast, V2R is coupled to $G\alpha_s$, which activates the adenylate cyclase, raising the cAMP concentration. [257]

The OXTR shares sequence homologies to V1aR (45%)[258], V1bR (45%)[258] and V2R (40%)[259], with the highest homology in the transmembrane helices and the extracellular loops. The intracellular loops and both termini show lower similarities.[260] Additionally, Oxytocin and Vasopressin are both part of the Vasotocin (VT) family and differ in two single amino acids (Figure 4.35), which means, both peptides share a homology of nearly 80%. Their genes are located on the chromosome 20, close to each other. It is considered, that Vasopressin and Oxytocin evolved by gene duplication from Vasotocin (Figure 4.35) over 400 million years ago.[261]

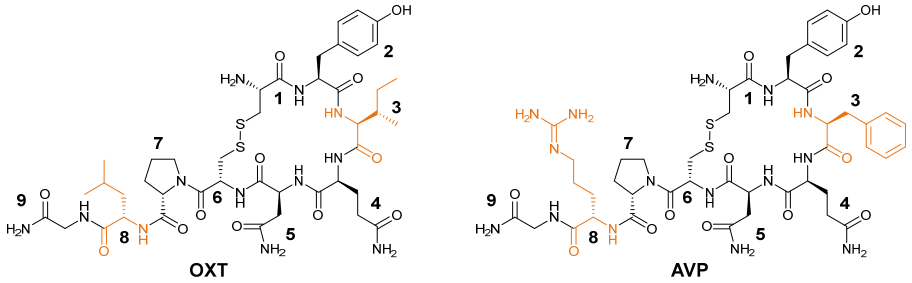

Figure 3.35: Oxytocin and Vasopressin are both part of the Vasotocin family.

Next to the structural similarity of Oxytocin and Vasopressin (Figure 4.34), the high extracellular homology between the OT and AVP receptors results in a low ligand selectivity (Table 3.1). Thus, receptor selectivity is achieved by several factors: a) the controlled release of the ligands, b) the cell specific up- and down-regulation of the receptor expression and c) the peptidases oxytocinase and vasopressinase.[262] Therefore, a highly selective and proteolytic stable OXTR-agonist is still subject of ongoing research.

Table 3.1: Affinity constants K_i (nM) from AVP and OT for the OXTR and AVPRs.[263]

	OTR	$V_{1a}R$	$V_{1b}R$	V_2R
OT	0.79	120	1782	1544
AVP	1.7	1.1	0.68	1.2

3.4.4 Oxytocin-ligand binding

For the design of novel and selective mimetic structures of ligands, ligand-bound crystal structures are essential, however, no crystal structure of OXTR and its ligand exist. Therefore, to address ligand binding, several strategies including construction of receptor chimeras[260, 264],

photoaffinity labeling[265], site directed mutagenesis and molecular modelling[266, 267] as well as *in silico* evolutionary studies[262] have been used. The Oxytocin receptor consists of seven transmembrane helices, which are arranged in an anticlockwise fashion and an extracellular amino-terminus.[260] Today, two different binding modes for OXTR agonists and antagonists are described. On the one hand, agonists bind to the extracellular domain, in particular to the amino terminus E1, which overlays the extracellular loops E2 and E3 (Figure 3.36).[264, 267] This binding site cannot distinguish between different agonists and therefore carbetocin, a partial agonist with improved proteolytic stability, binds to these domains in a similar fashion but with 10-fold lower affinity.[268] The partial agonist carbetocin will be discussed in detail in the next chapter. On the other hand, antagonists like barusiban, don't interact with the extracellular amino-terminus[264, 265, 269] of the oxytocin receptor and prefer binding to the bottom of the pocket, possibly to the transmembrane helices 1 and 2 via hydrophobic interactions.[260]

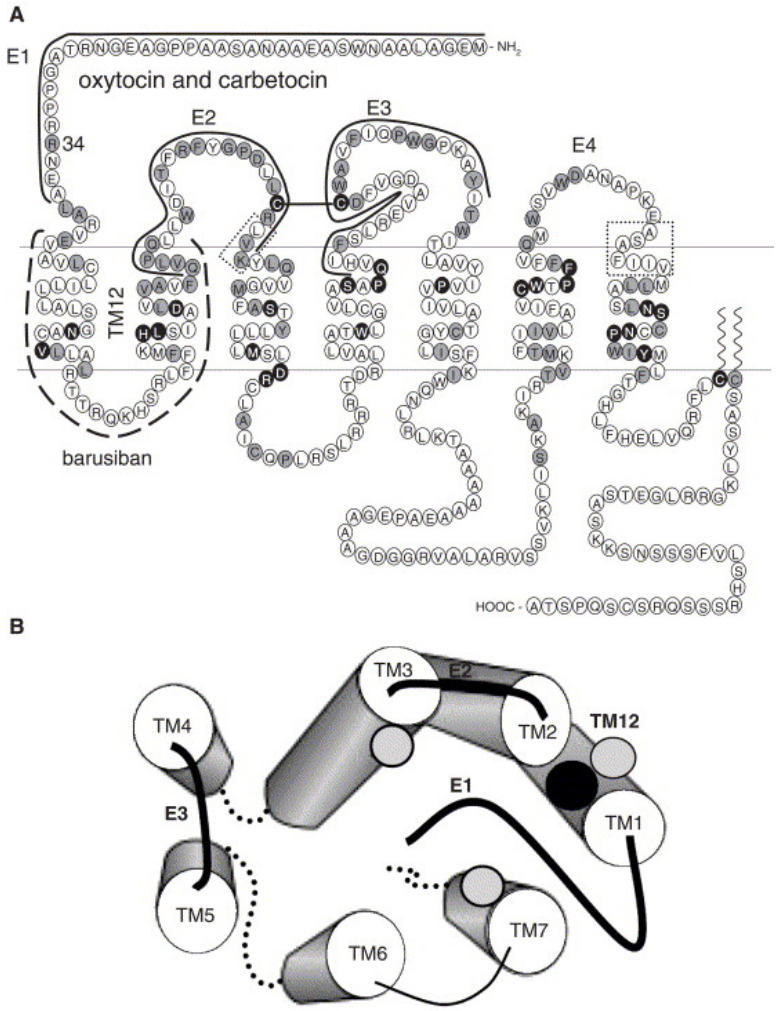

Figure 3.36: A) Binding domains of the OXTR. B) Anticlockwise-arrangement of the seven transmembrane helices.[260]

Besides receptor investigations, a closer look to the ligand can also give insights into peptide activity. Consisting of a six-membered ring with a highly conserved glycine-amide C-terminus, Oxytocin shows a high variability in position 2-5 and 8 between different species[270], suggesting that these positions are possibly responsible for species-selective recognition.[262] Furthermore, early structure-activity studies of oxytocin and its peptide analogues enclose the possibilities for modifications. The disulfide bridge is essential for the agonistic activity and either sulfur can be replaced by a methylene group.[271] The importante role of Tyr2 has been proofed in alanine-scans, as exchange led to complete loss in binding affinity to OTR.[272] While the changing the stereochemistry of Tyr2 lowers activity[271], exchange of Tyr2 by bulky aromatic residues results in antagonism.[272] The hydrophobic character of Ile3 is important for potency, hence, position 3 is only exchangeable against hydrophobic residues.[263, 271] The same applies for aliphatic H-bond donating character of Gln4, which has to be preserved.[271] Whereas Asn in position 5 is crucial,[273, 274] the *C*-terminal tail allows modifications. *Wiśnieski et. al*.[231] synthesized a number of potent OTR agonists by replacement of the Pro7 against *N*-alkylated glycines. Next, Leu8 allows a number of modifications.[275, 276] The introduction of bulky substituents at this position retains the affinity for the OXTR, but the bulkiness decides over activation or inhibition of the receptor. The fluorescent ligand nile red attached to the amine of Lys8-CBT resulted in a derivative with antagonistic effects while the same fluorophore attached to Lys8-CBT over a PEG-linker retained agonistic effects.[276]

At least, the hydrophobic interactions are meant to be part of the antagonistic binding properties[260], which has to be considered in the synthesis strategy of photoswitchable OTR-ligands.

After completing this work, further papers were published that provide insight into the ligand-receptor binding of AVPRs and OXTR. These data were not included in the consideration of the synthesis strategy, but will help to discuss the results.

A single particle cryo-EM structure analysis of the active OXTR im complex with OXT by *Waltenspühl et. al.*[277] provides an insight in the binding interactions. The cyclic part is described to be buried in the binding pocket. The *C*-terminal tripeptide looks towards the extracellular loops E2 and E3, with Leu8 in orientation to the extracellular surface. The amidated *C*-terminus possibly interacts with the trans membrane helices I and II, due to vicinity. Pro7 and Asn5 is packed against the extracellular surface of the loops 2 and 3. Gln4 stabilize the ring position via a hydrogen bond, while Ile3 is buried in the hydrophobic pocket. The

interactions of Tyr2 are based on hydropbic interactions of the pheyl ring as well es an additional hydrogen bond to a nearby backbone amide. At least, the backbone oxygen of Cys1 forms a polar cluster with several residues in close proximity.

First photoswitchable OT- and AVP-mimetics have been published by *Wirth. et. al.*[278] in 2023 (Figure 3.37). By introduction of the side-chain photoswitch AzoPhe and several different azobenzene and arylazopyrazole photoswitches into the backbone, they synthezised a small library of photoswichtable ligands. For the OTR, the photoswitchable mimetic OT10 showed agonstic activity with an EC_{50} = 30.7 ± 4 nM in the Z-conformation with an E/Z-ratio of 3.1. In OT10, the amino acids Pro7 and Leu8 were replaced by a *para*/*para*-substituted azobenze with an additional methylene spacer at amino function. While in OT10 the backbone-photowitch maintains the linar conformation of the *C*-terminus, a different strategy showed success for the AVP-mimetic. In VP12, the amino acid Phe3 was replaced by AzoPhe, resulting in a photoswitchable side-chain. VP12 showed reduced potency for V1aR but showed full agonstic activity for V1bR with an EC_{50} = 20.2 ± 6 in the Z-conformation with an E/Z-ratio of 5.3.

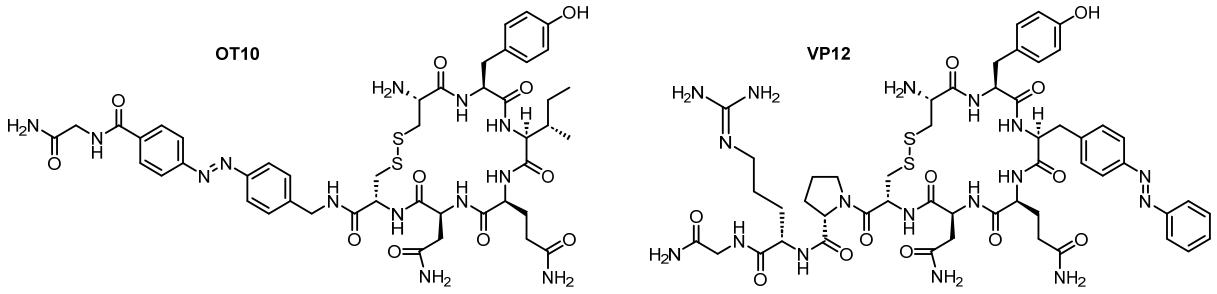

Figure 3.37: Photoswitchable OT- and AVP-mimetic showing success with two different strategies.[278]

3.4.4.1 Ligands of the oxytocin receptor

The search for effective and stable ligands for the oxytocin receptor has been going on for several dacades. In this time, a number of peptidic and non-peptidic agonists and antagonists have been developed for the treatment of premature ejaculation[279], postpartum hemorrhage[280] (OTR-agonists), preterm labor (OTR antagonists) and psychologic disorders.[281] Some of these ligands are being testet in clinical trials or have already been approved. For example, the antagonist Atosiban reduces the contraction rate and is clinically used in the treatment of preterm labor.[282] Because of preverable binding of Atosiban to the V1aR[283], Barusiban (Figure 3.38) with it's 300-fold higher affinity[284] (OTR vs. V1aR) and greater potency has been developed. However, Barusiban failed in Phase II clinical trial for the treatment of preterm labor.[285]

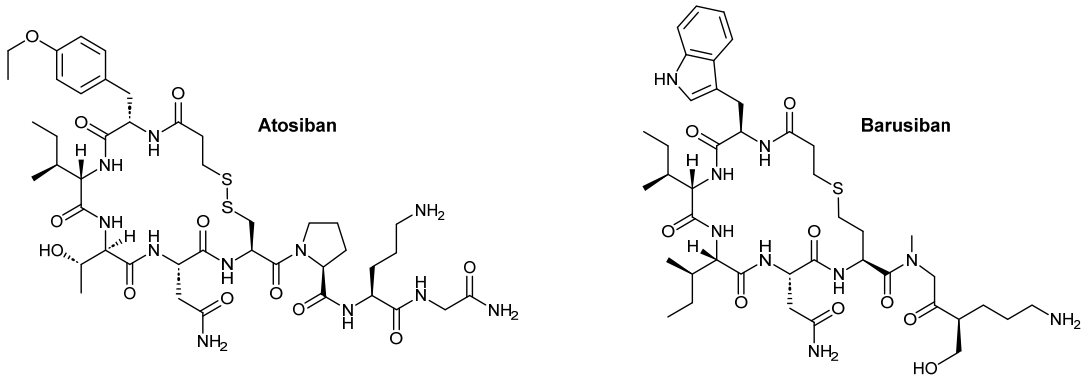

Figure 3.38: Structure of the OTR-antagonist Atosiban and Barusiban.[282]

In the early 1970s, the first deamino-1-monocarba analogue of OXT was synthesized.[18] Later, a proteolytic stable and selective OXT-mimetic, the deamino-1-monocarba-(2-O-methyltyrosin)-oxytocin dubbed carbetocin (**CBT**) was introduced. The high biostability (peripheral circulation half-life 85-100 min)[19] and increased efficacy was achieved by substitution of the disulfide bridge against a thioether, by introducing of a deaminated *N*-terminal butyric acid[286] and *O*-methoxy-tyrosine. The structural differences are accompanied with a prolonged milk let-down reflex[287] and a prolonged post-partum uterine activity with higher frequency and amplitude.[288] Therefore, CBT is sold under the name Pabal® for the prevention of postpartum haemorrhage, which is the most common cause[289] of maternal morbidity. In behavioural studies, CBT shows different and even opposite results on diverse pharmacological characteristics in comparison with oxytocin. In research on brown Norwegian rats, oxytocin but not carbetocin showed anti-psychotic properties[290] and in tests with Wistar rats, only Carbetocin reduced stress induced locomotor enhancement, ameliorating behavioural changes.[291] While OT is already in off-label use for autism spectrum disorder (ASD)[292], these findings recommend a careful use of CBT for the treatment of neurodevelopmental and psychiatric disorders.[20]

Besides the improved proteolytic stability and efficacy *in vivo*, CBT shows differences in receptor selectivity compared to the native OXT. CBT binds selectively to the G_q protein-coupled OXTR leading to a β-arrestin independent internalisation pathway but without receptor recycling.[20] While OT has activating properties on V1aR and V1bR at high concentrations, CBT appearas to acts as competitive antagonist on both receptors.[20] At least, carbetocin is only a partial agonist, with 50% − 58% efficiency on the G_q-coupled OXTR.[20, 21]

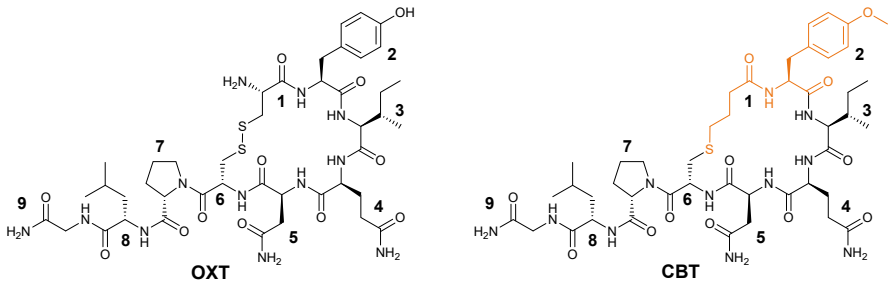

Figure 3.39: Oxytocin (OXT) and Carbetocin (CBT).

The roles of OXTR and AVPRs in neurodevelopmental and psychiatric conditions are still in ongoing research and tools for studying signalling pathways are still in need.[20] The search for selective and stable peptidic and non-peptidic OXTR ligands provides new insights into the binding properties of the OXTR. Nevertheless, strong tools for the unravelling of signalling pathways and controllable receptor manipulation are needed. Photo-pharmacology[187, 293] with its spatiotemporal precision provides a high selectivity of target distribution and dosing by adjustment of light intensity and wavelengths. Due to light controllable *cis*/*trans*-isomerisation of azobenzene moieties and the difference in geometry and dipole of the two isomers, the secondary structure of a photo-switchable peptide can be altered and thus receptor binding can be regulated by light. Hence, a photo-switchable peptide can be used as a tool for the controlled unravelling of signalling pathways and receptor systems.[192] Therefore, the aim was to design photo-switchable OTR ligands on the basis of CBT, which allow the external control of activity and selectivity by light. Although CBT is only a partial agonist, the high selectivity and stability predominates.

3.4.4.2 Results and discussion

For the synthesis of photoswitchable Carbetocin-based ligands several chromophores were incorporated into the peptide sequence by exchange of single amino acids. The position for amino acid substitution was chosen on the basis of structure-activity studies (Figure 3.40). After azobenzene introduction, the chromophoric ligands should preserve a high potency and gain a substantial difference in receptor activation upon *cis*/*trans*-isomerisation. Nevertheless, over millions of years, nature perfected receptor-ligand systems and every modification usually is at expense of potency.

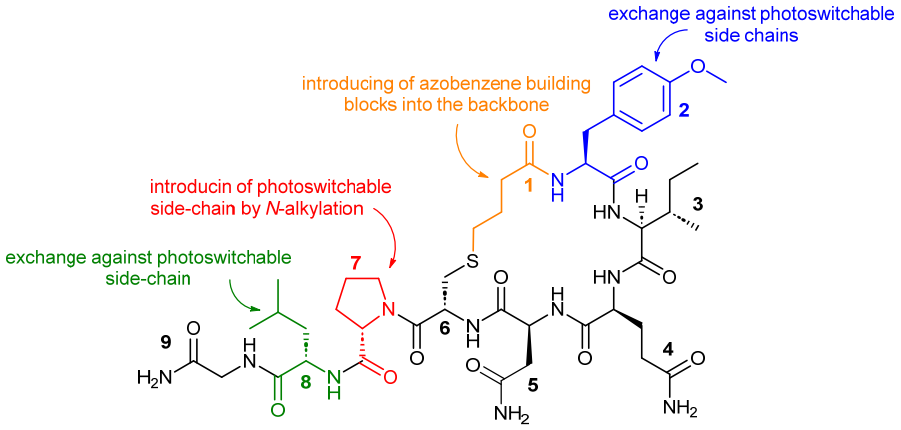

Figure 3.40: Positions chosen for the incorporation of photoswitches.

3.4.5 Introducing of photoswitchable side-chains by SPPS building blocks

The most evident choice for introducing azobenzene motifs was the substitution of Tyr(OMe)2, as the exchange of aromatic amino acids against aromatic azobenzene usually proves to be the least problematic. Therefore, *Fmoc*-AzoPhe-OH (**3.3**) was introduced by SPPS on position 2 (Scheme 3.11).

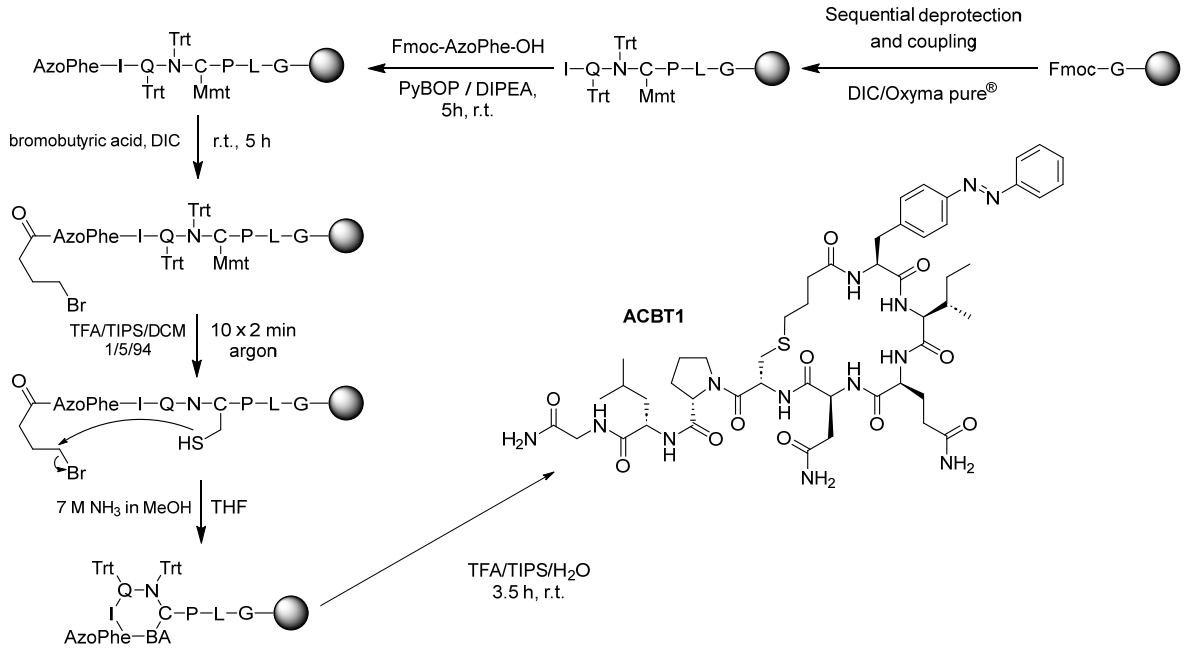

Scheme 3.11: Synthesis of photoswitchable CBT derivate **ACBT1**.

For the coupling of standard amino acids, DIC was used as an activator and Oxyma pure® as an activator base. The activator base solution was laced with 0.1 M DIPEA to improve purity and to avoid cysteine epimerisation.[294] Furthermore, the addition of a base improves the stability of the hyper-acid sensitive Methoxytrityl-protecting (Mmt) group at 90°C. For the

coupling of the photoswitch, coupling with PyBOP/DIPEA at room temperature for one hour provided the coupling of *Fmoc*-AzoPhe-OH **3.3**. Bromobutyric acid was coupled by room temperature for 5 h to the exclusion of nucleophiles using DIC solely. For the selective cleavage of the cysteine protecting group Mmt the resin was treated with 1% v/v TFA and 1.5% v/v triisopropylsilane (TIPS) in DCM for 10 x 2 min under argon. After cyclisation under basic conditions (1 mL 7 M NH_3 in MeOH, 4 mL THF), the resin was freed from DMF by washing with 5 x 10 mL DCM. The resin was cleaved from the solid support and the remaining side-chain protecting groups were removed using TFA/TIPS/H_2O (9.5/0.25/0.25) under argon.[57] After precipitation the crude peptide was purified by reversed-phase HPLC to furnish **A**zo**C**arbe**toc**in**1** (**ACBT1)**.

Leu8 of CBT was then chosen for the substitution with azobenzene side-chain mimetic motifs as it was shown that the introduction of bulky substituents[276] at this position has little influence on the affinity of the peptide for OXTR, although it modulates the functional activity. The fluorescent ligand nile red attached to the amine of Lys8-CBT resulted in a derivative with antagonistic effects while the same fluorophore attached to Lys8-CBT over a PEG-linker retained agonistic effects. However, introducing aromatic systems at position 8 retains receptor affinity, while the sterically hindrance decides over activation or inhibition of the receptor.[276] Next to AzoPhe, the analogue phenylalanine-4‘-azo (3,5-bis-tert-butyl)-benzene (*t*BuAzoPhe) **4.9** was introduced at position 8. In comparison to AzoPhe, the bulkier *t*BuAzoPhe has reduced π-stacking and a larger difference in the bulkiness of the *cis*- and *trans*-isoforms. The synthesis of peptides **ACBT2** and **ACBT3** (Figure 3.41) was different from the above-mentioned procedure. In **ACBT2** and **ACBT3** all coupling steps were carried out with DIC/Oxyma pure®. All amino acid were coupled in a single step, whereas *double coupling* was used in the coupling of the photoswitch AzoPhe **3.3** (2 x 8 min, 75 °C) and the adjacent amino acid *Fmoc*-Pro-OH (2 x 2 min, 90 °C). For the synthesis of **ACBT3**, all amino acids were coupled by *double coupling* (2 x 2 min, 90 °C), whereas the photoswith **3.9** was coupled in a singe step (8 min, 75 °C). The *Fmoc*-Cys(Mmt)-OH was also couped in a single step (2 min, 90 °C). Bromobutyric acid was coupled by room temperature for 2 x 5 h to the exclusion of nucleophiles using DIC solely. After selective deprotection of the Cys-side-chain, cyclization was carried out in 0.3 M DIPEA in DMF. The solid support and the remaining side-chain protecting groups were cleaved using TFA/EDT/Thioanisole/Anisole (9.0/0.3/0.5/0.2) under argon.[57] After precipitation the crude peptides was purified by reversed-phase HPLC to furnish **ACBT2** and **ACBT3**.

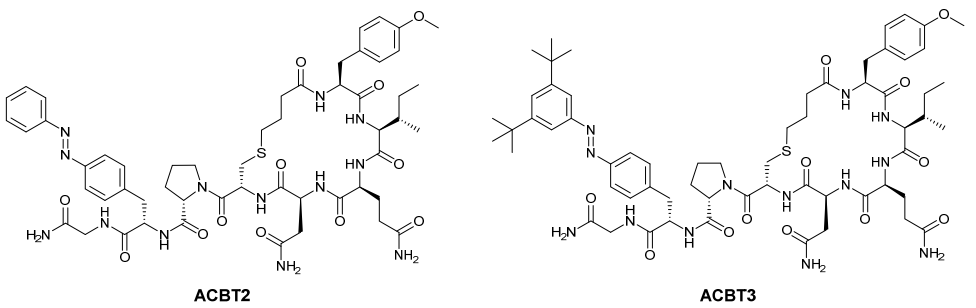

Figure 3.41: Structure of photoswitchable CBT analogues **ACBT2** and **ACBT3**.

All peptides were investigated by UV/VIS spectroscopy and both showed only minimal photobleaching or degradation and both exhibit a high bistability. Therefore, **ACBT1**, **ACBT2** and **ACBT3** can be used in biological assay.

3.4.6 Introduction of photoswitchable side-chains by *N*-alkylation

In the search for a highly selective agonist, Wiśniewski et al.[231] synthesised carba-1-[4-FBzlGly7]dOT, also called merotocin, where Pro7 of oxytocin is substituted by a 4-fluorobenzyl *N*-alkylated glycine (Figure 3.42). Analogues to Carbetocin, a sulphur atom of the disulfide bridge is replaced by a methylene group, resulting in an improved selectivity for the OXTR versus V2R. This peptide is now in phase II clinical trial for preterm mothers with lactation failure.[231] Hence, we decided to *N*-alkylate Gly7 with 4-aminomethyl-azobenzene **4.22** after introducing bromoacetic acid into the peptide backbone.

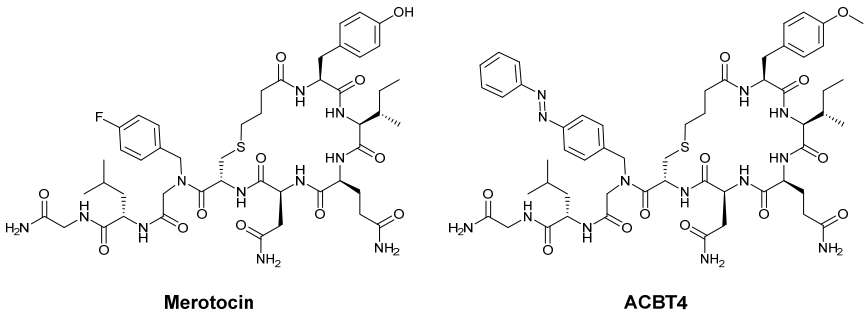

Figure 3.42: Structure of Merotocin/FE 202767[231] and **ACBT4**.

The synthesis of *N*-alkylated glycine in **ACBT4** followed a procedure[295] used in peptoid chemistry (Scheme 3.12). After the coupling of *Fmoc*-Leu-OH and subsequent deprotection with 20% piperidine in DMF, bromoacetic acid was coupled with DIC solely for an extended time of 2 x 5 h. The resin was then treated with the primary amine **4.22** in 0.3 M DIPEA in DMF. For the following coupling step of *Fmoc*-Cys(Mmt)-OH, double coupling (2 x 8 min, 75 °C) was used, as the sterically hindered secondary amine tends to have poor coupling

properties. The remaining amino acids were coupled by *double coupling* (2 x 2 min, 90 °C). Bromobutyric acid was coupled by room temperature over night to the exclusion of nucleophiles using DIC solely. The remaining synthesis followed the procedure of **ACBT2** and **ACBT3**.

While peptide-bonds usually have trans-configurations, peptidyl-prolyl fragments can exist in both *cis*- and *trans*-configuration. Peptide **ACBT4** contains a tertiary amide at position 7, resulting in a *cis*- and a *trans*-isomer at the alkylated glycine. The *N*-alkylation mimics the Pro-Cys-sequence, which tends to be presented in *cis*- and *trans* configuration, depending on the solvent and complex ions like Zn^{2+}.[296] Therefore, signals of two conformers can be found in the NMR-spectra. Spectroscopic investigations of peptide **ACBT4** showed a high stability of the *cis*-isomer and only minimal photobleaching or degradation in the switching measurements.

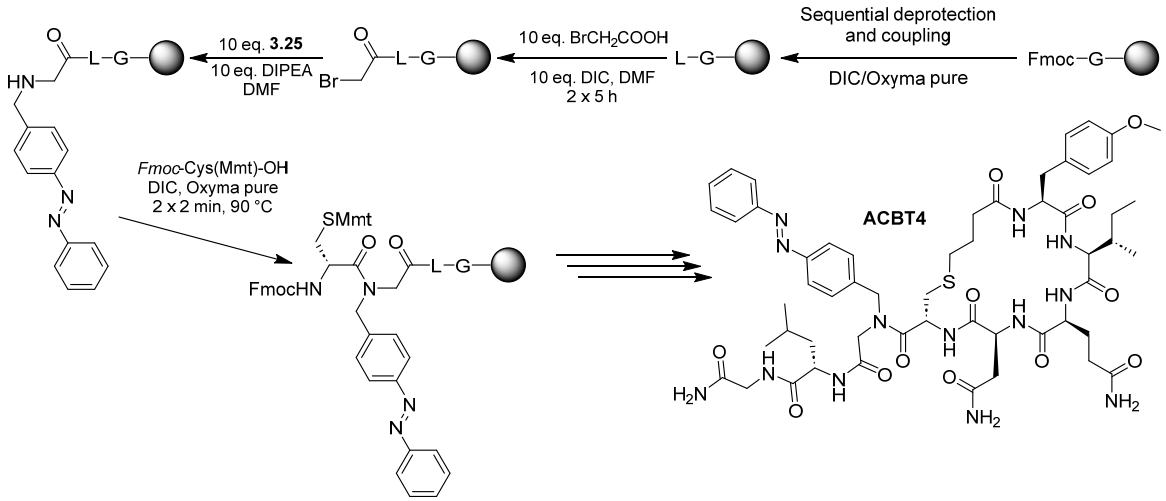

Scheme 3.12: Synthesis of **ACBT4** under use of *N*-alkylation.

3.4.7 Introducing of side-chain linked photoswitches

Peptides **ACBT1**, **ACBT2**, **ACBT3** and **ACBT4** contain photoswitchable side-chains. These sidechains usually cause local perturbations and rearrangements. To gain higher impact on the secondary structure, photoswitches **4.16** and **4.19** were introduced into the backbone of the ring by substitution of the butyric acid using solely DIC as coupling reagent. Both photoswitches contain a halogenated carbon atom, suitable for the substitution by the thiol group of the Cys6 side-chain.

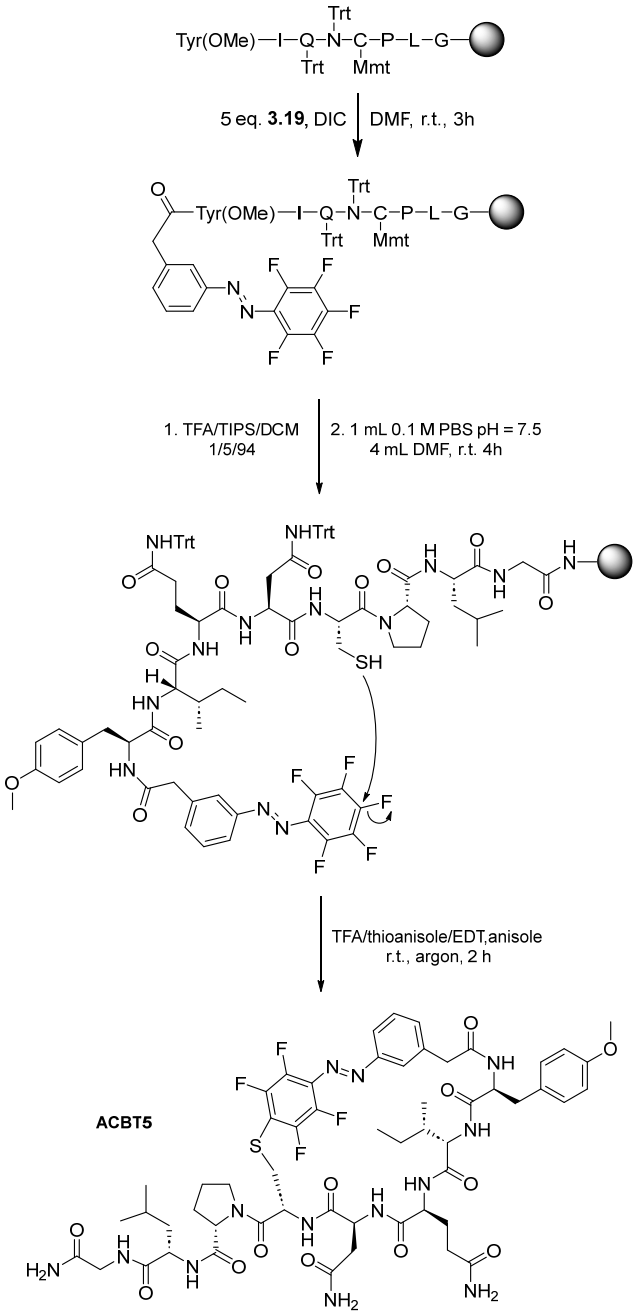

Scheme 3.13: Synthesis of **ACTB5**.

The cyclisation of **ACBT5** was carried out in 1 mL PBS (pH = 7.5) and 4 mL DMF for 4 h at room temperature (Scheme 3.13). The *para*-position of the perfluorinated benzene is electron deficient enough for the cysteine to attack in an aromatic nucleophile substitution.[219, 220] The selectivity of the *para*-position can be seen in the ^{19}F-NMR by the two doublets of doublets with J = 24 Hz for *ortho*-coupling and J = 12.5 Hz, for *meta*-coupling (Figure 3.43).

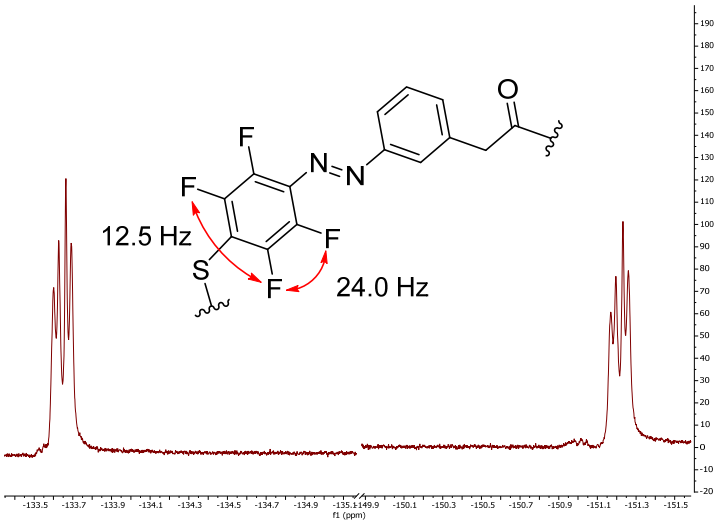

Figure 3.43: ^{19}F-NMR of **ACBT5**. The chemical splitting shows the *para*-substitution of the pentafluorobenzene moiety by the thiol group.

The transitions of the azobenzene of the photoswitch **4.19** in peptide **ACBT5** are shifted to higher wave lengths (Figure 3.44) by two effects, the substitution of the fluorine (mainly of the *ortho*-fluorine-atoms) and the sulphur atom in *para*-position. The fluorine atoms reduce the electron density of the azo-bridge, resulting in a lower energy of the n-orbital of the *cis*-isomer and a small red-shift of the n → π* absorption of the *trans*-isomer relative to the *cis*-isomer[182, 219]. In addition, the electron-donating sulfur in *para*-position causes a red-shift of the π → π* transition.[219] Both effects result in distinct transition bands and different switching wavelengths compared with "unsubstituted" azobenzenes. For the *trans* to *cis* isomerisation two wavelengths, UV-light (λ = 365 nm) and green light (λ = 540 m), can be used, whereas *cis* to *trans* isomerisation occurs with blue (λ = 405 nm). The red-shift allows switching in both directions without the use of UV-light. This is of interest, when the chromophoric ligand should be switched in biological assays. Additionally, the σ-electron-withdrawing fluorine-atoms stabilises the *cis*-isoform and improve its thermal stability.[182]

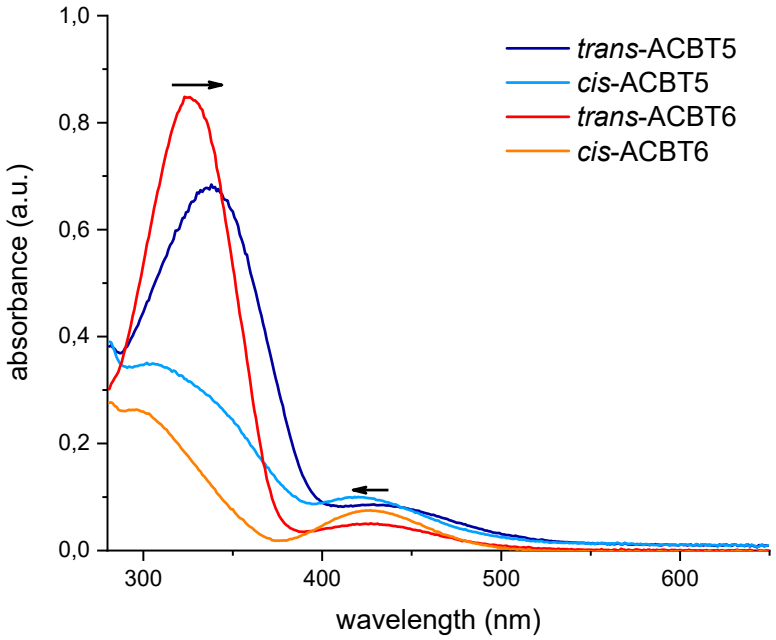

Figure 3.44: UV/VIS-spectra of **ACBT5** and **ACBT6**. The fluorine-substitutents in **ACBT5** red-shifts the π-π* transition and separates the n-π* bands.

While **ACBT5** has a slightly sterically restrained ring, photoswitch **4.16** which was introduced into **ACBT6** has an additional CH_2-spacer (Scheme 3.14). The methylene group extends the ring and allows a higher flexibility due to reduced constraints. For the synthesis of **ACBT6** *double coupling* (2 x 2 min, 90 °C) was used for all amino acids. The chromophore **4.16**, which is derived from AMPP, was coupled with DIC solely at room temperature over night. After selective deprotection of the Cys6 side-chain, cyclisation took place under basic conditions (0.3 DIPEA in DMF).

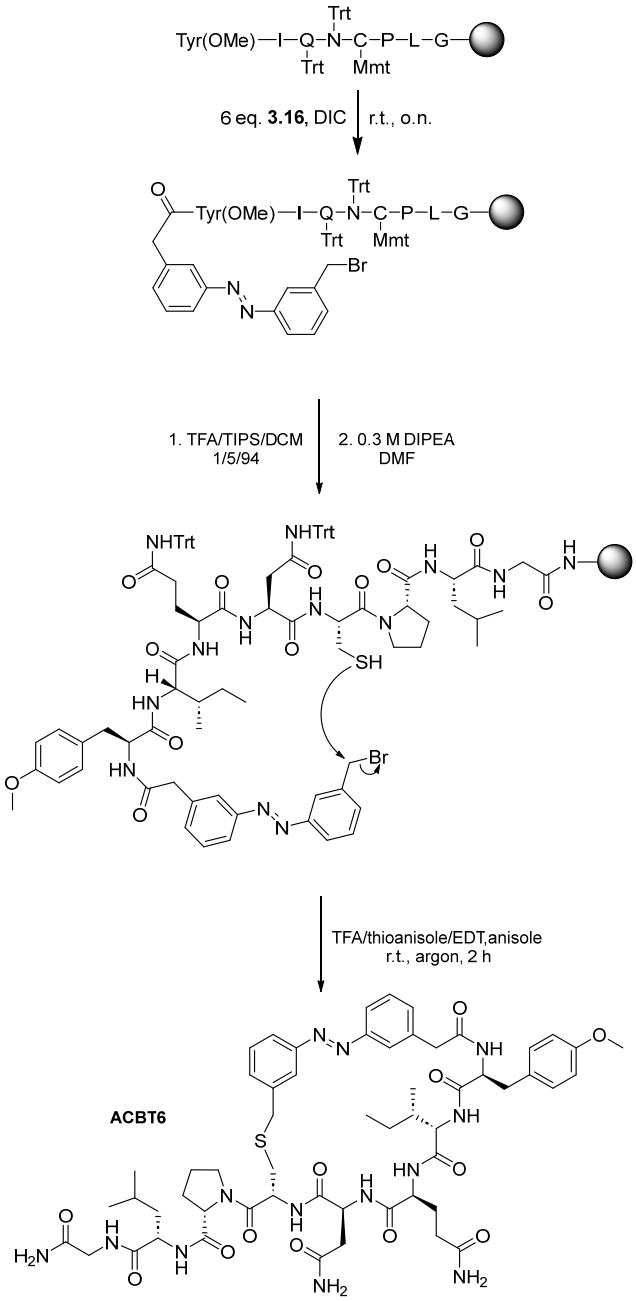

Scheme 3.14: Synthesis of **ACBT6**.

The *cis-trans* isomerisation of all peptides was investigated by UV/VIS spectroscopy (Figure 3.45). All peptides showed a decrease of the π-π* absorption band and an increase of the n-π* absorption band upon illumination with UV light or green light depending on the photoswitch (340 nm, 365 nm or 540 nm). A reversion of the isomerisation was induced by illumination with blue light (405 nm, 445 or 455 nm). Only minimal bleaching or degradation occurred after a switching cycle of ten repeats. This aspect is important for the biological application, as bleaching is the result of triplet state formation and subsequent generation of reactive oxygen species.[14] At least, all peptides showed a long-lasting *cis*-isoform in the dark

(< 2 h). The high bistability allows pre-illumination of all peptide before application to cells and no need of UV-light exposure of cells during biological assays.

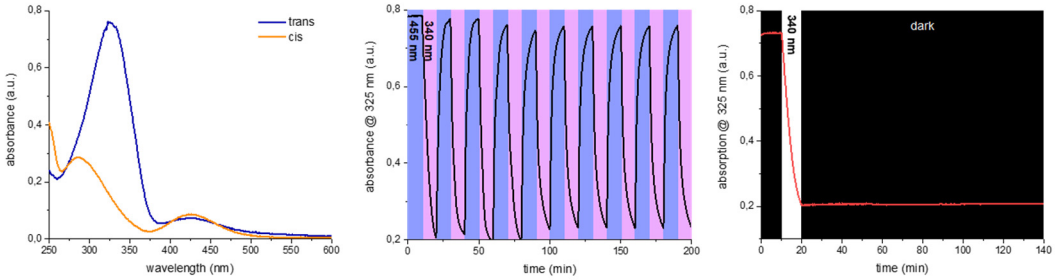

Figure 3.45: Photophysical properties of **ACBT1**: UV/VIS spectrum of trans-(blue) and cis-(orange) **ACBT1** (left); reversible cis/trans-isomerisation of **ACBT1** shows only minimal photobleaching (middle); illumination of trans-**ACBT1** with 340 nm for 10 min and subsequently leaving in the dark for two hours shows a high stability of the cis-isomer (right).

3.4.8 Functional evaluation by Ca^{2+}-imaging

Our cooperation partner, Dr. Iuliia Karpenko (Faculty of Pharmacy, University of Strasbourg) did the functional evaluation of all peptides. Therefore, in the following only the results of the work of Dr. Iuliia Karpenko (Table 3.2) are shown without the description of applied procedures.

All peptides (Figure 3.46) were tested for their activity towards the OXTR and the related vasopressin receptor family (V1aR, V1bR and V2R) by measuring of intracellular Ca^{2+} accumulation in HEK293 cells overexpressing OXTR, V1aR, V1bR or V2R and using Fluo-4 for Ca^{2+} detection. Additionally, the functional activity of CBT, a functional selective G_q-coupled OXTR agonist[20], was tested at the OXTR.

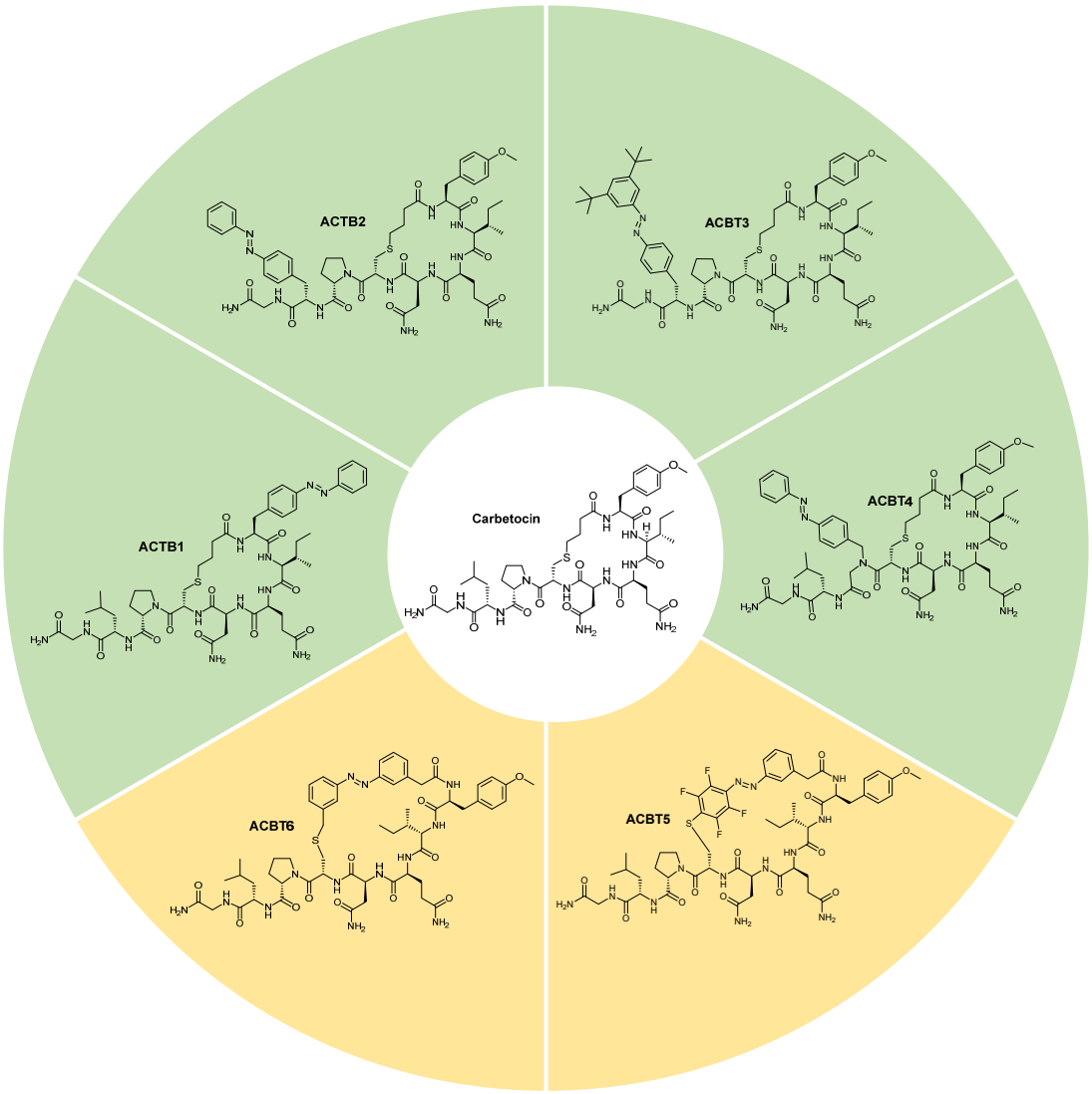

Figure 3.46: Carbetocin and the synthesised photoswitchable ACTBs.

For **ACBT1**, exchange of Tyr(OMe) in position 2 by AzoPhe resulted in a loss of activity for the OXTR. In contrast, **ACBT1** gained a moderate antagonistic activity for V1aR and a weak antagonistic activity for OXTR. With a selectivity of 5.3 for *cis*- and *trans*-**ACBT1** towards V1aR over OXTR and the 7.3-times increase in activity upon photoconversion to the *cis*-isomer for both receptors **ACBT1** shows a potential for a photoswitchable V1aR-ligand.

Introduction of AzoPhe on the *C*-terminal part by substitution of Leu8 retained small but very selective agonistic activity for the OXTR. Although binding in the low nanomolar range, **ACBT2** turned out to be a partial agonist with less than 20% of OXTR activation compared to the endogenous ligand. Noteworthy, Carbetocin is also a partial agonist with 50% Gq activation. Additional, **ACBT2** has a two-fold difference in activity upon isomerisation to the *cis*-isoform.

The next step was the replacement of Leu8 by the bulkier photoswitch *t*BuAzoPhe **4.9**, which should have reduced π-stacking and higher sterical difference of both isoforms. However, imaging of **ACBT3** showed a complete loss in agonistic activity for OXTR. Moreover, the bulkier photoswitch turned **ACBT3** into an OXTR antagonist with almost no difference in activity for both isoforms. At least, the selectivity for the OXTR was negligible. The merotocin derivative **ACBT4**, in which the azobenzene moiety was introduced by *N*-alkylation of glycine under replacement of Pro7, lost the agonistic activity for OXTR. Nevertheless, **ACBT4** possess agonistic activity for OXTR and V1aR in the low nanomolar range, but with a negligible difference between both isoforms and low selectivity for OXTR.

Table 3.2: Results of the Ca^{2+}-imaging of the photoswitchable CBT analogues **ACBT1-ACBT6**.

Peptide		**Agonism (EC_{50}, nM)**				**Antagonism (IC_{50}, nM)**				**Selectivity**
		OXTR	$V_{1a}R$	$V_{1b}R$	V_2R	OXTR	$V_{1a}R$	$V_{1b}R$	V_2R	
CBT		1.41 ± 0.67	nd	nd	nd	nd	nd	nd	nd	
ACBT1	*trans*	> 3000	> 3000	> 3000	> 3000	1380 ± 294	262 ± 99	> 3000	> 3000	V1aR/OXTR
	cis	> 3000	> 3000	> 3000	> 3000	188 ± 115	36 ± 17	> 3000	> 3000	*trans*: 5.3 *cis*: 5.3
	trans/*cis*					7.3	7.3			
ACBT2	*trans*	1.37 ± 0.64	> 3000	nd	nd	> 3000	202 ± 184	Nd	nd	OXTR/V1aR
	cis	0.70 ± 0.40	> 3000	nd	nd	> 3000	189 ± 130	Nd	nd	*trans*: 147 *cis*: 417
	trans/*cis*	2.0					1.1			
ACBT3	*trans*	> 3000	> 3000	nd	nd	412 ± 231	503 ± 102	Nd	nd	OXTR/V1aR
	cis	> 3000	> 3000	nd	nd	269 ± 120	260 ± 107	Nd	nd	negligible
	trans/*cis*					1.5	1.9			
ACBT4	*trans*	> 3000	> 3000	nd	nd	14.7 ± 9.1	43.5 ± 19.8	Nd	nd	OXTR/V1aR
	cis	> 3000	> 3000	nd	nd	14.5 ± 11.6	36.3 ± 22.3	Nd	nd	*trans*: 2.7 *cis*: 2.3
	trans/*cis*					1.0	1.2			
ACBT5	*trans*	> 3000	> 3000	> 3000	> 3000	64.1 ± 51.6	> 3000	> 3000	> 3000	OXTR/V1aR
	cis	> 3000	> 3000	> 3000	> 3000	29.1 ± 23.4	> 3000	> 3000	> 3000	selective
	trans/*cis*					2.2				
ACBT6	*trans*	> 3000	> 3000	> 3000	> 3000	51.4 ± 33.5	389 ± 155	> 3000	> 3000	OXTR/V1aR
	cis	> 3000	> 3000	> 3000	> 3000	14.7 ± 8.9	56.5 ± 14.5	> 3000	> 3000	*trans*: 3.0 *cis*: 2.9
	trans/*cis*					3.5	6.9			

Consequently, the conformational rigid photoswitch **4.19** was introduced into the peptide backbone by substitution of the butyric acid, resulting in a conformational rigid peptide **ACBT5**. The peptide revealed antagonistic activity and showed a complete selectivity for the OXTR. Nonetheless, **ACBT5** showed only a small two-fold difference in activity upon *trans* to *cis* isomerisation. At least, the insertion of the AMPP derivative **4.16** extended the ring and allowed a higher degree of flexibility. The higher flexibility converted peptide **ACBT6** into a potent antagonist in the low nanomolar range for both receptors, V1aR and OXTR, but with three-fold selectivity for the latter. Upon *trans*- to *cis*-isomerisation, **ACBT6** showed a 3.5-fold change in activity for the OXTR and even a 7-fold change at the V1aR.

In summary, the insertion of photoswitchable building blocks into Carbetocin leads to high differences in activity depending on the position of substitution. Tyr(OMe) in position 2 has a crucial role in receptor selectivity and **ACBT1** could potentially provide insight into the positioning of ligands in the binding pocket of OXTR and V1aR. However, **ACBT1** showed the highest difference in activity between both isoforms. Side-chain substitution in position 8 with AzoPhe resulted in the only AzoCarbetocin with partial agonistic activity for the OXTR. Additionally, **ACBT2** retains the antagonistic behaviour of Carbetocin towards V1aR.[20] A bulkier substituent in position 8 abolishes agonistic activity and led to the antagonist **ACBT3** for OXTR and V1aR. This is consistent with the results of Karpenko et. al.[276], where the bulky nile red attached at Lys8 provided an antagonist. Increasing the bulkiness at position 7 also resulted in an antagonist but with the smallest difference in activity upon isomerisation. This might be an outcome of the high flexibility of **ACBT4**. Substitution of the butyric acid in position 1 by photoswitchable backbone building blocks also led potent antagonists **ACBT5** and **ACBT6**. With the results of Ca^{2+} imaging in hand, the importance of hydrophobicity for antagonistic behaviour of OXTR ligands can be confirmed. Raising the hydrophobicity by incorporation of aromatic moieties in or near the ring resulted antagonists with different potency and selectivity, which coincides with the postulation of Gimpl et. al.[260]

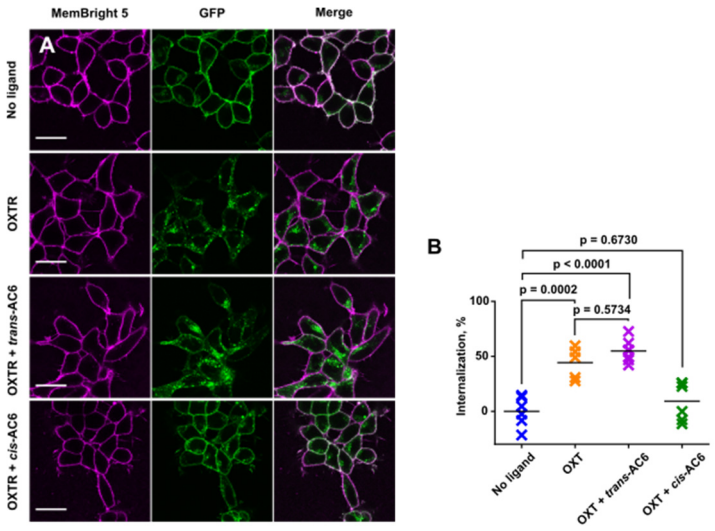

Figure 3.47: Internalisation of the OXTR in the presence of carbazotocins followed by confocal microscopy. (A) HEK293T cells stably expressing OXTR-eGFP fusion were incubated for 15 min at 37° C either without any ligand or in the presence of 10 nM OXT, 10 nM OXT and 15 nM trans-AC6 or 10 nM OXT and 15 nM cis-AC6. Fluorescence of the membrane probe MemBright 5 (excitation 635 nm, emission 650-750 nm) is shown in magenta, fluorescence of eGFP (excitation 488 nm, emission 500-550 nm) is shown in green. Scale bar, 30 µm. (B) Quantification of the OXTR internalisation induced by OXT and inhibited by carbazotocins trans-AC6 and cis-AC6 was calculated as a relative decrease of the mean membrane eGFP fluorescence. Data from two independent experiments. Statistics: one-way ANOVA with Tukey's multiple comparison test (confidence interval 99%).

Optical control of OXTR internalisation in living cells

Furthermore, Dr. Iuliia Karpenko (Faculty of Pharmacy, University of Strasbourg) demonstrated the applicability of the agonist **ACBT2** and the most potent antagonist **ACBT6** to control the activity of OXTR in living cells (Figure 3.47). Thus, the internalisation of OXTR fused to eGFP in HEK cells was studied by confocal microscopy. The application of oxytocin (10 nm) activates OXTR, followed by complete internalisation within 15 min. After addition of 0.7 nM **ACBT2** no internalisation could be observed, neither in *trans* nor in *cis*. In order to test the antagonistic activity of **ACBT6**, cells were treated with 15 nM of *trans*-**ACBT6**. No decrease in activation by oxytocin could be observed, which is consistent with its IC_{50} of 51 nM. In contrast, addition of the same quantity of *cis*-**ACBT6** significantly blocked the Oxytocin-depended activation of OXTR, which reflects the 3.5-times higher activity of *cis*-**ACBT6** measured by Ca^{2+}-imaging. Finally, introducing the AMPP-derivative **4.16** into the backbone of Carbetocin results in a potent light-controllable peptidic OXTR antagonist with a sufficient difference in *trans*-to-*cis* isomerisation.

3.4.9 Analytical Data of the AzoCarbetocins

Synthesis was carried out on preloaded *Fmoc* Gly TentaGel® S RAM low loading resin using DIC/Oxyma® as coupling reagents. *Fmoc*-deprotection was achieved by treatment with 20%

piperidine in DMF. Coupling conditions are shown in table 3.3 and table 3.4. Bromoacylacids as well as photoswitches **3.16** and **3.19** were coupled without base, using solely DIC and extended reaction time at room temperature. For synthesis of **ACTB4** the photoswitch **4.22** was introduced under basic conditions, shaking the resin in a 0.3 M DIPEA-solution in DMF overnight. To ensure complete coupling of the secondary amine, cysteine coupling was done twice. For cyclisation, Mmt protection group of the cysteine side chain was removed by treating the resin ten times for 2 min with 1% TFA in DCM under argon. Cyclisation of **ACBT1** was carried out in 7 M NH_3 in THF (2 x 2 h, r.t.). For peptides **ACBT2**, **ACBT3**, **ACBT4** and **ACBT6** cyclisation took place under basic conditions using a 0.3 M DIPEA-solution in DMF overnight. For the cyclization of **ACBT5** a solution of 1 mL PBS (pH = 7.5) in 4 mL DMF was used. Afterwards, the resin was freed from DMF by washing with DCM several times and global deprotection of the peptide was done with TFA, thioanisole, EDT, anisole (9 mL, 0.5 mL, 0.3 mL and 0.2 mL) for 2 h under argon to prevent oxidation of the thioether. Peptides were precipitated in cold diethyl ether, centrifuged and washed with Et_2O for five times. For purification by reverse-phase HPLC, the peptides were first purified in *trans*-isoform, lyophilised, solved, illuminated with UV-light and purified again in *cis*-isoform to receive high purity.

Table 3.3: Coupling conditions of **ACTB1**, **ACTB2** and **ACTB3**.

Compound	ACTB1				ACTB2				ACBT3			
	step	*t* [s]	*p* [W]	*T* [°C]	step	*t* [s]	*p* [W]	*T* [°C]	step	*t* [s]	*p* [W]	*T* [°C]
*Fmoc*LeuOH	1	120	30	90								
*Fmoc*AzoPheOH **3.3**	1				1&2	480	28	75				
Fmoc(14,-16 di-tert-butyl)-AzoPheOH **3.9**	1								1	480	28	75
*Fmoc*ProOH	1	120	30	90	1&2	120	30	90	1&2	120	30	90
*Fmoc*CysMmtOH	1	120	30	90	1	120	30	90	1	120	30	90
*Fmoc*AsnTrtOH	1	120	30	90	1	120	30	90	1&2	120	30	90
*Fmoc*GlnTrtOH	1	120	30	90	1	120	30	90	1&2	120	30	90
*Fmoc*IleOH	1	120	30	90	1	120	30	90	1&2	120	30	90
*Fmoc*Tyr(OMe)OH	1				1	120	30	90	1&2	120	30	90
*Fmoc*AzoPheOH **3.3**	1	480	28	75								
4-Bromobutyric acid	1	18000	0	r.t.	1&2	0	18000	r.t.	1&2	0	0	r.t.

Table 3.4: Coupling conditions of ACTB4, ACTB5 and ACTB6.

Compound	ACTB4				ACTB5				ACTB6			
	step	*t* [s]	*p* [W]	*T* [°C]	step	*t* [s]	*p* [W]	*T* [°C]	step	*t* [s]	*p* [W]	*T* [°C]
*Fmoc*LeuOH	1	120	30	90	1	120	30	90	1&2	120	30	90
*Fmoc*ProOH					1	120	30	90	1&2	120	30	90
Bromoacetic acid	1&2	18000	0	r.t.								
*Fmoc*CysMmtOH	1&2	120	30	90	1	120	30	90	1&2	120	30	90
*Fmoc*AsnTrtOH	1&2	120	30	90	1	120	30	90	1&2	120	30	90
*Fmoc*GlnTrtOH	1&2	120	30	90	1	120	30	90	1&2	120	30	90
*Fmoc*IleOH	1&2	120	30	90	1	120	30	90	1&2	120	30	90
*Fmoc*Tyr(OMe)OH	1&2	120	30	90	1	120	30	90	1&2	120	30	90
3-((perfluorophenyl)-diazenyl)phenyl)acetic acid **3.19**					1	10800	0	r.t.				
3-((3-(bromomethyl)-phenyl)diazenyl)phenyl)-acetic acid **3.16**									1	o.n.		r.t.
Bromobutyric acid	1&2	18000		r.t.								

Analytical Data of ACBT1

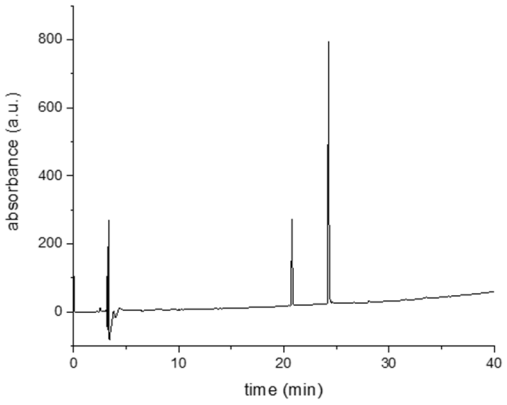

Figure 3.48: Analytical HPLC spectrum of **ACTB1** with a water/acetonitrile gradient of 95/5 →20/80 in 40 min. R_f: 20.7 min (cis) and 24.2 min (trans).

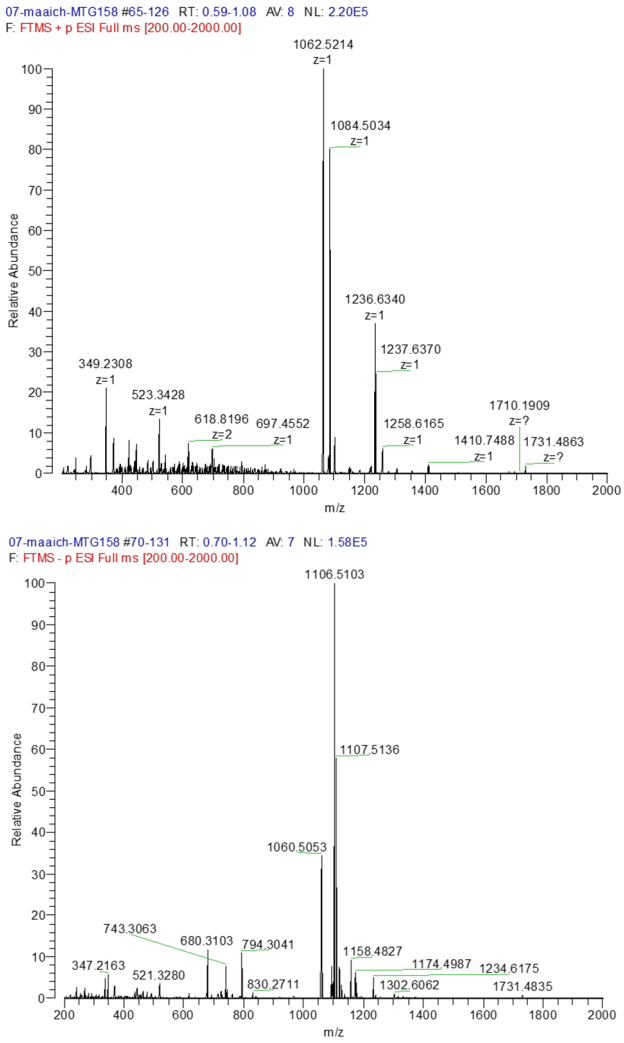

Figure 3.49: HRMS spectrum of **ACTB1**: HRMS (+ESI) m/z calc. for $C_{50}H_{72}N_{13}O_{11}S^+$ $[M + H]^+$: 1062.5189; found: 1062.5214. Calc. for $C_{50}H_{72}N_{13}NaO_{11}^+$ $[M + Na]^+$: 1084.5009; found: 1084.5034. HRMS (−ESI) m/z calc. for $C_{51}H_{72}N_{13}O_{13}S^-$ $[M+ FA – H]^-$: 1106.5099; found: 1106.5103.

Table 3.5: ^{1}H- and ^{13}C-NMR chemical shifts of trans-**ACTB1** in DMSO-d_6.

residue	^{1}H-NMR	^{13}C-NMR
Butyric acid	Hα$_1$ 2.20, Hα$_2$ 2.02, Hβ$_1$ 1.79, Hβ$_2$ 1.71, Hγ$_1$ 2.59, Hγ$_2$ 2.44	Cα 34.3, Cβ 26.7, Cγ 32.0
3.3	NH 8.09, H1 4.68, H2$_a$ 3.51, H2$_b$ 2.89, H4/8 7.53, H5/7 7.86, H12/16 7.88, H13/15 7.60, H14 7.57	C1 53.8, C2 35.8, C3 142.3, C4/8 129.7, C5/7 122.2, C6 150.6, C11 151.9, C12/16 122.2, C13/15 129.3, C14 131.2
Ile	NH 7.98, Hα 3.96, Hβ 1.79, Hγ$_{1a}$ 1.46, Hγ$_{1b}$ 1.17, Hγ$_2$ 0.92, Hδ 0.90	Cα 58.4, Cβ 36.1, Cγ$_1$ 24.7, Cγ$_2$ 15.1, Cδ 11.3
Gln	NH 8.45, Hα 3.89, Hβ 1.81, Hγ 2.19, Hδ$_1$ 7.34, Hδ$_2$ 6.88	Cα 54.5, Cβ 25.7, Cγ 31.1
Asn	NH 7.65, Hα 4.47, Hβ 2.60, Hδ$_1$ 7.44, Hδ$_2$ 7.01	Cα 50.4, Cβ 36.0
Cys	NH 7.74, Hα 4.60, Hβ$_1$ 2.93, Hβ$_2$ 2.54	Cα 51.4, Cβ 32.9
Pro	Hα 4.34, Hβ$_a$ 2.04, Hβ$_b$ 1.80, Hγ$_a$ 1.83, Hγ$_b$ 1.80, Hδ 3.47	Cα 60.2, Cβ 28.6, Cγ 24.3, Cδ 46.6
Leu	NH 7.84, Hα 4.20, Hβ$_a$ 1.56, Hβ$_b$ 1.48, Hγ 1.58, Hδ$_1$ 0.89, Hδ$_2$ 0.82	Cα 50.9, Cβ 39.7, Cγ 24.1, Cδ$_1$ 22.8, Cδ$_2$ 21.1
Gly	NH 7.79, Hα$_a$ 3.67, Hα$_b$ 3.49, CONH$_2$ 7.11	Cα 41.7

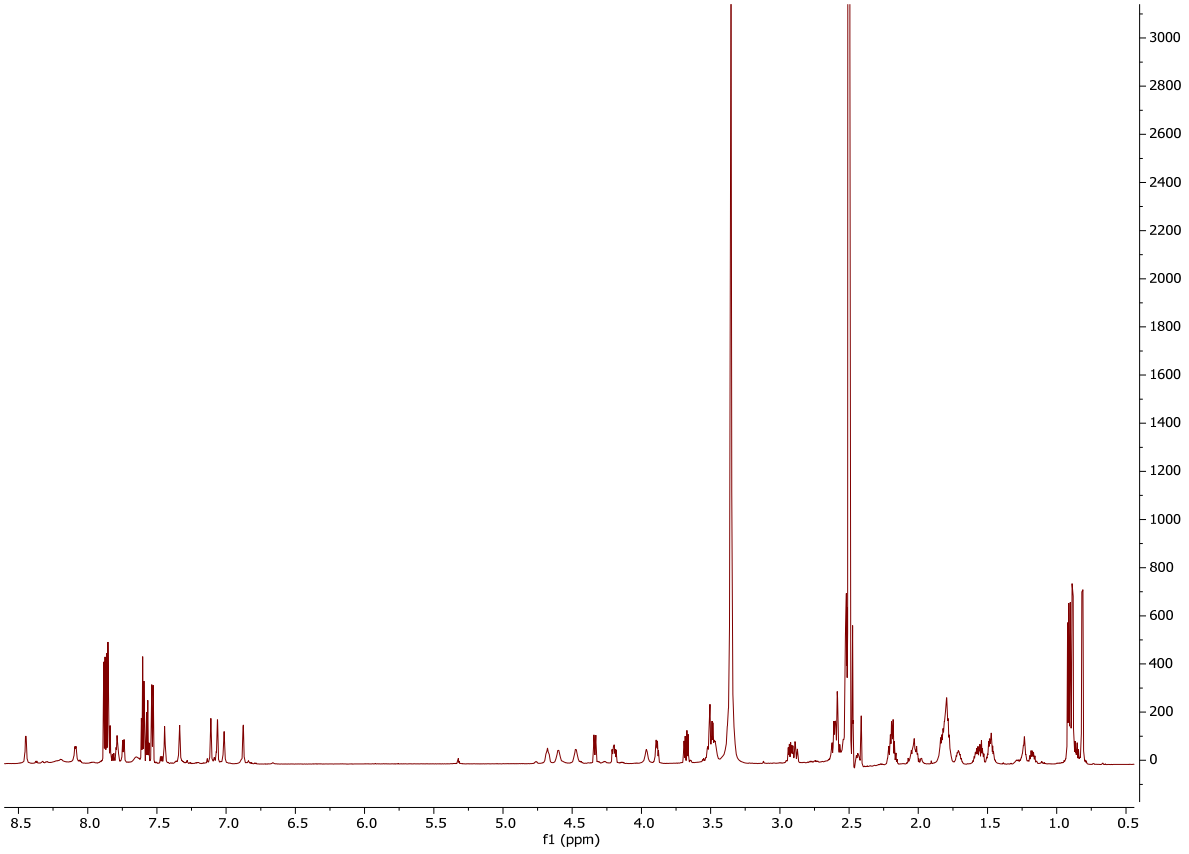

Figure 3.50: ^{1}H-NMR of **ACTB1**.

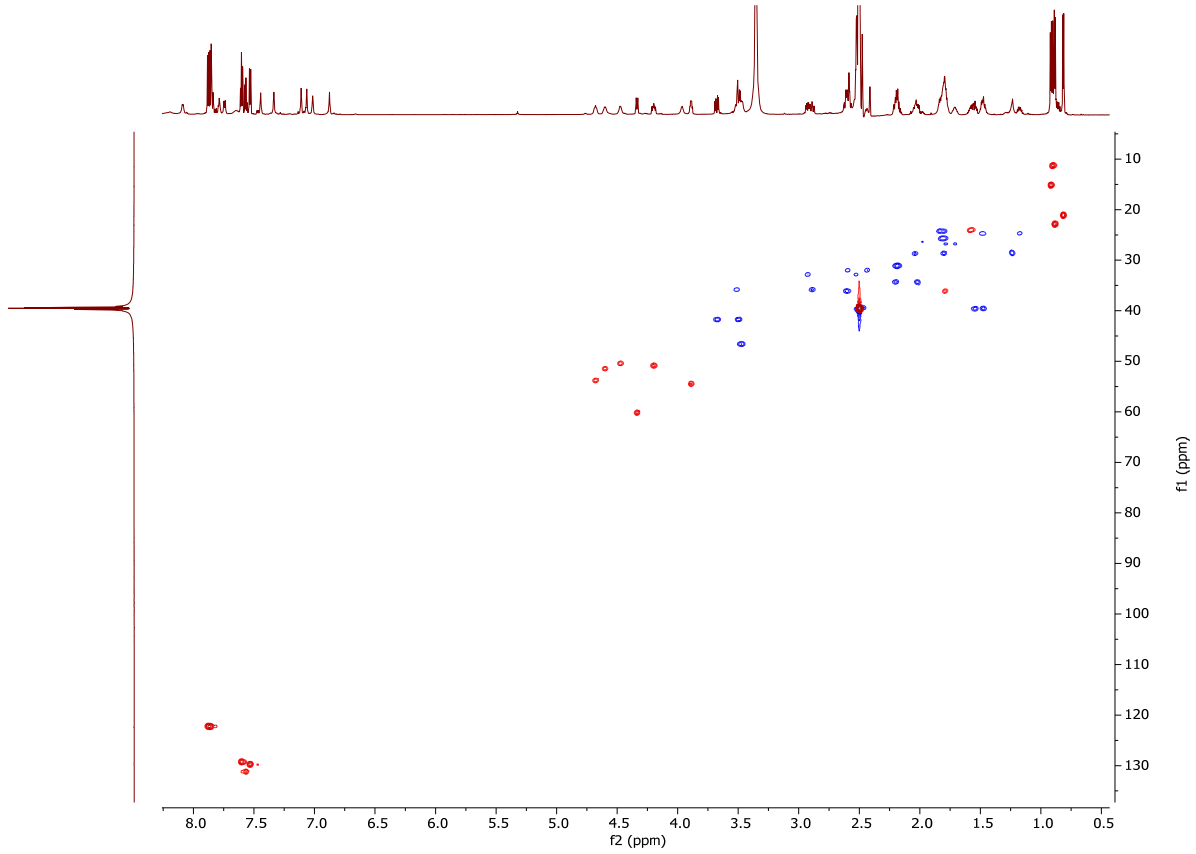

Figure 3.51: $^{1}H,^{13}C$-HSQC of **ACTB1**.

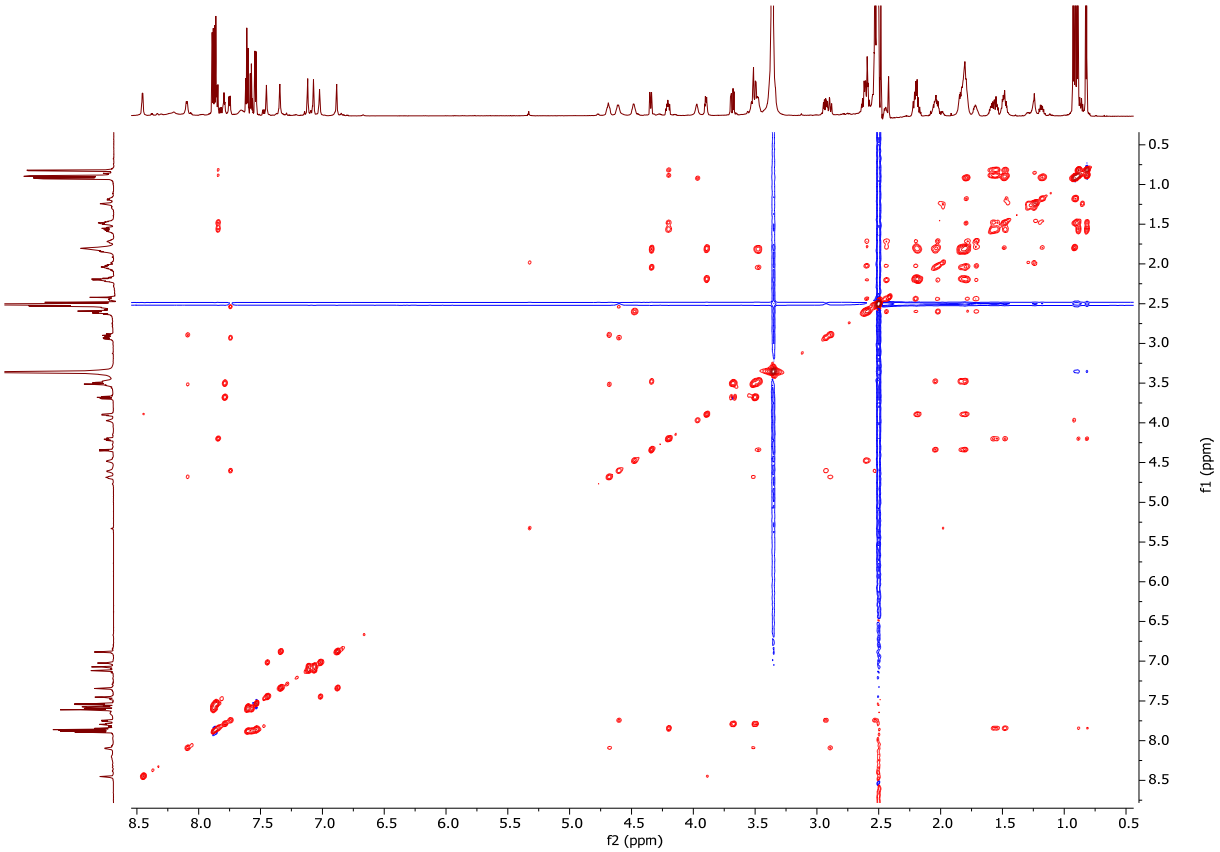

Figure 3.52: $^{1}H,^{1}H$-TOCSY of **ACTB1**.

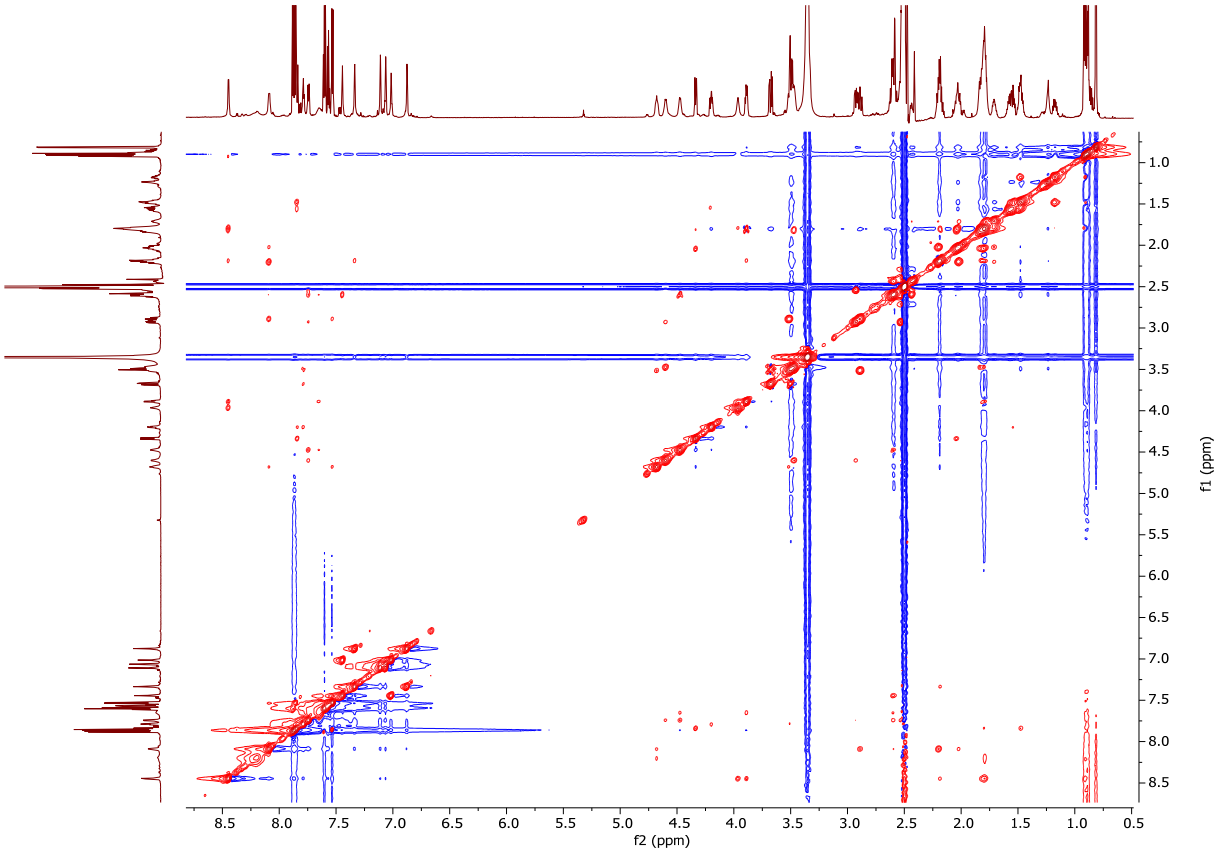

Figure 3.53: ^{1}H,^{1}H-NOESY of **ACTB1**.

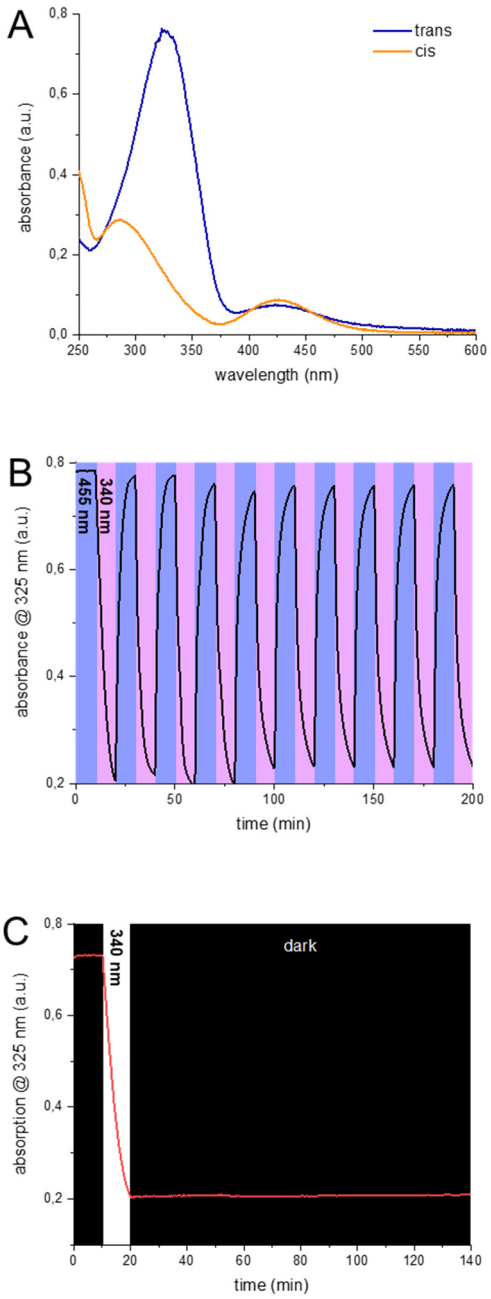

Figure 3.54: A) UV/VIS spectra of trans- and cis-**ACTB1**; illumination with 340 nm (trans→cis) and 455 nm (cis→trans). B) Kinetics of **ACTB1**. C) Bistabilty of **ACTB1**.

Analytical Data of ACBT2

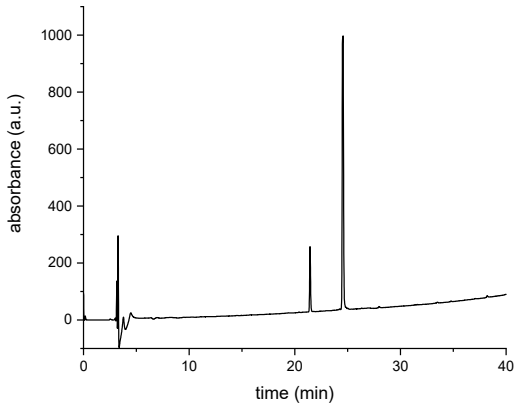

Figure 3.55: Analytical HPLC spectrum of **ACTB2** with a water/acetonitrile gradient of 95/5 →20/80 in 40 min. R_f: 21.4 min (cis) and 246 min (trans).

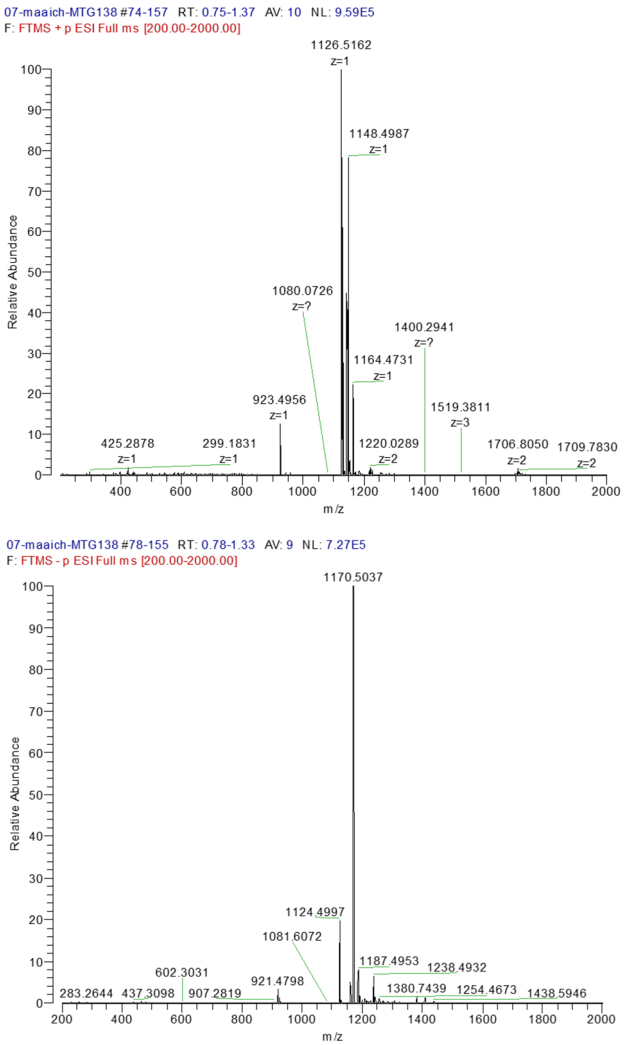

Figure 3.56: HRMS spectrum of **ACTB2**: HRMS (+ESI) m/z calc. for $C_{54}H_{72}N_{13}O_{12}S^+$ $[M + H]^+$: 1126.5139; found: 1126.5162. HRMS (−ESI) m/z calc. for $C_{55}H_{72}N_{13}O_{14}S^-$ [M+ FA – H] $^-$: 1170.5048; found: 1106.5037.

Table 3.6: ^{1}H- and ^{13}C-NMR of trans-ACTB2 in DMSO-d_6.

Residue	^{1}H-signals	^{13}C-signals
Butyric acid	Hα$_1$ 2.17, Hα$_2$ 2.00, Hβ$_1$ 1.78, Hβ$_2$ 1.69, Hγ$_1$ 2.60, Hγ$_2$ 2.43	Cα 34.4, Cβ 26.8, Cγ 32.0
Tyr(Ome)	NH 7.96, Hα 4.52, Hβ$_1$ 3.31, Hβ$_2$ 2.70, Hδ 7.21, Hε 6.86, Hη 3.72	Cα 54.4, Cβ 35.0, Cγ 157.8, Cδ 129.6, Cε 113.4, Cζ 157.8, Cη 54.7
Ile	Hα 3.93, Hβ 1.76, Hγ$_{1a}$ 1.46, Hγ$_{1b}$ 1.15, Hγ$_2$ 0.88, Hδ 0.88	Cα 58.4, Cβ 36.0, Cγ$_1$ 24.7, Cγ$_2$ 15.1, Cδ 11.2
Gln	NH 8.36, Hα 3.86, Hβ$_1$ 1.79, Hβ$_2$ 1.76, Hγ 2.17	Cα 54.4, Cβ 25.7, Cγ 31.1
Asn	NH 7.66, Hα 4.47, Hβ 2.59	Cα 50.7, Cβ 36.1
Cys	NH 7.74, Hα 4.58, Hβ$_1$ 2.92, Hβ$_2$ 2.55	Cα 51.6, Cβ 33.3
Pro	Hα 4.27, Hβ$_1$ 1.92, Hβ$_2$ 1.59, Hγ$_1$ 1.73, Hγ$_2$ 1.64, Hδ$_1$ 3.44, Hδ$_2$ 3.48	Cα 60.5, Cβ 28.7, Cγ 24.3, Cδ 46.8
3.3	NH 7.95, H1 4.54, H2$_a$ 3.72, H2$_b$ 2.91, H4/8 7.44, H5/7 7.81, H12/16 7.88, H13/15 7.59, H14 7.56	C1 53.4, C2 36.4, C3 142.9, C4/8 129.9, C5/7 122.1, C6 150.3, C11 151.7, C12/16 122.3, C13/15 129.2, C14 131.1
Gly	NH 7.44, Hα$_1$ 3.72, Hα$_2$ 3.57	Cα 41.8

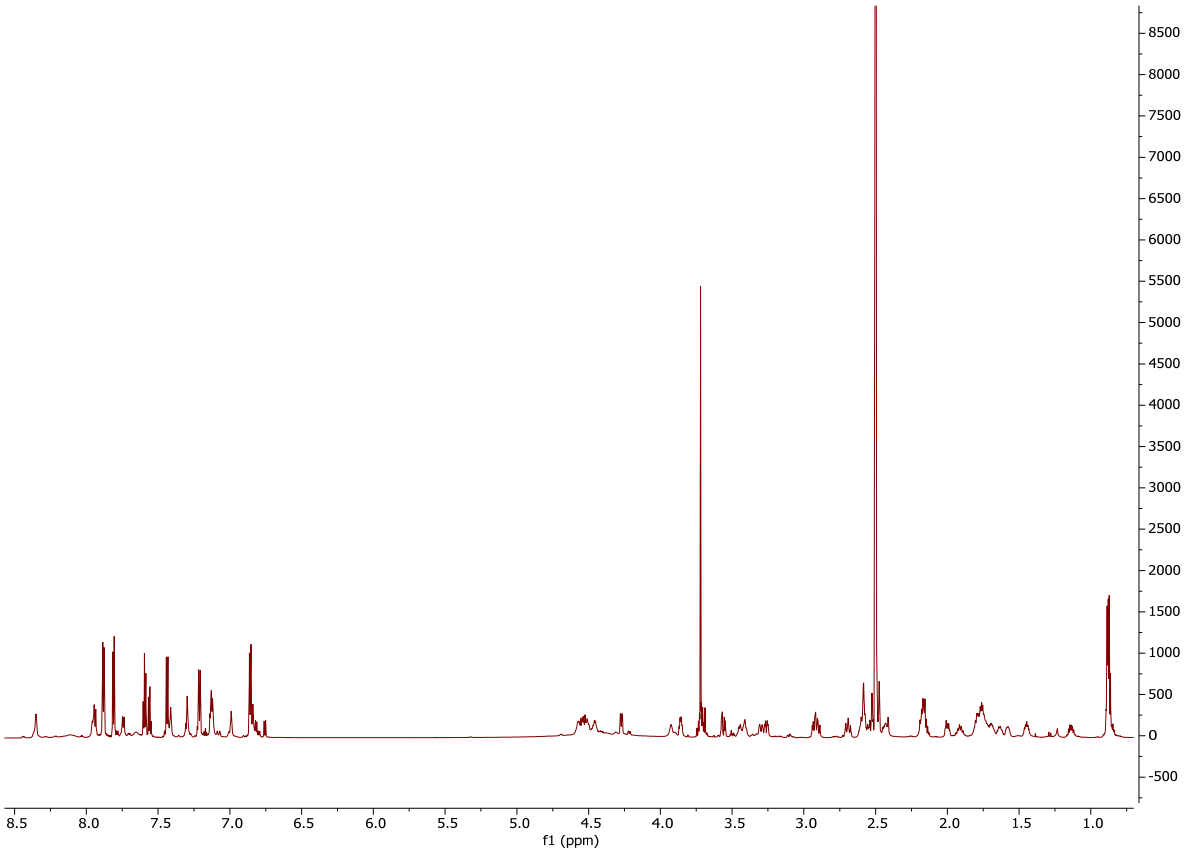

Figure 3.57: ^{1}H-NMR of **ACTB2**.

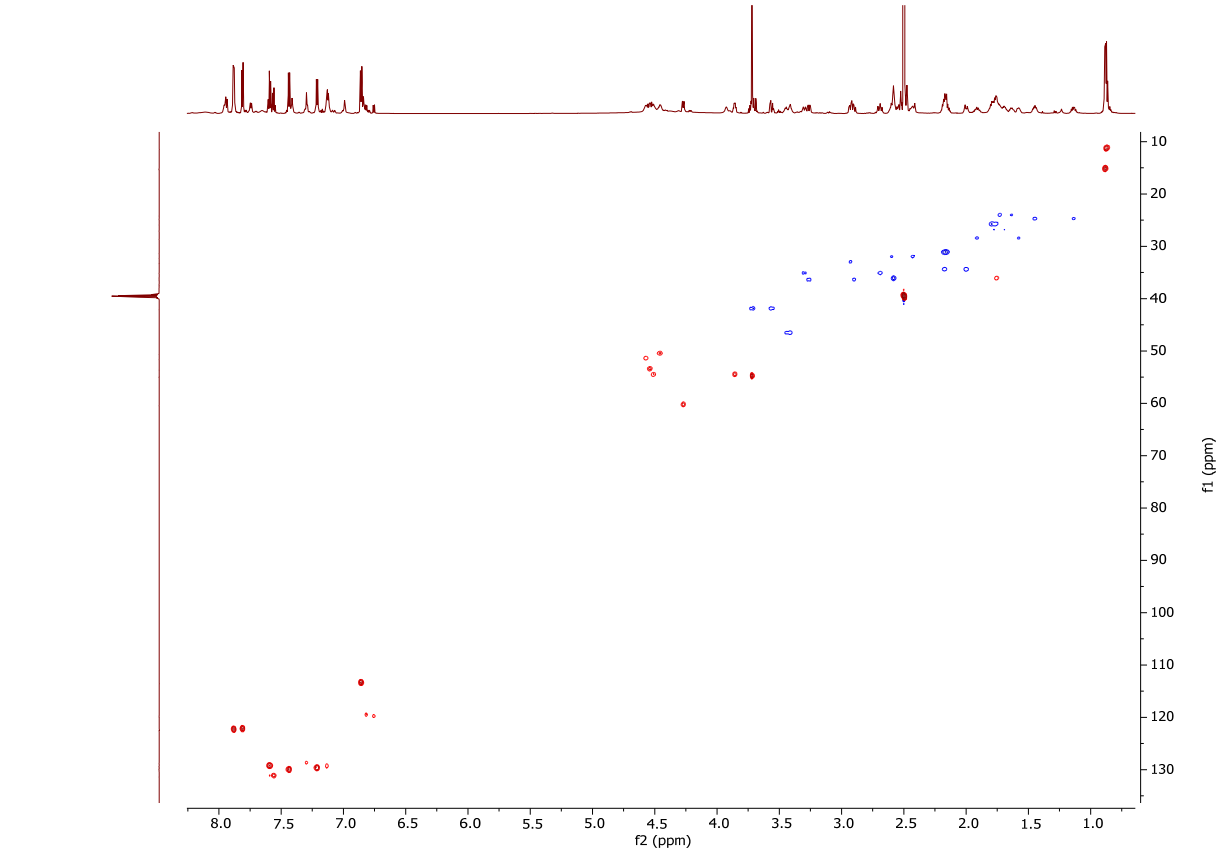

Figure 3.58: ^{1}H, ^{13}C-HSQC of **ACTB2**.

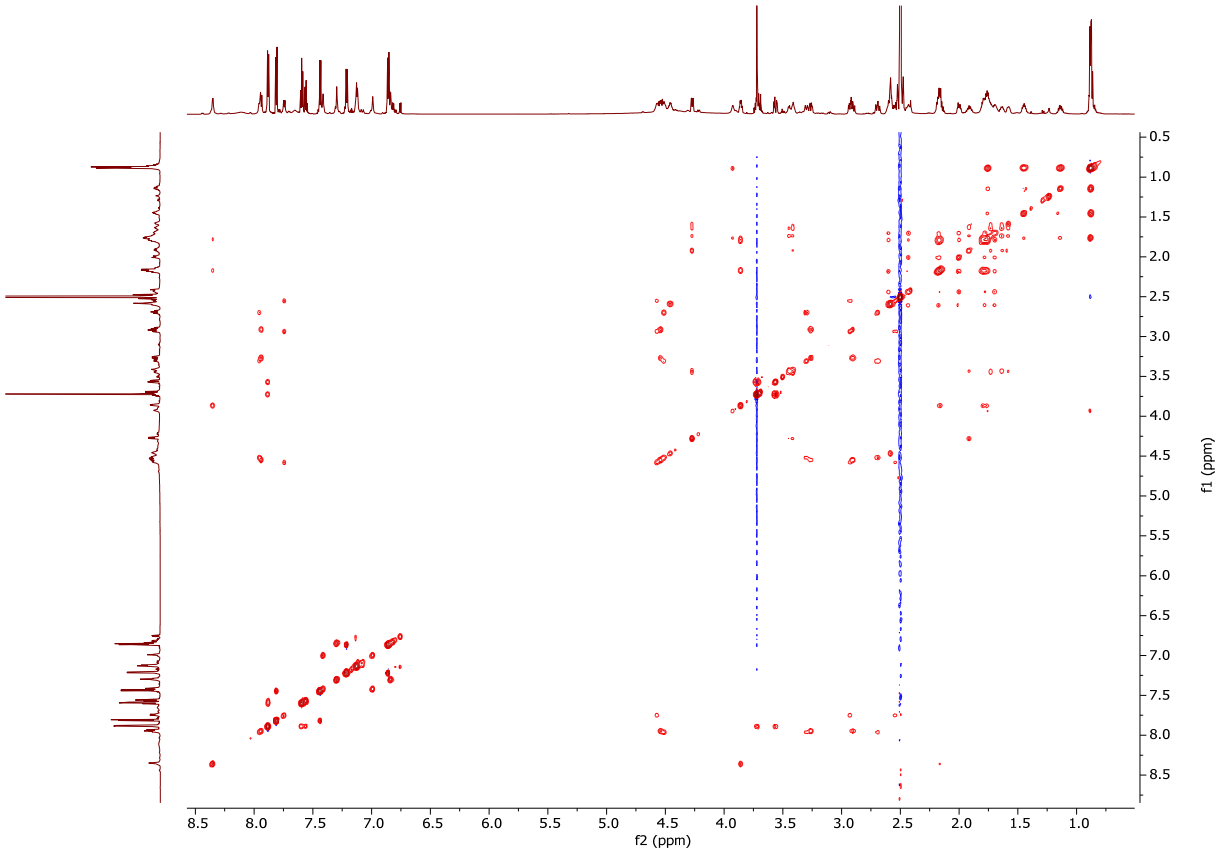

Figure 3.59: ^{1}H,^{1}H-TOCSY of **ACTB2**.

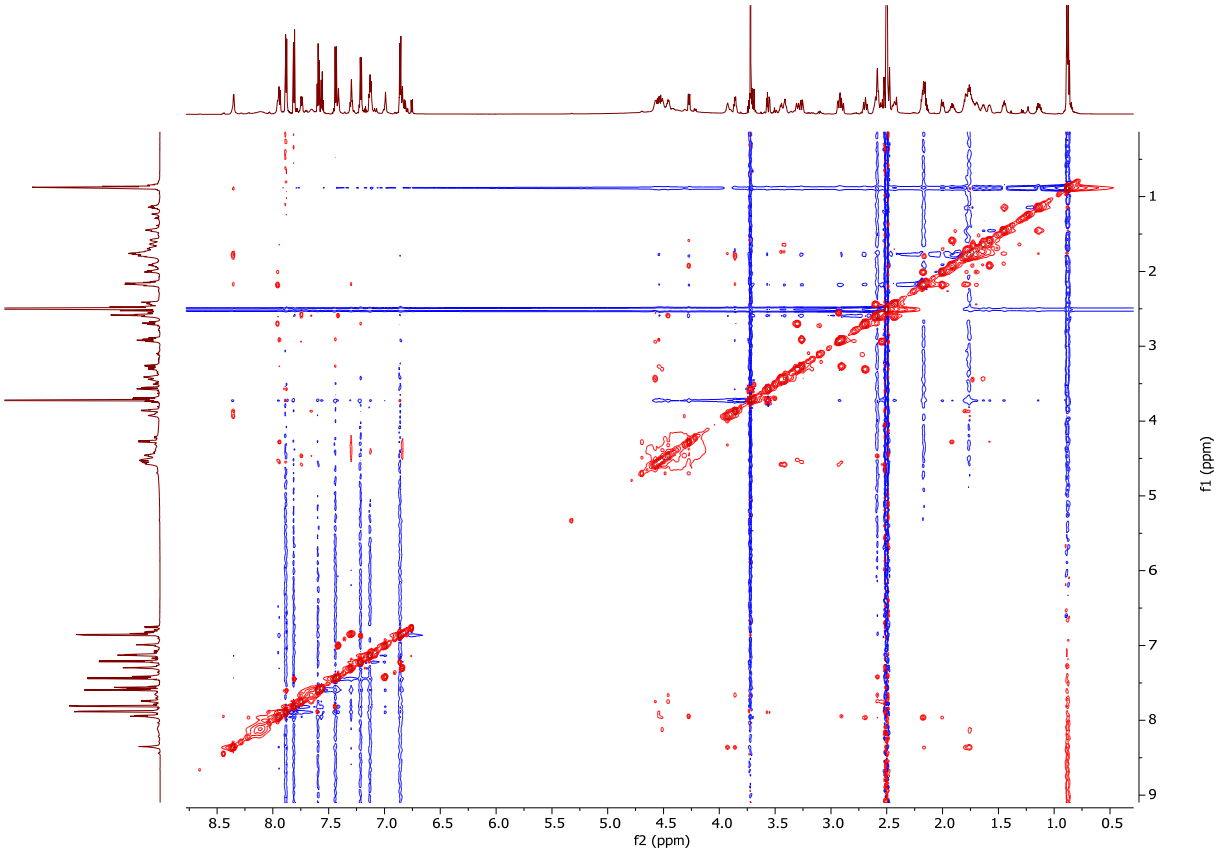

Figure 3.60: ^{1}H, ^{1}H-NOESY of **ACTB2**.

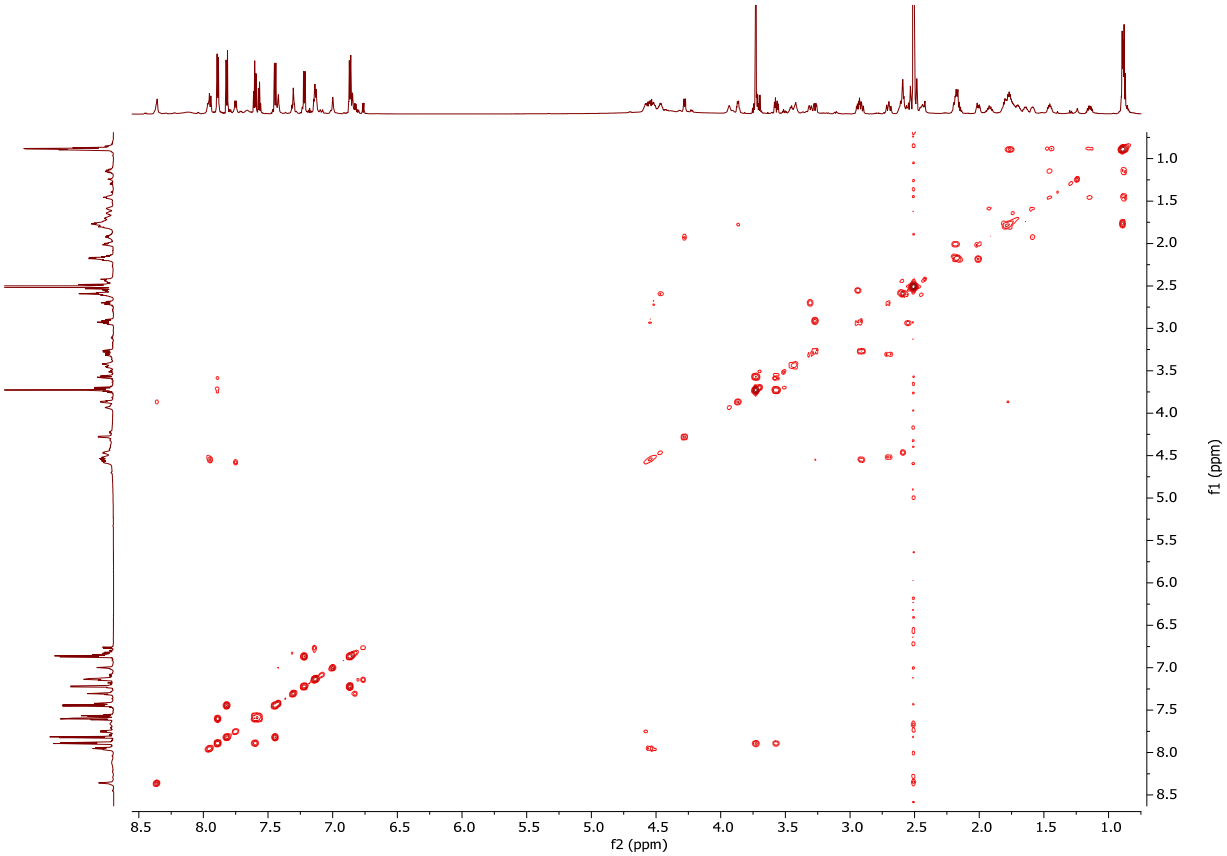

Figure 3.61: ^{1}H, H-COSY of **ACTB2**.

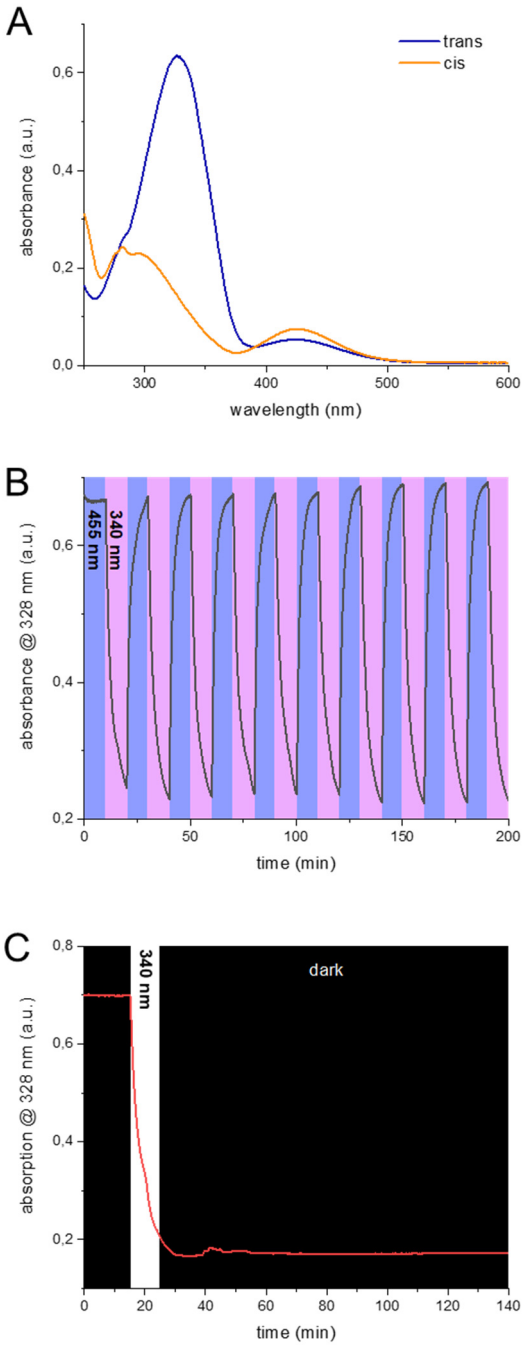

Figure 3.62: A) UV/VIS spectra of trans- and cis-**ACTB2**; illumination with 340 nm (trans→cis) and 455 nm (cis→trans). B) Kinetics of **ACTB2**. C) Bistabilty of **ACTB2**.

Analytical Data of ACTB3

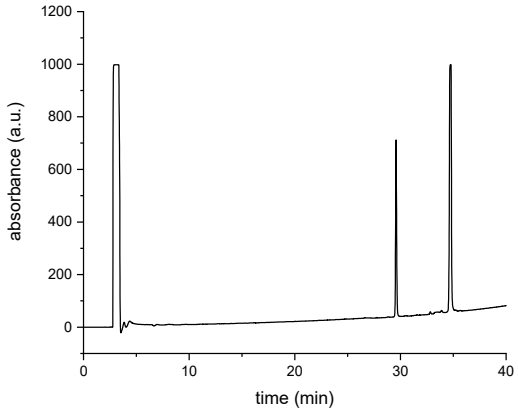

Figure 3.63: Analytical HPLC spectrum of **ACTB3** with a water/acetonitrile gradient of 95/5 →20/80 in 40 min. R_f: 29.6 min (cis) and 34.8 min (trans).

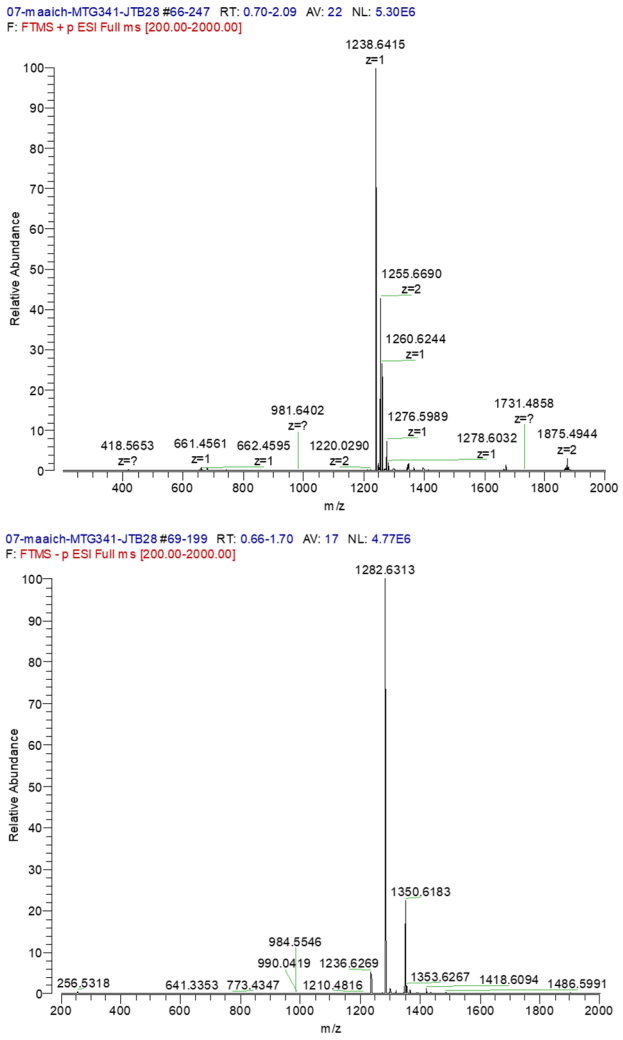

Figure 3.64: HRMS spectrum of **ACTB3**: HRMS (+ESI) m/z calc. for $C_{62}H_{88}N_{13}O_{12}S^+$ $[M + H]^+$: 1138.6391; found: 1138.6415. : HRMS (−ESI) m/z calc. for $C_{63}H_{88}N_{13}O_{12}S^-$ $[M + FA−H]^-$: 1282.6300; found: 1282.6313.

Table 3.7: Chemical shifts of ^{1}H- and ^{13}C-NMR of trans-**ACTB3**.

residue	^{1}H-NMR	^{13}C-NMR
Butyric acid	Hα$_1$ 2.17, Hα$_2$ 1.99, Hβ$_1$ 1.77, Hβ$_2$ 1.69, Hγ$_1$ 2.60, Hγ$_2$ 2.41	Cα 34.4, Cβ 26.9, Cγ 32.0
Tyr(OMe)	NH 7.94, Hα 4.51, Hβ$_1$ 3.30, Hβ$_2$ 2.68, Hδ 7.21, Hε 6.86, Hη 3.72	Cα 54.5, Cβ 35.1, Cγ 157.8, Cδ 129.6, Cε 113.3, Cζ 157.8, Cη 54.7
Ile	Hα 3.91, Hβ 1.75, Hγ$_{1a}$ 1.45, Hγ$_{1b}$ 1.1, Hγ$_2$ 0.88, Hδ 0.87	Cα 58.4, Cβ 36.0, Cγ$_1$ 24.7, Cγ$_2$ 15.1, Cδ 11.2
Gln	NH 8.36, Hα 3.91, Hβ$_1$ 1.78, Hγ 2.16	Cα 54.5, Cβ 25.7, Cγ 31.1
Asn	NH 7.64, Hα 4.46, Hβ 2.58	Cα 50.4, Cβ 36.1
Cys	NH 7.74, Hα 4.57, Hβ$_1$ 2.93, Hβ$_2$ 2.52	Cα 51.3, Cβ 32.9
Pro	Hα 4.27, Hβ$_1$ 1.92, Hβ$_2$ 1.58, Hγ 1.73, Hδ$_1$ 3.42	Cα 60.2, Cβ 28.4, Cγ 23.9, Cδ 46.5
3.9	NH 7.81, H1 4.54, H2$_a$ 3.26, H2$_b$ 2.89, H4/8 7.42, H5/7 7.81, H12/16 7.71, H14 7.61	C1 53.6, C2 36.5, C3 141.9, C4/8 129.9, C5/7 122.1, C6 150.4, C11 151.8, C12/16 116.5, C13/15 151.7, C14 125.1
Gly	NH 7.88, Hα$_1$ 3.71, Hα$_2$ 3.57	Cα 41.8

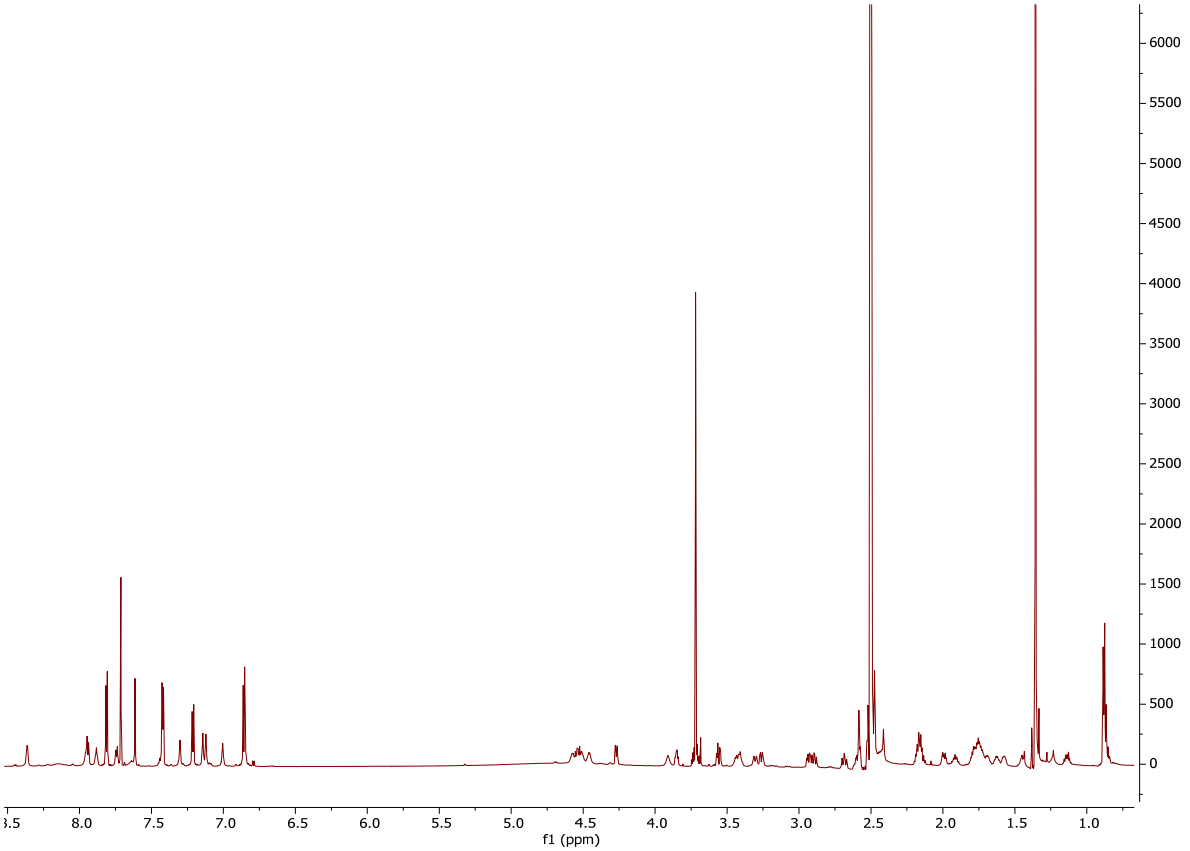

Figure 3.65: ^{1}H-NMR of **ACTB3**.

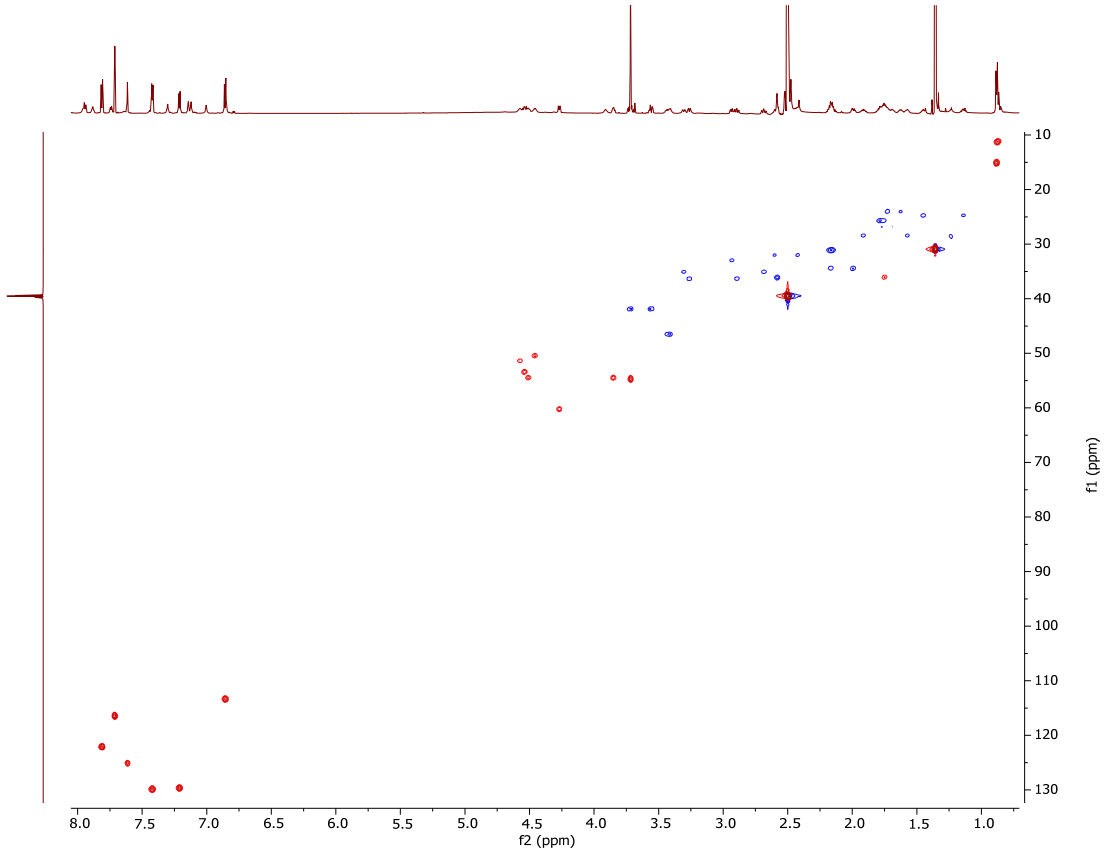

Figure 3.66: ^{1}H, ^{13}C-HSQC of **ACTB3**.

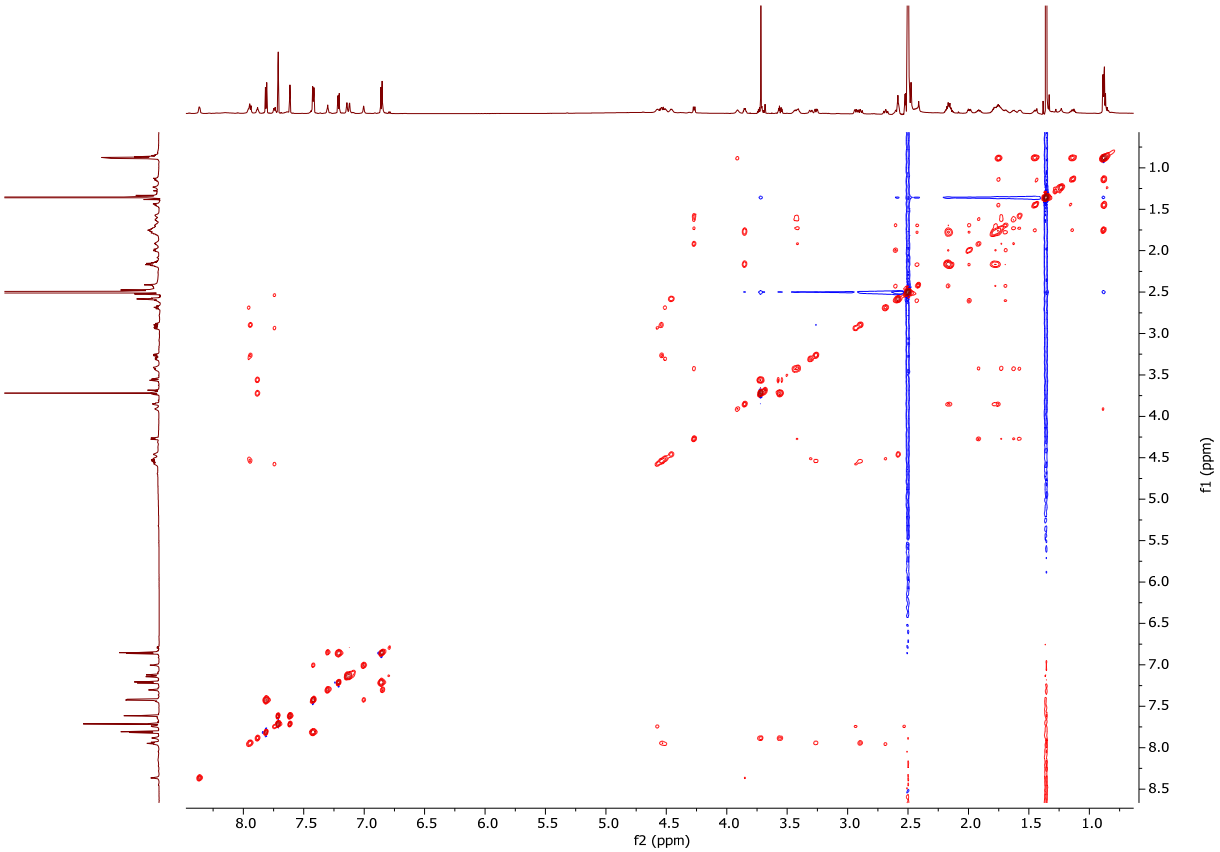

Figure 3.67: ^{1}H, ^{13}C-TOCSY of **ACTB3**.

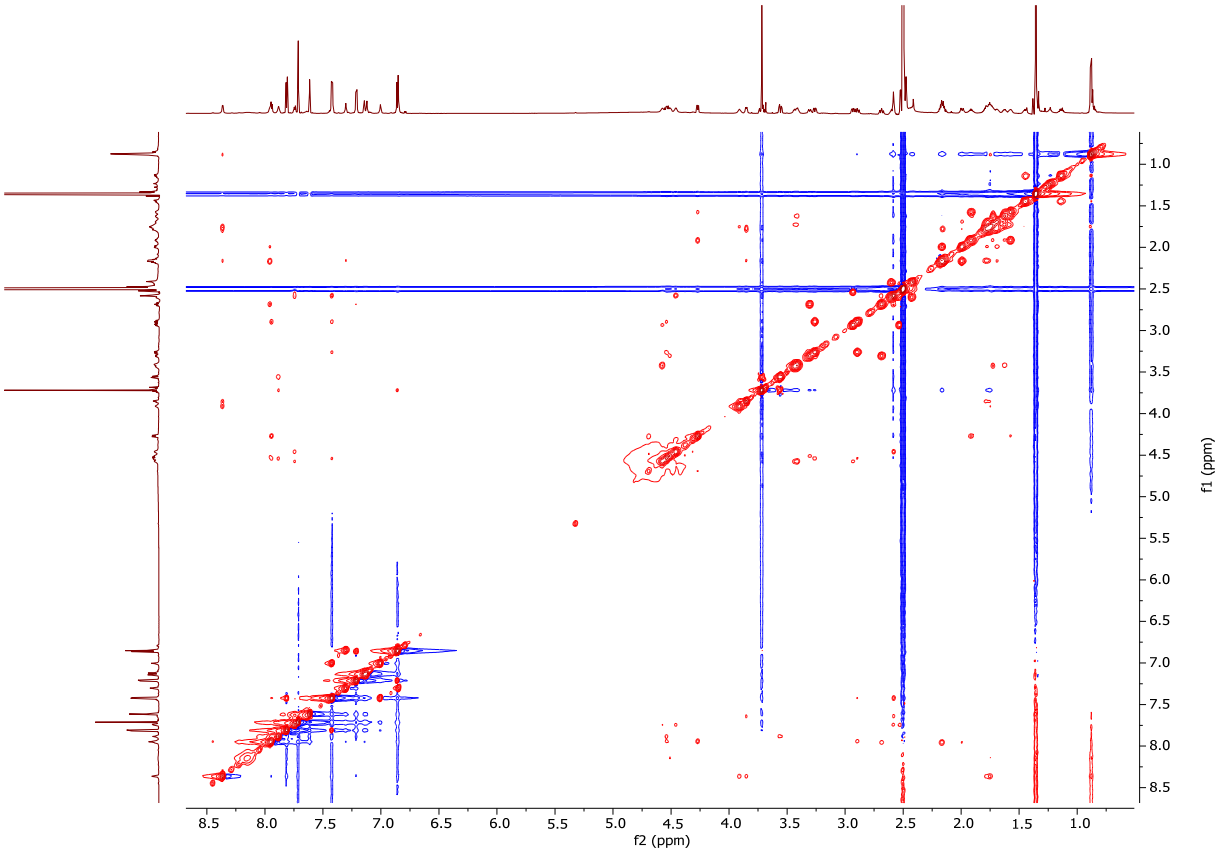

Figure 3.68: ^{1}H, ^{1}H-NOESY of **ACTB3**.

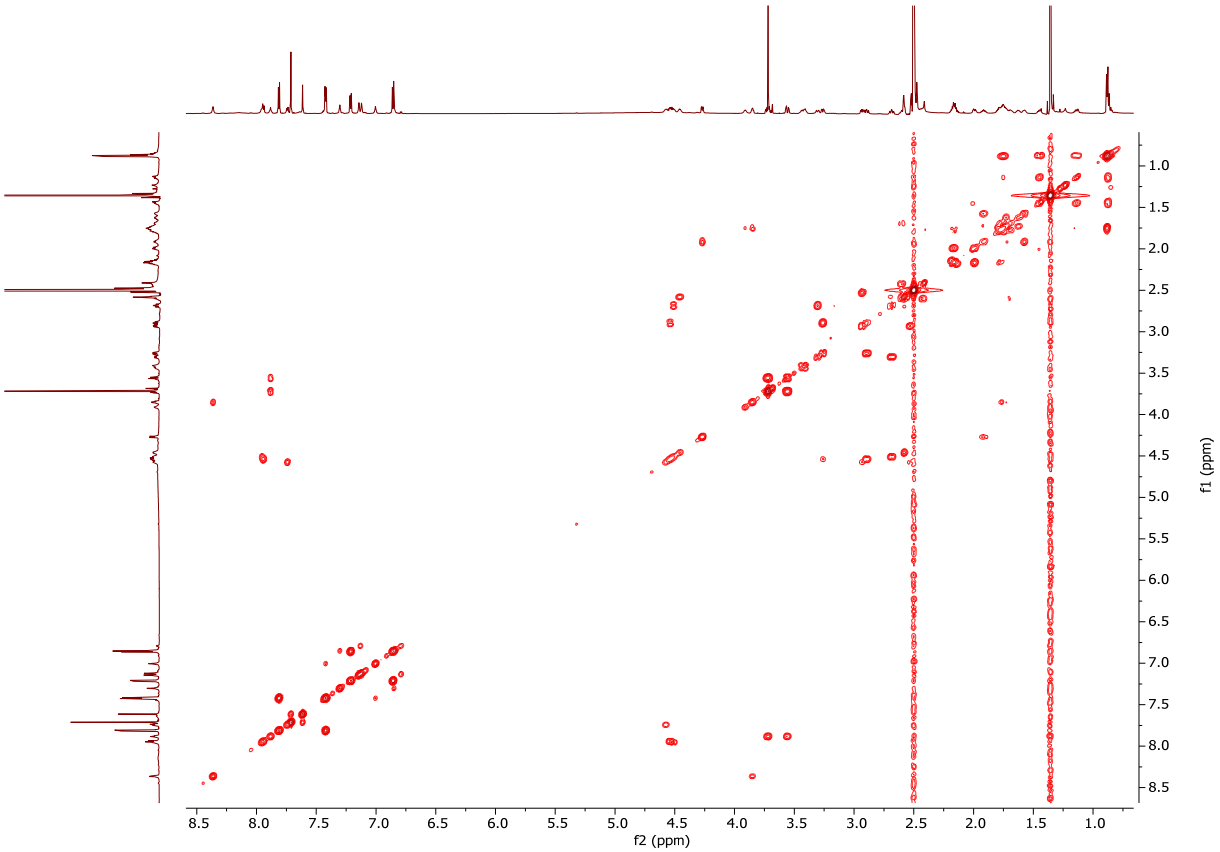

Figure 3.69: ^{1}H, ^{1}H-COSYvof **ACTB3**.

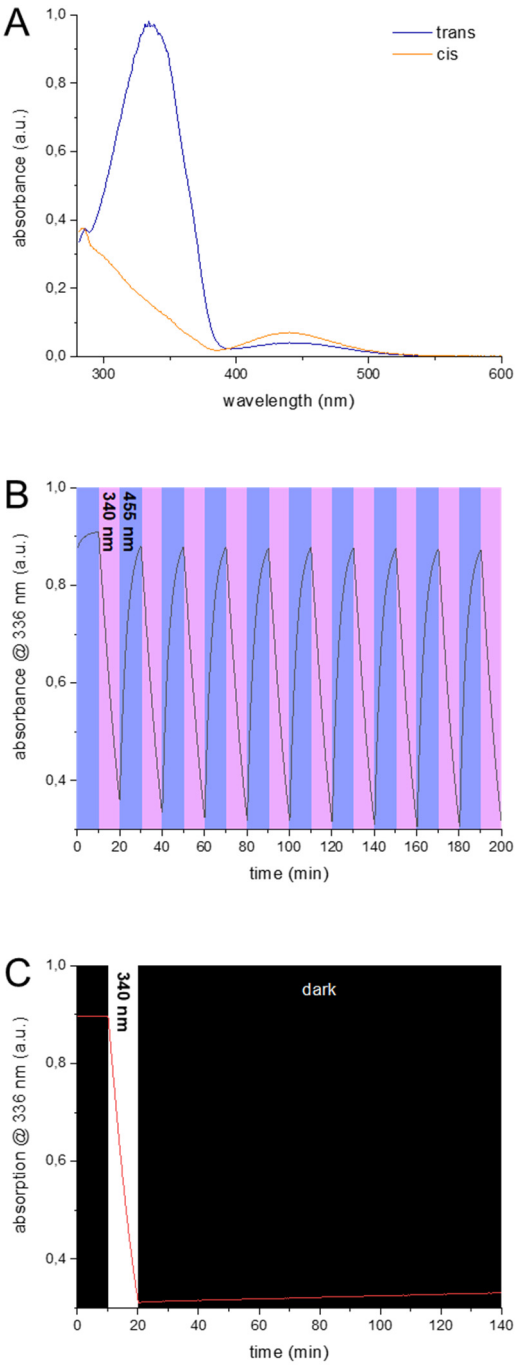

Figure 3.70: A) UV/VIS spectra of trans- and cis-**ACTB3**; illumination with 340 nm (trans→cis) and 455 nm (cis→trans). B) Kinetics of **ACTB3**. C) Bistabilty of **ACTB3**.

Analytical Data of ACTB4

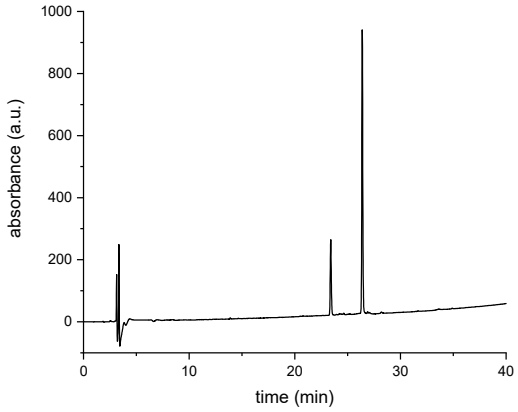

Figure 3.71: Analytical HPLC spectrum of **ACTB4** with a water/acetonitrile gradient of 95/5 →20/80 in 40 min. R_f: 23.4 min (cis) and 26.4 min (trans).

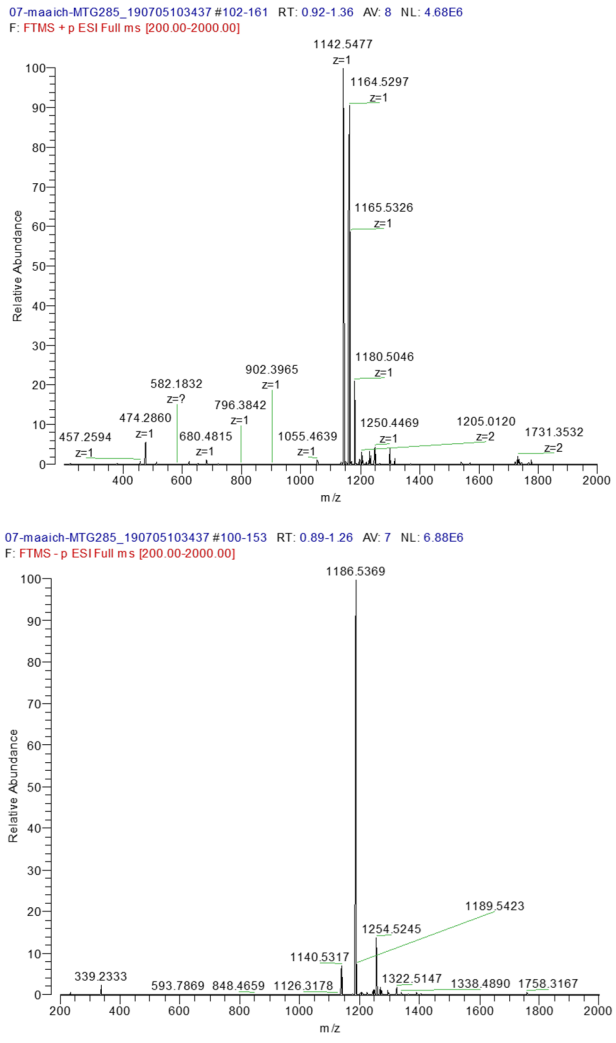

Figure 3.72: HRMS spectrum of **ACTB4**: HRMS (+ESI) m/z calc. for $C_{55}H_{76}N_{13}O_{12}S^+$ $[M + H]^+$: 1142.5452; found: 1142.5477. HRMS (−ESI) m/z calc. for $C_{56}H_{76}N_{13}O_{14}S^-$ $[M + FA-H]^-$: 1186.5361; found: 1186.5369.

Table 3.8: Chemical shifts of ^{1}H- and ^{13}C-NMR of **ACTB4**.

residue	^{1}H-NMR	^{13}C-NMR
Butyric acid	Hα$_1$(K1) 2.20, Hα$_2$(K1) 2.07, Hα$_1$(K2) 2.03, Hα$_2$(K2) 1.90, Hβ$_1$ 1.70, Hβ$_2$ 1.62, Hγ$_1$(K1) 2.53, Hγ$_2$(K1) 2.48, Hγ$_1$(K2) 2.40, Hγ$_2$(K2) 2.33	Cα(K1) 34.4, Cα(K2) 34.2, Cβ 25.6, Cγ(K1) 31.9, Cγ$_1$(K2) 31.8
Tyr(OMe)	NH 7.94, Hα(K1) 4.49, Hα(K2) 4.47, Hβ$_1$(K1) 3.23, Hβ$_1$ 3.21(K2), Hβ$_2$ 2.71, Hδ(K1) 7.19, Hδ(K2) 7.16, Hε 6.84(K1), Hε 6.83(K2), Hη 3.72(K1), Hη 3.72(K2)	Cα(K1) 54.4, Cα(K2) 54.2, Cβ(K1) 35.4, Cβ(K2) 35.3, Cγ 157.7, Cδ 129.6, Cε 113.3, Cζ 157.7, Cη 54.7
Ile	Hα(K1) 4.18, Hα(K2) 4.11, Hβ(K1) 1.85, Hβ(K2) 1.75, Hγ$_{1a}$(K1) 1.46, Hγ$_{1a}$(K2) 1.42, Hγ$_{1b}$(K1) 1.14, Hγ$_{1b}$(K2) 1.08, γ$_2$(K1) 0.86, Hγ$_2$(K2) 0.82, Hδ(K1) 0.90, Hδ(K2) 0.84	Cα(K1) 57.6, Cα(K2) 57.4, Cβ 36.5, Cγ$_1$(K1) 24.4, Cγ$_1$(K2) 24.1, Cγ$_2$(K1) 15.2, Cγ$_2$(K2) 15.2, Cδ(K1) 11.2, Cδ(K2) 11.0
Gln	NH(K1) 8.34, NH(K2) 8.27, Hα 3.93, Hβ$_1$ 1.87, Hβ$_2$ 1.81, Hγ 2.18	Cα 54.0, Cβ 26.0, Cγ 31.2
Asn	NH(K1) 7.95, NH(K2) 7.93, Hα(K1) 4.45, Hα(K2) 4.38 Hβ(K1) 2.62, Hβ(K2) 2.60	Cα(K1) 50.2, Cβ(K1) 35.8, Cβ(K2) 35.5
Cys	NH(K1) 7.82, NH(K2) 2.97, Hα(K1) 4.73, Hα(K1) 4.70 Hβ$_1$ 2.74, Hβ$_2$ 2.64	Cα(K1) 49.4, Cα(K2) 49.9, Cβ 33.3
Gly-N(R)$_2$	Hα$_1$(K1) 4.36, Hα$_2$(K1) 3.91, Hα(K2) 3.93	Cα(K1) 49.5, Cα(K2) 48.7
3.22	H1$_1$(K1) 4.84, H1$_2$(K1) 4.75, H2$_1$(K2) 4.64, H2$_2$(K2) 4.49, H3/7(K1) 7.55, H3/7(K2) 7.45, H4/6(K1) 7.89, H4/6(K2) 7.82, H11/15 7.89, H12/14 7.60, H13 7.57	Cα(K1) 50.9, Cα(K1) 49.2, C2(K1) 151.6, C2(K2) 151.0, C3/7(K1) 128.2, H3/7(K2) 128.5, H4/6 122.3, C5(K1) 151.2, C5(K2) 151.0, C10 151.9, H11/15 122.3, H12/14 129.3, H13 131.2
Leu	NH(K1) 8.30, NH(K2) 8.00, Hα 4.22, Hβ(K1) 1.48, Hβ$_1$(K2) 1.43, Hβ$_2$(K2) 1.37, Hγ(K1) 1.56, Hγ(K2) 1.47, Hδ$_1$(K1) 0.87, Hδ$_2$(K1) 0.83, Hδ$_1$(K2) 0.82, Hδ$_2$(K2) 0.78	Cα 51.2, Cβ 40.4, Cγ 23.7, Cδ$_1$ 22.7, Cδ$_2$ 21.3
Gly	NH(K1) 8.10, NH(K2) 8.21, Hα$_1$(K1) 3.65, Hα$_2$(K1) 3.60, Hα(K2) 3.63	Cα(K1) 41.6, Cα(K2) 41.7

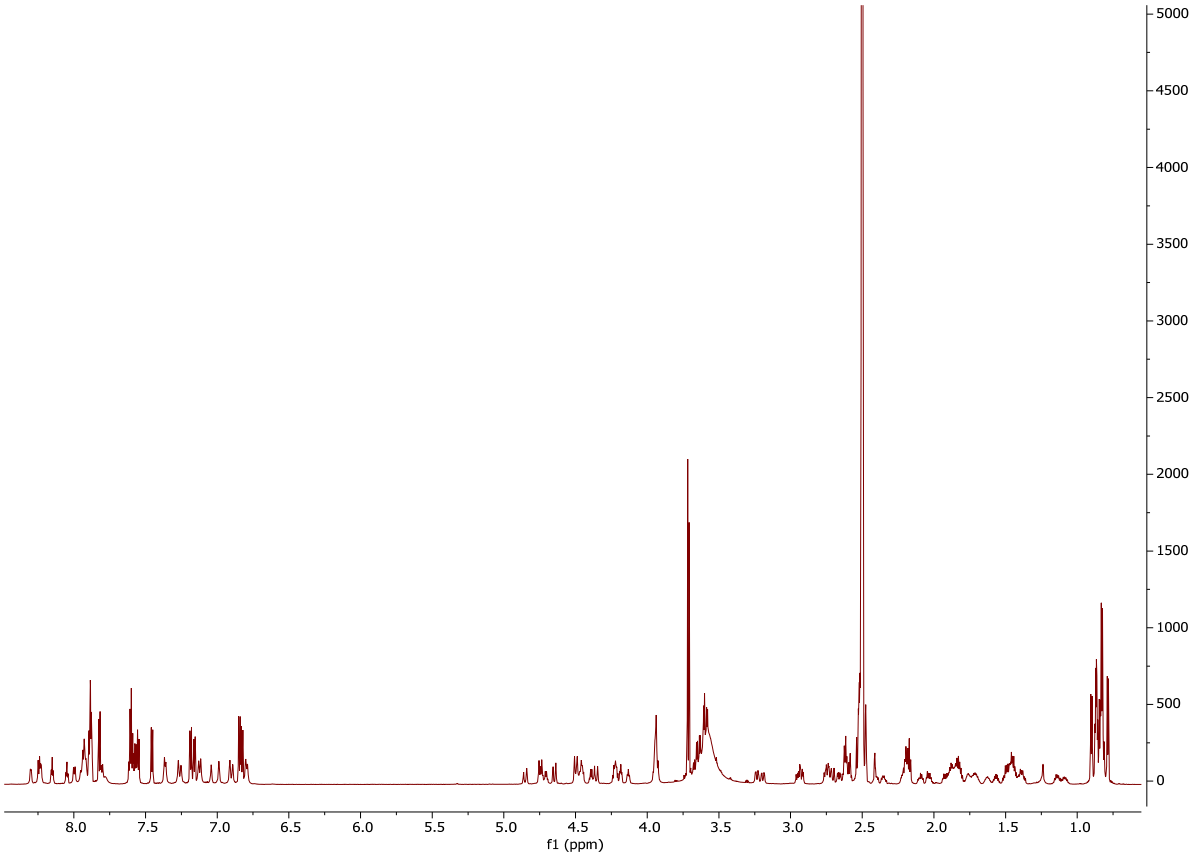

Figure 3.73: ^{1}H-NMR of **ACTB4**.

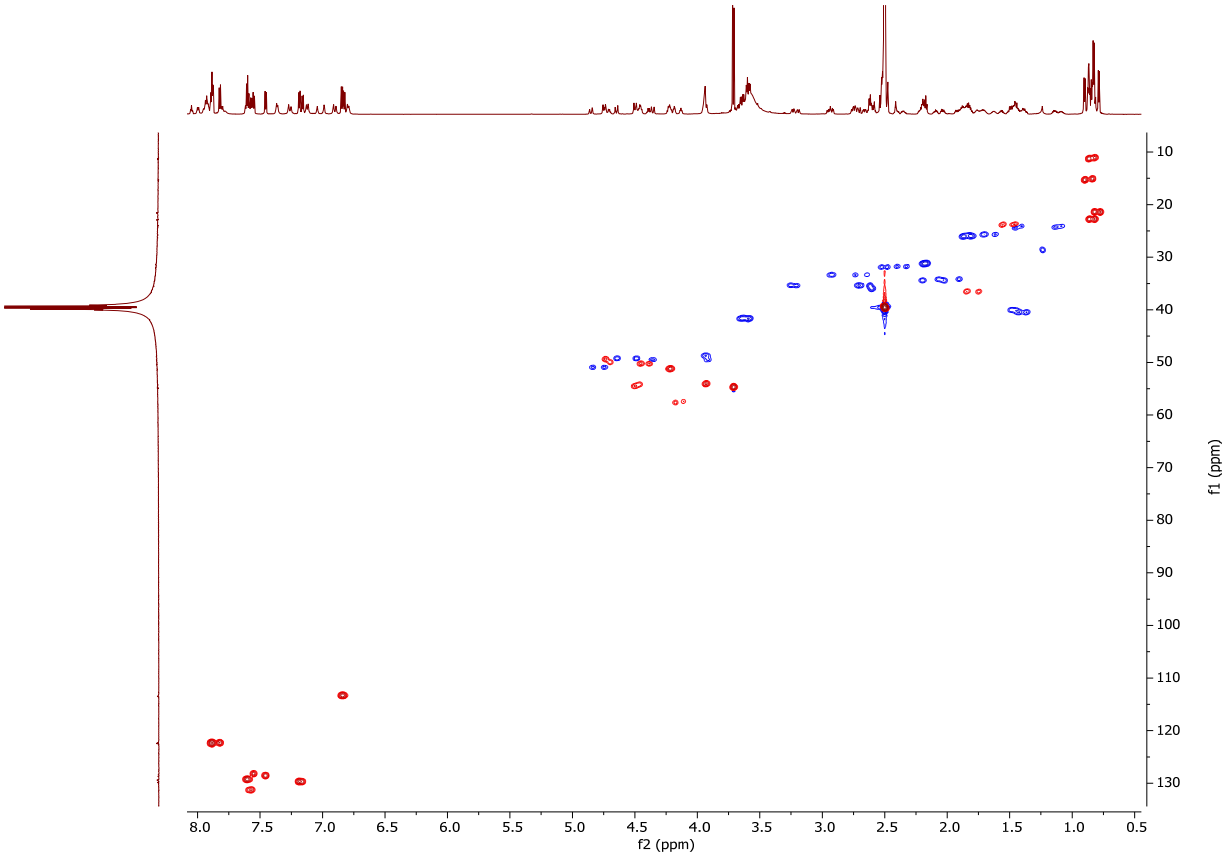

Figure 3.74: ^{1}H, ^{13}C-HSQC-NMR of **ACTB4**.

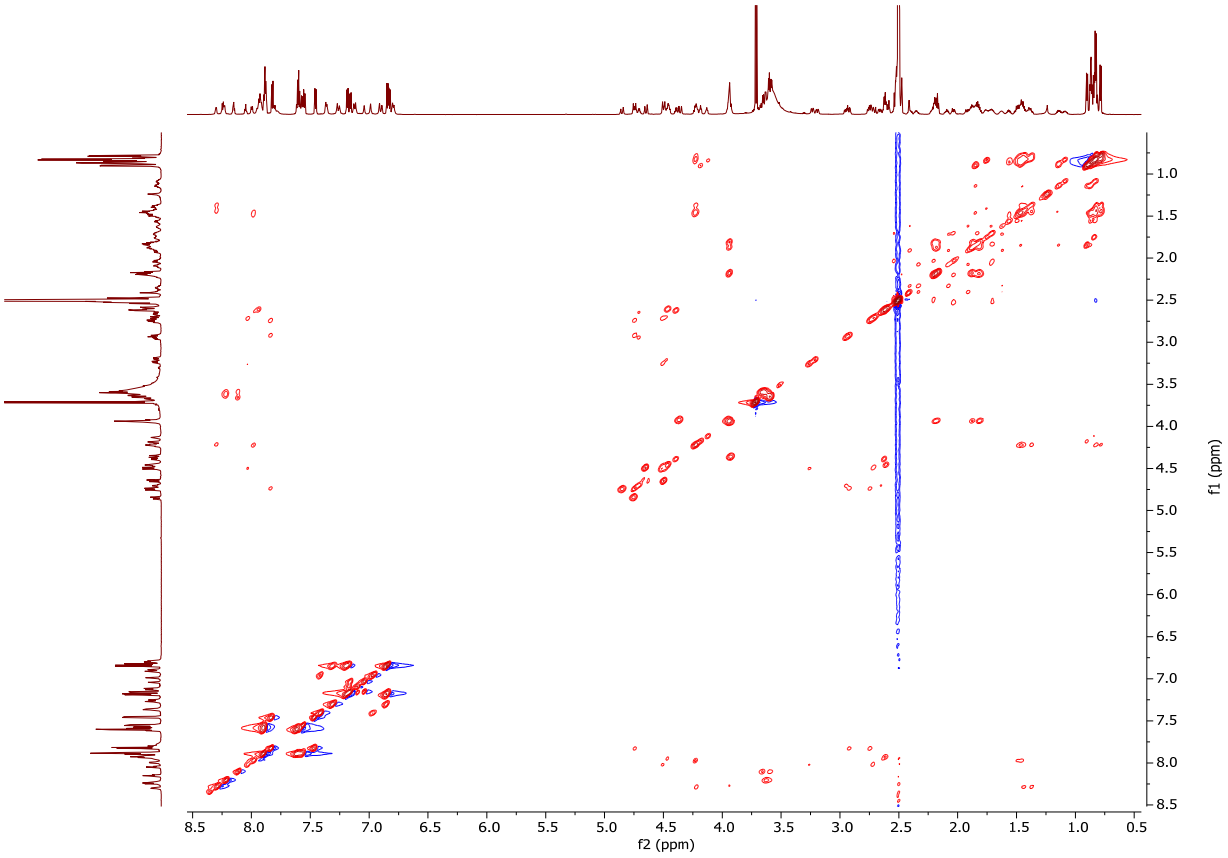

Figure 3.753: ^{1}H, ^{1}H-TOCSY of **ACTB4**.

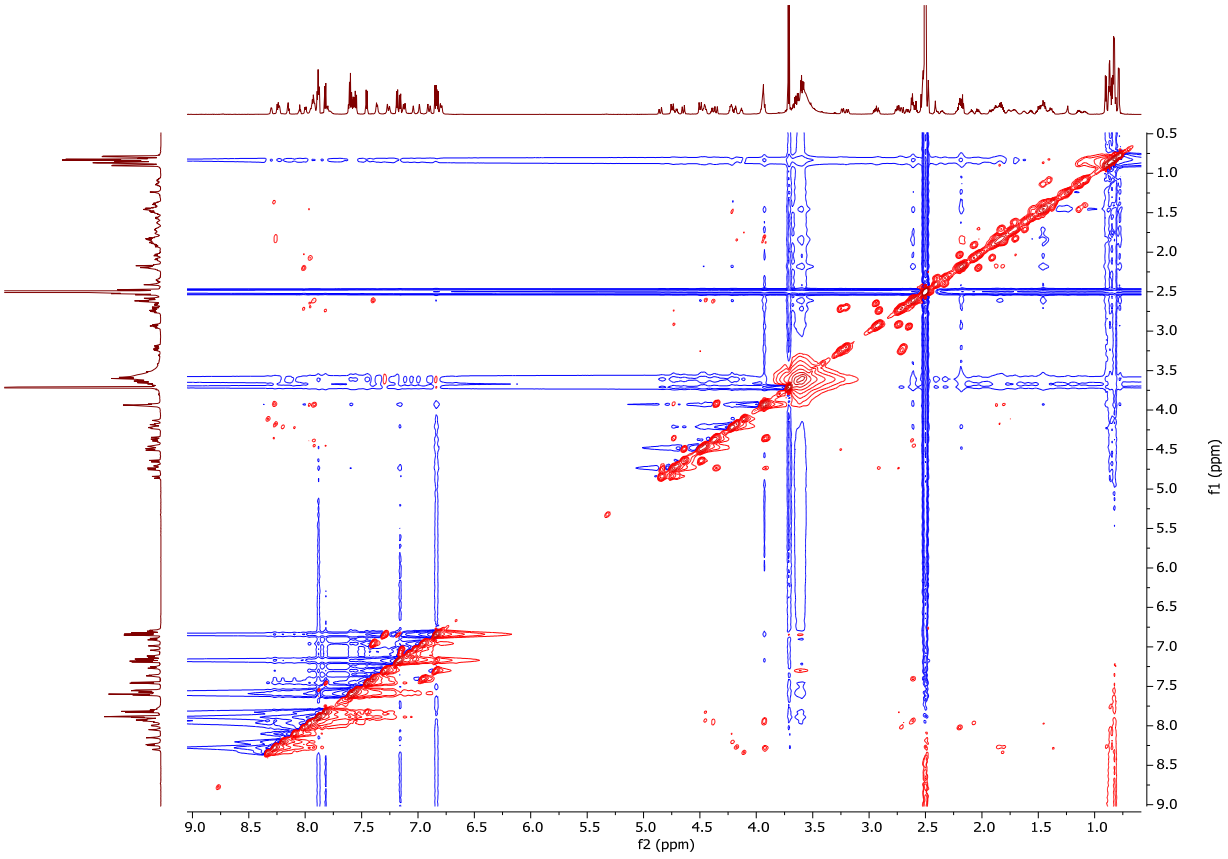

Figure 3.76: ^{1}H, ^{1}H-NOESY-NMR of **ACTB4**.

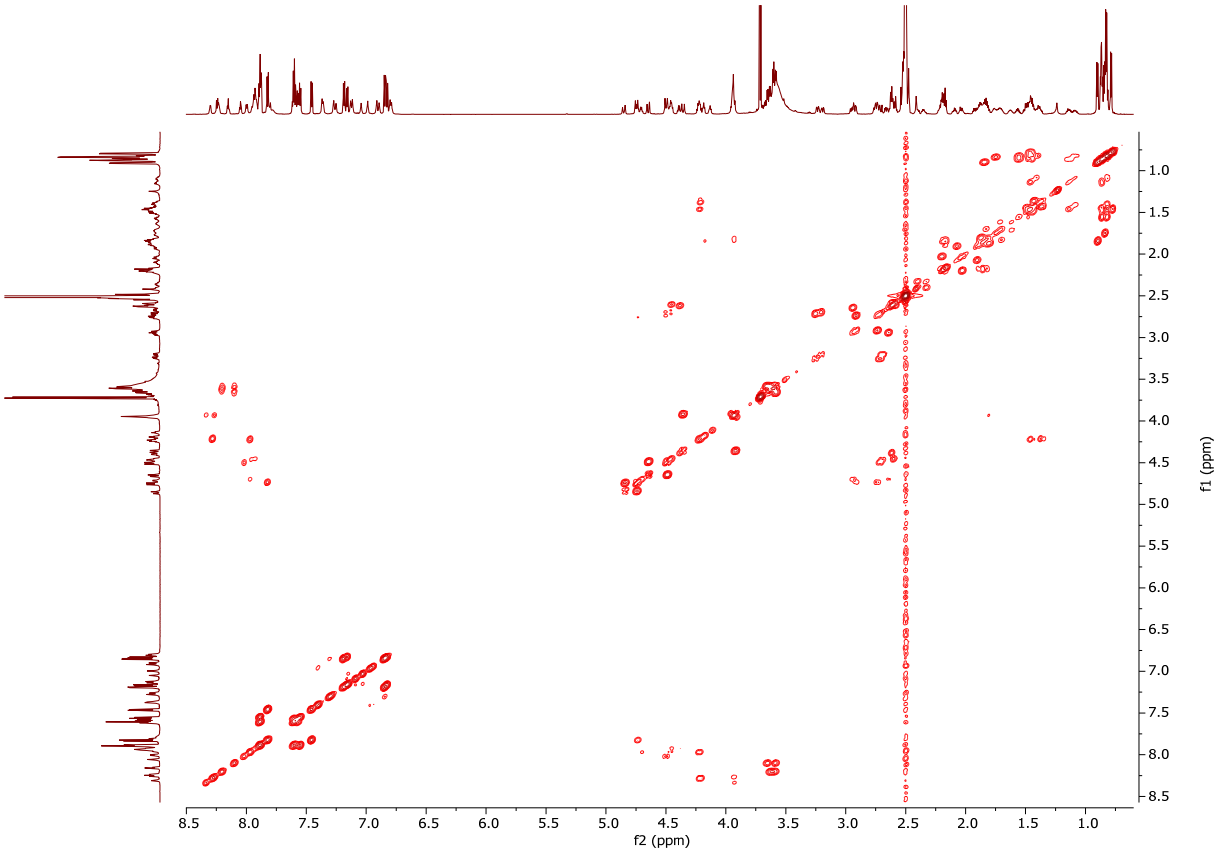

Figure 3.77: ^{1}H, ^{1}H-COSY of **ACTB4**.

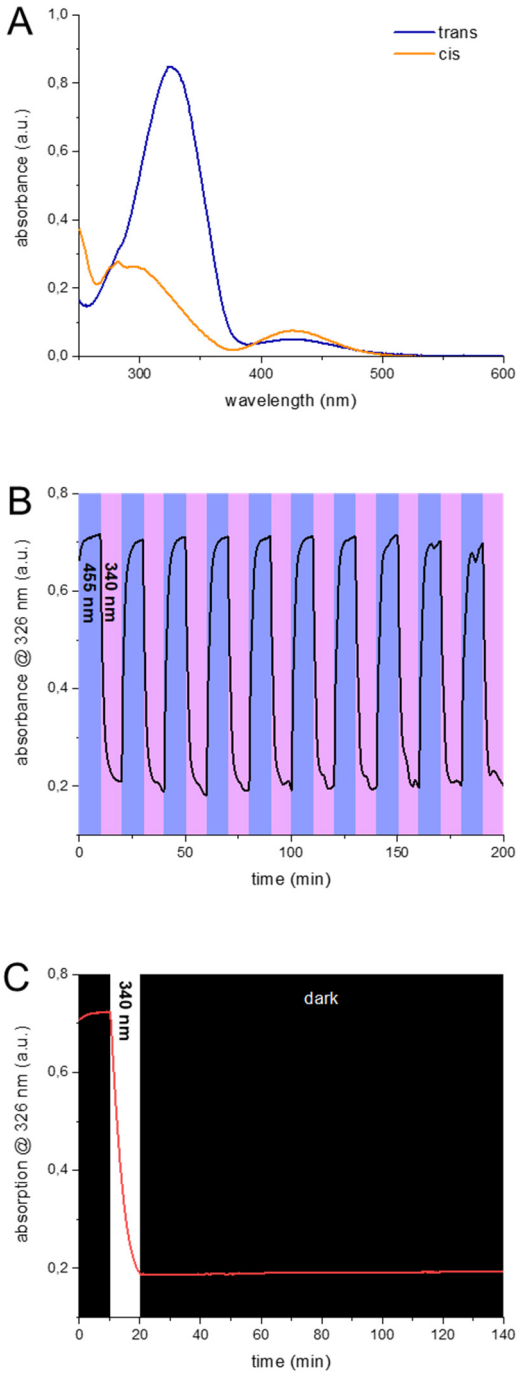

Figure 3.78: A) UV/VIS spectra of trans- and cis-**ACTB4**; illumination with 340 nm (trans→cis) and 455 nm (cis→trans). B) Kinetics of **ACTB4**. C) Bistabilty of **ACTB4**.

Analytical Data of ACTB5

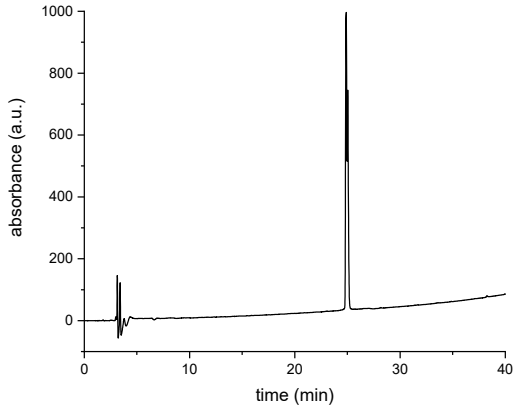

Figure 3.79: Analytical HPLC spectrum of **ACTB5** with a water/acetonitrile gradient of 95/5 →20/80 in 40 min. R_f: 24.9 min (trans) and 25.0 min (cis).

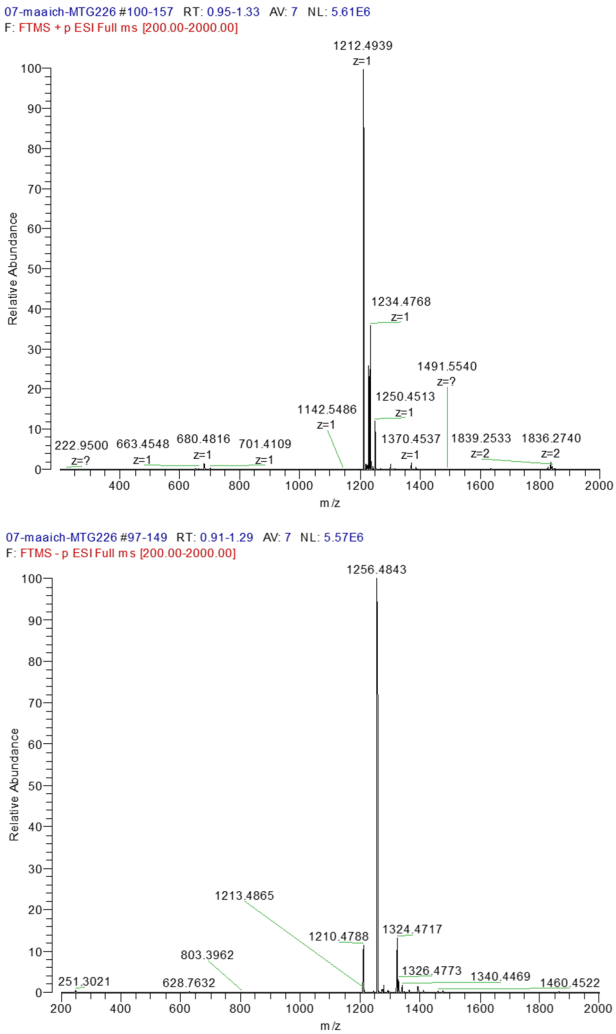

Figure 3.80: HRMS spectrum of ACTB5: HRMS (+ESI) m/z calc. for $C_{55}H_{70}F_4N_{13}O_{12}S^+$ $[M + H]^+$: 1212.4918; found: 1212.4939. HRMS (−ESI) m/z calc. for $C_{56}H_{70}F_4N_{13}O_{12}S^-$ $[M + FA-H]^-$: 1256.4827; found: 1256.4843.

Table 3.9: Chemical shifts of the ^{1}H- and ^{13}C-NMR of **ACTB5** in DMSO-d_6.

residue	^{1}H-NMR	^{13}C-NMR
3.19	$H1_a$ 3.73, $H1_b$ 3.40, H3 7.49, H4 7.54, H5 7.72, H7 7.81	C1 41.3, C2 128.0, C3 134.4, C4 129.2, C5 119.6, C6 152.5, C7 123.5
Tyr(OMe)	NH 8.60, Hα 4.49, $H\beta_1$ 2.94, $H\beta_2$ 2.74, Hδ 7.19, Hε 6.85, Hη 3.72	Cα 54.4, Cβ 35.9, Cγ 157.6, Cδ 129.9, Cε 113.3, Cζ 157.6, Cη 54.7
Ile	NH 7.60, Hα 4.09, Hβ 1.59, $H\gamma_{1a}$ 1.28, $H\gamma_{1b}$ 0.81, $H\gamma_2$ 0.56, Hδ 0.60	Cα 56.5, Cβ 36.4, $C\gamma_1$ 23.6, $C\gamma_2$ 15.0, Cδ 10.5
Gln	NH 8.23, Hα 4.06, $H\beta_1$ 1.79, $H\beta_2$ 1.63, $H\gamma_{1a}$ 1.28, $H\gamma_{1b}$ 0.81, $H\gamma_2$ 0.56, Hδ 0.60	Cα 52.2, Cβ 27.5, Cγ 31.0
Asn	NH 7.35, Hα 4.43, Hβ 2.44	Cα 48.9, Cβ 37.4
Cys	NH 8.70, Hα 4.85, $H\beta_1$ 3.33, $H\beta_2$ 2.29	Cα 51.2, Cβ 36.3
Pro	Hα 4.31, $H\beta_1$ 2.03, $H\beta_2$ 1.85, $H\gamma_1$ 1.88, $H\gamma_2$ 1.85, $H\delta_1$ 3.56, $H\delta_2$ 3.49	Cα 59.8, Cβ 28.7, Cγ 24.1, Cδ 46.4
Leu	NH 8.06, Hα 4.22, Hβ 1.52, Hγ 1.66, $H\delta_1$ 0.91, $H\delta_2$ 0.85	Cα 51.2, Cβ 39.9, Cγ 23.9, $C\delta_1$ 23.9, $C\delta_2$ 21.3
Gly	NH 7.97, $H\alpha_1$ 3.68, $H\alpha_2$ 3.49	Cα 46.4

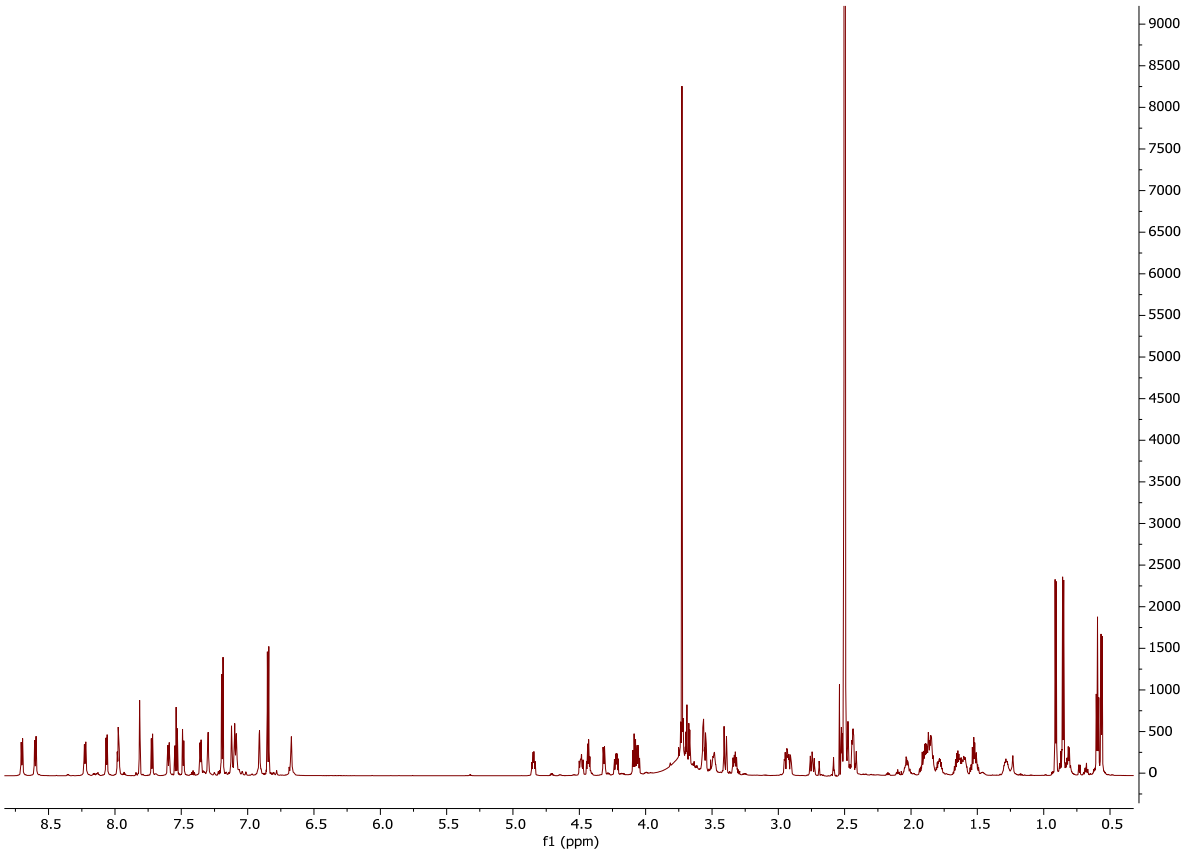

Figure 3.81: ^{1}H-NMR of **ACTB5**.

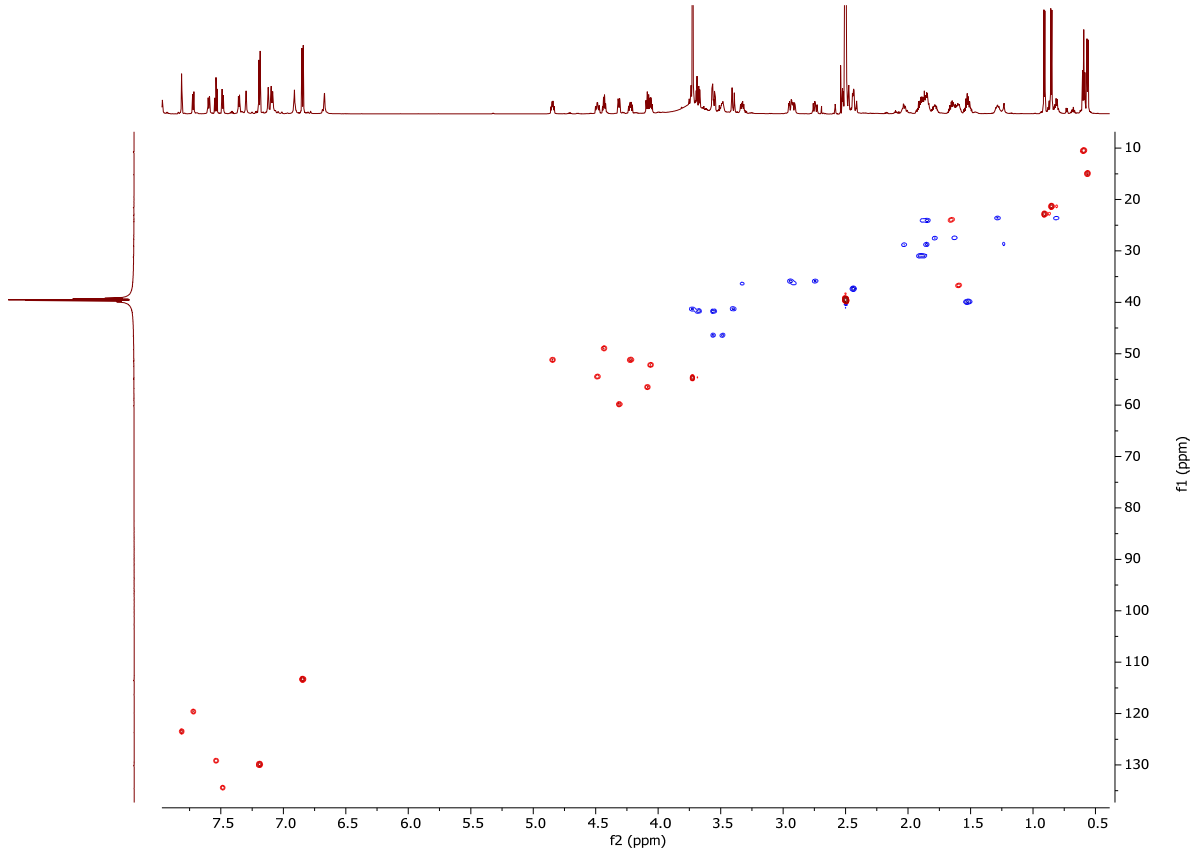

Figure 3.82: $^{1}H,^{13}C$-HSQC of **ACTB5**.

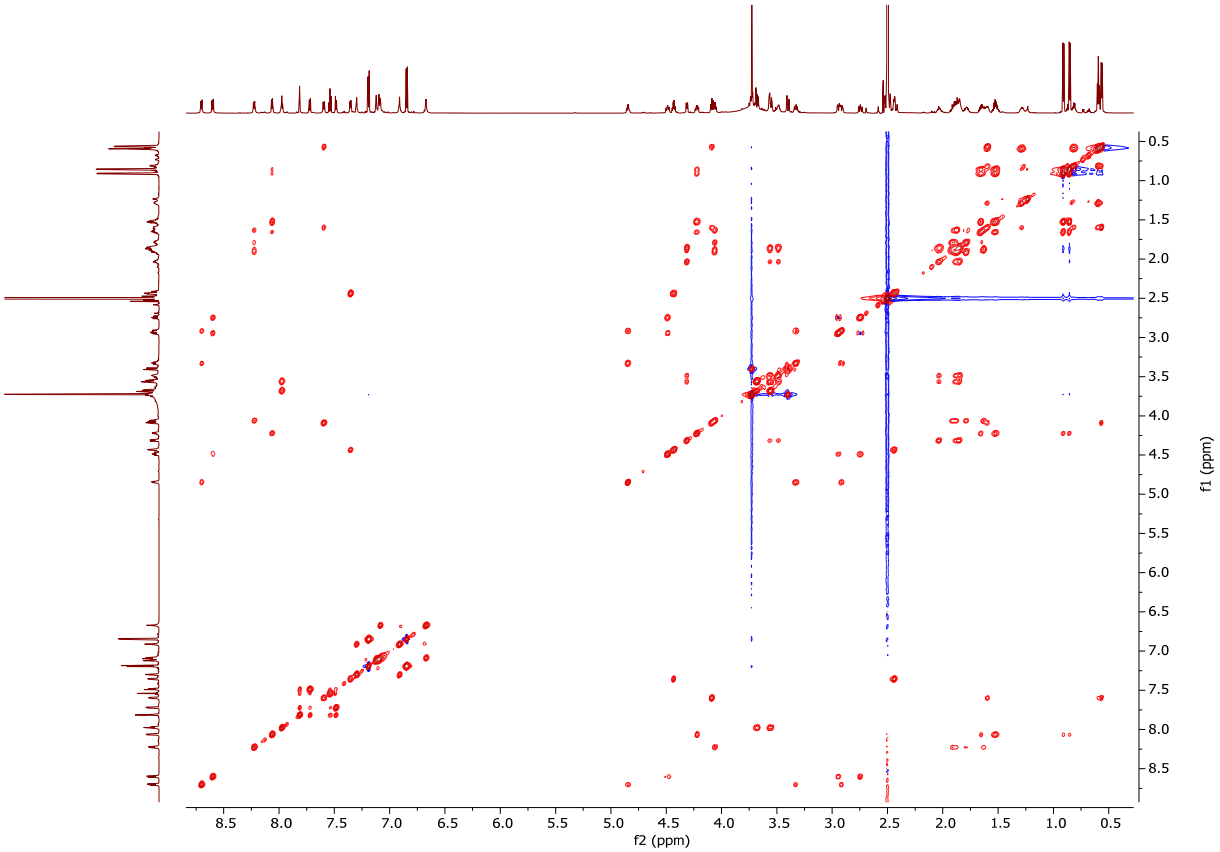

Figure 3.83: ^{1}H, ^{1}H-TOCSY of **ACTB5**.

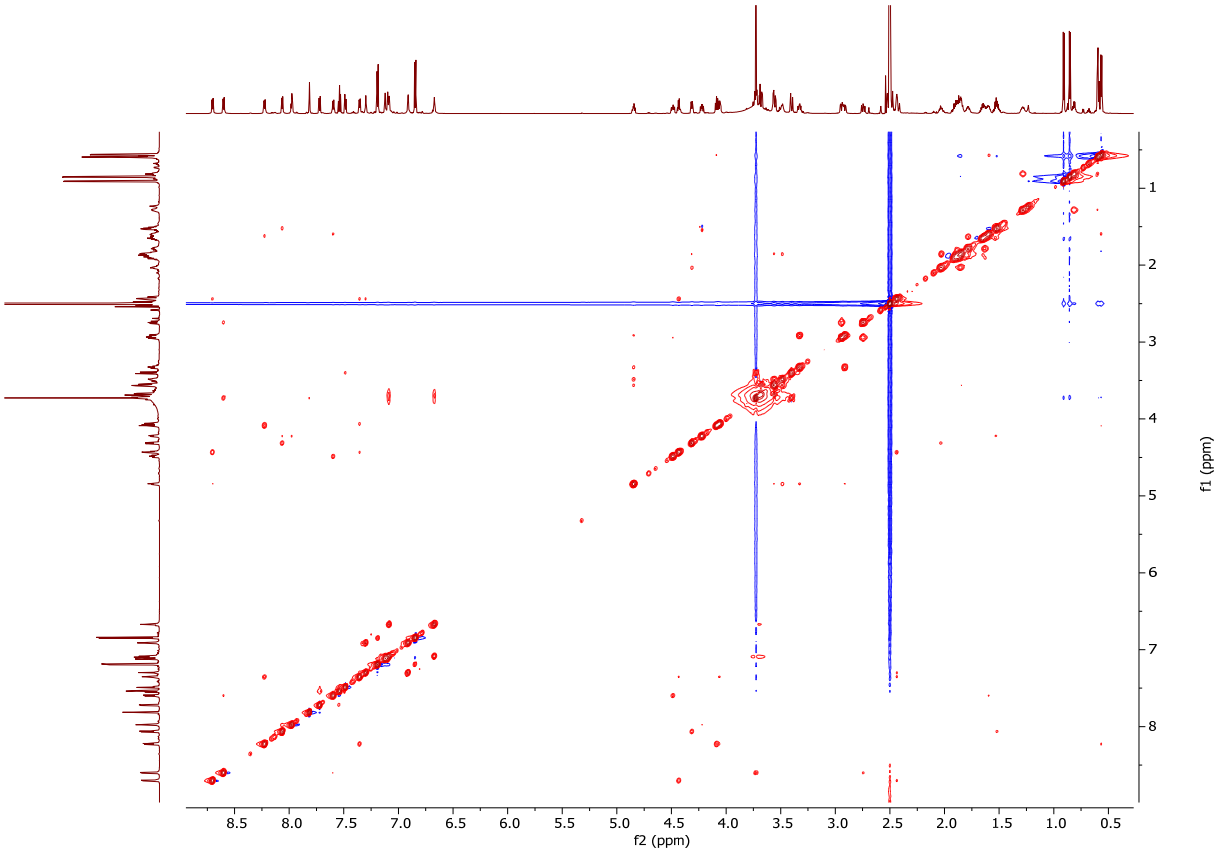

Figure 3.84: ^{1}H, ^{1}H-NOESY of **ACTB5**.

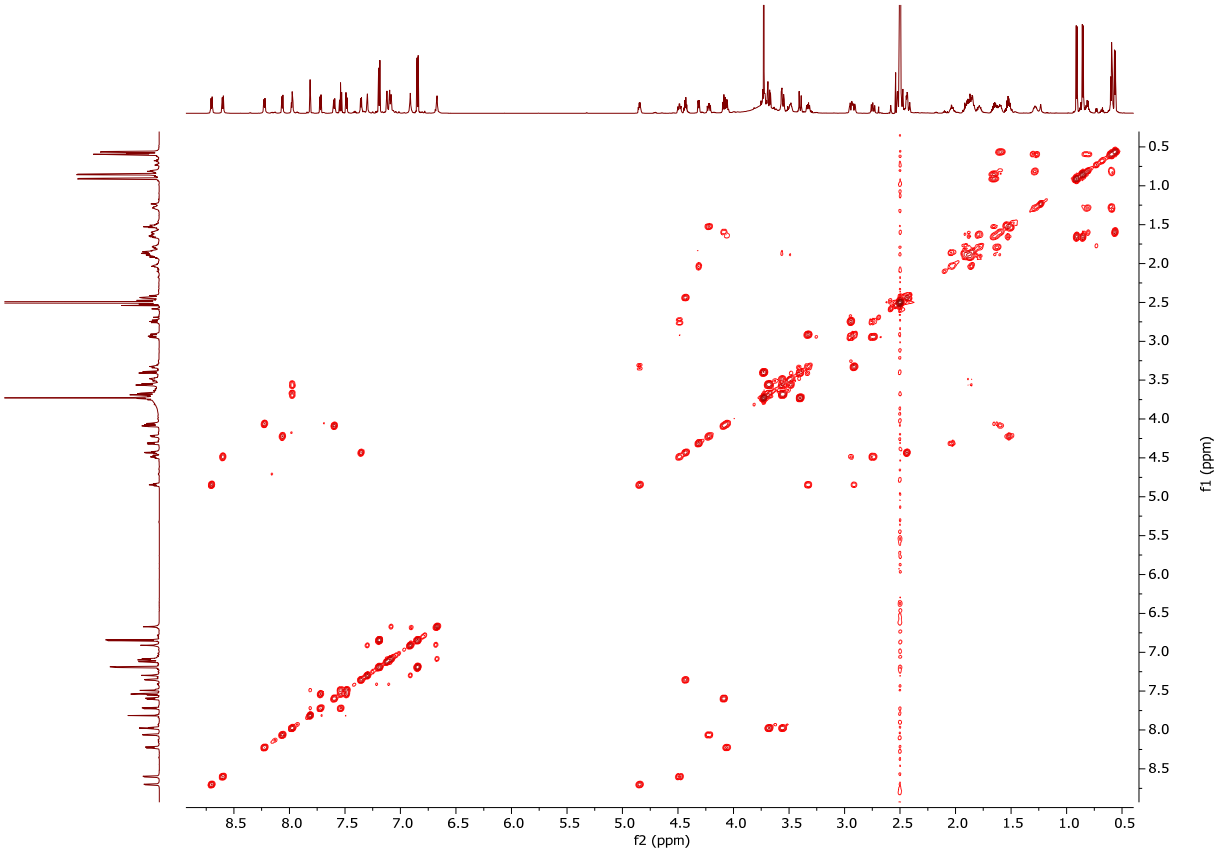

Figure 3.85: ^{1}H, ^{1}H-COSY of **ACTB5**.

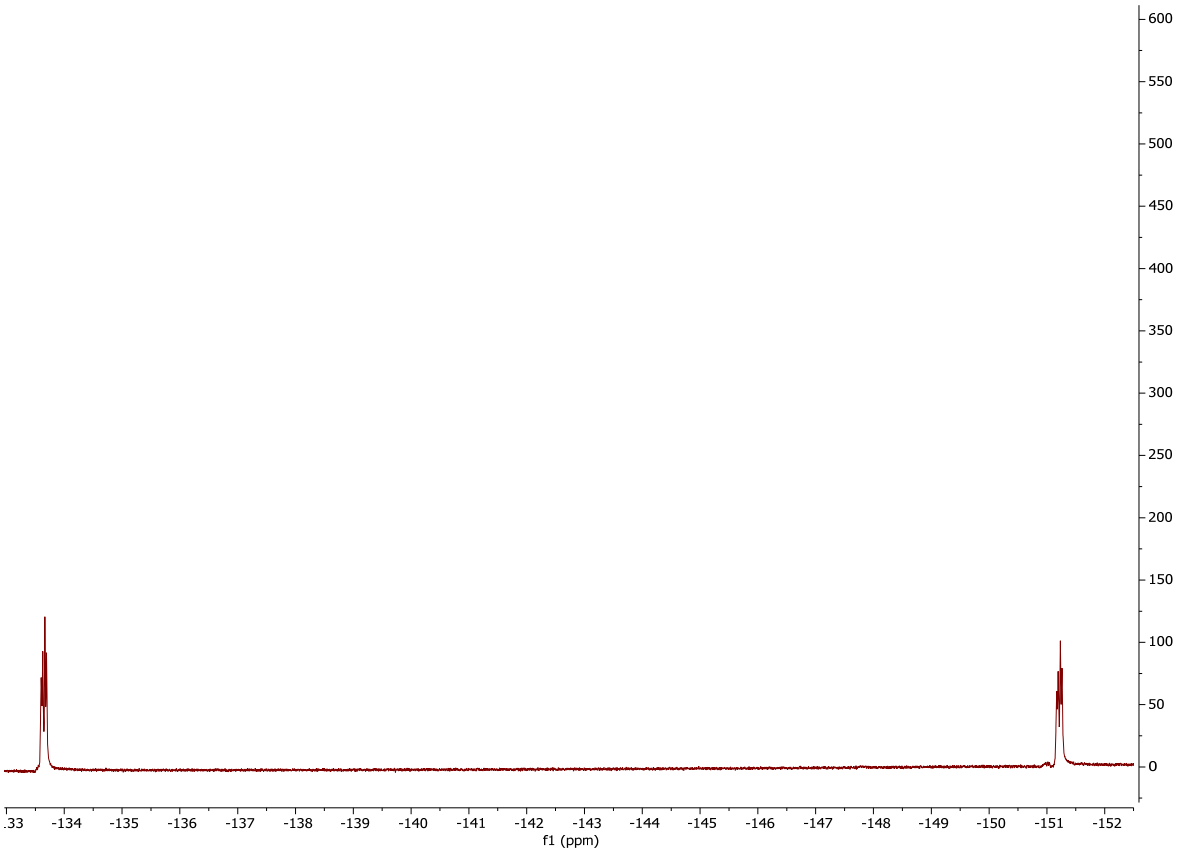

Figure 3.86: ^{19}F-NMR of **ACTB5**.

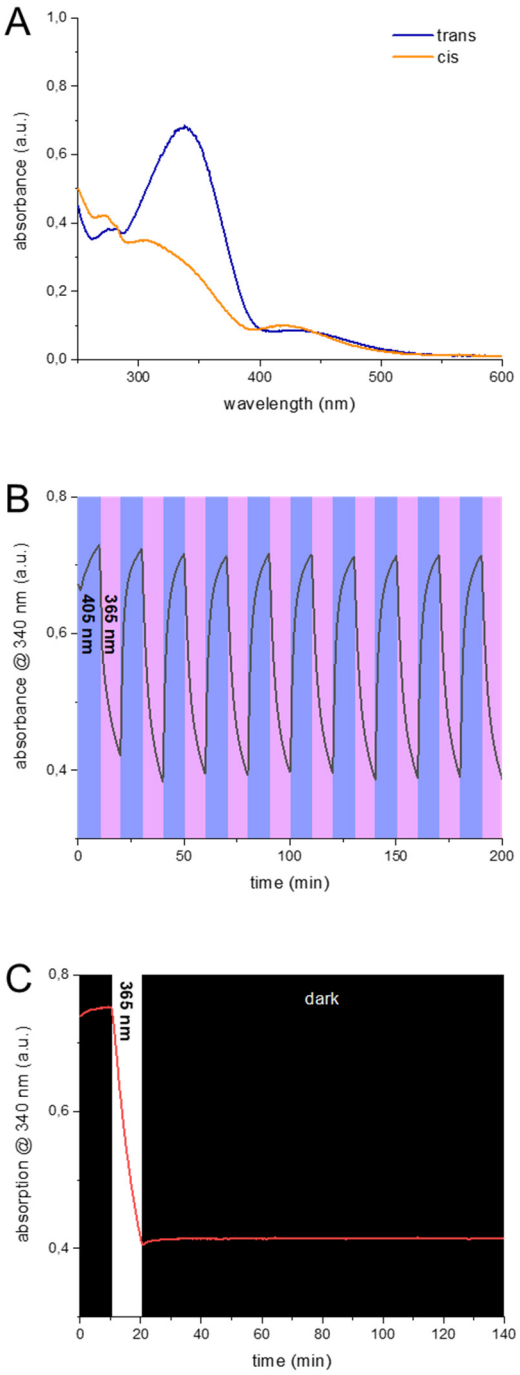

Figure 3.87: UV/VIS spectra of trans- and cis-**ACTB5**; illumination with 365 nm (trans→cis) and 405 nm (cis→trans). B) Kinetics of **ACTB5**. C) Bistabilty of **ACTB5**.

Analytical Data of ACTB6

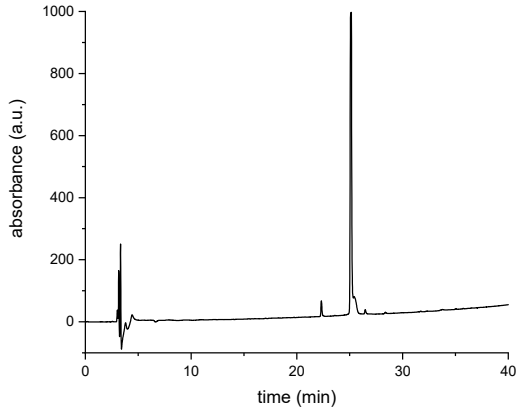

Figure 3.88: Analytical HPLC spectrum of **ACTB6** with a water/acetonitrile gradient of 95/5 →20/80 in 40 min. R_f: 22.3 min (cis) and 25.1 min (trans).

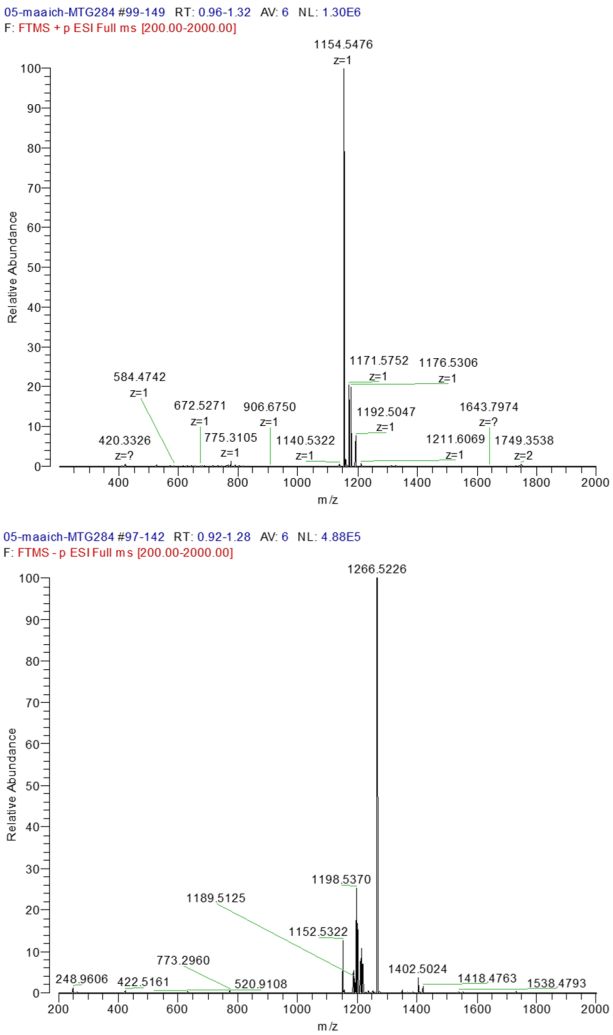

Figure 3.89: HRMS spectrum of **ACTB5**: HRMS (+ESI) m/z calc. for $C_{56}H_{76}N_{13}O_{12}S^+$ $[M + H]^+$: 1154.5452; found: 1154.5476. . HRMS (−ESI) m/z calc. for $C_{55}H_{72}F_3N_{13}O_{14}S^-$ $[M + TFA - H]^-$: 1266.5235; found: 1266.5226.

Table 3.10: Chemical shifts of the ^{1}H- and ^{13}C-NMR of **ACTB6** in DMSO-d_6.

residue	^{1}H-NMR	^{13}C-NMR
3.16	$H2_a$ 3.64, $H2_b$ 3.44, H4 7.80, H6 7.73, H7 7.49, H8 7.37, H12 7.84, H14 7.53, H15 7.76, H16 7.80, $H17_a$ 3.94, $H17_b$ 3.88	C2 41.7, C3 138.1, C4 123.1, C5 152.0, C6 120.8, C7 152.0, 129.2, C8 133.3, C11, C12 122.4, C13 140.9, C14 132.0, C15 121.8, C16 122.6, C17 35.8
Tyr(OMe)	NH 8.59, Hα 4.53, $Hβ_1$ 3.04, $Hβ_2$ 2.77, Hδ 7.22, Hε 6.81, Hη 3.71	Cα 57.3, Cβ 36.2, Cγ 157.6, Cδ 130.1, Cε 113.5, Cζ 157.7, Cη 54.9
Ile	NH 7.67, Hα 4.10, Hβ 1.63, $Hγ_1$ 1.27, $Hγ_2$ 0.65, Hδ 0.64	Cα 57.3, Cβ 36.2, $Cγ_1$ 24.1, $Cγ_2$ 15.4, Cδ 11.1
Gln	NH 8.12, Hα 4.12, $Hβ_1$ 1.80, $Hβ_2$ 1.70, Hγ 2.03	Cα 52.9, Cβ 27.5, Cγ 31.2
Asn	NH 7.76, Hα 4.47, $Hβ_1$ 2.55, $Hβ_2$ 2.41	Cα 49.7, Cβ 36.9
Cys	NH 8.09, Hα 4.64, $Hβ_1$ 2.86, $Hβ_2$ 2.61	Cα 51.3, Cβ 32.7
Pro	Hα 4.31, Hβ 2.02, Hγ 1.86, $Hδ_1$ 3.58, $Hδ_2$ 3.53	Cα 59.9, Cβ 29.0, Cγ 24.8, Cδ 46.9
Leu	NH 8.00, Hα 4.21, Hβ 1.51, Hγ 1.63, $Hδ_1$ 0.89, $Hδ_2$ 0.83	Cα 51.4, Cβ 40.2, Cγ 24.2, $Cδ_1$ 23.1, $Cδ_2$ 21.6
Gly	NH 7.98, $Hα_1$ 3.67, $Hα_2$ 3.56	Cα 42.0

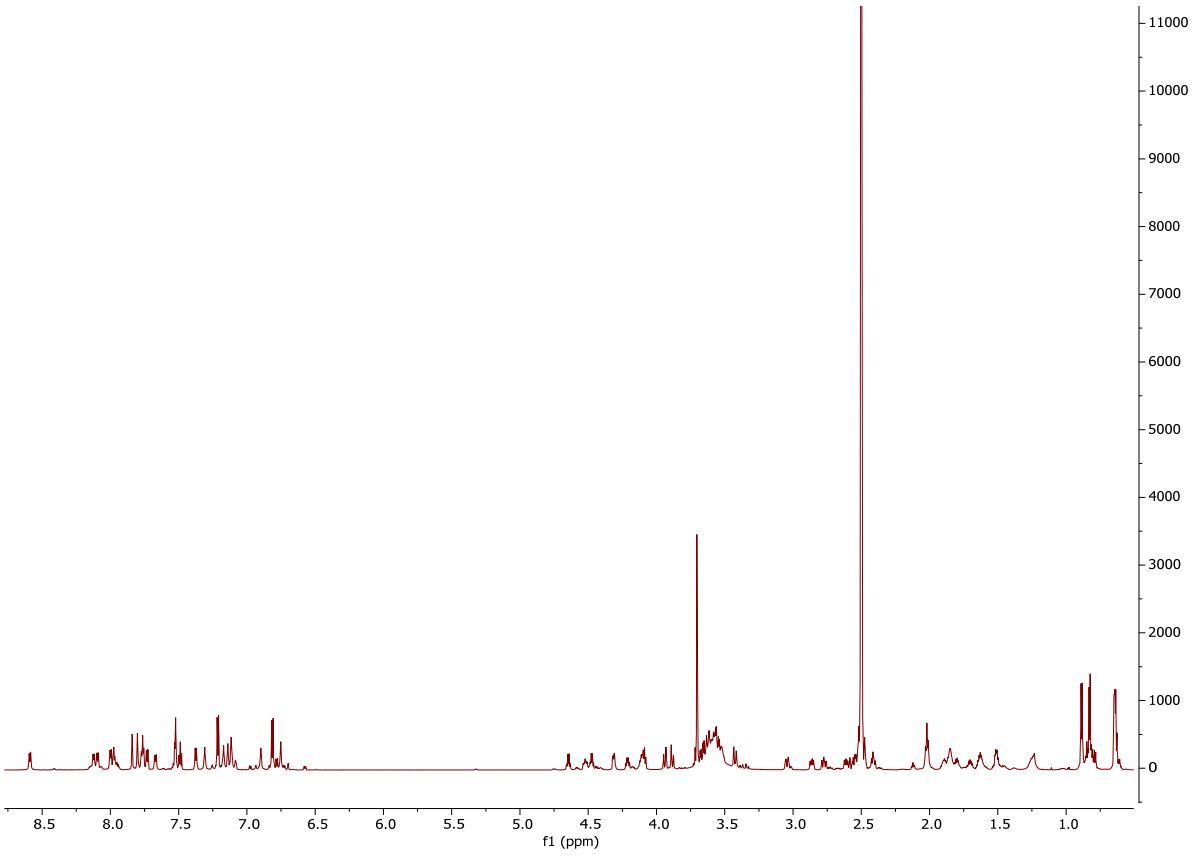

Figure 3.90: ^{1}H-NMR of **ACTB6**.

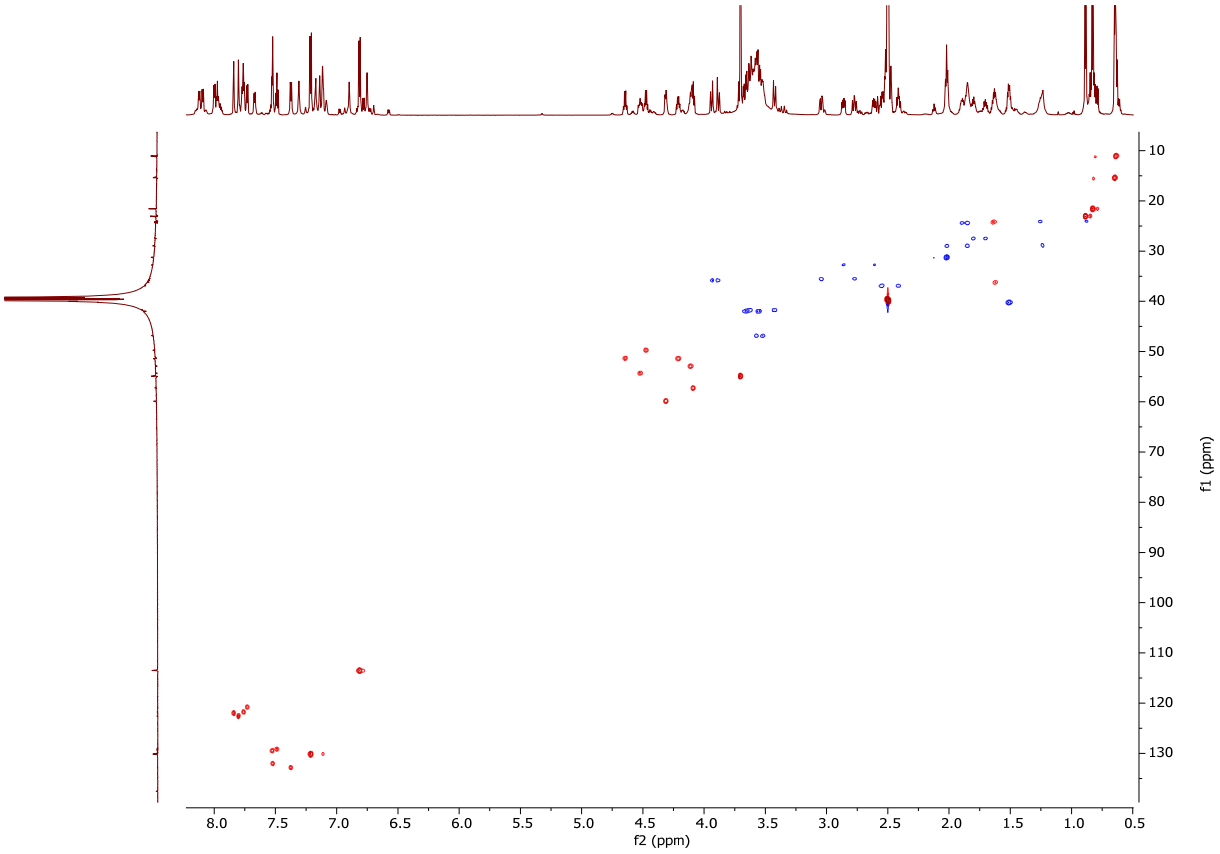

Figure 3.91: ^{1}H, ^{13}C-HSQC of **ACTB6**.

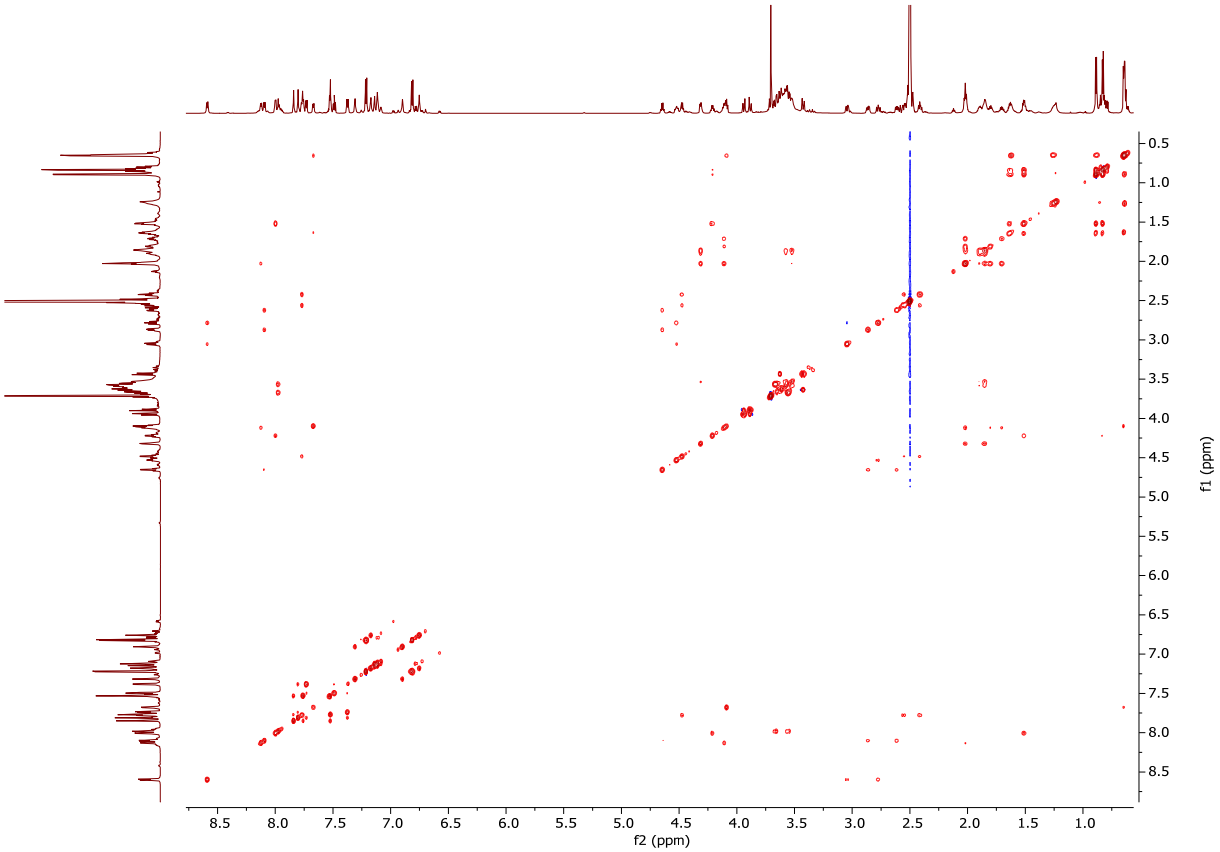

Figure 3.92: ^{1}H, ^{1}H-TOCSY of **ACTB6**.

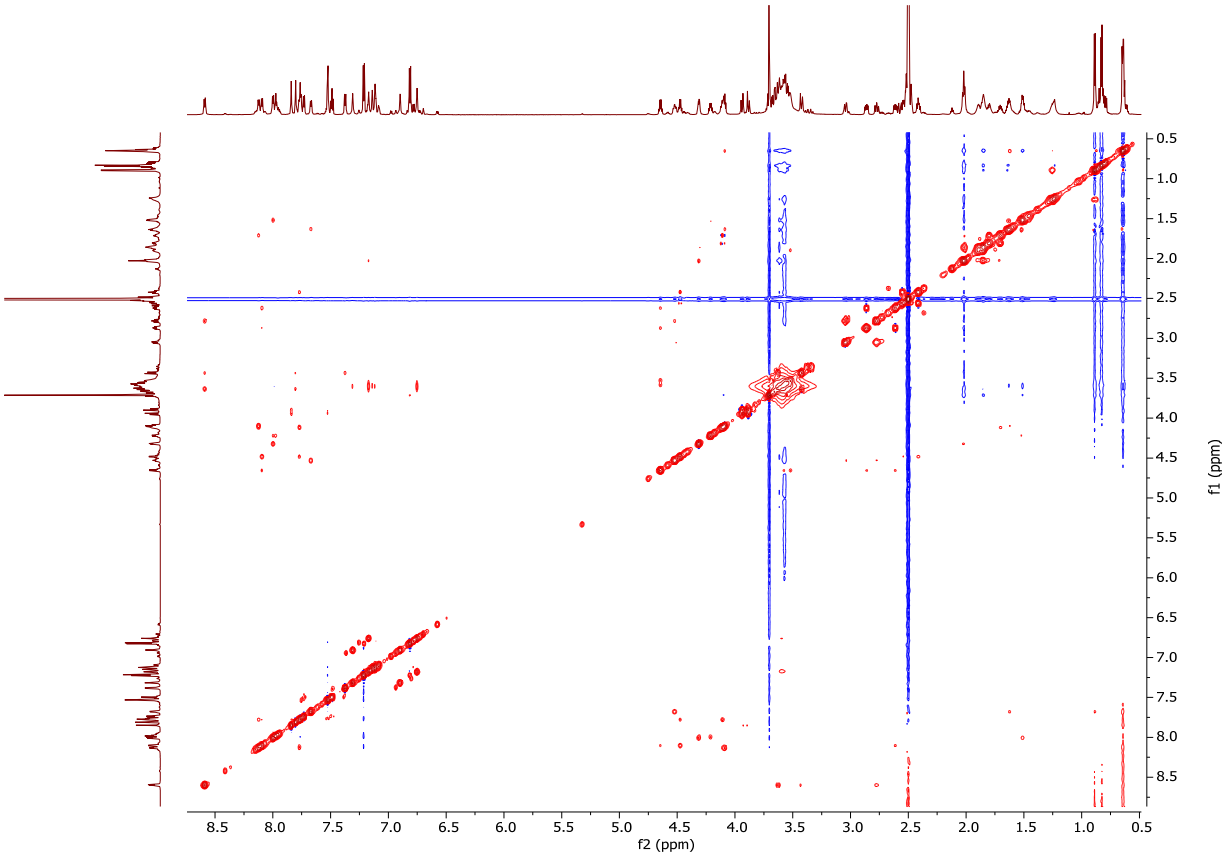

Figure 3.93: ^{1}H,^{1}H-NOESY of **ACTB6**.

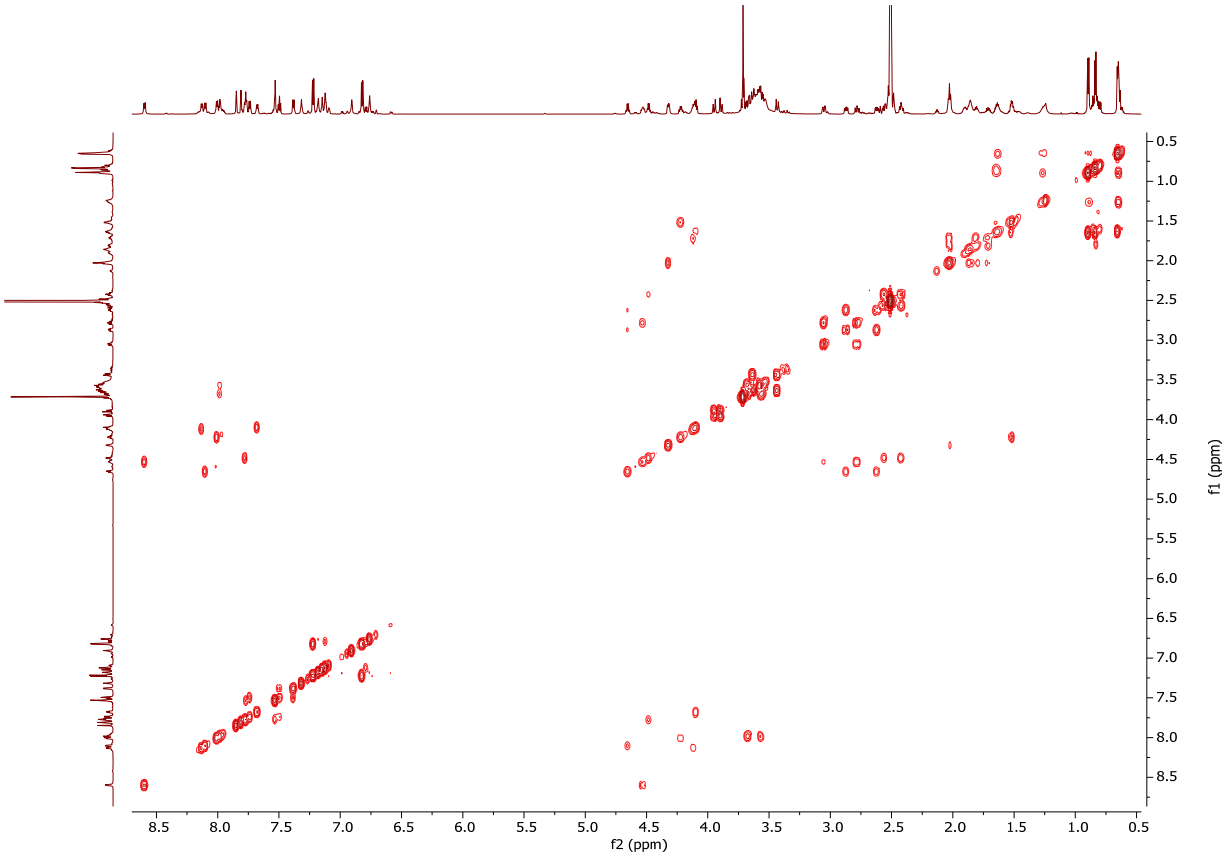

Figure 3.94: ^{1}H, ^{1}H-COSY of **ACTB6**.

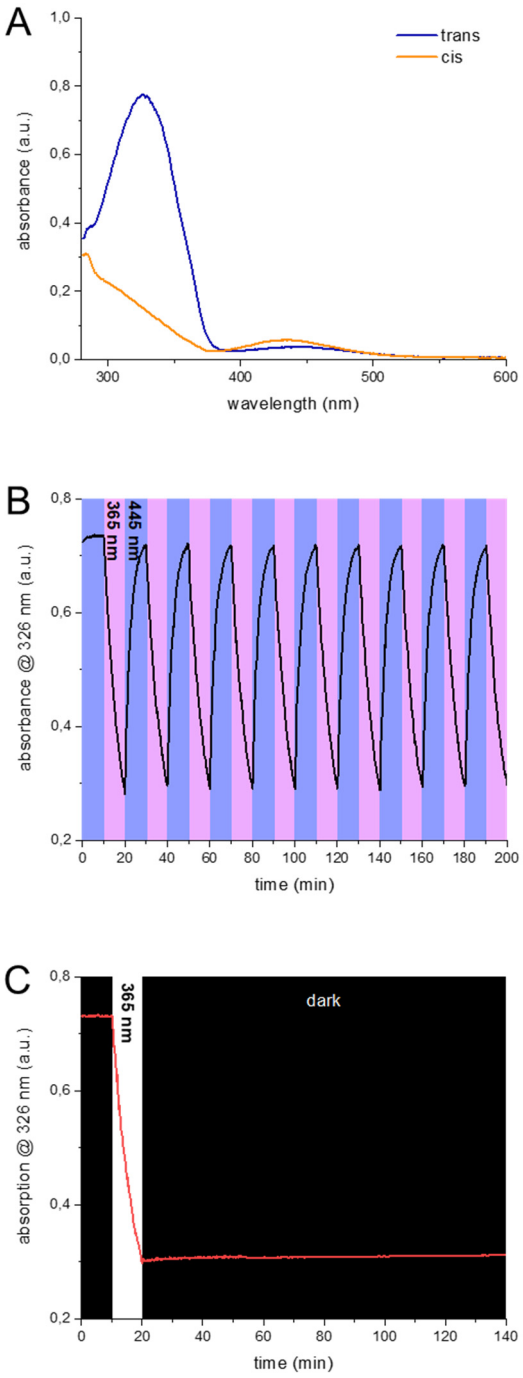

Figure 3.95: A) UV/VIS spectra of trans- and cis-**ACTB6**; illumination with 365 nm (trans→cis) and 445 nm (cis→trans). B) Kinetics of **ACTB6**. C) Bistabilty of **ACTB6**.

3.5 DAMGO

3.5.1 Introduction

Nature provides a huge library for the modification of canonical building blocks. One of the most appearing alterations is the introduction of methyl groups. The DNA building blocks adenine and cytosine can be methylated at N^6 or C^5 respectively by a number of methyl transferases, which play big role not only in epigenetics but also in diseases like cancer.[297-299] In histones lysine[300] and arginine,[301] side-chains can be methylated and demethylated in order to alter gene transcription by binding of non-histone proteins.[302] In contrast, *N*-methylation of peptide amide bonds is not a post-translational modification. Synthesised in multifunctional groups in the non-ribosomal peptide synthetases[303, 304], *N*-methylated peptides can have several benefits, like enzymatic stability, intestinal permeability and increase in activity.[305] Often isolated from marine sponges[306] and fungi[307], *N*-methylated peptides like cyclosporine A[308] give blueprints for the modification of bioactive peptidic drugs. With its seven *N*-methyl amides, cyclosporine A violates two of the four Lipinski rules[309]: ≤ 500 Da (1.2 kDa), ≤ 5 H-donors (5), ≤ 10 H-acceptors (12), distribution coefficient ≤ 5 (2-3), but is sold as an orally available drug. The introduction of a *N*-methyl group into the backbone can improve the peptide activity as it was shown with cilengitide, a small cyclic peptide developed for the treatment of glioblastoma by Kessler in cooperation with Merck-Serono.[310] A single *N*-methylation of a backbone amide lowered the IC_{50} from 2.5 nM to 0.58 nM.[310, 311] Therefore, *N*-methylation of peptides became an effective tool for the modification and improvement of peptidic drugs. This and other modifications were used in the synthesis of [D-Ala2, *N*-MePhe4, Gly5-ol]enkephalin, DAMGO, first described in 1980[312], to furnish a μ-opioid receptor (MOR) selective and proteolytic stable analogue of Leu- and Met-Enkephalin. DAMGO, a five amino acid long peptide exhibits D-alanine, C-terminal glycinol and a *N*-methylated phenylalanine. Whereas opioids usually have a low half-life of up to five minutes, these modifications stabilise DAMGO against enzymatic degradation and doubles the half-life to 9.2 ± 2.1 min[313]. More important, in mouse writhing nociception test, it had a 140-fold higher potency then morphine.[312] Rats, medicated with both, morphine and DAMGO, become less tolerant to the analgesic effect of morphine than rats, treated just with morphine.[314] Whereas endogenous peptide ligands (e.g. enkephalins) and some synthetic agonists (DAMGO, Fentanyl) induce a rapid receptor endocytosis followed by recycling, morphine shows only little endocytosis.[315, 316] The differences between morphine and DAMGO is a consequence of altered molecular mechanism upon activation of MOR.[315]

3.5.2 Activation of the μ-opioid receptor

Located pre- and post-synaptically in the brain, spinal cord and in the intestinal tract, the μ-opioid receptor modulates a wide range of functions, e.g. reward properties and pain perception (analgesia). MOR belongs to the family of rhodopsin-like G protein-coupled receptors (Class A, see chapter 3.3.2).[317]

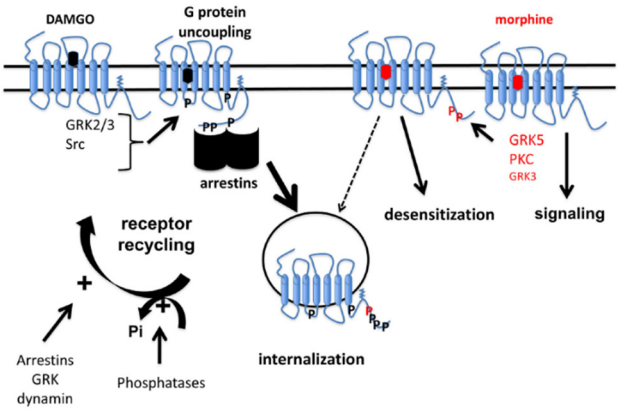

Figure 3.96: Different mechanism of activation and phosphorylation of MOR by DAMGO and morphine.[318]

Agonistic activation of MOR causes analgesic effects, mediated by classical G_i protein downstream signalling. Binding of an agonist induces a conformational change of the receptor, resulting in the dissociation of the α-subunit of the G protein complex.[319] Inhibition of the adenylyl cyclase (AC) by the α-subunit, decreases the cAMP level, which impedes the Na^{2+} influx of the cyclic nucleotide-gated ion channels, suppressing the neuronal excitability.[320] Furthermore, reduced cAMP concentration decreases the activation of the protein kinase A (PKA).[321] The dimeric βγ subunit on the one hand inhibits T-type Ca^{2+} channels, on the other hand activates the G protein inwardly rectifying potassium (GIRK) channels. The net effect is a neuronal hyperpolarisation and a decreased neurotransmitter release from the pre-synaptic nerve terminal, which causes analgesia.[320, 322]

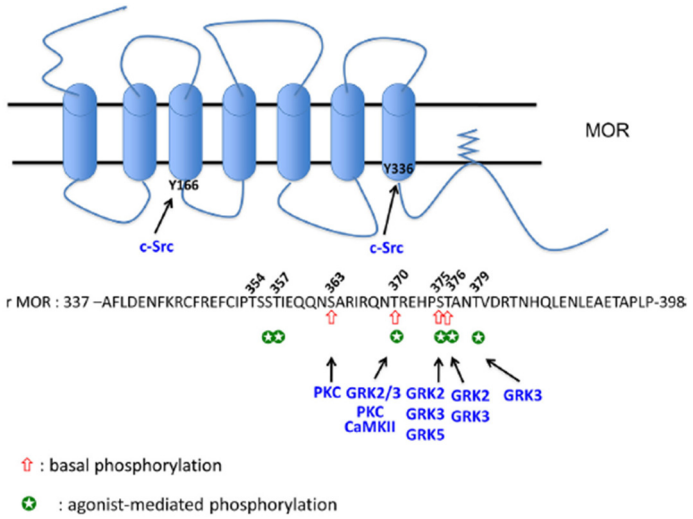

Figure 3.97: Phosphorylation position of MOR by different kinases.[318]

Kinases usually phosphorylate the intracellular *C*-terminal part of the receptor, which induces the recruitment of β-arrestin followed by receptor internalisation and recycling. But the phosphorylation of threonine- and serine side chains of MOR differs between agonists: activation by morphine essentially recruits protein kinase C (PKC) mediated phosphorylation leading to reduced endocytosis. In contrast, activation of G protein-coupled receptor kinase (GRK) and β-arrestin recruitment by DAMGO strongly induces receptor internalisation and recycling (Figure 3.96). A possible explanation is the difference in phosphorylation sites of the kinases and thus, differences in the subsequent recruitment of β-arrestin (Figure 3.97).[323]

However, unravelling the agonist depending mechanism of desensitisation, phosphorylation, internalisation and recycling is an ongoing research area and photopharmacology is proven to provide suitable tools. Hence, introduction of photoswitchable amino acids into the sequence of DAMGO could furnish a light-controllable tool for the manipulation of MOR, called AZODAMGO[324].

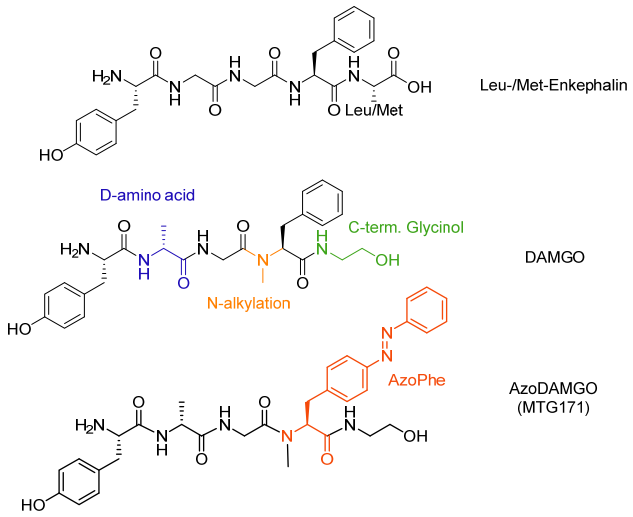

Figure 3.98: Structure of enkephalins, DAMGO and AzoDAMGO.

In structure models, the side-chain of *N*(Me)Phe interacts with a conserved hydrophobic pocket of the μ-receptor, whereas the Tyr side-chain undergoes a water-mediated interaction with the binding pocket.[325] With this in mind, we decided to substitute *N*(Me)F4 against the photoswitchable amino acid AzoPhe (Figure 3.98) in order to furnish a light controllable μ-receptor agonist. For methylation of backbone amides, nature provides non-ribosomal synthase complexes as mentioned above. In SPPS, selective *N*-methylation was introduced by MILLER and SCANLAN (Scheme 3.15).[326]

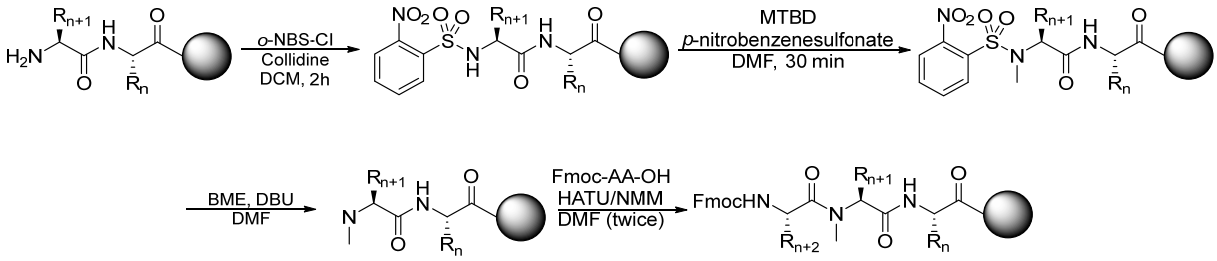

Scheme 3.15: Synthetic route of selective N-methylation during SPPS.[326]

This three-step procedure starting with protection and activation of an α-amine, methylation and at least deprotection of the secondary amine. This procedure, improved by *Kessler and coworkers*[305] was used for the synthesis of AzoDAMGO.

3.5.3 Results and Discussion

For the SPPS of AzoDAMGO, unloaded 1.35 mmol/g 2-chlorotrityl resin was treated with *N*-*Fmoc*-ethanolamine in DMF under basic conditions for 18 h. The extant free positions were capped with MeOH and the resin was washed and dried under high vacuum. For the

determination of the resin loading 10 mg resin were allowed to swell in 800 µL DMF. After addition of 200 µL piperidine, *Fmoc* was deprotected and the 100 µL were diluted in 10 mL DMF. Finally, the absorption of at 301 nm was measured by UV/VIS to determine the resin loading of 0.72 mmol/g. All amino acids were coupled using PyBOP/DIPEA in DMF at room temperature and without the assistance of microwave irradiation. The coupling reagent Pybop was chosen for its high coupling efficiency at room temperature. Additional, instead of uronium salts like HATU or HBTU, coupling with PyBOP requires no pre-activation, which facilitates manual synthesis. After coupling and *Fmoc*-deprotection of AzoPhe, the N-terminal amine was protected with *o*-Nitrobenzenesulfonyl chloride in NMP for 15 min using Collidin as a base. Furthermore, *o*-NBS additionally activates the N-terminal amine for methylation without forming sulfenes. Afterwards, 1,8-Diazabicyclo[5.4.0]undec-7-en (DBU) in NMP was added, and the resin was shaked for 3 min prior the addition of dimethylsulfate. The solution was shaked for 2 min and the methylation step was then repeated once. Simultaneous addition of DBU und dimethyl sulfate leads to side reactions of base and methylation reagent. Deprotection of *o*-NBS was achieved with β-mercapto ethanol and DBU in NMP for 5min.[305] This step was repeated once and could be monitored by the slightly greenish solution of the free *o*-NBS. Coupling of the next amino acid glycine was carried out by double coupling with PyBOP/DIPEA in the Liberty Blue Peptide Synthesizer. After coupling of D-alanine and tyrosine with DIC/Oxyma® by automated microwave-assisted SPPS, the peptide was cleaved from the resin and deprotected with TFA/water/phenol/TIPS/ (88/5/5/2). After precipitation in cold diethyl ether and purification by reversed phase HPLC, 10.4 mg of AzoDAMGO were furnished.

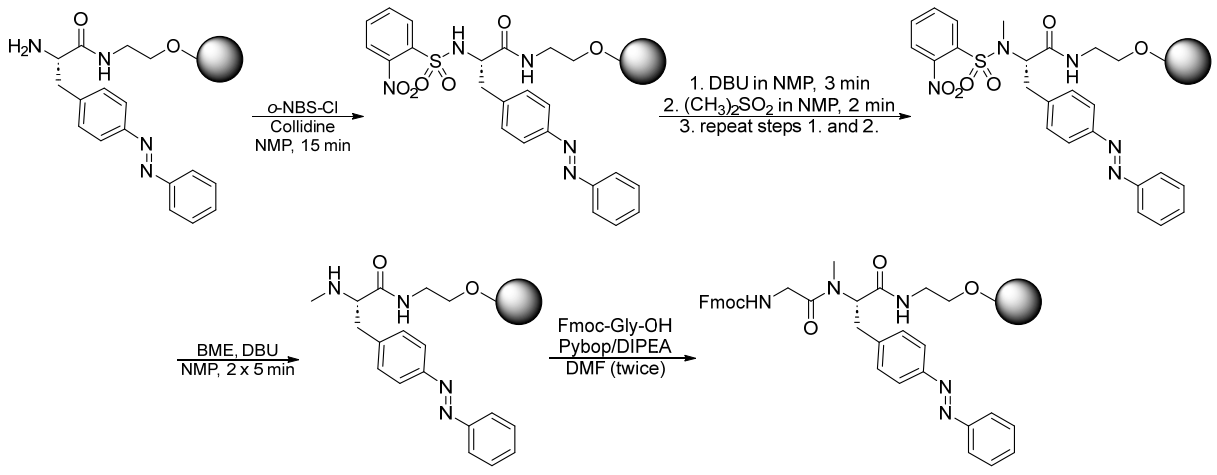

Scheme 3.16: Synthesis of AzoDAMGO: *N*-methylation of the resin-bound peptide by the procedure of KESSLER and coworkers.[305]

Purity was controlled by HPLC and mass spectroscopy and spectroscopic properties were examined by UV/VIS spectroscopy. AzoDAMGO could be switched from *trans* to *cis* with UV light (340 nm) and back with blue light (455 nm). A decrease of the π-π* absorption band and an increase of the n-π* absorption band was observed by illumination with UV light and vice versa by subsequent exposure to blue light. Only minimal bleaching occurred after several switching cycles. This secures prevention of the formation of triplet states and reactive oxygen species, which is crucial for biocompatibility.[14] The compound possesses also a high bistability when switched to the *cis* state and subsequently left in the dark for 2 hours allowing for pre-illumination of the peptides before being applied to cells and no need of UV-light exposure of cells.

In collaboration with Dr. Philipp Leippe (Trauner group, LMU Munich), the functional activity in MOR-transfected HEK-GIRK assays of AzoDAMGO was tested by Dr. Leippe.[324] Addition (at 60 sec) of a 1 µM solution of DAMGO resulted in a hyperpolarization, which can be seen in a drop in the curve. After washout, AzoDAMGO was added in concentration of 10 µM (at 360 sec). No hyperpolarization could be observed neither in *cis*- nor in *trans*-AzoDAMGO. The incorporation of AzoPhe into DAMGO lead to an inactive compound, which could not activate the µ-opioid receptor.

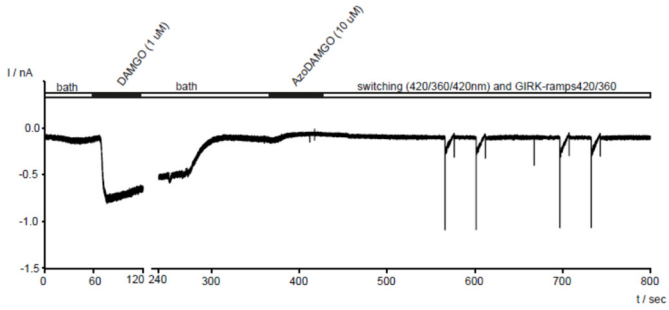

Figure 3.99: Electrophysiologcal charaterization of AzoDAMGO.[324]

3.5.4 Analytical data of AzoDAMGO

3.5.4.1 Synthesis of SPPS building blocks

***N*-Fmoc-aminoethanol[327]**

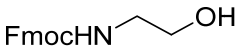

To a solution of 1.00 g (16.4 mmol, 2.0 eq.) ethanolamine in 50 mL DCM and 100 mL aqu. sat. $NaHCO_3$ solution, 2.76 g (8.20 mmol, 1.0 eq.) *Fmoc-O*Su dissolved in 15 mL DCM were added dropwise. The solution was stirred for 18 h at room temperature. The organic phase was separated and the aqueous phase was extracted with DCM (3 x 30 mL). The combined organic phases were washed with 1 N HCl (3 x 30 mL) and sat. NaCl solution (3 x 30 mL) and dried over $NaSO_4$. After removal of the solvent, the product (2.32 g, quant.) was furnished as colorless amorphous solid.

C17H17NO3 (283.33 g/mol) [283.1208]

Rf (CHex/EtOAc, 1:1 + 1% AcOH): 0.30.

HR ESI-MS (positiv), m/z: 306.1102 ($[M+Na]^+$, ber.: 306.1100), 284.1281 ($[M+H]^+$, ber.: 284.1286).

HR ESI-MS (negativ), m/z: 328.1194 ($[M+HCO_2]^-$, ber.: 328.1190).

^{1}H-NMR (400 MHz, $CDCl_3$): δ = 7.76 (d, $J_{H4,H3}$ = 7.5 Hz, 2H, ***H***4-, ***H***5-*Fmoc*), 7.58 (d, $J_{H5,H6}$ = 7.4 Hz, 2H, ***H***1-, ***H***8-*Fmoc*), 7.40 (m, 7.42 – 7.37, 2H, ***H***3-, ***H***6-*Fmoc*), 7.31 (td, $J_{H2,H1/H3 = JH7,H6/H8}$ = 7.5 Hz, $J_{H2,H4 = JH7,H5}$ = 1.2 Hz, 2H, ***H***2-, ***H***7-*Fmoc*), 5.25 (bs, 1H, N***H***-*Fmoc*), 4.43 (d, $J_{CH2Fmoc,H9Fmoc}$ = 6.7 Hz, 2H, C***H***$_2$-*Fmoc*), 4.21 (t, $J_{H9Fmoc,CH2Fmoc}$ = 6.6 Hz, 1H, ***H***9-*Fmoc*), 3.74 – 3.62 (m, 1H, C***H***$_2$), 3.33 (d, J_{CH2-CH} = 1.6 Hz, 2H, C***H***$_2$), 2.23 (bs, OH) ppm.

^{13}C-NMR (100 MHz, $CDCl_3$): δ = 157.3 (***C***=O-*Fmoc*), 144.0 (***C***1a-, ***C***8a-Fmoc), 141.4 (***C***4a-, ***C***5a-*Fmoc*), 127.8 (***C***3-, ***C***6-*Fmoc*), 127.2 (***C***2-, ***C***7-*Fmoc*), 125.1 (***C***1-, ***C***8-*Fmoc*), 120.1 (***C***4-, ***C***5-*Fmoc*), 66.9 (***C***H$_2$-*Fmoc*), 62.3 (***C***H$_2$OH), 47.3 (***C***9-*Fmoc*), 43.6 (***C***H$_2$-NH*Fmoc*) ppm.

3.5.4.2 Synthesis of AzoDAMGO

A Merrifield reactor was loaded with 405 mg 2-chlorotrityl resin (1.35 mmol/g, 0.3 mmol) and the resin was swollen for 2 h. After addition of 1.0 eq. *N-Fmoc*-ethanolamine solved in 3 mL

DMF, 6 eq. DIPEA were added. The Merrifield reactor was shacked for 18 h and the resin was freed from the reaction mixture. The extant free positions were capped with a mixture of DCM/MeOH/DIPEA (17:2:1) for 1 h. The resin was washed with DCM (3 x 10 mL), DMF (5 x 10 mL) and again with DCM (5 x 10 mL) and dried under high vacuum. For the determination of the resin loading 10 mg resin were allowed to swell in 800 µL DMF. After addition of 200 µL piperidine, *Fmoc* was cleaved and the 100 µL were diluted in 10 mL DMF. Finally, the absorption of 301 nm was measured by UV/VIS to determine the resin loading of 0.72 mmol/g. The synthesis of **AzoDAMGO** is based on the work of *Biron et. al.*[305] For the synthesis of AzoDAMGO, 138 mg (0.1 mmol) of resin were swollen in a Merrifield reactor. Fmoc-AzoPhe-OH **3.3** (5.0 eq.) were coupled using Pybop/DIPEA (5.0 eq./10 eq.) in DMF at room temperature for 10 h. *Fmoc*-deprotection was achieved by treatment with 20% piperidine in DMF. The procedure of *N*-methylation by *Kessler and coworkers*[305] was used for the synthesis of AzoDAMGO. After *Fmoc*-deprotection of AzoPhe, the N-terminal amine was protected with 89.0 mg (0.4 mmol, 4 eq.) *o*-Nitrobenzenesulfonyl chloride in 5 mL NMP for 40 min using 0.13 mL collidine as a base. Afterwards, 46 mg (0.3 mmol, 3 eq.) 1,8-Diazabicyclo[5.4.0]undec-7-en (DBU) in 3 mL NMP was added, and the resin was shaken for 10 min prior the addition of 95 µL (1.0 mmol, 10 eq.) dimethylsulphate in 2 mL NMP. The solution was shaken for 5 min and the methylation step was then repeated once. Deprotection of *o*-NBS was achieved with 70 µL (1.0 mmol, 10 eq.) β-mercapto ethanol and 74 µL (0.5 mmol, 5.0 eq.) DBU in 5 mL NMP for 10 min. The deprotection step was repeated once. The resin was transferred into the Liberty Blue reactor and for the remaining coupling reactions DIC/Oxyma pure® (120 s, 30 W, 90 °C) was used. Coupling of *Fmoc*-Gly-OH was carried out by double coupling. For *Fmoc*-Ala-OH and *Fmoc*-Tyr-OH single coupling was used. The peptide was cleaved from the resin and deprotected with TFA/water/phenol/TIPS (88/5/5/2). After precipitation in cold diethyl ether and purification by reversed phase HPLC, 10.4 mg (17%) of AzoDAMGO were furnished.

$$L_R = (V \cdot A_{301} \cdot d)/(E_c \cdot M \cdot w)$$

A_{301} = absorbance at 301 nm = 0.56
d = dilution = 10
E_c = extinction coefficient = 7800 mL/mmol·cm
V = volume = 1 mL
w = width of the cuvette = 1 cm
M = weight of the resin sample = 10 mg

$$L_R = 0.72 \text{ mmol/g}$$

3.5.4.3 HR-MS, HPLC and NMR

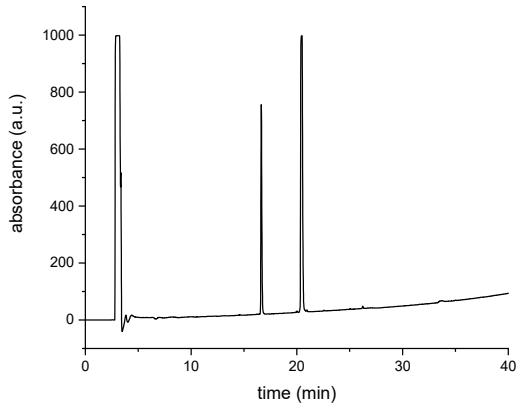

Figure 3.100: Analytical HPLC spectrum of **AzoDAMGO** with a water/acetonitrile gradient of 95/5 →20/80 in 40 min. Rf: 16.6 min (cis) and 20.5 min (trans).

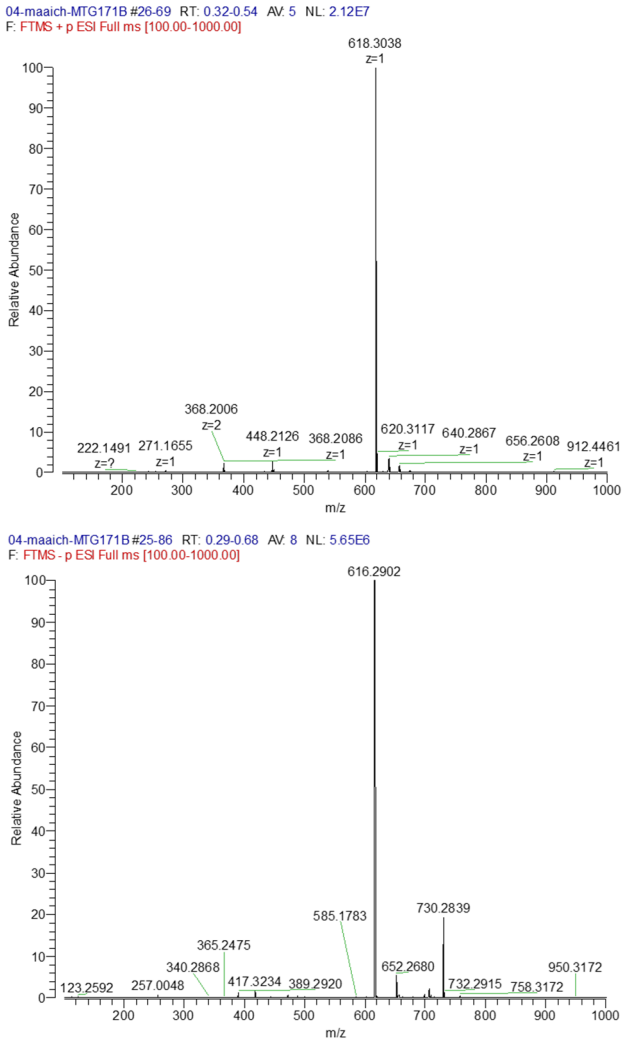

Figure 3.101: HRMS spectrum of **AzoDAMGO**: HRMS (+ESI) m/z calc. for $C_{32}H_{40}N_7O_6^+$ $[M + H]^+$: 618.3035; found: 618.3038. HRMS (−ESI) m/z calc. for $C_{32}H_{38}N_7O_6^+$ $[M - H]^-$: 616.2889; found: 616.2902.

Table 3.11: ^{1}H- and ^{13}C-NMR of trans-**AzoDAMGO** in DMSO-d_6

residue	^{1}H-NMR	^{13}C-NMR
Glycinol	NH 7.93, Hα 3.14, Hβ 3.39, OH 4.67	Cα 41.4, Cβ 59.4
AzoPhe	H1 5.23, $H2_a$ 3.32, $H2_b$ 3.03, H4/8 (K1) 7.44 H4/8 (K2) 7.52, H5/7 (K1) 7.79, H5/7 (K2) 7.82, H12/16 7.87, H13/H15 7.60, H14 131.2	C1 57.5, C2 33.8, C3 (K1) 142.2, C3 (K2) 141.5, C4/8 (K1) 129.7, C4/8 (K2) 129.9, C5/7 (K1) 122.3, C5/7 (K2) 122.4, C6 150.2, C11 151.7, C12/16 122.2, C13/15 129.2, C14 131.2
Gly	NH8.08, $H\alpha_1$ 3.99, $H\alpha_2$ 3.73	Cα 40.3
Ala	NH 8.48, Hα (K1) 4.42, Hα (K2), 4.35, Hβ (K1) 1.04, Hβ (K2) 1.01	Cα 47.6, Cβ (K1) 18.6, Cβ (K2) 18.3
Tyr	Hα 3.96, $H\beta_1$ 2.86, $H\beta_2$ 2.82, Hδ 7.00, Hε 6.69, Hη 9.33	Cα 53.1, Cβ 36.1, Hγ 124.5, Hδ 130.3, Hε 115.0, Cζ 156.3

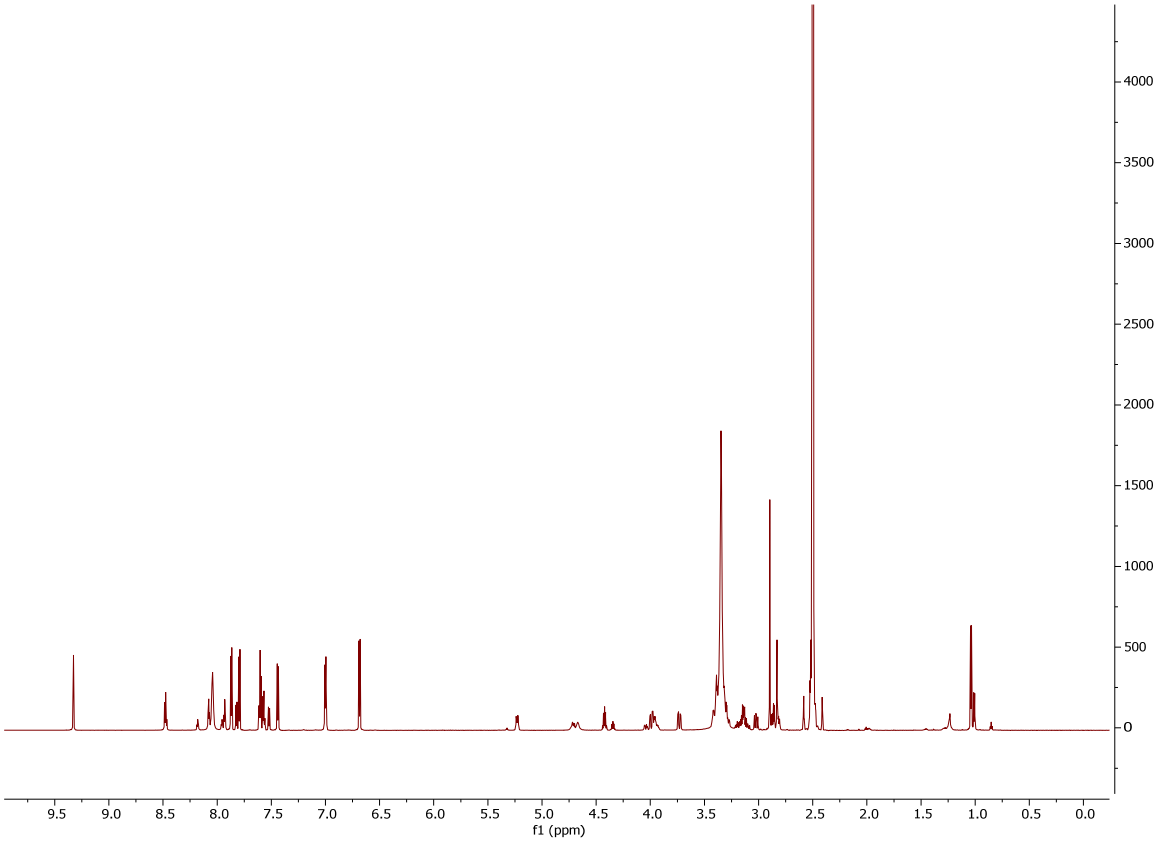

Figure 3.102: ^{1}H-NMR of **AzoDAMGO**.

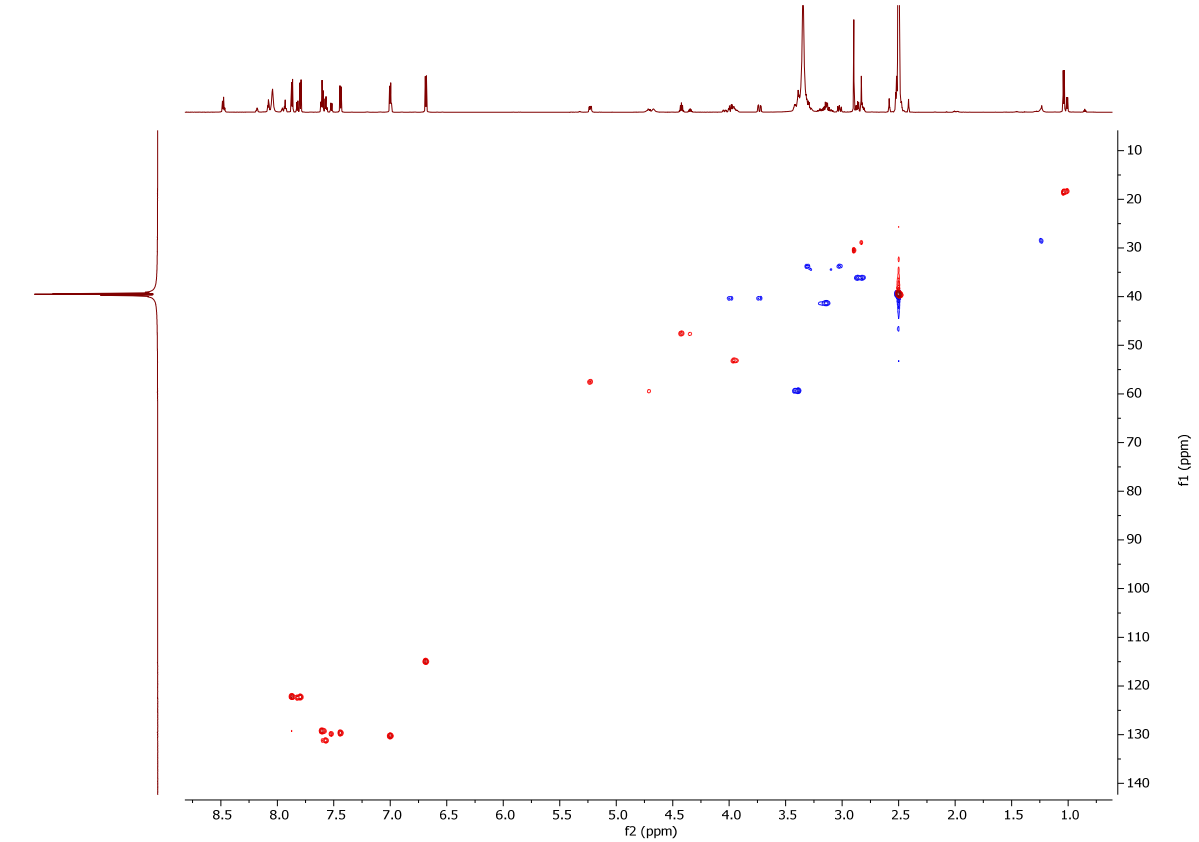

Figure 3.103: ^{1}H, ^{13}C-HSQC-NMR of **AzoDAMGO**.

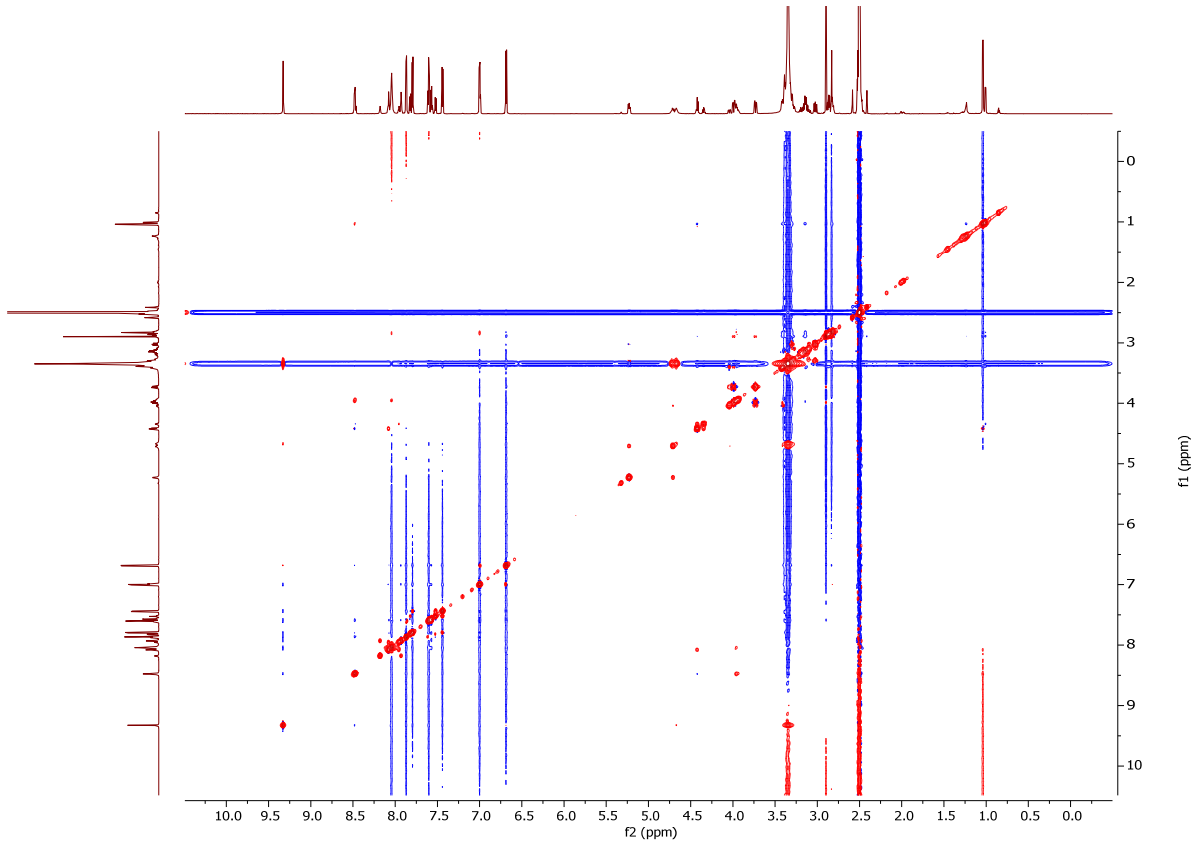

Figure 3.104: ^{1}H, ^{1}H-TOCSY-NMR of **AzoDAMGO**.

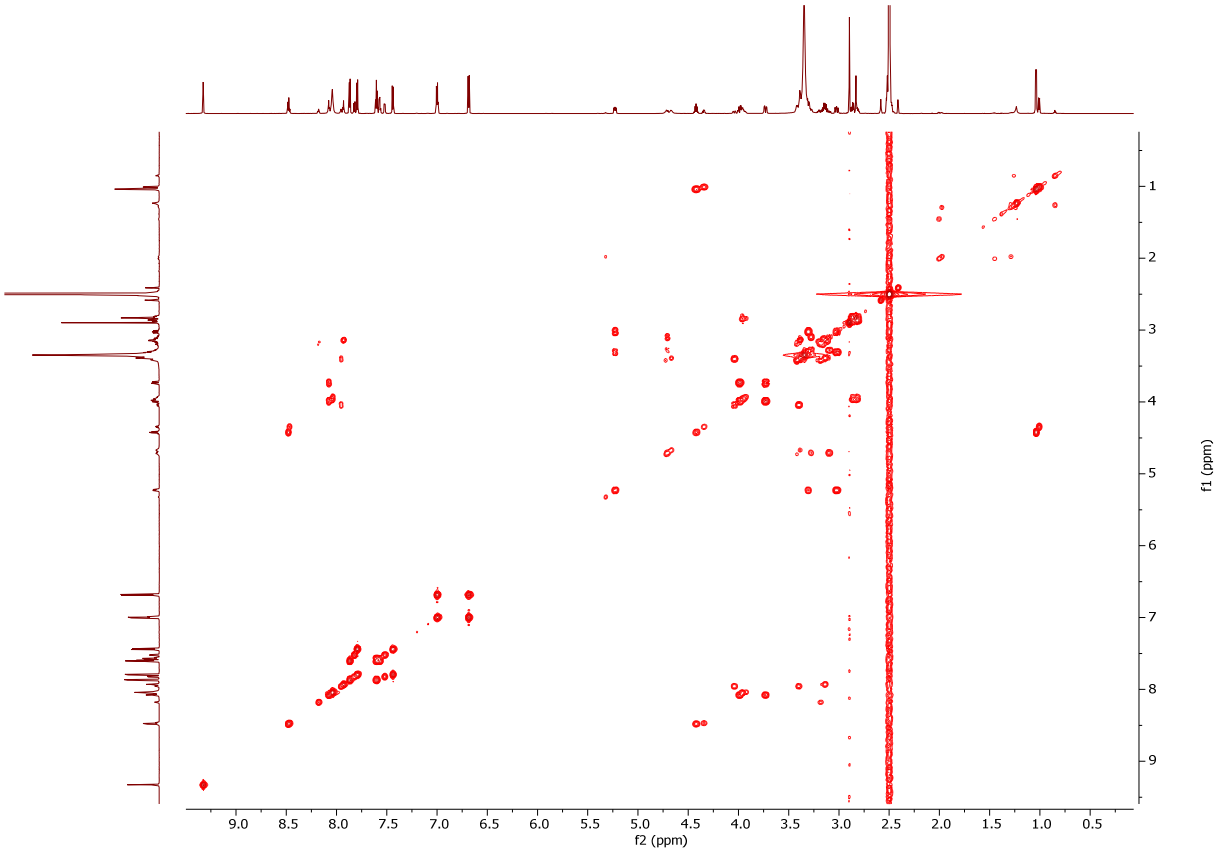

Figure 3.105: ^{1}H, ^{1}H-NOESY-NMR of **AzoDAMGO**.

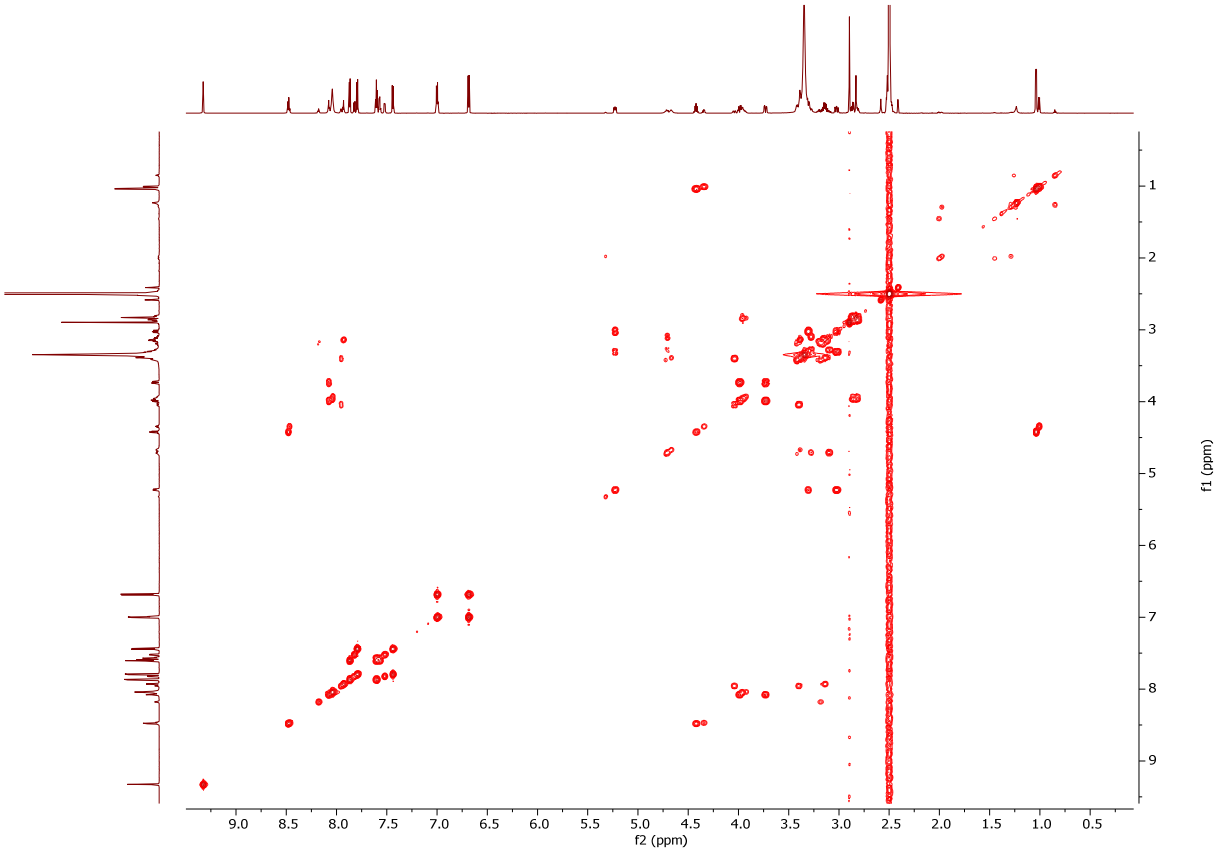

Figure 3.106: ^{1}H, ^{1}H-COSY-NMR of **AzoDAMGO**.

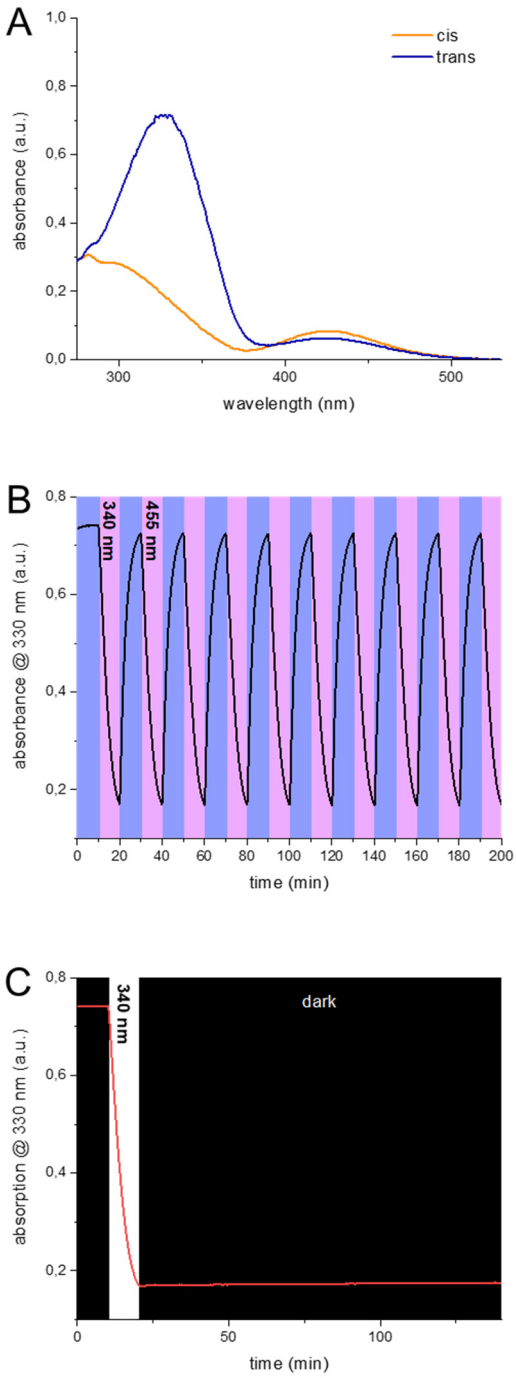

Figure 3.107: A) UV/VIS spectra of trans- and cis-**AzoDAMGO**; illumination with 340 nm (trans→cis) and 455 nm (cis→trans). B) Kinetics of **AzoDAMGO**. C) Bistabilty of **AzoDAMGO**.

3.6 Photoswitchabe Kisspeptin-Analogues

3.6.1 Introduction

Kisspeptin was first discovered in 1996 as a metastasis suppressor of skin and breast cancer, giving it the name metastin.[22] Five years later, the products of the KISS-1 gene were identified to be the endogenous ligands of the G protein coupled receptor GPR54.[328] Translation of the KISS-1 gene results in a 145 amino acid precursor peptide.[328] After proteolysis, several small bioactive peptides are derived (Kisspeptin-54 (Metastin), 14, 13 and 10), all part of the RF-amide (Arg-Phe-NH_2) family,[328-330] binding to the orphan G protein-coupled receptor GPR54.[328-331] Expressed in the pituitary and in gonadotropin-releasing hormone (GnRH) neurons, the activation of GPR54 leads to gonadotropin secretion. Therefore, in 2003 mutation in GPR54 was identified as cause for autosomal recessive idiopathic hypogonadotropic hypogonadism[24, 25] and furthermore defective sexual development as well as reproductive failure was identified as a result of a deletion of GPR54 in mice.[25, 332] Therefore the expression of GPR54 on gonadotropin releasing hormone (GnRH) neurons plays a crucial role in the regulation of the sexual maturation via the hypothalamic-pituitary-gonadal (HPG) axis.

3.6.2 GPR54- a G-coupled receptor

After the discovery of its endogenous ligands, GPR54 was also termed KISS1R for the human and Kiss1r for the non-human receptors by Gottsch *et. al.*[333] GPR54 is widely expressed in a variety of tissues, especially in a variety of brain regions (e.g. midbrain, hypothalamus, amygdala, pituitary gland) and peripheral regions (e.g. intestine, placenta, gonadotrophs).[334] GPR54 is a $G_{q/11}$-coupled 7-transmembrane receptor of the rhodopsin family (see chapter 3.3.2).[328, 330]

Ligand binding to GPR54 (Figure 3.108) causes the dissociation of the α-subunit of the G protein, which activates phospholipase C (PLC). PLC cleaves phosphatidylinositol 4,5-bisphosephate into DAG and IP_3.[328] The latter one causes Ca^{2+}-release from the endoplasmic reticulum which leads the activation of Ca^{2+}-dependent signalling pathways in GnRH neurons. DAG activates transient receptor potential cation (TRPC) channels and inhibition of inwardly rectifying potassium channels (K_{ir}).[335] Furthermore, DAG activates the Ca^{2+} dependent protein kinase C (PKC), which itself stimulates extra-cellular regulated kinase (ERK) 1/2.[328]

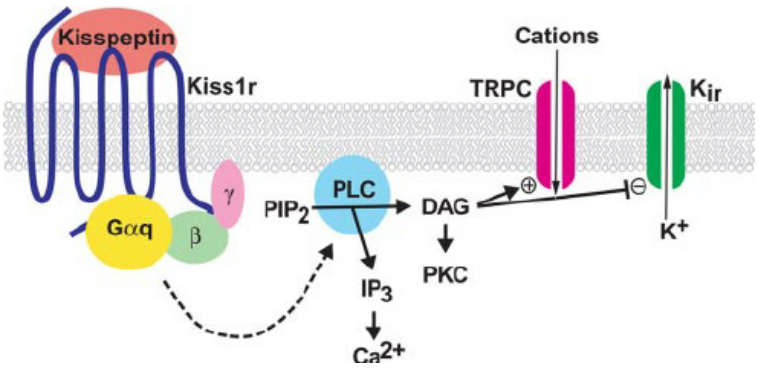

Figure 3.108: Cellular response on kisspeptin-mediated activation of GPR54.[336]

A consequence is the depolarisation of the GnRH neurons and a subsequent release of GnRH stimulating the hypophysis. The hypophysis releases the gonadotropins luteinizing hormone (LH) and follicle-stimulating hormone (FSH).[23] Both gonadotropins cause gonadal secretion of the sex steroids testosterone, estrogen and progesterone. While GnRH neurons lack the estrogen receptor alpha (ERα), a feedback loop must involve kisspeptin neurons.[337-339] It is assumed that estrogen (testosterone is aromatised to estrogen[338]) binds to ERα in kisspeptin neurons in the arcuate nucleus (ARC) followed by inhibition of GnRH release.[337]

Both, kisspeptin and GPR54 play a crucial role in the reproductive system. Gen mutation of GPR54 leads to abnormal developments in sexual maturation, ranking from partial sexual development to severe hypogandism.[340] Therefore, a micropenis is an early clinical indicator for GnRH definciency.[341] Later, GnRH is important for the onset of puberty and mutation lead to absence of pubertal development and infertility in both sexes, which can be overtaken by GnRH administration. Furthermore, kisspeptin plays a crucial role in the female reproduction cycle, especially in the genesis of the LH preovulatory peak[342-344] in the ovarian cycle, pregnancy[345, 346] and lactation.[347]

Besides its affinity to GPR54, kp-54 and kp-10 are also binding to the NPFFR1 receptor (or GPR147)[348], which is the receptor for gonadotropin inhibitory hormone (GnIH).[349] Upon binding of its ligands, for example the Gonadotropin inhibitory hormone RFRP-3, NPFFR1 inhibits the firing of GnRH neurons and therefore plays a key role in suppression of the HPG axis.[350] The low selectivity (IC_{50}, GPR54: 0.12 nM, NPFFR1: 4.7 nM, NPFFR2: 76 nM) might seem incompatible, but the receptor expression level and the projection pattern of neurons should regulate GnRH secretion.[351]

3.6.3 Kisspeptin

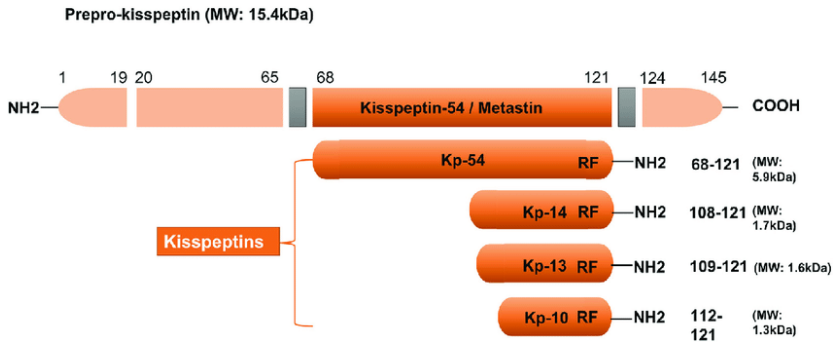

Figure 3.109: Proteolysis of the precursor prepro-kisspeptin reveal four shorter fragments kp-54, kp-14, kp-13 and kp-10, all able to activate GPR54.[26]

The human KISS-1 gene encodes a 145 amino acid long precursor peptide, the prepro-kisspeptin.[22, 328] Prepro-kisspeptin consists of a 19 amino acid long signal peptide and 54-amino acid central region.[352] After proteolysis, an amino group is transferred to the *C*-terminal phenylalanine Phe121 from the adjacent glycine Gly122 by carboxypeptidase, which is essential for the stimulation of intracellular Ca^{2+}-increase.[329, 330] This fragment kp-54 is also called metastin (Figure 3.109) and degradation from the *N*-terminus produces the shorter sequences kp-14, kp-13 and kp-10 (DLNPYNWNSFGLRF-NH_2).[328] The highly conserved 10 amino acid long *C*-terminal RF-amide core sequence YNWNSFGLRF-NH_2 is sufficient for a full activation of the GPR54.[353] Furthermore, with 4.13 nM, kp-10 has the lowest EC_{50} value upon the short kisspeptin equences.[202]

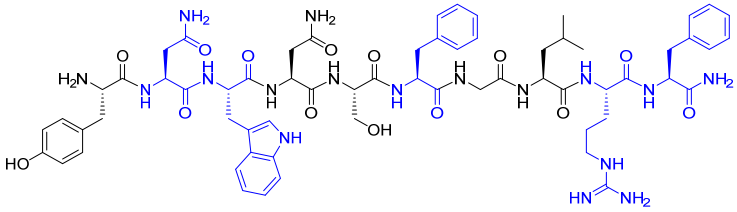

Figure 3.110: Kisspeptin-10 and its residues important for GPR54 activation.[27, 354-357]

kp-10 is a highly aromatic linear peptide, with a low solubility in aqueous solution[355]. Both, rat kp-10 and human kp-13 show a α-helical domain from Asn4 to Tyr/Phe10.[27, 354] With a 1-4 min half-life, kp-10 has a low proteolytic stability and a low bioavailability.[358] In the search for stable and potent GPR54 agonists and antagonists, structure-activity studies revealed the amino acids, which are crucial for receptor binding (Figure 3.110). Alanine scans of the kiss1-R ligand kisspeptin-10 showed the importance of aromatic side-chains for GPR54 binding.

Aromatic positions F6 and F10 are known to be essential for receptor activity.[27, 354] Furthermore, F6A-kp-10-analogue showed antagonistic effects on GPR54 in transfected CHO-K1 cells.[354] Substitution of Tyr1 against D-Tyr or D-Ala, Ser5 against Gly or D-Ser and Leu8 against D-Trp or D-Leu resulted in a high-affinity GPR54 antagonists, too.[359] At least, the five *C*-terminal part with its hydrophobic and charged residues is thought to be essential for receptor binding, whereas the five *N*-terminal amino acids form the activation domain. The two phenyl-rings are meant to form a hydrophobic cluster (Figure 3.111), flanked by the side-chain of Leu8 and Arg9.[27, 355] These results stress out the importance of the RF-amide motive for receptor binding, whereas Phe10 can be substituted by aromatic tryptophan, increasing the metabolic stability.[356, 357]

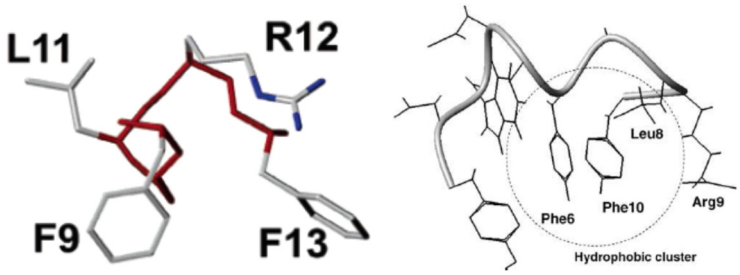

Figure 3.111: Hydrophobic cluster in the C-terminal part of kp-13[27] and kp-10[355], which is essential for receptor binding.

3.6.4 Results and Discussion

3.6.4.1 Development and Synthesis of photoswitchable Kisspeptin-analogues

In this context, the aim was the development of light-controlled mimetics of kp-10. Spatiotemporal approaches provide a high level of selectivity concerning target distribution and dosing by adjustment of light intensity and wavelength. However, photopharmacology offers the possibility of converting molecules into photoswitchable tools enabling targeting drug activity to the tissue of interest and thus representing a potent tool to disclose yet unknown signalling pathways.[14, 187, 188, 360] These are the first examples of photoswitchable kisspeptin-10 peptides, which are possible tools to understand molecular mechanism of receptor activation, the control of HPG-axis and can serve as blueprint for therapeutic targets of kisspeptin-related diseases like diabetes, cancer and defective sexual development.

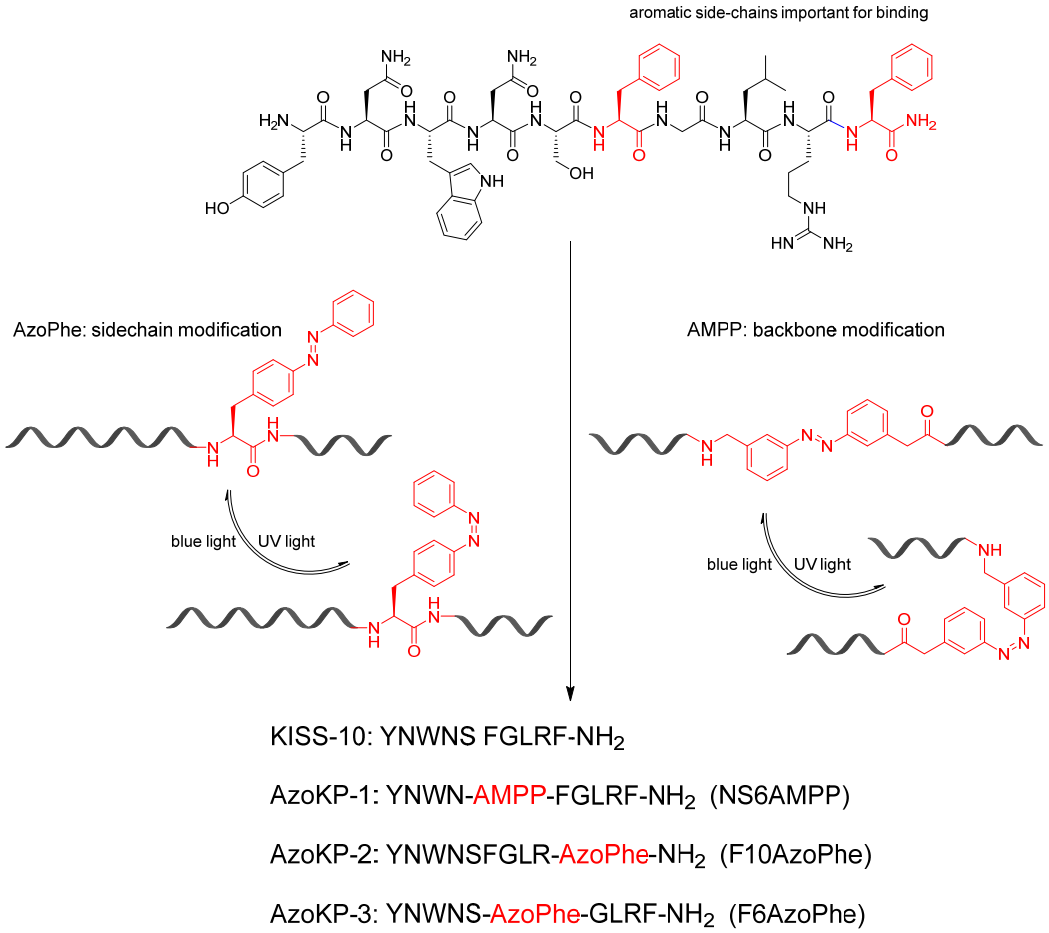

Scheme 3.17: Design of photowitchable Kisspeptin-Analogues: by substitution of amino acids critical for receptor binding, spatiotemporal control over peptide activity can be gained.

The most evident choice for the introduction of the chromophoric units was the substitution of Phe6 and Phe10 of the hydrophobic cluster (Scheme 3.17). Substitution of Phe10 by Trp already showed the acceptance of a bulkier side-chain in this position.[357] Therefore, incorporation of AzoPhe should be less problematic for receptor binding. Furthermore, the chromophoric backbone SPPS building block AMPP was introduced by substitution of Asn4 an Ser5 to get a high impact on the adjacent and important F6 and thus, giving control over the hydrophobic cluster.

The photoswitches AzoPhe **3.3** and AMPP **3.1** were introduced into kp-10 as Fmoc-protected amino acids using HBTU/HOBt and DIPEA for coupling (Figure 3.112). Natural amino acids were coupled by microwave assisted SPPS using DIC/Oxyma pure®. All coupling conditions are summarised in table 3.12. The peptides were characterised by NMR and high-resolution mass spectrometry and their purity was controlled by reverse-phase HPLC. All three peptides were <1.9 ppm of the calculated mass and RP-HPLC confirmed high purity.

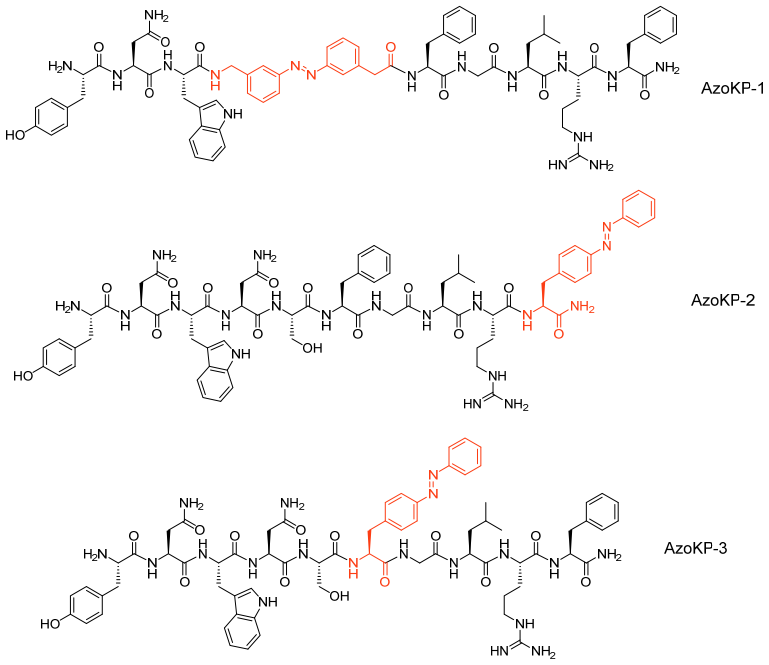

Figure 3.112: Structure of the three synthesised Azo-KP.

To examine the structure relations, we recorded CD spectra of Kisspetin-10 and our kisspeptin-mimetics in PBS/TFE 20:80, whereas TFE is known to induce secondary structure formation,[361-363] and as it was also shown with Kisspeptin-14.[364] All photoswitchable peptides were measured in *cis*- and *trans*-configuration. The recorded spectra were smoothed with a 20-point Savitzky-Golay[365] filter and secondary structure prediction was done with BeStSeL[366-368]. The closest fit to the Kisspeptin-10 curve could be received with *cis*-AzoKP-2. For *trans*-AzoKP-2 we gained a higher content of β-strand and a lower α-helical content, whereas *cis*-AzoKP-2 and Kisspeptin-10 showed a quite similar secondary structure prediction with a higher amount of α-helix. AzoKP-1 and AzoKP-3 showed smaller differences between *cis* and *trans* forms. Nevertheless, CD-spectroscopic secondary structure estimation for short peptides should be regarded carefully. Furthermore, the secondary structure analysis of human kp-13[27] in the presence of DPC micelles (NMR) and rat kp-10 analogues[354] in a diphenylcarbodiimide-water solution (NMR and MD-simulations) in one hand and of human kp-10 analogues[355] in the presence of SDS micelles (NMR and CD) showed different results. While human kp-13 and rat kp-10 analogues possess an α-helix between Asn7 and Phe13 and Asn4 to Tyr10 respectively, the human kp-10 analogues showed several tight turn structures between Trp3 and Phe10, but no helical conformation. An explanation might be the use of different solution materials. Diphenylcarbodiimide and the zwitterionic DPC have both neutral surfaces, whereas SDS micelles form negatively charged surfaces.[27, 354, 355]

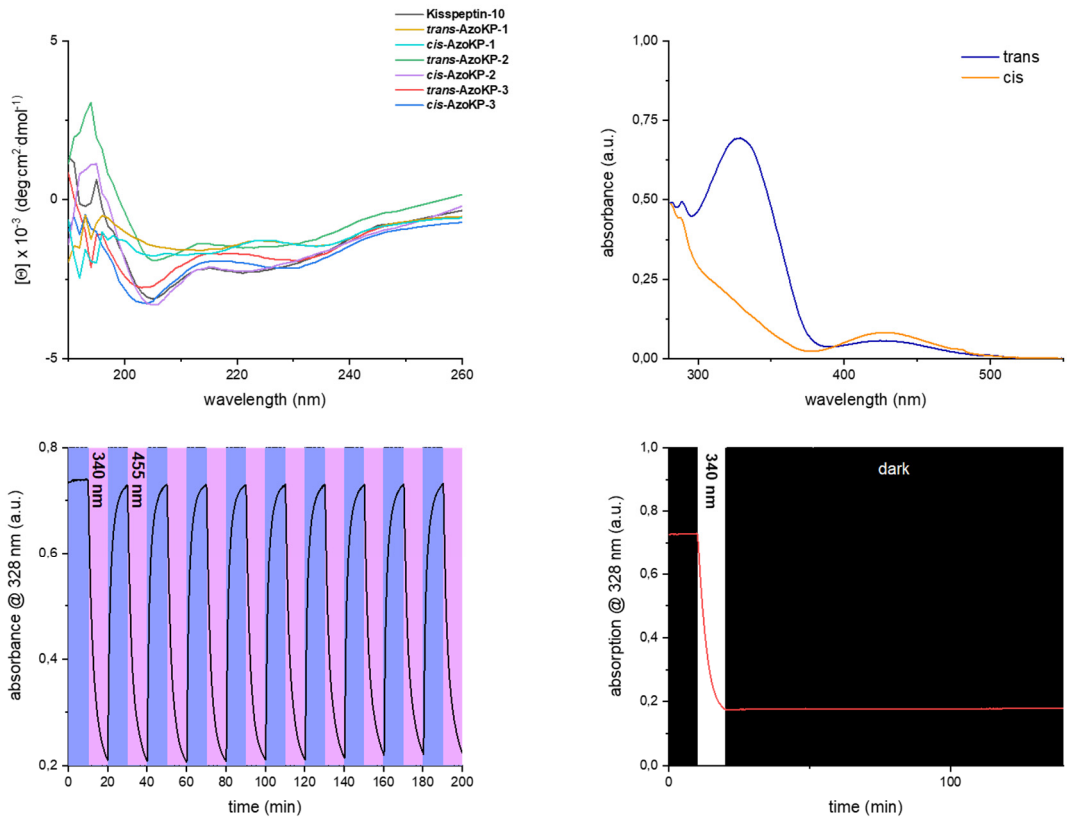

Figure 3.113: Photoisomerisation. A) CD-spectra of Kisspeptin-10 and its photoswitchable mimetics. B) Representative UV/VIS spectra for *cis*- and *trans*-AzoKP-2. C) Representative reversible switching of AzoKP-2 between the *cis*- and *trans*-Isomers using blue (λ = 455 nm) and UV (λ = 340 nm). D) Representative bistability of the *cis*-Isomer over 2 h.

Spectroscopic properties of the compounds were examined using UV/VIS spectroscopy (Figure 3.113) by switching azobenzene moieties from *trans* to *cis* with UV light (365 nm) and back with blue light (445 nm). A decrease of the π-π* absorption band and an increase of the n-π* absorption band was observed by illumination with UV light and vice versa by subsequent exposure to blue light. Only minimal bleaching occurred after several switching cycles. The high photostability prevents the formation of triplet states and reactive oxygen species, which is crucial for biocompatibility.[14] The compounds also possess a high bistability when switched to the *cis* state and subsequently left in the dark for 2 hours allowing for pre-illumination of the peptides before being applied to cells.

3.6.4.2 Pharmaceutical evaluation

Patch clamp recordings

To investigate the pharmaceutical properties, for all compounds, whole-cell patch-clamp recordings were performed in voltage clamp and current clamp on GnRH neurons by Dr. Jian

Qiu (Group of Prof. Dr. Martin J. Kelly, Oregon Health and Science University). The results of Dr. Qiu are described in the following.

Using voltage clamp method, a constant electrical voltage is applied to the cell. This technique is used to measure changes in the conductivity of the membrane, whereas the applied voltage ist used as reference.[369] The purpose of voltage clamp technology is the measurement of the current flow or ionic currents of a cell. In contrast, the current clamp method measures the change in the membrane potential, i.e. the voltage.[369] At least, reversal potential is determined by plotting the maximum current versus the voltage ramp.[370]

After addition of each peptide in a concentration of 100 nM, the neurons were illuminated with a 375 nm LED-source. Addition of AzoKP-1 showed no effect in a voltage clamp assay, neither in *trans*- nor in *cis*-conformation, whereas a positive control with kp-10 showed strong neuronal firing (Figure 3.115E). The substitution of two polar amino acid side-chains by an unpolar azobenzene moiety in AzoKP-1 results in an inactive peptide.

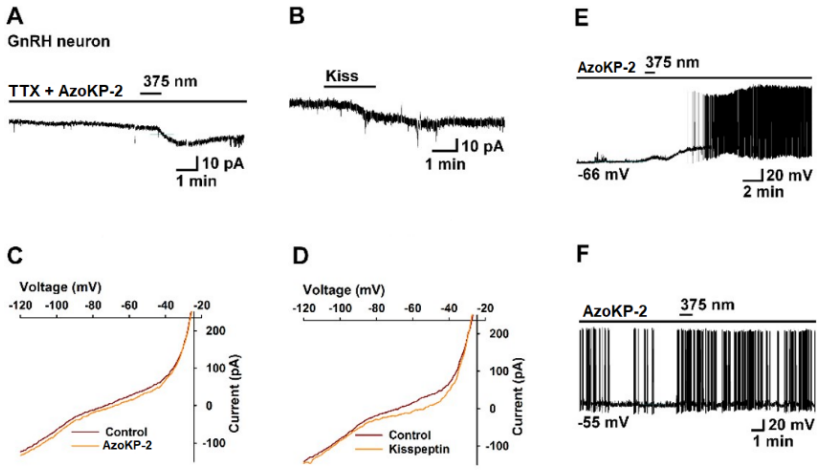

Figure 3.114: Patch clamp experiments on GnRH-neurons: A) representative trace of inward current in GnRH neurons in voltage clamp (Vhold= −60 mV) upon light-induced isomerisation of AzoKP-2 (100 nM). B) rapid bath application of kp-10 (100 nM) induced an inward current in the presence of fast sodium channel and ionotropic glutamatergic blockade (Vhold = - 60 mV). C and D) comparison of voltage ramps from 0 to -100 mV (over 2 s) before and after *trans* to *cis* isomerisation of AzoKP-2 or during treatment with kp-10: both showed a reversal at -30 mV. E) *trans* to *cis* isomerisation of AzoKP-2 (100 nM) induced depolarization in GnRH neuron. F) photoactivation increased bursting firing frequency of AzoKP-2 (100 nM) in GnRH neurons.

AzoKP-2, the F10AzoPhe Kisspeptin derivative, instead showed a clear response on GnRH neurons upon photoactivation at 100 nM in voltage clamp experiments. Upon illumination, GnRH neurons showed a prolonged inward current of 12 pA (Figure 3.114A), which is slightly lower than kp-10 (100 nM) induced inward current of 20 pA.[335] The lower inward current

of *cis*-AzoKP-2 in comparison to the native kp-10 suggests an incomplete activation of GPR54. Although 10 nM concentration of kp-10 also leads to prolonged and intense activation of GnRH neurons (Figure 3.114B), a saturating concentration of 100 nM is usually used to minimise fluctuation of the effective peptide concentration and to guarantee maximal response.[335, 371] Furthermore, illumination with 375 nm showed an increased firing in current clamp method as a result of *trans* to *cis* isomerization (Figure 3.114F). Hence, *cis*-AzoKP-2 shows a stronger receptor activation then *trans*-AzoKP-2.

Current-voltage (I/V) curves by running a voltage ramp from 0 mV to −100 mV in the presence of *cis*- and *trans*-AzoKP-2 in comparison to kp-10 were also recorded. Nearly identical I/V curves with a reversal potential of −30 mV of AzoKP-2 and kp-10 in the voltage ramp experiments suggest the same mechanism of receptor activation and thus neuronal excitation of both peptides (Figure 3.114C/D).

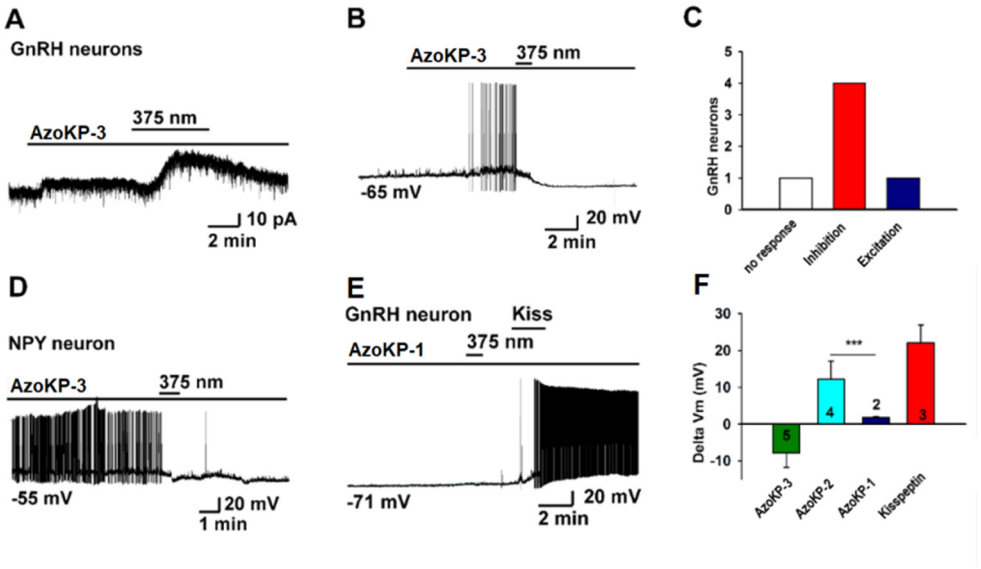

Figure 3.115: Effects by light-induced photoactivation of AzoKP-1 and AzoKP-3 on GnRH neurons: A) representative trace of the inward-current. AzoKP-3 (100 nM) was added 7 min before activating with a 375 nm light pulse (Vhold= −60 mV). B) Hyperpolarisation and inhibited firing of GnRH neurons after photoactivation of AzoKP-3 in current clamp. C) Number of GnRH neurons with different respond to photoactivation of AzoKP-3. D) Hyperpolarisation and inhibited firing of NPY neurons after photoactivation of AzoKP-3 in current clamp. E) AzoKP-1 shows no effect on GnRH neurons. F) Summary of the effects of the photoswitchable kisspeptin-10 analogues in comparison to kp-10 on GnRH neurons.

In contrast the excitatory properties of AzoKP-2, addition of AzoKP-3 (F6AzoPhe) lead to inhibition of firing of GnRH neurons in current clamp upon isomerisation from *trans* to *cis* with 375 nm (Figure 3.115A/B). While four of six cells were inhibited and one showed no response, one of six showed excitation (Figure 3.115C). The predominantly inhibitory effects of *cis*-

AzoKP-3 on GnRH neurons coincides with the dose-dependent effect of RFRP-3 on GnRH neurons.[372] RFRP-3 is a RF-amide peptide with the sequence VPNLPQRF-NH2 and belongs to the Gonadotropin-inhibitory Hormone (GnIH) group.[373] Upon binding to the receptors NPFFR-1 and NPFFR-2, RFPR-3 inhibits GnRH neurons.[374] Whether AzoKP-3 binds directly to GPR54 or to NPFFR-1/NPRFFR-2, further current clamp experiments on NPY neurons were carried out. NPY neurons do not express GPR54 but NPFFR1 mRNA.[375] Reported by Oishi et. al. besides kp-54, kp-10 binds to NPFFR1 with an IC50 = 4.7 nM as assessed by binding inhibition assays.[348] In accordance current clamp experiments on NPY neurons showed also a clear inhibition of firing (Figure 3.115D) upon *trans*- to *cis*-isomerisation of AzoKP-3. These findings suggest binding of *cis*-AzoKP-3 to NPFFR1.

3.6.4.3 *in vitro* cell studies

The observed effects on GPR54 could be underlined by in vivo cell studies on transfected GPR54-GFP tagged HeLa cells, carried out by Dr. Jan-Erik Hoffmann (Group of Prof. Dr. Carsten Schulz, Oregon Health and Science University). The results of Dr. Hoffmann are shown below. The GPR54 transducts signals through the phospholipase C/IP_3 pathway, leading to calcium efflux from the endoplasmic reticulum[328], which can be monitored by R-GECO as readout for receptor activation.

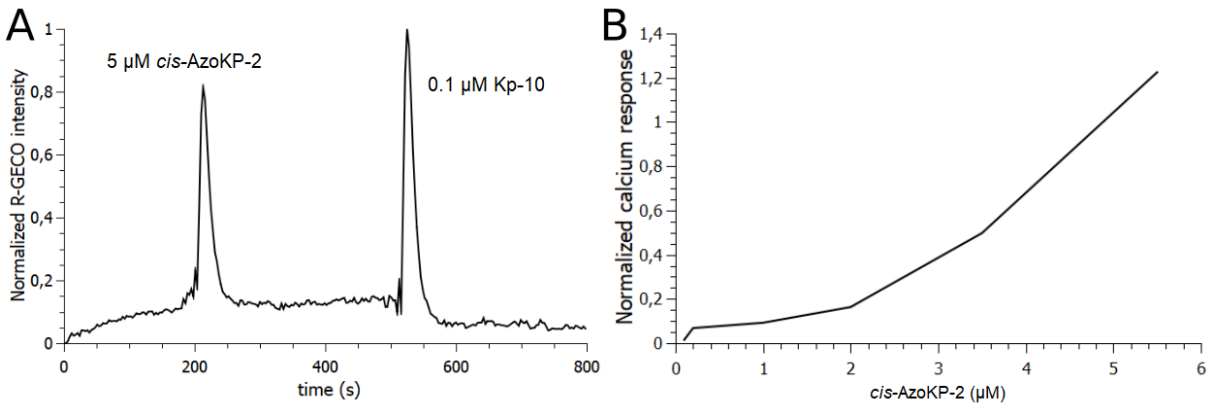

Figure 3.116: A) *cis*-AzoKP-2 stimulates Gpr54-transfected HeLa cells. B) Dose-response curve calculated by kisspeptin/*cis*-AzoKP-2 ratio.

In the *in vitro* cell studies, the addition of pre-illuminated *cis*-AzoKP-2 lead to a clear fluorescence signal, however, not as potent as with native kp-10. (Figure 3.116) The lower excitation of GnRH neurons upon binding of *cis*-AzoKP-2 in comparison to native kp-10 agrees with cell assays on transfected HeLa cells, where first reliable responses can be seen at concentration of 500 nM and a maximum response at 3-5 µM. However, low saturation effects

were observed upon addition of kp-10 to GPR54 after high concentrations of AzoK-2, giving a weaker response. Furthermore, different concentrations of *cis*-AzoKP-2 were used to stimulate HeLa cells, followed by addition of 0.1 µM KP-10. The KP-10/*cis*-AzoKP-2 ratio was used to calculate a dose-response curve.

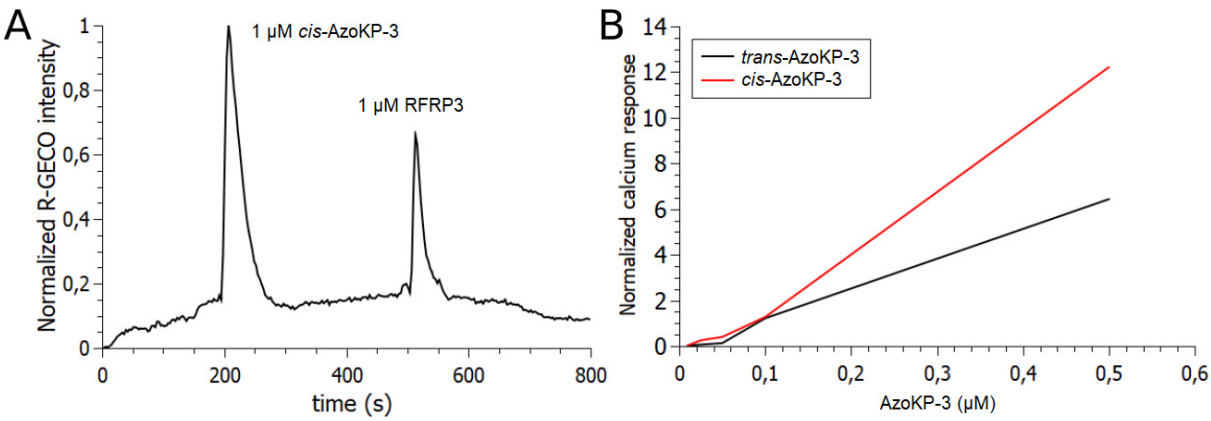

Figure 3.117: A) cis-AzoKP-3 stimulates NPFFR1 transfected HeLa cells. B) Dose-response curve for trans- and cis- AzoKP-3 calculated by RFRP-3/AzoKP-3 ratio.

In accordance to GPR54 *in vitro* tests, cell assays on NPFFR1 expressing HeLa cells were confirmed (Figure 3.117). Whereas *cis*- or *trans*-AzoKP-2 doesn't bind to NPFFR1, we could observe a maximum response by addition of AzoKp-3 at 500 nM. Additionally, due to its affinity of kp-10 to NPFFR1, introducing photoswitches into kp-10 leads to a GPR54 selective agonist AzoKP-2. Furthermore, stimulating with higher concentrations of one peptide has a fatigue effect on the other peptide resulting in a lack of stimulation when added 5 minutes later. The dose-response curve was calculated from integrated Ca^{2+}-spikes of AzoKP-3 and RFRP3. Both conformations of AzoKP-3 activate NPFFR1 in lower concentration then RFRP-3.

However, experiments in HeLa cells and patch clamp experiments on GnRH and NPY neurons show some differences. First, results from experiments in HeLa cells showed signalling upon addition of both *cis*- and *trans*-AzoKP-3 in concentration higher than 50 nM, which is in contrast to the *cis*/*trans*-selectivity shown in patch clamp experiments on GnRH and NPY neurons. This can be explained by the used technique of transfected HeLa cells. Reconstituted HeLa cells are a very artificial system, giving only qualitative results. Nevertheless, these experiments confirm the binding of AzoKP-3 on NPFFR1, which causes inhibition GnRH neurons.

In summary, introduction of chromophoric side chains by substitution of relevant aromatic amino acids lead to potent and selective photoswitchable GPR-54 agonist AzoKP-2 and

AzoKP-3. Whereas the exchange of the *C*-terminal phenylalanine against AzoPhe led to a GPR54-agonist, the exchange of Phe6 against AzoPhe abolished binding to GPR-54 but gained a highly potent NPFFR1-agonist. With both photoswitchable KP-10 analogues, the control of the HPG axis is possible. Next step would be to test AzoKP-2 and AzoKP-3 in *in vitro* experiments to get reliable dissoziation constants. Finally, experiments with GnRH-GFP and NPY-GFP mice could be used to visualize the structure and function of GnRH- and NPY-neurons.

3.6.5 Analytical Data of the AzoKisspeptins

A solid-phase *Fmoc*-L-Phenylalanine TentaGel S RAM resin (RAPP Polymere®), pre-loaded with 0.23 mmol/g amino acid, was used for peptides **AzoKP-1** and **AzoKP-3**. An unloaded TentaGel S RAM resin (RAPP Polymere®) with 0.23 mmol/g resin loading was used for the synthesis of **AzoKP-2**. The peptides were synthesised in 0.1 mmol scale with the coupling reagents DIC 0.5 M as an activator and Oxyma Pure® 1.0 M as an activator base in DMF. Amino acids were coupled in fivefold excess (0.2 M solutions) as Fmoc-protected compounds with standard residual protecting groups. Coupling of photoswitch **3.1** was carried out with HBTU/HOBt in NMM for 1 h at room temperature. Fmoc deprotection was achieved by treatment with 20% piperidine in DMF. Coupling conditions are summarised in Table 3.12. After peptide synthesis, the resin-bound peptide was transferred into a Merrifield reactor followed by global deprotection with TFA/Thioanisole/1,2-Ethanedithiole/Anisole (9.5/0.5/0.3/0.2) solution within 2 h. The solvent was then evaporated and the residue was precipitated in 45 mL chilled diethyl ether. The precipitated peptide was centrifuged, washed five times with diethyl ether and after decantation of the solution, the residue was dried and purified with RP-HPLC to yield the desired peptide.

-

Table 3.12: Coupling conditions of **AzoKP-1**, **AzoKP-2**, **AzoKP-3**.

Compound	AzoKP-1				AzoKP-2				AzoKP-3			
	step	*t* [s]	*p* [W]	*T* [°C]	step	*t* [s]	*p* [W]	*T* [°C]	step	*t* [s]	*p* [W]	*T* [°C]
*Fmoc*AzoPheOH **3.3**					1&2	480	28	75				
*Fmoc*Arg(Pbf)OH	1&2	120	30	90	1&2	120	30	90	1&2	120	30	90
*Fmoc*LeuOH	1&2	120	30	90	1	120	30	90	1	120	30	90
*Fmoc*GlyOH	1&2	120	30	90	1	120	30	90	1	120	30	90
*Fmoc*PheOH	1&2	120	30	90	1	120	30	90	1	120	30	90
*Fmoc*AzoPheOH **3.3**									1&2	480	28	75
*Fmoc*AMPPOH **3.1**	1	3600	0	r.t.								
*Fmoc*Ser(*t*Bu)OH					1	120	30	90	1	120	30	90
*Fmoc*Asn(Trt)OH					1	120	30	90	1	120	30	90
*Fmoc*Trp(Boc)OH	1&2	120	30	90	1	120	30	90	1	120	30	90
*Fmoc*Asn(Trt)OH	1&2	120	30	90	1	120	30	90	1	120	30	90
*Fmoc*Tyr(*t*Bu)OH	1&2	120	30	90	1	120	30	90	1	120	30	90

AzoKP-1

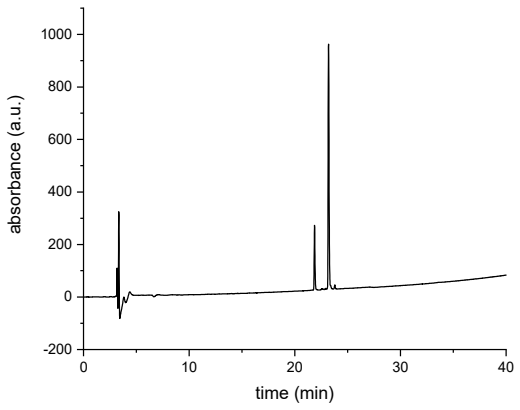

Figure 3.118: Analytical HPLC spectrum of **AzoKP-1** with a water/acetonitrile gradient of 95/5 →20/80 in 40 min. Rf: 21.9 min (cis) and 23.2 min (trans).

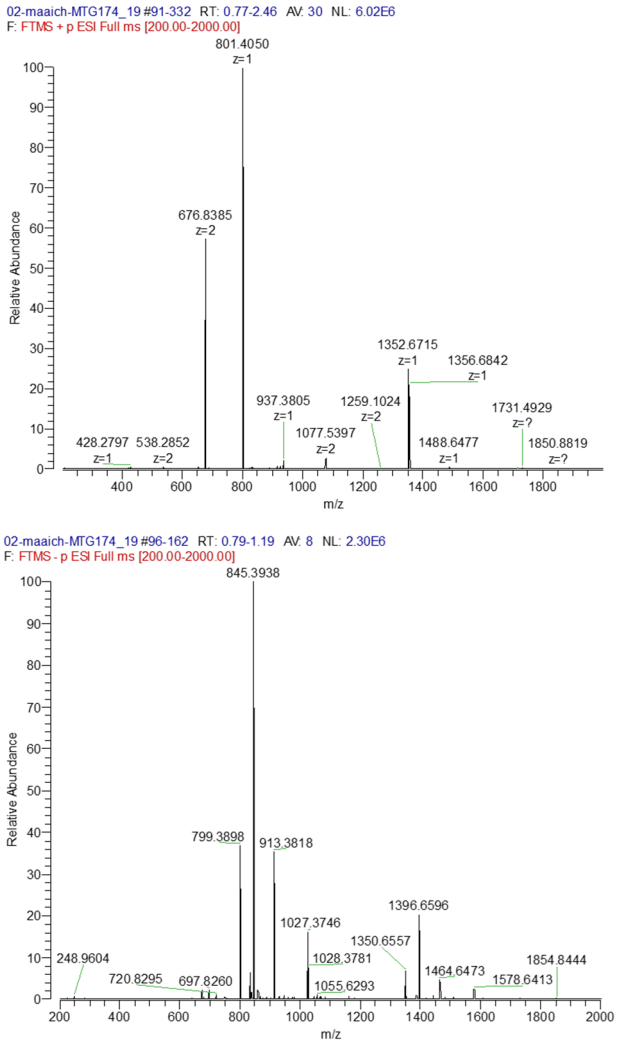

Figure 3.119: HRMS spectrum of **AzoKP-1**: HRMS (+ESI) m/z calc. for $C_{71}H_{87}N_{17}O_{11}^{2+}$ $[M + 2H]^+$: 676.8380; found: 676.8385. Calc. for $C_{71}H_{86}N_{17}O_{11}^{+}$ $[M + H]^+$: 1352.6687; found: 1352.6715. HRMS (−ESI) m/z calc. for $C_{72}H_{86}N_{17}O_{13}$ $[M + FA - H]^-$: 1396.6596; found: 1396.6596.

Table 3.13: Chemical shifts of ^{1}H- and ^{13}C-NMR of **AzoKP-1** DMSO-d_6.

residue	^{1}H-signals	^{13}C-signals
Tyr	NH 7.95, Hα 3.90, Hβa 2.91, Hβb 2.69, Hδ 6.69, Hε 7.03	Cα 54.1, Cβ 36.7, Cγ 125.3, Cδ 115.8, Cε 131.0, Cζ 157.0
Asn	NH 8.70, Hα 4.66, Hβa 2.64, Hβb 2.47	Cα 50.3, Cβ 37.7
Trp	NH 8.26, Hα 4.56, Hβa 3.25, Hβb 3.04, Hδ1 7.14, Hε3 7.58, Hζ3 6.96, Hη2 7.03, Hζ2 7.30	Cα 54.5, Cβ 28.1, Cδ1 124.0, Cζ3 118.8, Cη2 121.3, Cζ2 111.8
AMPP	NH 8.58, H2a 3.60, H2b 3.50, H4 7.67, H6 7.26, H7 7.43, H8 7.72, H12 7.76, H14 7.29, H15 7.49, H16 7.76, H17 4.37	C2 42.3, C3 138.1, C4 123.4, C5 152.3, C6 132.6, C7 129.6, C8 121.5, C11 152.0, C12 121.5, C13 141.5, C14 130.5, C15, 129.8, C16 121.5, C17 42.5
Phe	NH 8.40, Hα 4.53, Hβa 3.04, Hβb 2.80, Hδ 7.20, Hε 7.16, Hζ 7.11	Cα 54.6, Cβ 38.1, Cγ 138.2, Cδ 129.6, Cε 126.7/128.4, Cζ 126.6
Gly	NH 8.33, Hα 3.75	Cα 42.4
Leu	NH 7.89, Hα 4.32, Hβ* 1.42, Hγ 1.59, $Hδ_1$ 0.86, $Hδ_2$ 0.83	Cα 51.5, Cβ 41.4, Cγ 24.6, Cδa 23.6, Cδb 22.1
Arg	NH 8.03, Hα 4.21, Hβ* 1.42, Hγa 1.64, Hγb1.50, Hδ 3.06	Cα 52.8, Cβ 25.3, Cγ 29.3, Cδ 40.9
Phe	NH 7.76, Hα 4.44, Hβa 3.01, Hβb 2.83, Cδ 7.20, Cε 7.23, Cζ 7.17	Cα 54.0, Cβ 38.1, Cγ 138.1 Cδ 129.6, Cε 128.5, Cζ 126.7

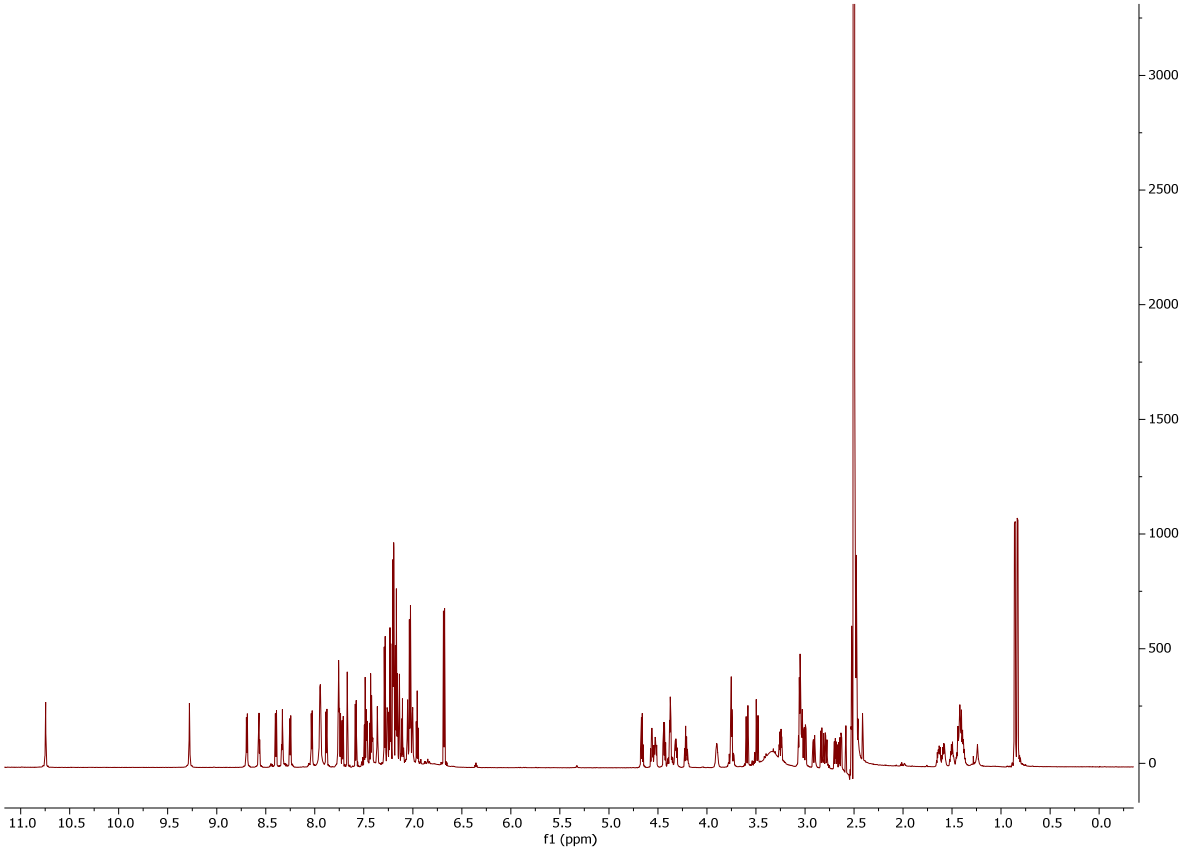

Figure 3.120: ^{1}H-NMR of **AzoKP-1**.

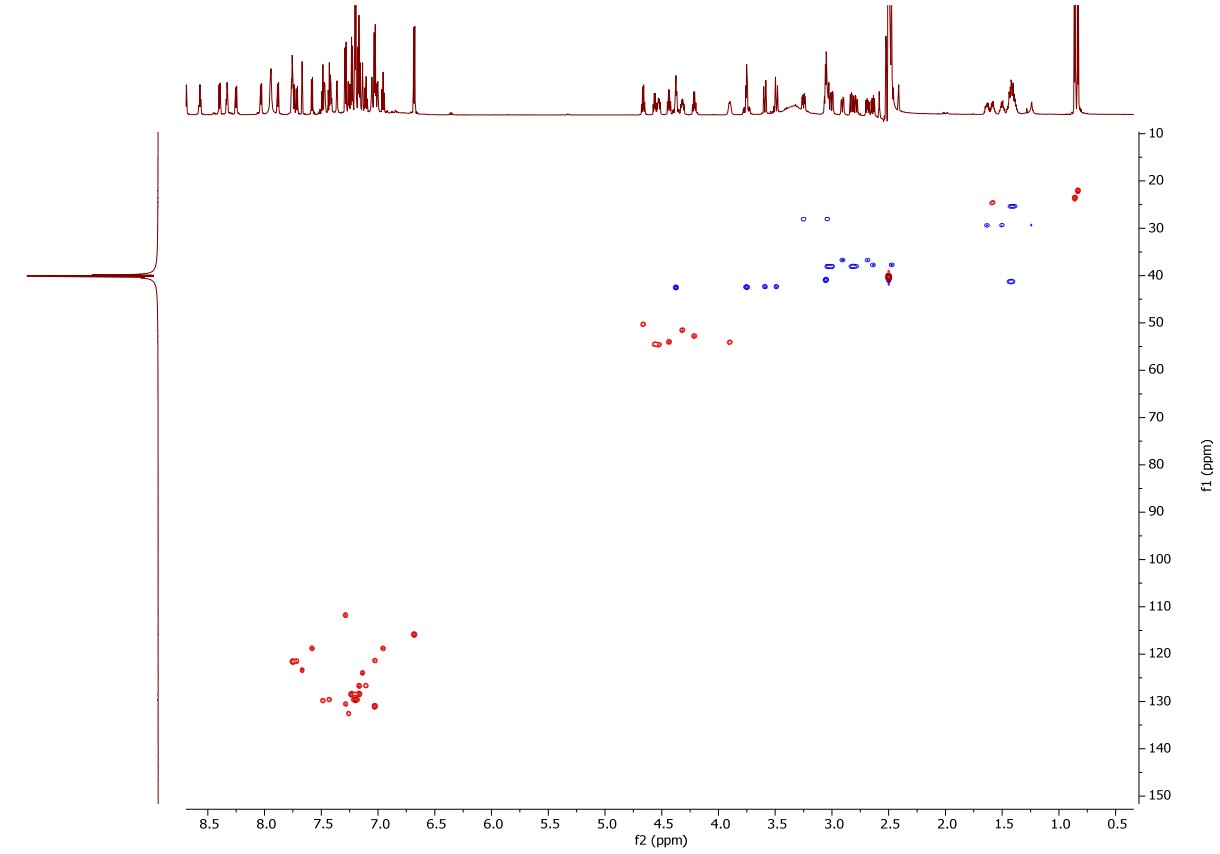

Figure 3.121: ^{1}H, ^{13}C-HSQC-NMR of **AzoKP-1**.

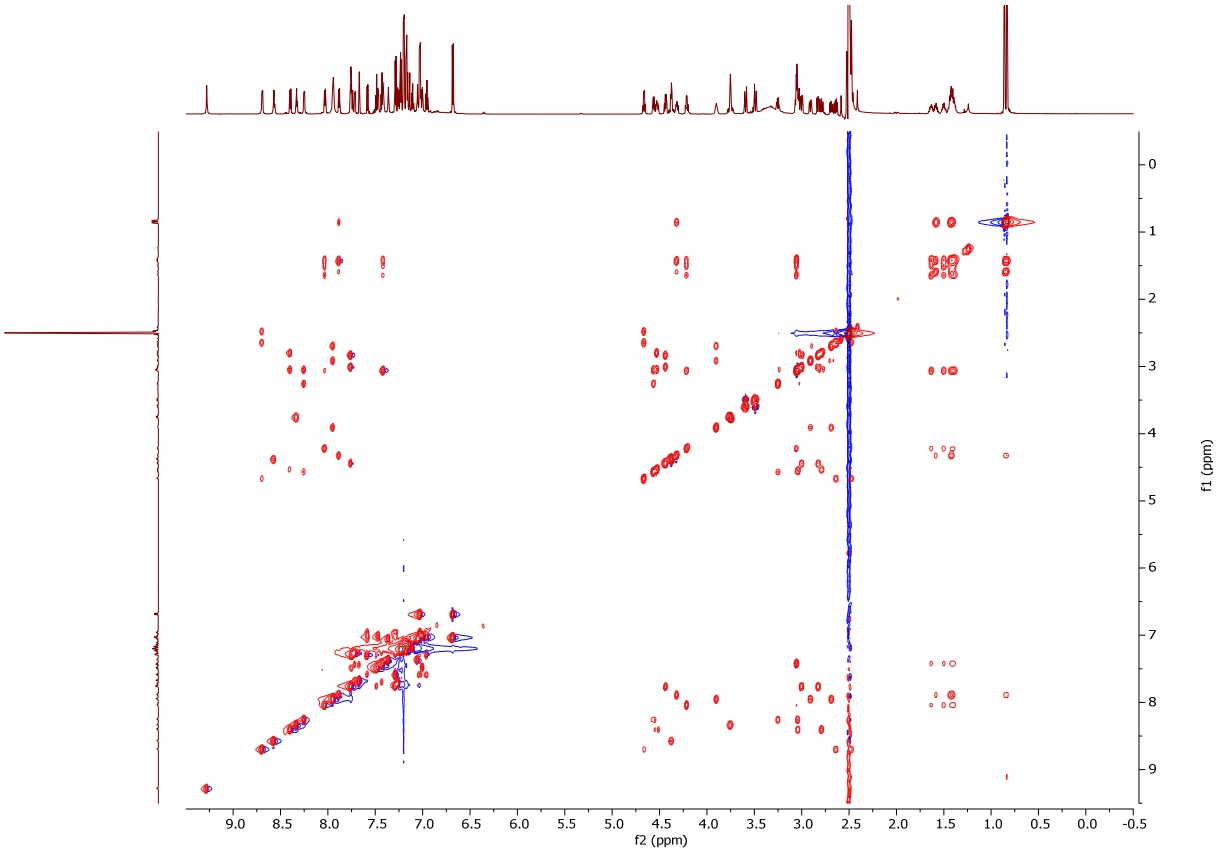

Figure 3.122: ^{1}H, ^{1}H- TOCSY-NMR of **AzoKP-1**.

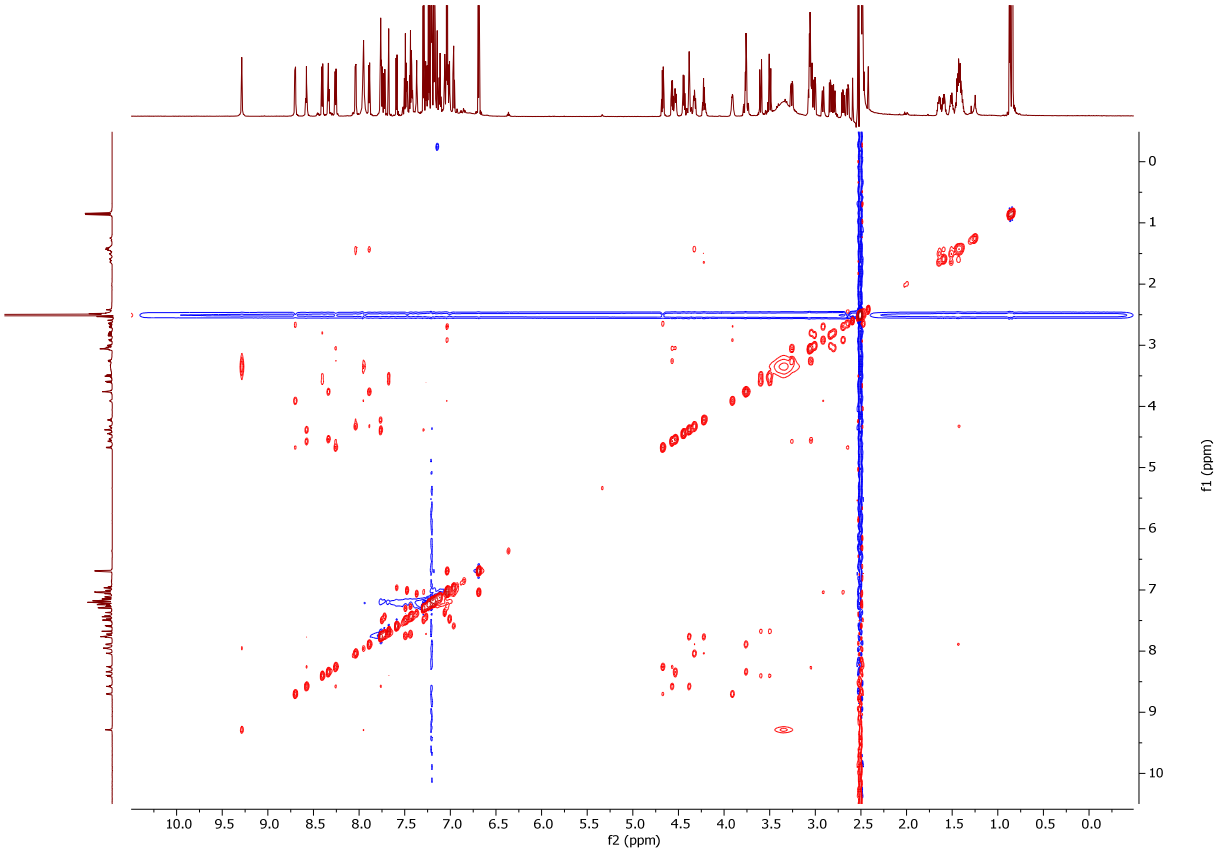

Figure 3.123: ^{1}H, ^{1}H-NOESY-NMR of **AzoKP-1**.

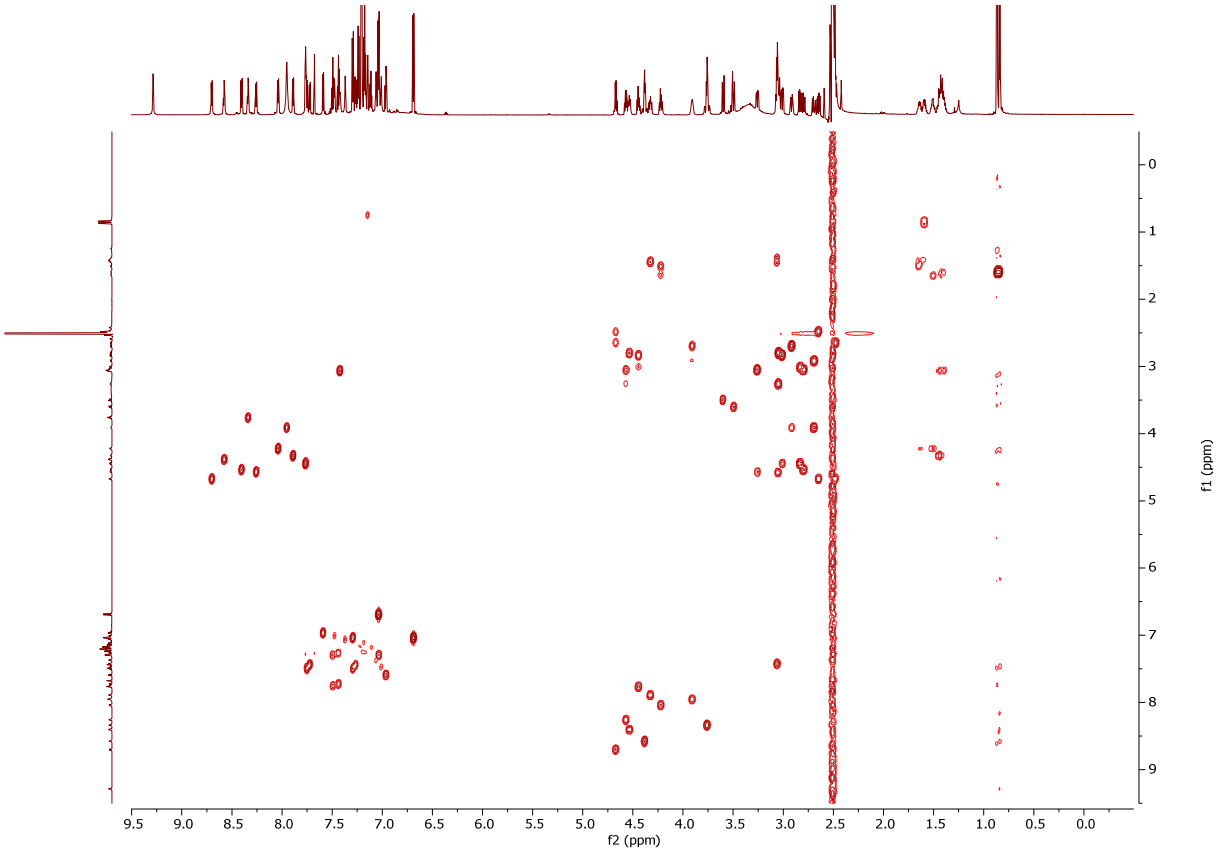

Figure 3.124: ^{1}H, ^{1}H-COSY-NMR of **AzoKP-1**.

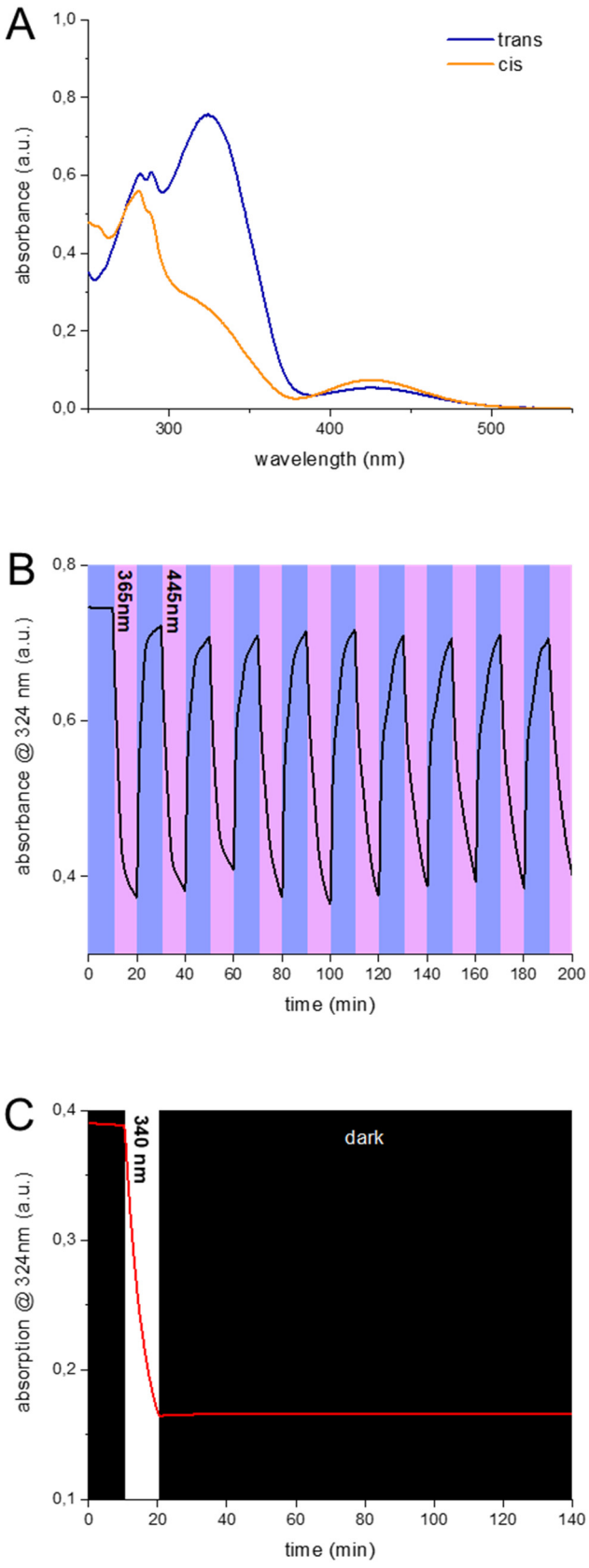

Figure 3.125: A) UV/VIS spectra of trans- and cis-**AzoKP-1**; illumination with 365 nm (trans→cis) and 445 nm (cis→trans). B) Kinetics of **AzoKP-1**. C) Bistability of **AzoKp-1**.

AzoKP-2

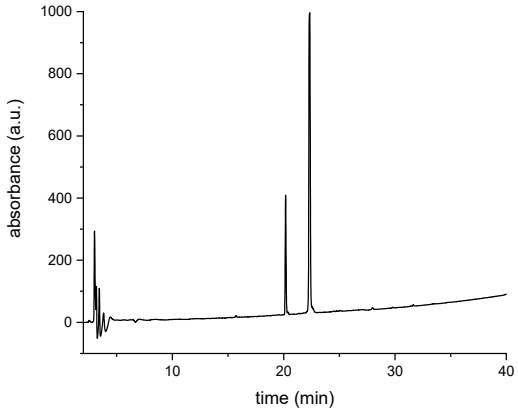

Figure 3.126: Analytical HPLC spectrum of **AzoKP-2** with a water/acetonitrile gradient of 95/5 →20/80 in 40 min. Rf: 20.1 min (cis) and 22.3 min (trans).

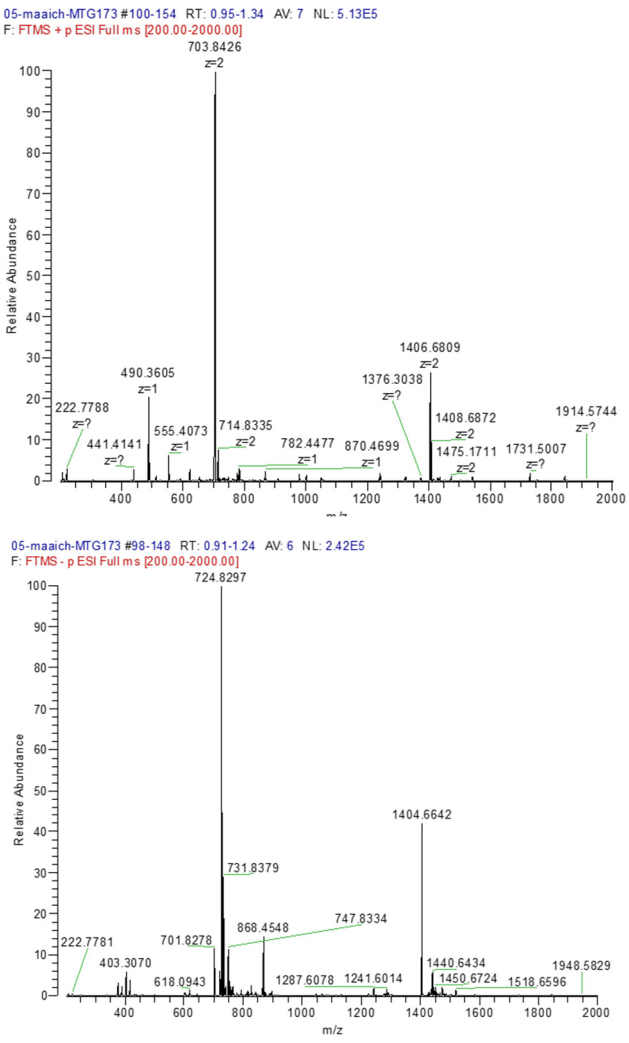

Figure 3.127: HRMS spectrum of **AzoKP-2**: HRMS (+ESI) m/z calc. for $C_{69}H_{89}N_{19}O_{14}^{2+}$ $[M + 2H]^{2+}$: 703.8413; found: 703.8426. Calc. for $C_{71}H_{86}N_{17}O_{11}^{+}$ $[M + H]^{+}$: 1406.6753; found: 1406.6809. : HRMS (−ESI) m/z calc. for $C_{69}H_{89}N_{19}O_{14}^{2-}$ $[M + FA - 2H]^{2-}$: 724.8294; found: 724.8297.

Table 3.14: Chemical shifts of ^{1}H-NMR and ^{13}C-NMR **AzoKP-2** in DMSO-d_6.

residue	^{1}H-NMR	^{13}C-NMR
Tyr	NH 7.96, Hα 3.89, Hβa 2.92, Hβb 2.66, Hδ 7.04, Hε 6.68,	Cα 54.1, Cβ 36.7, Cγ 125.3, Cδ 115.8, Cε 131.0
Asn	NH 8.71, Hα 4.62, Hβa 2.61, Hβb 2.50	Cα 50.2, Cβ 37.6
Trp	NH 8.20, Hα 4.51, Hβa 3.16, Hβb 2.96, Hδ1 7.15, Hε2 7.58, Hζ3 6.94, Hη2 7.02, Hζ2 7.28	Cα 53.9, Cβ 27.9, Cγ 110.3, Cδ1 124.1, Cε2 118.8, Cζ3 118.7, Cη2 121.3, Cζ2 111.7
Asn	NH 8.30, Hα 4.63, Hβa 2.61, Hβb 2.50	Cα 50.2, Cβ 37.6
Ser	NH 8.01, Hα 4.19, Hβa 3.55, Hβb 3.50, Hγ 4.97	Cα 56.2, Cβ 61.8
Phe	NH 8.08, Hα 4.43, Hβa 3.07, Hβb 2.89, Cδ 7.22, Hε 7.24, Hζ 7.16	Cα 55.0, Cβ 37.4, Cγ 138.3, Cδ 129.6, Cε 128.5, Cζ 126.7
Gly	NH 8.11, Hα 3.72	Cα 42.5
Leu	NH 7.86, Hα 4.30, Hβa 1.44, Hβb 1.36, Hγ 1.56, Hδa 0.81, Hδb 0.78	Cα 51.4, Cβ 41.2, Cγ 24.4, Cδa 23.6, Cδb 22.0
Arg	NH 8.12, Hα 4.24, Hβ* 1.45, Hγa 1.66, Hγb1.53, Hδ 3.05	Cα 25.7, Cβ 25.4, Cγ 29.3, Cδ 40.9
AzoPhe	NH 7.92, H1 4.51, H2a 3.11, H2b 2.93, H4/8 7.43, H5/7 7.80, H12/16 7.86, H13/15 7.59, H14 7.59	C1 53.9, C2 37.9, C3 142.2, C4/8 130.7, C5/7 122.8, C6 151.0, C12/16 122.9, C13/15 129.9, C14 131.8

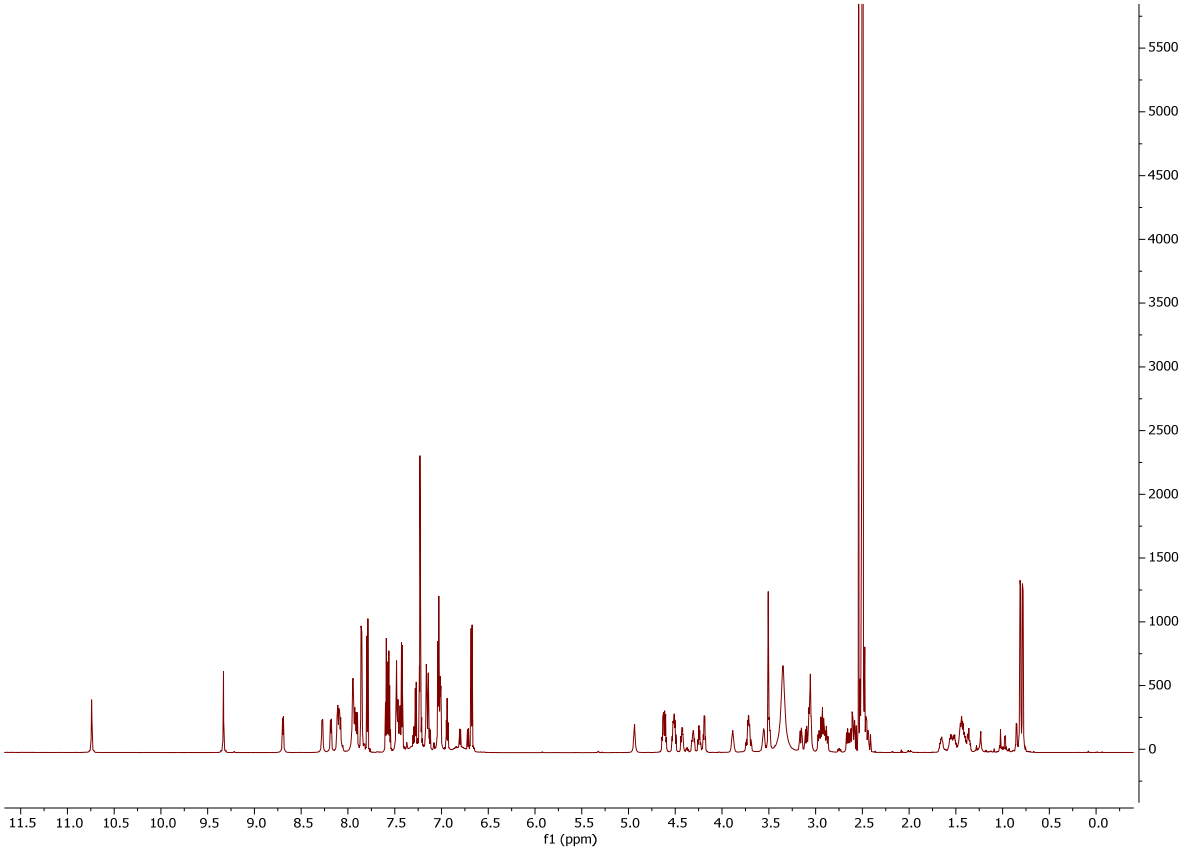

Figure 3.128: ^{1}H-NMR of **AzoKP-2**.

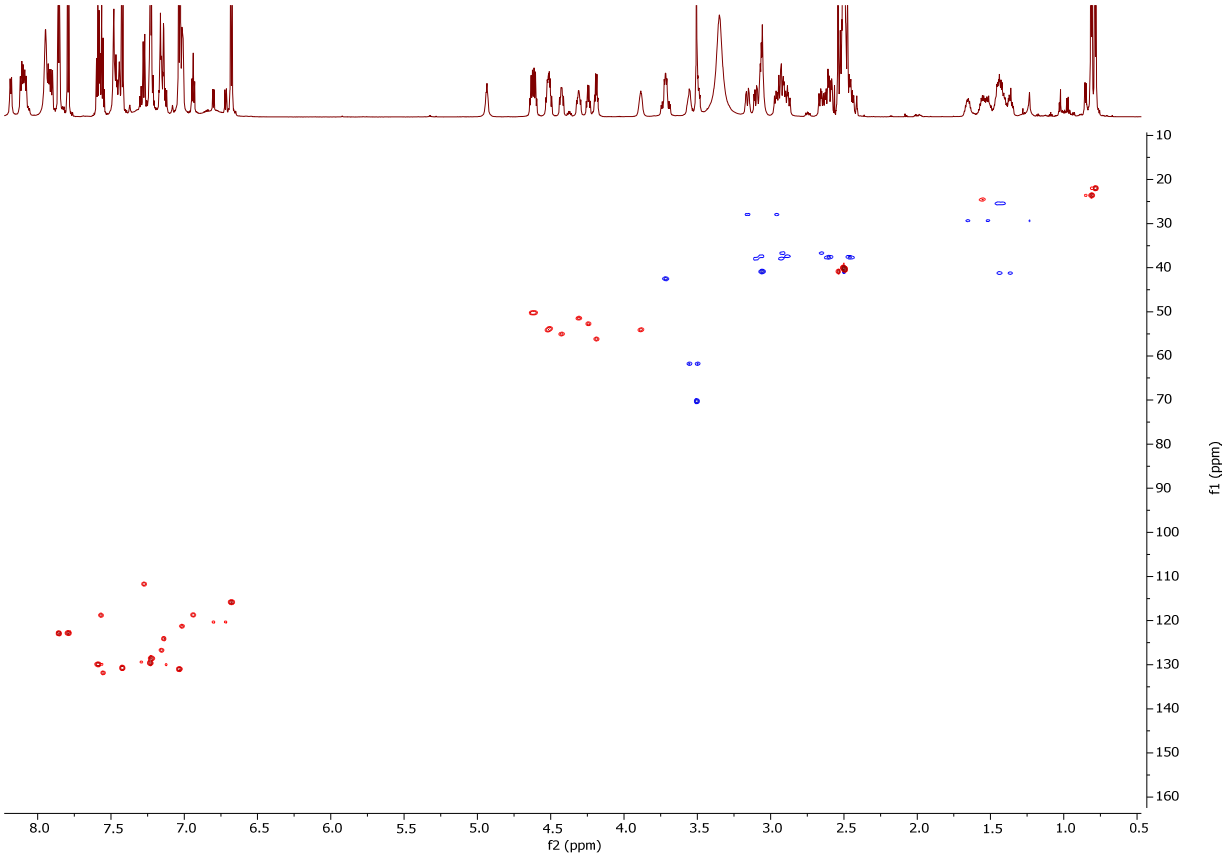

Figure 3.129: ^{1}H, ^{13}C-HSQC-NMR of **AzoKp-2**.

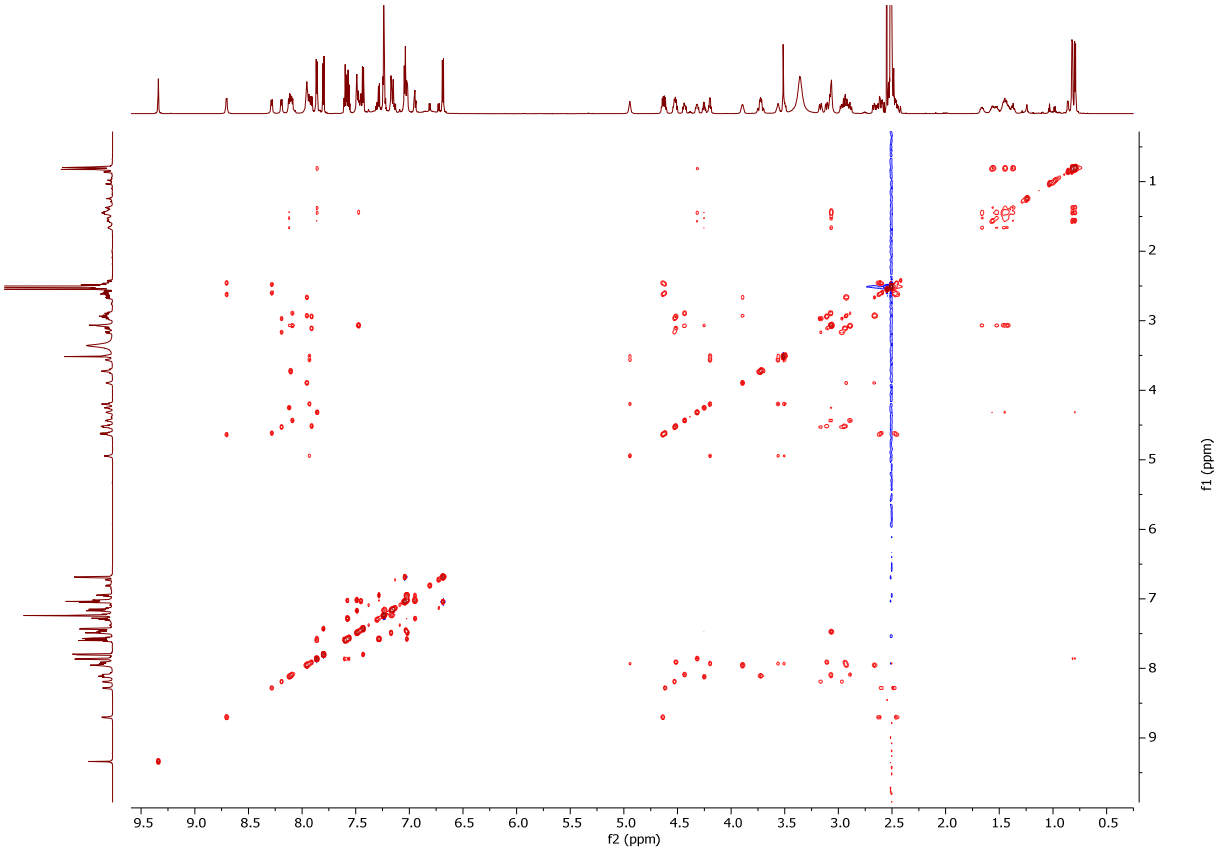

Figure 3.130: ^{1}H, ^{1}H-TOCSY-NMR of **AzoKP-2**.

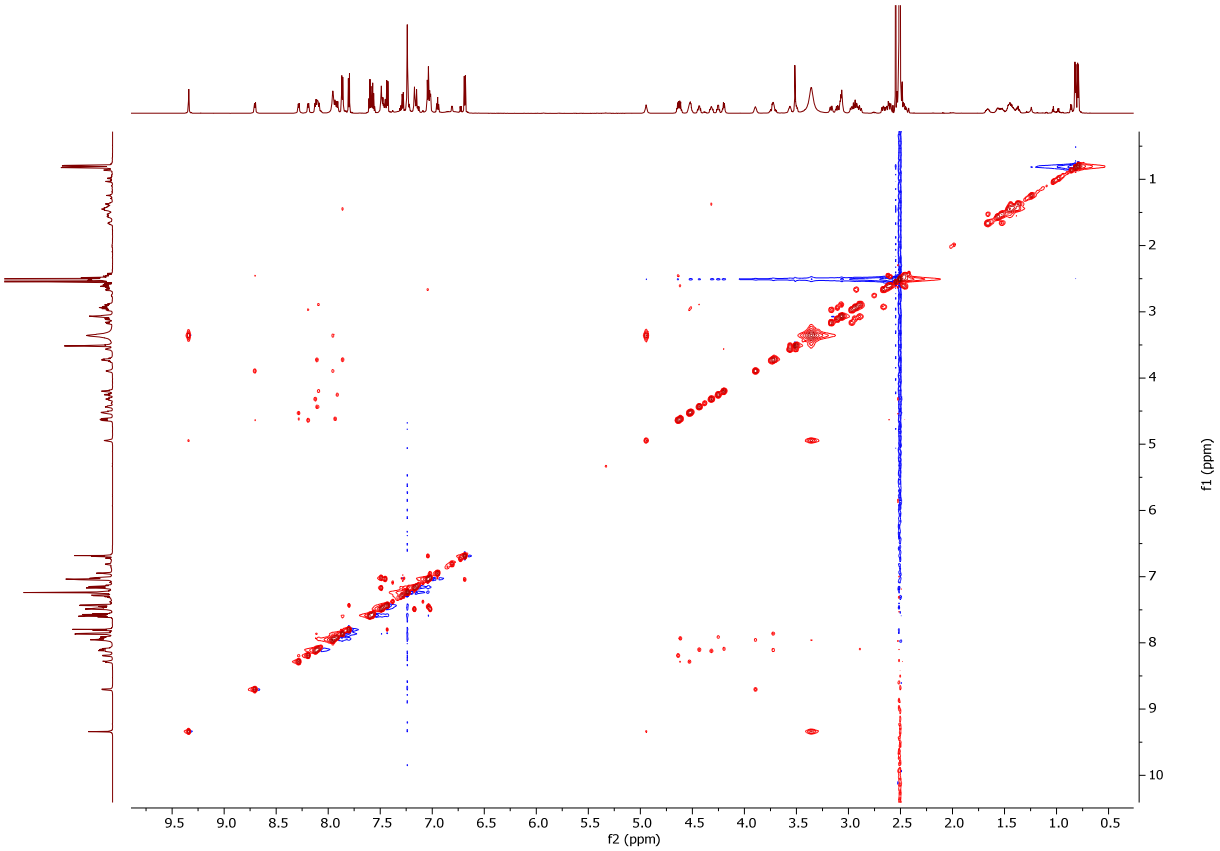

Figure 3.131: ^{1}H, ^{1}H-NOESY-NMR of **AzoKP-2**.

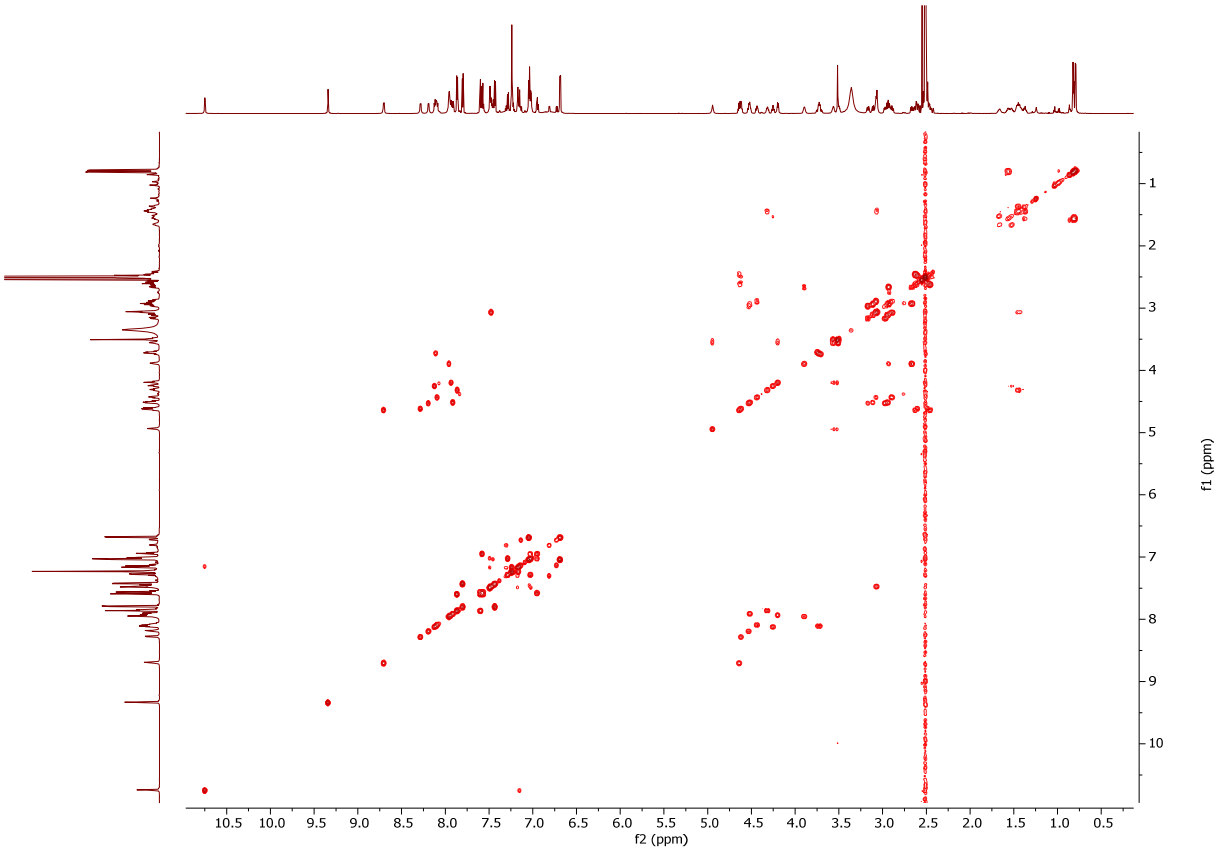

Figure 3.132: ^{1}H, ^{1}H-COSY-NMR of **AzoKP-2**.

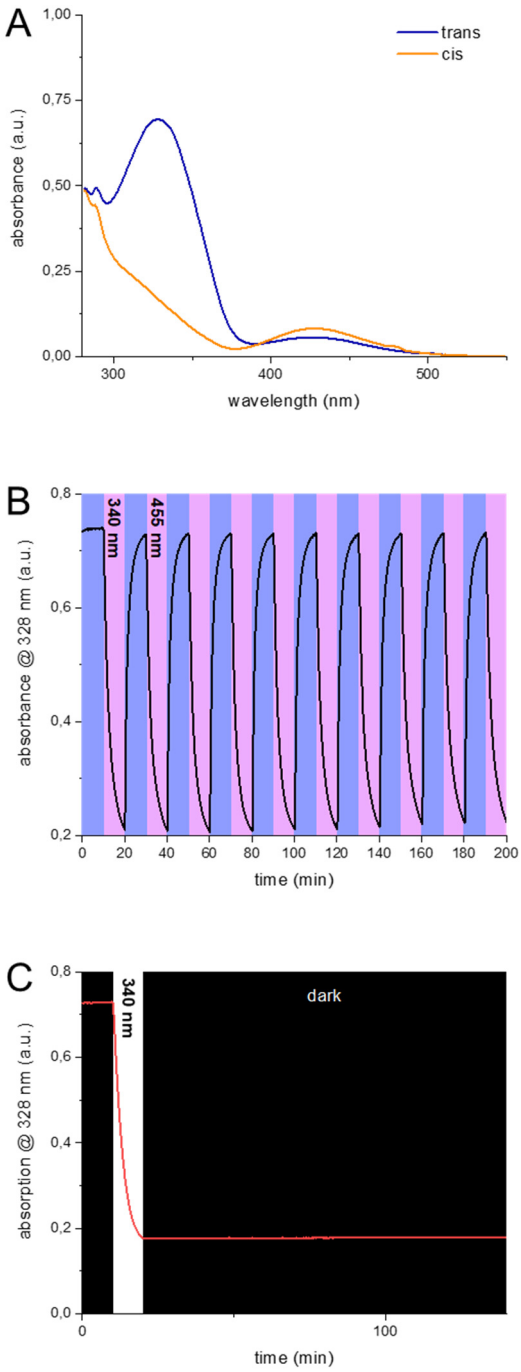

Figure 3.133: A) UV/VIS spectra of trans- and cis-**AzoKP-2**; illumination with 340 nm (trans→cis) and 455 nm (cis→trans). B) Kinetics of **AzoKP-2**. C) Bistability of **AzoKp-2**.

AzoKP-3

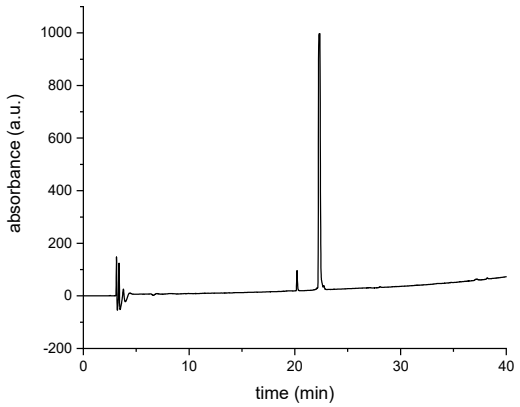

Figure 3.134: Analytical HPLC spectrum of **AzoKP-3** with a water/acetonitrile gradient of 95/5 →20/80 in 40 min. Rf: 20.2 min (cis) and 22.4 min (trans).

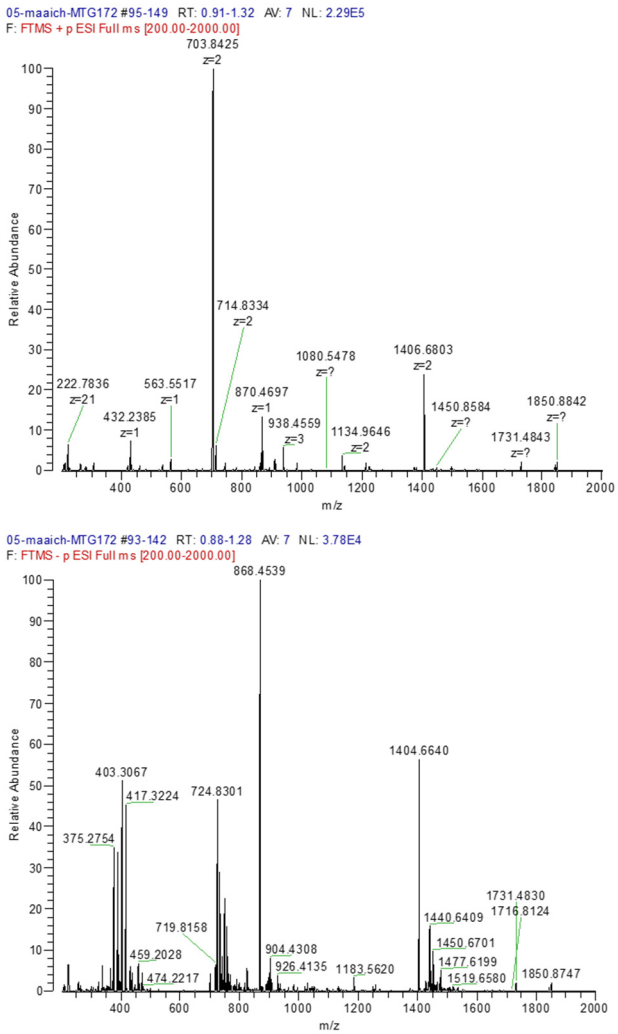

Figure 3.135: HRMS spectrum of **AzoKP-2**: HRMS (+ESI) m/z calc. for $C_{69}H_{89}N_{19}O_{14}$ $[M + 2H]^+$: 703.8413; found: 703.8425. Calc. for $C_{71}H_{86}N_{17}O_{11}$ $[M + H]^+$: 1406.6753; found: 1406.6804. : HRMS (−ESI) m/z calc. for $C_{69}H_{87}N_{19}O_{14}^-$ $[M – H]^-$: 1404.6607; found: 1404.6640.

Table 3.15: Chemical shifts of ^{1}H- and ^{13}C-NMR of **AzoKP-3** in DMSO-$_6$.

residue	^{1}H-NMR	^{13}C-NMR
Tyr	NH 7.97, Hα 3.90, Hβa 2.93, Hβb 2.67, Hδ 7.03, Hε 7.67	Cα 54.1, Cβ 36.9, Cγ , Cδ 125.3, 131.0, Cε 115.8, Cζ 157.0
Asn	NH 8.72, Hα 4.63, Hβa 2.61, Hβb 2.50, Hδa 7.05, Hδb 7.48	Cα 50.2, Cβ 37.6
Trp	NH 8.19, Hα 4.53, Hβa 3.18, Hβb 3.02, Hδ2 7.15, Hε3 7.58, Hζ3 6.94, Hη2 7.03, Hζ2 7.27	Cα 54.3, Cβ 37.3, Cδ2 124.1, Cε3 118.8, Cζ3 118.7, Cη2 121.3, Cζ2 111.7
Asn	NH 8.30, Hα 4.63, Hβa 2.61, Hβb 2.50, Hδ 6.67, Hδa 7.05, Hδb 7.48	Cα 50.2, Cβ 37.6
Ser	NH 8.01, Hα 4.21, Hβa 3.59, Hβb 3.54, Hγ 4.96	Cα 56.2, Cβ 61.7
AzoPhe	NH 8.19, H1 4.53, H2a 3.18, H2b 2.98, H4/8 7.47, H5/7 7.80, H12/16, 7.87, H13/15 7.60, H14 7.57	C1 54.3, C2 27.9, C3 142.4, C4/8 130.8, C5/7 122.9, C6 151.0, C11 152.4, C12/16 122.9, C13/15 129.9, C 14 131.8
Gly	NH 8.18, Hα 3.75	Cα 42.5
Leu	NH 7.89, Hα 4.33, Hβa 1.46, Hβb 1.41, Hγ 1.60, Hδa 0.87, Hδb 0.83	Cα 51.4. Cβ 41.2, Cγ 24.5, Cδa 23.6, Cδb 22.0
Arg	NH 8.10, Hα 4.21, Hβa 1.44, Hβb 1.39, Hγa 1.63, Hγb1.51, Hδ 3.06, Hε7.03,	Cα 52.8, Cβ 25.4, Cγ 29.3, Cδ 40.9
Phe	NH 7.82, Hα 4.43, Hβa 3.01, Hβb 2.82, Hδ 7.21, Hε 7.24, Hζ 7.16	Cα 54.0, Cβ 38.0, Cγ 138.1, Cδ 129.6, Cε 128.5, Cζ 126.7

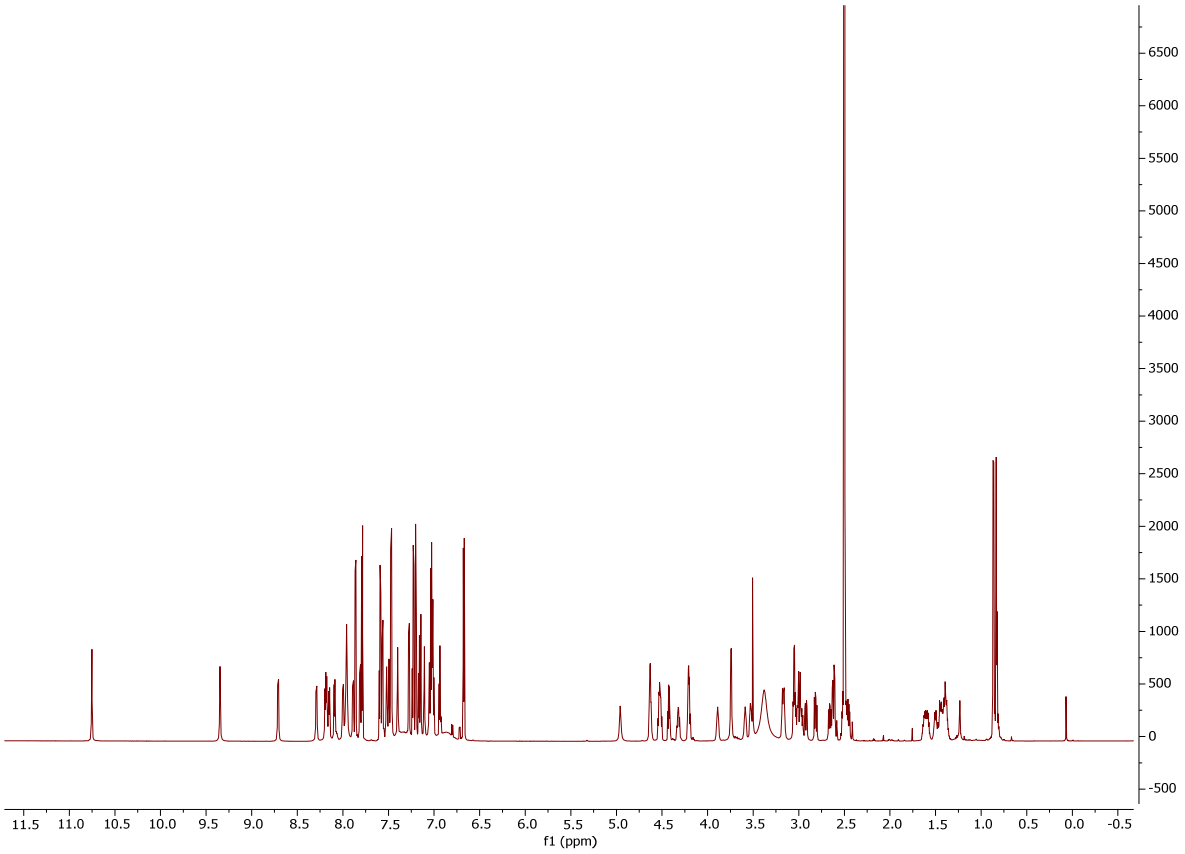

Figure 3.136: ^{1}H-NMR of **AzoKP-3**.

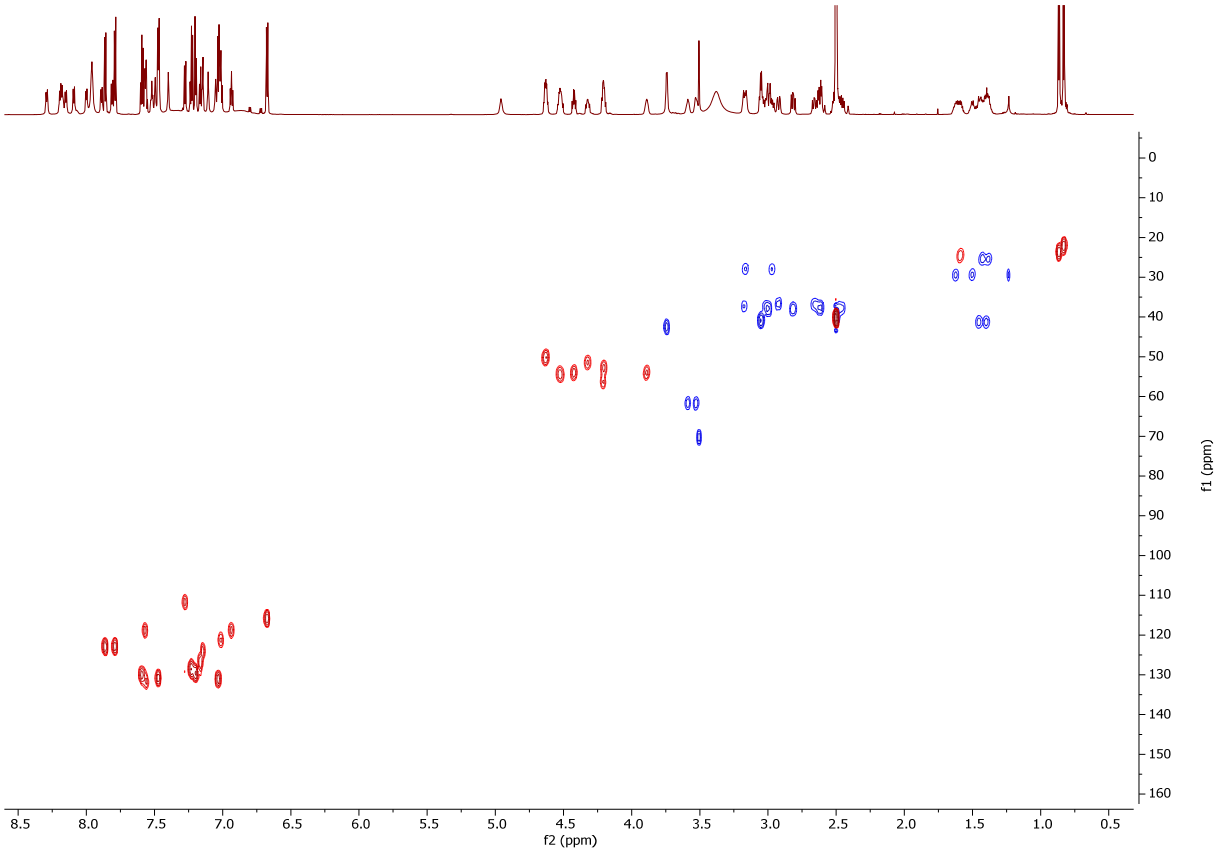

Figure 3.137: ^{1}H, ^{13}C- HSQC-NMR of **AzoKP-3**.

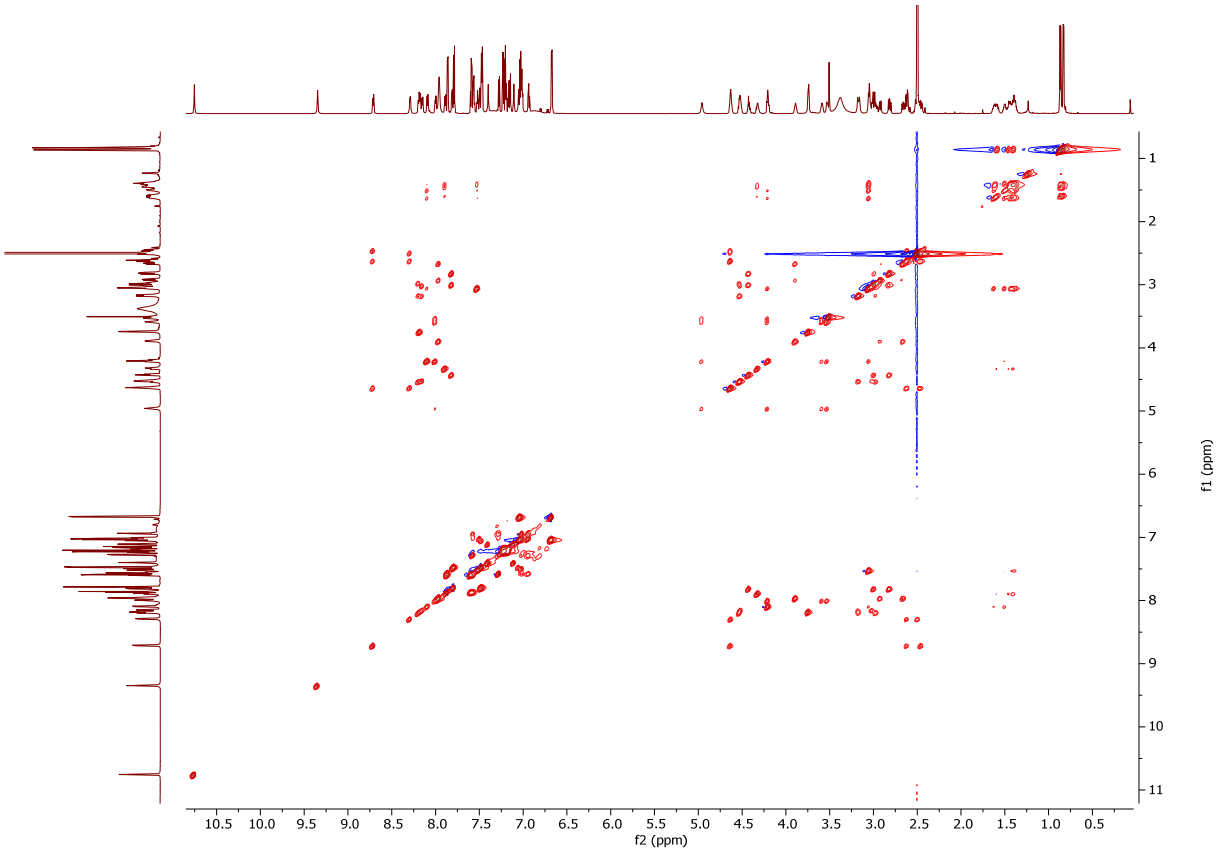

Figure 3.138: ^{1}H, ^{1}H-TOCSY-NMR of **AzoKP-3**.

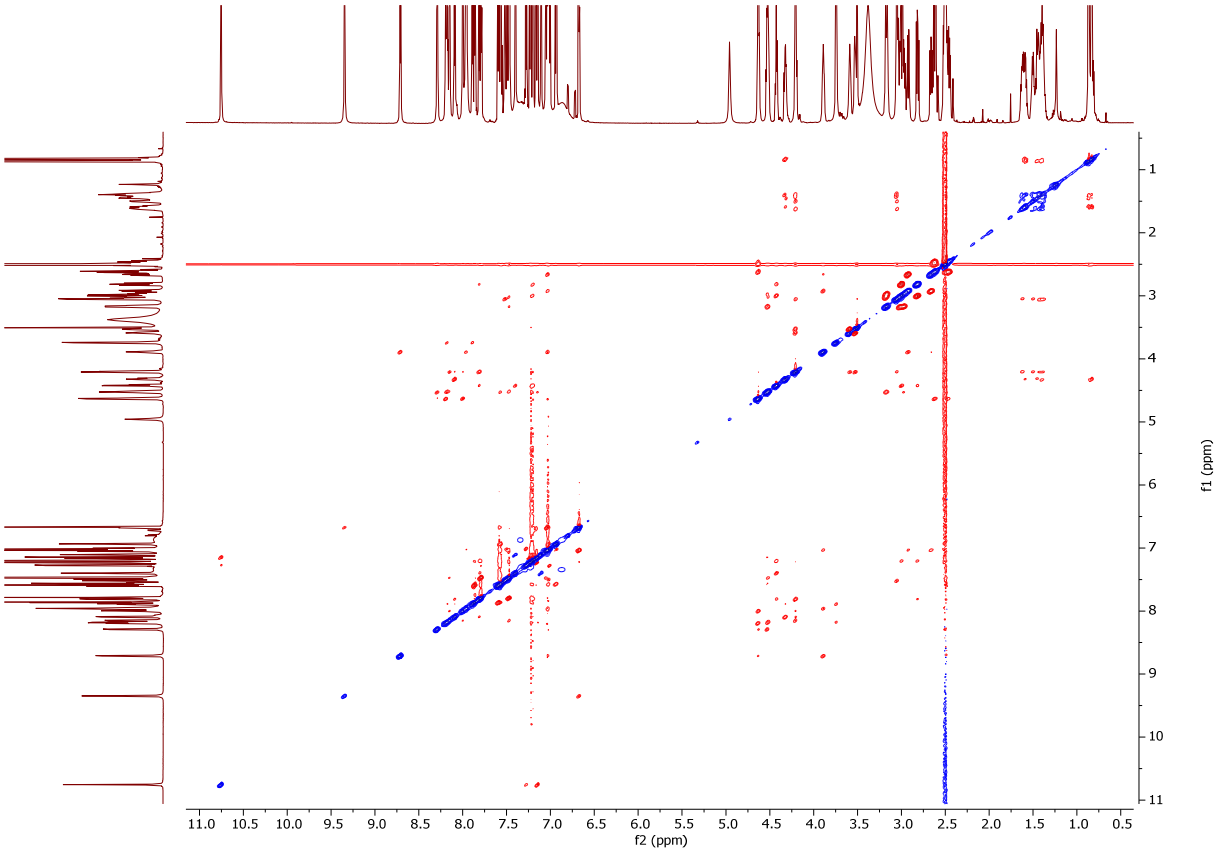

Figure 3.139: ^{1}H, ^{1}H-NOESY-NMR of **AzoKP-3**.

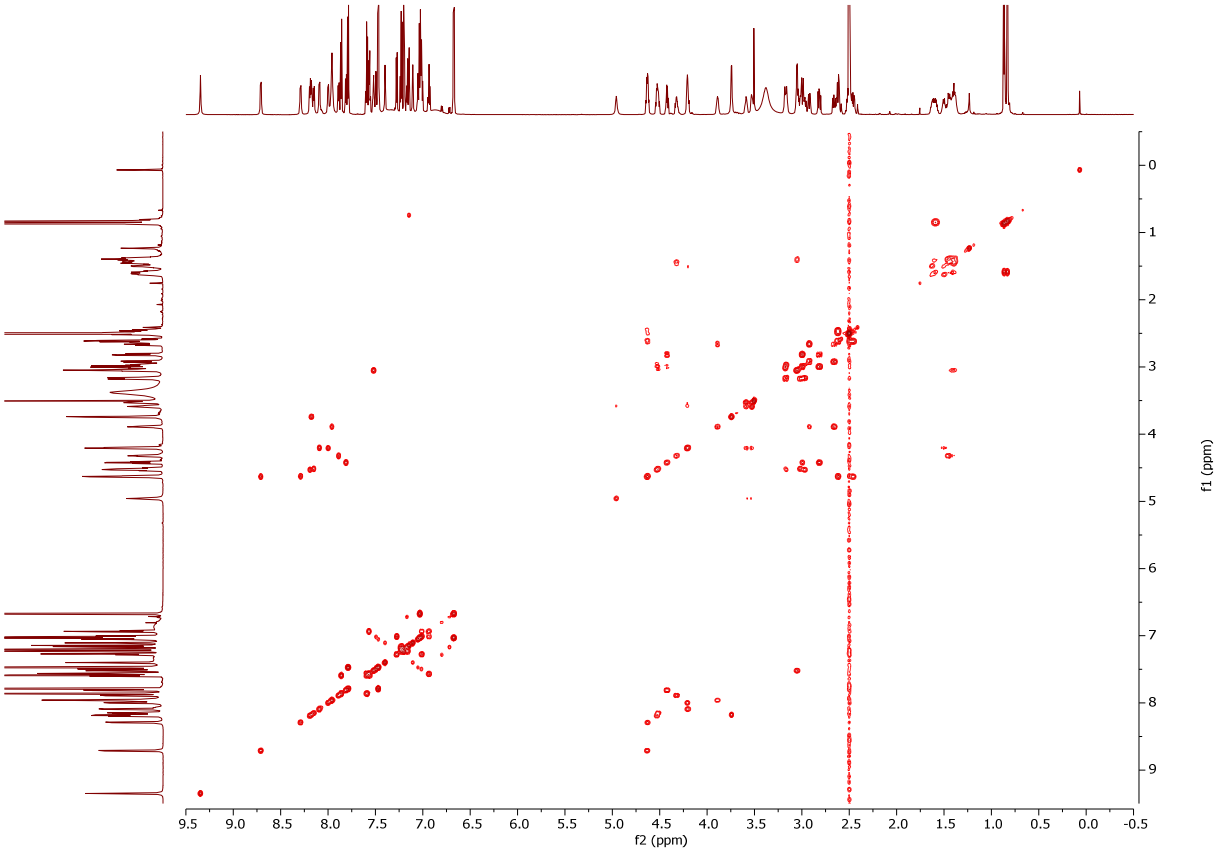

Figure 3.140: ^{1}H, ^{1}H-COSY-NMR of **AzoKP-3**.

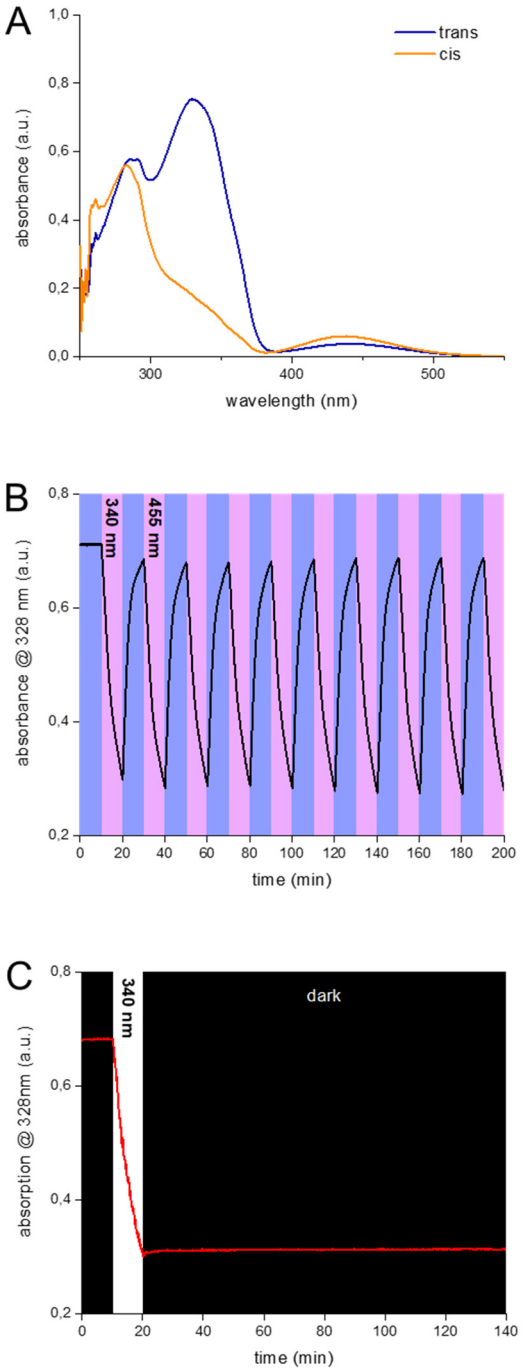

Figure 3.141: A) UV/VIS spectra of trans- and cis-**AzoKP-3**; illumination with 340 nm (trans→cis) and 455 nm (cis→trans). B) Kinetics of **AzoKP-3**. C) Bistability of **AzoKp-3**.

General Remarks

Apparatus and glass ware

Magnetic stirring was used for all reactions and, if necessary, the Schlenk technique was used with oven dried glassware under nitrogen or argon atmosphere.

Chemicals, solutions and compounds

The chemicals and solutions (p.a.) used were either purchased from Sigma-Aldrich (Munich/Germany), ABCR (Karlsruhe/Germany) or VWR (Ismaning/Germany). Compounds and resins for SPPS were purchased from, Orpegen Peptide Chemicals, Rapp Polymere or NovaBiochem. If necessary, solvents were distillied over sodium and benzophenone prior to use.

Flash column chromatography and thin-layer chromatography

Flash chromatography was done on silica gel (grain size 35-70 µm, Acros Organics, Geel/Belgium) with nitrogen pressure. Thin-layer chromatography reaction control was undertaken on aluminium foils (silicagel 60 F254, Merck KGaA, Grafen/Germany). Compounds were detected utilising either fluorescence quenching at λ = 254 nm or by dyeing with *ninhydrin solution* (1.5 g ninhydrin, 15 mL glacial acetic acid and 500 mL methanol) or Seebach-reagent (2.5 g Phosphomolybdic acid, 1.0 g Cerium (IV) sulfate tetrahydrate, 6 mL conc. Sulfuric acid and 94 mL dest. water).

Peptide Synthesizer

Unless otherwise mentioned, peptides were synthesized CEM Liberty Blue Peptide Synthesizer with a CEM Discovery Microwave (CEM GmbH, Kamp-Lintfort/Germany) under standard Fmoc conditions (with or without microwave).

Analytical reversed-phase HPLC

Analytical RP-HPLCs were performed on Jasco (Jasco Germany GmbH, Groß-Umstadt/Germany) devices (HPLC-pump PU-2080 Plus, gradient unit LG-2080-02-S, degasser DG-2080-53 and diode array detector MD-2010 Plus) with a Phenomenex (Aschaffenburg/Germany) Aeris column (C18, 5 µm, 250 x 4.6 mm) for peptides and

Phenomenex Luna column (C18, 5 µm, 250 x 4.6 mm) for all other molecules. As eluent, a water/acetonitrile gradient with 0.1% TFA with a flow of 1 mL/min was used.

Semi-preparative reversed-phase HPLC

Semi-preparative RP-HPLCs was performed on Jasco (Groß-Umstadt/Germany) devices (PU-2087 Plus, LG-2080-02-S and UV/Vis detector UV-2075 Plus) with a Phenomenex (Torrance/USA) Aeris column (XBC18, 5 µm, 250 x 21.2 mm) for peptides and Phenomenex Luna column (XBC18, 5 µm, 250 x 20 mm) for all other molecules. As eluent, a water/acetonitrile gradient with 0.1% TFA and 18-20 mL/min flow was used.

NMR spectroscopy

NMR spectra were recorded on Varian (Darmstadt/Germany) AC 300 (300 MHz), WH 400 (400 MHz) and AMX 600 (600 MHz), as well as on Bruker (Billerica/USA) AV-III (800 MHz) devices. Chemical shifts δ are denoted in ppm based on TMS ($\delta = 0$) as external standard. Deuterated solvents $CDCl_3$, CD_3OD, CD_3OH and DMSO-d_6 were used for all measurements and the residual solvent peaks [δ ($CDCl_3$) = 7.26, δ (CD_3OD) = 3.31 and δ (DMSO-d_6) = 2.50 ppm] were used as internal standard. *J*-coupling constants are given in Hz and the multiplicity is abbreviated as s = singlet, d = doublet, t = triplet, q = quartet and m = multiplet. The analysis of the NMR spectra was carried out with the help of MestReC V14.3.1-31739 (Mestrelab Research, Santiago de Compostela/Spain) software.

Mass spectrometry

The resolution of EI-MS is 1000 u and of HR-EI-MS is 5000 u. Electron spray ionisation (ESI) measurements were performed on a Thermo Finnigan LTQFT (Thermo Fisher Scientific Inc., Waltham/USA) mass spectrometer. The measured values are denoted in m/z.

UV/Vis spectroscopy

UV spectra were recorded on a VARIAN Cary 50 UV/Vis spectrometer. Compunds stirred in phosphate buffer (10 mM pH 7.5) and 1% dmso were illuminated in Quartz cuvettes (d = 1 cm) by a light fiber cable from above.

CD spectroscopy

CD measurements were done on a Jasco 810 CD spectrometer with a Jasco CDF-4265 Peltier-Element (Jasco Germany GmbH, Groß-Umstadt/Germany) and phosphate buffer (10 mM, pH 7.5) and trifluoroethanol (80:20) and 1 mm cuvettes. Recorded spectra were evaluated with the software Origin 2018 (OriginLab Corporation, Northampton/USA) and smoothed with a 20-point Savitzky-Golay[365] filter and secondary structure prediction was done with BeStSeL (Beta Structure Selection, BeStSel™ (2014-2024) – ELTE Eötvös Loránd University, Budapest, Hungary)[366-368].

References

[1] T. Podewin, J. Ast, J. Broichhagen, N. H. F. Fine, D. Nasteska, P. Leippe, M. Gailer, T. Buenaventura, N. Kanda, B. J. Jones, C. M'Kadmi, J.-L. Baneres, J. Marie, A. Tomas, D. Trauner, A. Hoffmann-Röder, D. J. Hodson; Conditional and Reversible Activation of Class A and B G Protein-Coupled Receptors Using Tethered Pharmacology, *ACS Central Science*, **2018**, *4*, 166-179.

[2] S. M. Hofmann, C. V. Frost, T. Podewin, M. Gailer, E. Weber, M. Zacharias, W. Zinth, A. Hoffmann-Röder; Folding and Unfolding of the Short Light-Triggered β-Hairpin Peptide AzoChignolin Occurs within 100 ns, *The Journal of Physical Chemistry B*, **2020**, *124*, 5113-5121.

[3] S. Gutenthaler, S. Tsushima, R. Steudtner, M. Gailer, A. Hoffmann-Röder, B. Drobot, L. Daumann; Lanmodulin peptides – unravelling the binding of the EF-Hand loop sequences stripped from the structural corset, *Inorganic Chemistry Frontiers*, **2022**, *9*, 4009-4021.

[4] X. Jing, H. Liang, C. Hao, X. Yang, X. Cui; Overexpression of MUC1 predicts poor prognosis in patients with breast cancer, *Oncology Reports*, **2019**, *41*, 801-810.

[5] M. N. Christiansen, J. Chik, L. Lee, M. Anugraham, J. L. Abrahams, N. H. Packer; Cell surface protein glycosylation in cancer, *Proteomics*, **2014**, *14*, 525-546.

[6] M. A. Hollingsworth, B. J. Swanson; Mucins in cancer: protection and control of the cell surface, *Nature Reviews Cancer*, **2004**, *4*, 45-60.

[7] N. Gaidzik, U. Westerlind, H. Kunz; The development of synthetic antitumour vaccines from mucin glycopeptide antigens, *Chemical Society Reviews*, **2013**, *42*, 4421-4442.

[8] E. Kobayashi, K. Motoki, T. Uchida, H. Fukushima, Y. Koezuka; KRN7000, a novel immunomodulator, and its antitumor activities, *Oncology Research*, **1995**, *7*, 529-534.

[9] S. Mahadevan, C. J. Dillard, A. L. Tappel; Degradation of polysaccharides, mucopolysaccharides, and glycoproteins by lysosomal glycosidases, *Archives of Biochemistry and Biophysics*, **1969**, *129*, 525-533.

[10] J. Vagner, H. Qu, V. J. Hruby; Peptidomimetics, a synthetic tool of drug discovery, *Current Opinion in Chemical Biology*, **2008**, *12*, 292-296.

[11] Y. Niu, Y. Hu, X. Li, J. Chen, J. Cai; γ-AApeptides: design, synthesis and evaluation, *New Journal of Chemistry*, **2011**, *35*, 542-545.

[12] M. Gailer; master's thesis thesis, Ludwig-Maximilians Universität München **2015**.

[13] A. A. Beharry, G. A. Woolley; Azobenzene photoswitches for biomolecules, *Chemical Society Reviews*, **2011**, *40*, 4422-4437.

[14] J. Broichhagen, J. A. Frank, D. Trauner; A Roadmap to Success in Photopharmacology, *Accounts of Chemical Research*, **2015**, *48*, 1947-1960.

[15] L. Albert, O. Vázquez; Photoswitchable peptides for spatiotemporal control of biological functions, *Chemical Communications*, **2019**, *55*, 10192-10213.

[16] J. J. Ferreira, A. Butler, R. Stewart, A. L. Gonzalez-Cota, P. Lybaert, C. Amazu, E. L. Reinl, M. Wakle-Prabagaran, L. Salkoff, S. K. England, C. M. Santi; Oxytocin can regulate myometrial smooth muscle excitability by inhibiting the Na+-activated K+ channel, Slo2.1, *The Journal of Physiology*, **2019**, *597*, 137-149.

[17] C. Jones, I. Barrera, S. Brothers, R. Ring, C. Wahlestedt; Oxytocin and social functioning, *Dialogues in clinical neuroscience*, **2017**, *19*, 193-201.

[18] O. Keller, J. Rudinger; Synthesis of [1, 6-α, α′-Diaminosuberic acid]oxytocin ('Dicarba-oxytocin'), *Helvetica Chimica Acta*, **1974**, *57*, 1253-1259.

[19] N. Cort, S. Einarsson, D. Schams, H. Vilhardt; Blood concentrations of oxytocin equivalents after single injections of deamino-1-monocarba-[2-O-methyltyrosine]-oxytocin in lactating sows, *American Journal of Veterinary Research*, **1981**, *42*, 1804-1806.

[20] I. Passoni, M. Leonzino, V. Gigliucci, B. Chini, M. Busnelli; Carbetocin is a Functional Selective Gq Agonist That Does Not Promote Oxytocin Receptor Recycling After Inducing β-Arrestin-Independent Internalisation, *Journal of Neuroendocrinology*, **2016**, *28*, https://doi.org/10.1111/jne.12363.

[21] M. C. Frantz, L. P. Pellissier, E. Pflimlin, S. Loison, J. Gandia, C. Marsol, T. Durroux, B. Mouillac, J. A. J. Becker, J. Le Merrer, C. Valencia, P. Villa, D. Bonnet, M. Hibert; LIT-001, the First Nonpeptide Oxytocin Receptor Agonist that Improves Social Interaction in a Mouse Model of Autism, *Journal of Medicinal Chemistry*, **2018**, *61*, 8670-8692.
[22] J. H. Lee, M. E. Miele, D. J. Hicks, K. K. Phillips, J. M. Trent, B. E. Weissman, D. R. Welch; KiSS-1, a novel human malignant melanoma metastasis-suppressor gene, *Journal of the National Cancer Institute*, **1996**, *88*, 1731-1737.
[23] T. M. Plant; Neurophysiology of puberty, *Journal of Adolescent Health*, **2002**, *31*, 185-191.
[24] N. de Roux, E. Genin, J.-C. Carel, F. Matsuda, J.-L. Chaussain, E. Milgrom; Hypogonadotropic hypogonadism due to loss of function of the KiSS1-derived peptide receptor GPR54, *Proceedings of the National Academy of Sciences*, **2003**, *100*, 10972-10976.
[25] S. B. Seminara, S. Messager, E. E. Chatzidaki, R. R. Thresher, J. S. Acierno, J. K. Shagoury, Y. Bo-Abbas, W. Kuohung, K. M. Schwinof, A. G. Hendrick, D. Zahn, J. Dixon, U. B. Kaiser, S. A. Slaugenhaupt, J. F. Gusella, S. O'Rahilly, M. B. L. Carlton, W. F. Crowley, S. A. J. R. Aparicio, W. H. Colledge; The GPR54 Gene as a Regulator of Puberty, *New England Journal of Medicine*, **2003**, *349*, 1614-1627.
[26] K.-L. Hu, H. Zhao, H.-M. Chang, Y. Yu, J. Qiao; Kisspeptin/Kisspeptin Receptor System in the Ovary, *Frontiers in Endocrinology*, **2018**, *8*, 365.
[27] M. J. Orsini, M. A. Klein, M. P. Beavers, P. J. Connolly, S. A. Middleton, K. H. Mayo; Metastin (KiSS-1) Mimetics Identified from Peptide Structure−Activity Relationship-Derived Pharmacophores and Directed Small Molecule Database Screening, *Journal of Medicinal Chemistry*, **2007**, *50*, 462-471.
[28] L. Wang, N. Wang, W. Zhang, X. Cheng, Z. Yan, G. Shao, X. Wang, R. Wang, C. Fu; Therapeutic peptides: current applications and future directions, *Signal Transduction and Targeted Therapy*, **2022**, *7*, 48.
[29] S. Marqus, E. Pirogova, T. J. Piva; Evaluation of the use of therapeutic peptides for cancer treatment, *Journal of Biomedical Science*, **2017**, *24*, 21.
[30] V. Erckes, C. Steuer; A story of peptides, lipophilicity and chromatography – back and forth in time, *RSC Medicinal Chemistry*, **2022**, *13*, 676-687.
[31] J. M. Collins, K. A. Porter, S. K. Singh, G. S. Vanier; High-Efficiency Solid Phase Peptide Synthesis (HE-SPPS), *Organic Letters*, **2014**, *16*, 940-943.
[32] A. Pech, J. Achenbach, M. Jahnz, S. Schülzchen, F. Jarosch, F. Bordusa, S. Klussmann; A thermostable d-polymerase for mirror-image PCR, *Nucleic Acids Research*, **2017**, *45*, 3997-4005.
[33] W. Xu, W. Jiang, J. Wang, L. Yu, J. Chen, X. Liu, L. Liu, T. F. Zhu; Total chemical synthesis of a thermostable enzyme capable of polymerase chain reaction, *Cell Discovery*, **2017**, *3*, 17008.
[34] V. du Vigneaud, C. Ressler, J. M. Swan, C. W. Roberts, P. G. Katsoyannis; The Synthesis of Oxytocin1, *Journal of the American Chemical Society*, **1954**, *76*, 3115-3121.
[35] A. Belgi, M. Akhter Hossain, G. W. Tregear, J. D. Wade; The Chemical Synthesis of Insulin: From the Past to the Present, *Immunology, Endocrine & Metabolic Agents in Medicinal Chemistry (Discontinued)*, **2011**, *11*, 40-47.
[36] E. Fischer, E. Fourneau; Ueber einige Derivate des Glykocolls, *Berichte der deutschen chemischen Gesellschaft*, **1901**, *34*, 2868-2877.
[37] E. Fischer, E. Koenigs; Synthese von Polypeptiden. XVIII. Derivate der Asparaginsäure, *Berichte der deutschen chemischen Gesellschaft*, **1907**, *40*, 2048-2061.
[38] M. Bergmann, L. Zervas; Über ein allgemeines Verfahren der Peptid-Synthese, *Berichte der deutschen chemischen Gesellschaft (A and B Series)*, **1932**, *65*, 1192-1201.
[39] F. C. McKay, N. F. Albertson; New Amine-masking Groups for Peptide Synthesis, *Journal of the American Chemical Society*, **1957**, *79*, 4686-4690.
[40] R. B. Merrifield; Solid Phase Peptide Synthesis. I. The Synthesis of a Tetrapeptide, *Journal of the American Chemical Society*, **1963**, *85*, 2149-2154.
[41] R. B. Merrifield; Solid-Phase Peptide Synthesis. III. An Improved Synthesis of Bradykinin*, *Biochemistry*, **1964**, *3*, 1385-1390.
[42] L. A. Carpino, G. Y. Han; 9-Fluorenylmethoxycarbonyl function, a new base-sensitive amino-protecting group, *Journal of the American Chemical Society*, **1970**, *92*, 5748-5749.

[43] M. Amblard, J.-A. Fehrentz, J. Martinez, G. Subra; Methods and protocols of modern solid phase peptide synthesis, *Molecular Biotechnology*, **2006**, *33*, 239-254.
[44] W. Chan, P. White; *Fmoc Solid Phase Peptide Synthesis: A Practical Approach*, Oxford University Press, **1999**.
[45] J. M. Palomo; Solid-phase peptide synthesis: an overview focused on the preparation of biologically relevant peptides, *RSC Advances*, **2014**, *4*, 32658-32672.
[46] V. Mäde, S. Els-Heindl, A. G. Beck-Sickinger; Automated solid-phase peptide synthesis to obtain therapeutic peptides, *Beilstein Journal of Organic Chemistry*, **2014**, *10*, 1197-1212.
[47] B. Yan, J. B. Fell, G. Kumaravel; Progression of Organic Reactions on Resin Supports Monitored by Single Bead FTIR Microspectroscopy, *The Journal of Organic Chemistry*, **1996**, *61*, 7467-7472.
[48] P. T. Shelton, K. J. Jensen; in *Peptide Synthesis and Applications* (Eds.: K. J. Jensen, P. Tofteng Shelton, S. L. Pedersen), Humana Press, Totowa, NJ, **2013**, pp. 23-41.
[49] S.-S. Wang; p-Alkoxybenzyl Alcohol Resin and p-Alkoxybenzyloxycarbonylhydrazide Resin for Solid Phase Synthesis of Protected Peptide Fragments, *Journal of the American Chemical Society*, **1973**, *95*, 1328-1333.
[50] Y. Yang, L. Hansen; Optimized Fmoc-Removal Strategy to Suppress the Traceless and Conventional Diketopiperazine Formation in Solid-Phase Peptide Synthesis, *ACS Omega*, **2022**, *7*, 12015-12020.
[51] K. Barlos, O. Chatzi, D. Gatos, G. Stavropoulos; 2-Chlorotrityl Chloride Resin—Studies on Anchoring of Fmoc-Amino Acids and Peptide Cleavage, *International Journal of Peptide and Protein Research*, **1991**, *37*, 513-520.
[52] D. s. M. M. Jaradat; Thirteen decades of peptide synthesis: key developments in solid phase peptide synthesis and amide bond formation utilized in peptide ligation, *Amino Acids*, **2018**, *50*, 39-68.
[53] K.-H. Kim, B. L. Seong; Peptide amidation: Production of peptide hormonesin vivo andin vitro, *Biotechnology and Bioprocess Engineering*, **2001**, *6*, 244-251.
[54] G. Barany, F. Albericio; Three-dimensional orthogonal protection scheme for solid-phase peptide synthesis under mild conditions, *Journal of the American Chemical Society*, **1985**, *107*, 4936-4942.
[55] G. Barany, R. B. Merrifield; A new amino protecting group removable by reduction. Chemistry of the dithiasuccinoyl (Dts) function, *Journal of the American Chemical Society*, **1977**, *99*, 7363-7365.
[56] R. Behrendt, P. White, J. Offer; Advances in Fmoc solid-phase peptide synthesis, *Journal of Peptide Science*, **2016**, *22*, 4-27.
[57] F. A. Paul Lloyd-Williams, Ernest Giralt; *Chemical Approaches to the Synthesis of Peptides and Proteins*, CRC Press, Boca Raton, **1997**.
[58] A. Isidro-Llobet, M. Álvarez, F. Albericio; Amino Acid-Protecting Groups, *Chemical Reviews*, **2009**, *109*, 2455-2504.
[59] J. R. Dunetz, J. Magano, G. A. Weisenburger; Large-Scale Applications of Amide Coupling Reagents for the Synthesis of Pharmaceuticals, *Organic Process Research & Development*, **2016**, *20*, 140-177.
[60] L. De Rosa, A. Russomanno, A. Romanelli, L. D. Andrea; Semi-Synthesis of Labeled Proteins for Spectroscopic Applications, *Molecules*, **2013**, *18*, 440-465.
[61] F. Albericio, A. El-Faham; Choosing the Right Coupling Reagent for Peptides: A Twenty-Five-Year Journey, *Organic Process Research & Development*, **2018**, *22*, 760-772.
[62] J. C. Sheehan, G. P. Hess; A New Method of Forming Peptide Bonds, *Journal of the American Chemical Society*, **1955**, *77*, 1067-1068.
[63] J. Sheehan, P. Cruickshank, G. Boshart; Notes- A Convenient Synthesis of Water-Soluble Carbodiimides, *The Journal of Organic Chemistry*, **1961**, *26*, 2525-2528.
[64] R. Subirós-Funosas, R. Prohens, R. Barbas, A. El-Faham, F. Albericio; Oxyma: An Efficient Additive for Peptide Synthesis to Replace the Benzotriazole-Based HOBt and HOAt with a Lower Risk of Explosion[1], *Chemistry – A European Journal*, **2009**, *15*, 9394-9403.

[65] V. Dourtoglou, B. Gross, V. Lambropoulou, C. Zioudrou; O-Benzotriazolyl-N,N,N′,N′-tetramethyluronium Hexafluorophosphate as Coupling Reagent for the Synthesis of Peptides of Biological Interest, *Synthesis*, **1984**, *1984*, 572-574.
[66] L. A. Carpino; 1-Hydroxy-7-azabenzotriazole. An efficient peptide coupling additive, *Journal of the American Chemical Society*, **1993**, *115*, 4397-4398.
[67] L. A. Carpino, A. El-Faham, F. Albericio; Racemization studies during solid-phase peptide synthesis using azabenzotriazole-based coupling reagents, *Tetrahedron Letters*, **1994**, *35*, 2279-2282.
[68] F. Albericio, J. M. Bofill, A. El-Faham, S. A. Kates; Use of Onium Salt-Based Coupling Reagents in Peptide Synthesis1, *The Journal of Organic Chemistry*, **1998**, *63*, 9678-9683.
[69] L. A. Carpino, H. Imazumi, B. M. Foxman, M. J. Vela, P. Henklein, A. El-Faham, J. Klose, M. Bienert; Comparison of the Effects of 5- and 6-HOAt on Model Peptide Coupling Reactions Relative to the Cases for the 4- and 7-Isomers, *Organic Letters*, **2000**, *2*, 2253-2256.
[70] A. El-Faham, F. Albericio; Peptide Coupling Reagents, More than a Letter Soup, *Chemical Reviews*, **2011**, *111*, 6557-6602.
[71] T. F. Scientific; Cleavage, Deprotection, and Isolation of Peptides after Fmoc Synthesis, Technical Bulletin, 1998527, https://www.google.com/url?sa=t&source=web&rct=j&opi=89978449&url=https://tools.thermofisher.com/content/sfs/brochures/cms_040654.pdf&ved=2ahUKEwi6-Z2anL-FAxWh_7sIHcJXDksQFnoECA8QAQ&usg=AOvVaw1goqzo6NzWNUt-ScNvSOJr.
[72] M. Kojima, H. Hosoda, Y. Date, M. Nakazato, H. Matsuo, K. Kangawa; Ghrelin is a growth-hormone-releasing acylated peptide from stomach, *Nature*, **1999**, *402*, 656-660.
[73] C. Delporte; Structure and physiological actions of ghrelin, *Scientifica (Cairo)*, **2013**, *2013*, 518909-518943.
[74] J. Yang, M. S. Brown, G. Liang, N. V. Grishin, J. L. Goldstein; Identification of the acyltransferase that octanoylates ghrelin, an appetite-stimulating peptide hormone, *Cell*, **2008**, *132*, 387-396.
[75] J. A. Gutierrez, P. J. Solenberg, D. R. Perkins, J. A. Willency, M. D. Knierman, Z. Jin, D. R. Witcher, S. Luo, J. E. Onyia, J. E. Hale; Ghrelin octanoylation mediated by an orphan lipid transferase, *Proceedings of the National Academy of Sciences, USA*, **2008**, *105*, 6320-6325.
[76] X. Zhu, Y. Cao, K. Voogd, D. F. Steiner; On the processing of proghrelin to ghrelin, *Journal of Biological Chemistry*, **2006**, *281*, 38867-38870.
[77] M. A. Cowley, R. G. Smith, S. Diano, M. Tschöp, N. Pronchuk, K. L. Grove, C. J. Strasburger, M. Bidlingmaier, M. Esterman, M. L. Heiman, L. M. Garcia-Segura, E. A. Nillni, P. Mendez, M. J. Low, P. Sotonyi, J. M. Friedman, H. Liu, S. Pinto, W. F. Colmers, R. D. Cone, T. L. Horvath; The Distribution and Mechanism of Action of Ghrelin in the CNS Demonstrates a Novel Hypothalamic Circuit Regulating Energy Homeostasis, *Neuron*, **2003**, *37*, 649-661.
[78] Y. Masuda, T. Tanaka, N. Inomata, N. Ohnuma, S. Tanaka, Z. Itoh, H. Hosoda, M. Kojima, K. Kangawa; Ghrelin Stimulates Gastric Acid Secretion and Motility in Rats, *Biochemical and Biophysical Research Communications*, **2000**, *276*, 905-908.
[79] J. C. Weikel, A. Wichniak, M. Ising, H. Brunner, E. Friess, K. Held, S. Mathias, D. A. Schmid, M. Uhr, A. Steiger; Ghrelin promotes slow-wave sleep in humans, *American Journal of Physiology-Endocrinology and Metabolism*, **2003**, *284*, E407-E415.
[80] T. R. Davis, M. R. Pierce, S. X. Novak, J. L. Hougland; Ghrelin octanoylation by ghrelin O-acyltransferase: protein acylation impacting metabolic and neuroendocrine signalling, *Open biology*, **2021**, *11*, 210080.
[81] J. Lukszo, D. Patterson, F. Albericio, S. A. Kates; 3-(1-Piperidinyl)alanine formation during the preparation of C-terminal cysteine peptides with the Fmoc/t-Bu strategy, *Letters in Peptide Science*, **1996**, *3*, 157-166.
[82] C. Wu, X. Fu, S. Li; New simple and recyclable O-acylation serine derivatives as highly enantioselective catalysts for the large-scale asymmetric direct aldol reactions in the presence of water, *Tetrahedron*, **2011**, *67*, 4283-4290.
[83] A. Paquet; Introduction of 9-fluorenylmethyloxycarbonyl, trichloroethoxycarbonyl, and benzyloxycarbonyl amine protecting groups into O-unprotected hydroxyamino acids using succinimidyl carbonates, *Canadian Journal of Chemistry*, **1982**, *60*, 976-980.

[84] A. K. Tickler, J. D. Wade; Overview of Solid Phase Synthesis of "Difficult Peptide" Sequences, *Current Protocols in Protein Science*, **2007**, *50*, 18.18.11-18.18.16.
[85] M. Muttenthaler, G. F. King, D. J. Adams, P. F. Alewood; Trends in peptide drug discovery, *Nature Reviews Drug Discovery*, **2021**, *20*, 309-325.
[86] D. Zane, P. L. Feldman, T. Sawyer, Z. Sobol, J. Hawes; Development and Regulatory Challenges for Peptide Therapeutics, *International Journal of Toxicology*, **2021**, *40*, 108-124.
[87] P. Vlieghe, V. Lisowski, J. Martinez, M. Khrestchatisky; Synthetic therapeutic peptides: science and market, *Drug Discovery Today*, **2010**, *15*, 40-56.
[88] E. Lenci, A. Trabocchi; Peptidomimetic toolbox for drug discovery, *Chemical Society Reviews*, **2020**, *49*, 3262-3277.
[89] M. Pelay-Gimeno, A. Glas, O. Koch, T. N. Grossmann; Structure-Based Design of Inhibitors of Protein–Protein Interactions: Mimicking Peptide Binding Epitopes, *Angewandte Chemie International Edition*, **2015**, *54*, 8896-8927.
[90] A. S. Ripka, D. H. Rich; Peptidomimetic design, *Current Opinion in Chemical Biology*, **1998**, *2*, 441-452.
[91] H.-J. Lee, J.-W. Song, Y.-S. Choi, H.-M. Park, K.-B. Lee; A Theoretical Study of Conformational Properties of N-Methyl Azapeptide Derivatives, *Journal of the American Chemical Society*, **2002**, *124*, 11881-11893.
[92] T. L. Graybill, M. J. Ross, B. R. Gauvin, J. S. Gregory, A. L. Harris, M. A. Ator, J. M. Rinker, R. E. Dolle; Synthesis and evaluation of azapeptide-derived inhibitors of serine and cysteine proteases, *Bioorganic & Medicinal Chemistry Letters*, **1992**, *2*, 1375-1380.
[93] J. J. Perez; Designing Peptidomimetics, *Current Topics in Medicinal Chemistry*, **2018**, *18*, 566-590.
[94] X. Li, Y.-D. Wu, D. Yang; α-Aminoxy Acids: New Possibilities from Foldamers to Anion Receptors and Channels, *Accounts of Chemical Research*, **2008**, *41*, 1428-1438.
[95] D. Yang, J. Qu, B. Li, F.-F. Ng, X.-C. Wang, K.-K. Cheung, D.-P. Wang, Y.-D. Wu; Novel Turns and Helices in Peptides of Chiral α-Aminoxy Acids, *Journal of the American Chemical Society*, **1999**, *121*, 589-590.
[96] D. Yang, B. Li, F.-F. Ng, Y.-L. Yan, J. Qu, Y.-D. Wu; Synthesis and Characterization of Chiral N−O Turns Induced by α-Aminoxy Acids, *The Journal of Organic Chemistry*, **2001**, *66*, 7303-7312.
[97] X. Li, D. Yang; Peptides of aminoxy acids as foldamers, *Chemical Communications*, **2006**, 3367-3379.
[98] A. S. Dutta, J. S. Morley; Polypeptides. Part XIII. Preparation of α-aza-amino-acid (carbazic acid) derivatives and intermediates for the preparation of α-aza-peptides, *Journal of the Chemical Society, Perkin Transactions 1*, **1975**, 1712-1720.
[99] I. Avan, C. D. Hall, A. R. Katritzky; Peptidomimetics via modifications of amino acids and peptide bonds, *Chemical Society Reviews*, **2014**, *43*, 3575-3594.
[100] H.-J. Lee, H. J. Jung, J. H. Kim, H.-M. Park, K.-B. Lee; Conformational preference of azaglycine-containing dipeptides studied by PCM and IPCM methods, *Chemical Physics*, **2003**, *294*, 201-210.
[101] R. E. Melendez, W. D. Lubell; Aza-Amino Acid Scan for Rapid Identification of Secondary Structure Based on the Application of N-Boc-Aza1-Dipeptides in Peptide Synthesis, *Journal of the American Chemical Society*, **2004**, *126*, 6759-6764.
[102] D. Boeglin, W. D. Lubell; Aza-Amino Acid Scanning of Secondary Structure Suited for Solid-Phase Peptide Synthesis with Fmoc Chemistry and Aza-Amino Acids with Heteroatomic Side Chains, *Journal of Combinatorial Chemistry*, **2005**, *7*, 864-878.
[103] D. Seebach, P. E. Ciceri, M. Overhand, B. Jaun, D. Rigo, L. Oberer, U. Hommel, R. Amstutz, H. Widmer; Probing the Helical Secondary Structure of Short-Chain β-Peptides, *Helvetica Chimica Acta*, **1996**, *79*, 2043-2066.
[104] R. P. Cheng, S. H. Gellman, W. F. DeGrado; β-Peptides: From Structure to Function, *Chemical Reviews*, **2001**, *101*, 3219-3232.
[105] J. A. Kritzer, O. M. Stephens, D. A. Guarracino, S. K. Reznik, A. Schepartz; β-Peptides as inhibitors of protein–protein interactions, *Bioorganic & medicinal chemistry*, **2005**, *13*, 11-16.

[106] K. Gademann, T. Hintermann, J. V. Schreiber; Beta-peptides: twisting and turning, *Current medicinal chemistry*, **1999**, *6*, 905-925.
[107] F. Karch, A. Hoffmann-Röder; Synthesis of glycosylated β3-homo-threonine conjugates for mucin-like glycopeptide antigen analogues, *Beilstein Journal of Organic Chemistry*, **2010**, *6*, 47.
[108] R. J. Simon, R. S. Kania, R. N. Zuckermann, V. D. Huebner, D. A. Jewell, S. Banville, S. Ng, L. Wang, S. Rosenberg, C. K. Marlowe; Peptoids: a modular approach to drug discovery, *Proceedings of the National Academy of Sciences of the United States of America*, **1992**, *89*, 9367-9371.
[109] Y. Hu, X. Li, S. M. Sebti, J. Chen, J. Cai; Design and synthesis of AApeptides: A new class of peptide mimics, *Bioorganic & Medicinal Chemistry Letters*, **2011**, *21*, 1469-1471.
[110] D. Gaspar, A. S. Veiga, C. Sinthuvanich, J. P. Schneider, M. A. Castanho; Anticancer peptide SVS-1: efficacy precedes membrane neutralization, *Biochemistry*, **2012**, *51*, 6263-6265.
[111] C. Sinthuvanich, A. S. Veiga, K. Gupta, D. Gaspar, R. Blumenthal, J. P. Schneider; Anticancer β-Hairpin Peptides: Membrane-Induced Folding Triggers Activity, *Journal of the American Chemical Society*, **2012**, *134*, 6210-6217.
[112] T. Podewin, M. S. Rampp, I. Turkanovic, K. L. Karaghiosoff, W. Zinth, A. Hoffmann-Röder; Photocontrolled chignolin-derived β-hairpin peptidomimetics, *Chemical Communications*, **2015**, *51*, 4001-4004.
[113] M. S. Rampp, S. M. Hofmann, T. Podewin, A. Hoffmann-Röder, L. Moroder, W. Zinth; Time-resolved infrared studies of the unfolding of a light triggered β-hairpin peptide, *Chemical Physics*, **2018**, *512*, 116-121.
[114] A. A. Deeg, M. S. Rampp, A. Popp, B. M. Pilles, T. E. Schrader, L. Moroder, K. Hauser, W. Zinth; Isomerization- and temperature-jump-induced dynamics of a photoswitchable β-hairpin, *Chemistry – A European Journal*, **2014**, *20*, 694-703.
[115] N. Regner, T. T. Herzog, K. Haiser, C. Hoppmann, M. Beyermann, J. Sauermann, M. Engelhard, T. Cordes, K. Ruck-Braun, W. Zinth; Light-switchable hemithioindigo-hemistilbene-containing peptides: ultrafast spectroscopy of the Z --> E isomerization of the chromophore and the structural dynamics of the peptide moiety, *Journal of Physical Chemistry B*, **2012**, *116*, 4181-4191.
[116] T. E. Schrader, T. Cordes, W. J. Schreier, F. O. Koller, S. L. Dong, L. Moroder, W. Zinth; Folding and unfolding of light-triggered beta-hairpin model peptides, *Journal of Physical Chemistry B*, **2011**, *115*, 5219-5226.
[117] T. E. Schrader, W. J. Schreier, T. Cordes, F. O. Koller, G. Babitzki, R. Denschlag, C. Renner, M. Loweneck, S. L. Dong, L. Moroder, P. Tavan, W. Zinth; Light-triggered beta-hairpin folding and unfolding, *Proceedings of the National Academy of Sciences, USA*, **2007**, *104*, 15729-15734.
[118] S.-L. Dong, M. Löweneck, T. E. Schrader, W. J. Schreier, W. Zinth, L. Moroder, C. Renner; A photocontrolled β-hairpin peptide, *Chemistry - A European Journal*, **2006**, *12*, 1114-1120.
[119] H. X. Xu, Wenbo; Dai, Jian; Lu, Qiangxi; Qin, Lixing; Zhou, Zhiguo; Method for preparing N-fluorenylmethyloxycarbonyl-O-caprylyl-serine/threonine, **2018**,
[120] Y. Shi, P. Teng, P. Sang, F. She, L. Wei, J. Cai; γ-AApeptides: Design, Structure, and Applications, *Accounts of Chemical Research*, **2016**, *49*, 428-441.
[121] N. Winssinger, R. Damoiseaux, D. C. Tully, B. H. Geierstanger, K. Burdick, J. L. Harris; PNA-Encoded Protease Substrate Microarrays, *Chemistry & Biology*, **2004**, *11*, 1351-1360.
[122] F. Debaene, J. A. Da Silva, Z. Pianowski, F. J. Duran, N. Winssinger; Expanding the scope of PNA-encoded libraries: divergent synthesis of libraries targeting cysteine, serine and metallo-proteases as well as tyrosine phosphatases, *Tetrahedron*, **2007**, *63*, 6577-6586.
[123] P. E. Nielsen; Peptide Nucleic Acid. A Molecule with Two Identities, *Accounts of Chemical Research*, **1999**, *32*, 624-630.
[124] J. Saarbach, P. M. Sabale, N. Winssinger; Peptide nucleic acid (PNA) and its applications in chemical biology, diagnostics, and therapeutics, *Current Opinion in Chemical Biology*, **2019**, *52*, 112-124.

[125] H. Wu, Y. Niu, S. Padhee, R. E. Wang, Y. Li, Q. Qiao, G. Bai, C. Cao, J. Cai; Design and synthesis of unprecedented cyclic γ-AApeptides for antimicrobial development, *Chemical Science*, **2012**, *3*, 2570-2575.

[126] H. Wu, Q. Qiao, Y. Hu, P. Teng, W. Gao, X. Zuo, L. Wojtas, R. W. Larsen, S. Ma, J. Cai; Sulfono-γ-AApeptides as a New Class of Nonnatural Helical Foldamer, *Chemistry – A European Journal*, **2015**, *21*, 2501-2507.

[127] F. She, A. Nimmagadda, P. Teng, M. Su, X. Zuo, J. Cai; Helical 1:1 α/Sulfono-γ-AA Heterogeneous Peptides with Antibacterial Activity, *Biomacromolecules*, **2016**, *17*, 1854-1859.

[128] O. Bolarinwa, A. Nimmagadda, M. Su, J. Cai; Structure and Function of AApeptides, *Biochemistry*, **2017**, *56*, 445-457.

[129] A. Nimmagadda, Y. Shi, J. Cai; γ-AApeptides as a New Strategy for Therapeutic Development, *Current medicinal chemistry*, **2019**, *26*, 2313-2329.

[130] Y. Niu, G. Bai, H. Wu, R. E. Wang, Q. Qiao, S. Padhee, R. Buzzeo, C. Cao, J. Cai; Cellular Translocation of a γ-AApeptide Mimetic of Tat Peptide, *Molecular Pharmaceutics*, **2012**, *9*, 1529-1534.

[131] C.-F. Le, C.-M. Fang, S. D. Sekaran; Intracellular Targeting Mechanisms by Antimicrobial Peptides, *Antimicrobial Agents and Chemotherapy*, **2017**, *61*, e02340-02316.

[132] Y. Li, H. Wu, P. Teng, G. Bai, X. Lin, X. Zuo, C. Cao, J. Cai; Helical Antimicrobial Sulfono-γ-AApeptides, *Journal of Medicinal Chemistry*, **2015**, *58*, 4802-4811.

[133] Y. Niu, S. Padhee, H. Wu, G. Bai, Q. Qiao, Y. Hu, L. Harrington, W. N. Burda, L. N. Shaw, C. Cao, J. Cai; Lipo-γ-AApeptides as a New Class of Potent and Broad-Spectrum Antimicrobial Agents, *Journal of Medicinal Chemistry*, **2012**, *55*, 4003-4009.

[134] Y. Li, C. Smith, H. Wu, P. Teng, Y. Shi, S. Padhee, T. Jones, A. M. Nguyen, C. Cao, H. Yin, J. Cai; Short antimicrobial lipo-α/γ-AA hybrid peptides, *Chembiochem*, **2014**, *15*, 2275-2280.

[135] T. Ju, V. I. Otto, R. D. Cummings; The Tn Antigen—Structural Simplicity and Biological Complexity, *Angewandte Chemie International Edition*, **2011**, *50*, 1770-1791.

[136] D. Roulois, M. Grégoire, J.-F. Fonteneau; MUC1-Specific Cytotoxic T Lymphocytes in Cancer Therapy: Induction and Challenge, *BioMed Research International*, **2013**, *2013*, 871936-871946.

[137] M. A. Cheever, J. P. Allison, A. S. Ferris, O. J. Finn, B. M. Hastings, T. T. Hecht, I. Mellman, S. A. Prindiville, J. L. Viner, L. M. Weiner, L. M. Matrisian; The Prioritization of Cancer Antigens: A National Cancer Institute Pilot Project for the Acceleration of Translational Research, *Clinical Cancer Research*, **2009**, *15*, 5323-5337.

[138] H. C. Hang, C. R. Bertozzi; The chemistry and biology of mucin-type O-linked glycosylation, *Bioorganic & medicinal chemistry*, **2005**, *13*, 5021-5034.

[139] T. A. Gerken, J. Raman, T. A. Fritz, O. Jamison; Identification of common and unique peptide substrate preferences for the UDP-GalNAc:polypeptide alpha-N-acetylgalactosaminyltransferases T1 and T2 derived from oriented random peptide substrates, *Journal of Biological Chemistry*, **2006**, *281*, 32403-32416.

[140] T. A. Gerken, K. G. Ten Hagen, O. Jamison; Conservation of peptide acceptor preferences between Drosophila and mammalian polypeptide-GalNAc transferase ortholog pairs, *Glycobiology*, **2008**, *18*, 861-870.

[141] C. Perrine, T. Ju, R. D. Cummings, T. A. Gerken; Systematic determination of the peptide acceptor preferences for the human UDP-Gal:glycoprotein-α-GalNAc β3 galactosyltranferase (T-synthase), *Glycobiology*, **2008**, *19*, 321-328.

[142] S. H. Brewer, B. Song, D. P. Raleigh, R. B. Dyer; Residue specific resolution of protein folding dynamics using isotope-edited infrared temperature jump spectroscopy, *Biochemistry*, **2007**, *46*, 3279-3285.

[143] T. Ju, R. D. Cummings, W. M. Canfield; Purification, characterization, and subunit structure of rat core 1 Beta1,3-galactosyltransferase, *Journal of Biological Chemistry*, **2002**, *277*, 169-177.

[144] M. F. Bierhuizen, M. Fukuda; Expression cloning of a cDNA encoding UDP-GlcNAc:Gal beta 1-3-GalNAc-R (GlcNAc to GalNAc) beta 1-6GlcNAc transferase by gene transfer into CHO cells expressing polyoma large tumor antigen, *Proceedings of the National Academy of Sciences, USA*, **1992**, *89*, 9326-9330.

[145] N. Kurosawa, N. Kojima, M. Inoue, T. Hamamoto, S. Tsuji; Cloning and expression of Gal beta 1,3GalNAc-specific GalNAc alpha 2,6-sialyltransferase, *Journal of Biological Chemistry*, **1994**, *269*, 19048-19053.
[146] Y. C. Lee, M. Kaufmann, S. Kitazume-Kawaguchi, M. Kono, S. Takashima, N. Kurosawa, H. Liu, H. Pircher, S. Tsuji; Molecular cloning and functional expression of two members of mouse NeuAcalpha2,3Galbeta1,3GalNAc GalNAcalpha2,6-sialyltransferase family, ST6GalNAc III and IV, *Journal of Biological Chemistry*, **1999**, *274*, 11958-11967.
[147] F. J. Irazoqui, G. A. Nores; Thomsen-friedenreich disaccharide immunogenicity, *Curr Cancer Drug Targets*, **2003**, *3*, 433-443.
[148] W. Kuhns, V. Rutz, H. Paulsen, K. L. Matta, M. A. Baker, M. Barner, M. Granovsky, I. Brockhausen; ProcessingO-glycan core 1, Galβ1-3GalNAcα-R. Specificities of core 2, UDP-GlcNAc: Galβ1-3GalNAc-R(GlcNAc to GalNAc) β6-N-acetylglucosaminyltransferase and CMP-sialic acid:Galβ1-3GalNAc-R α3-sialyltransferase, *Glycoconjugate Journal*, **1993**, *10*, 381-394.
[149] S. Hakomori; Glycosylation defining cancer malignancy: new wine in an old bottle, *Proceedings of the National Academy of Sciences, USA*, **2002**, *99*, 10231-10233.
[150] F. Santos-Silva, A. Fonseca, T. Caffrey, F. Carvalho, P. Mesquita, C. Reis, R. Almeida, L. David, M. A. Hollingsworth; Thomsen-Friedenreich antigen expression in gastric carcinomas is associated with MUC1 mucin VNTR polymorphism, *Glycobiology*, **2005**, *15*, 511-517.
[151] I. Brockhausen, J.-M. Yang, J. Burchell, C. Whitehouse, J. Taylor-Papadimitriou; Mechanisms Underlying Aberrant Glycosylation of MUC1 Mucin in Breast Cancer Cells, *European Journal of Biochemistry*, **1995**, *233*, 607-617.
[152] S. Nath, P. Mukherjee; MUC1: a multifaceted oncoprotein with a key role in cancer progression, *Trends in Molecular Medicine*, **2014**, *20*, 332-342.
[153] N. Martínez-Sáez, J. M. Peregrina, F. Corzana; Principles of mucin structure: implications for the rational design of cancer vaccines derived from MUC1-glycopeptides, *Chemical Society Reviews*, **2017**, *46*, 7154-7175.
[154] R. M. Wilson, S. J. Danishefsky; A Vision for Vaccines Built from Fully Synthetic Tumor-Associated Antigens: From the Laboratory to the Clinic, *Journal of the American Chemical Society*, **2013**, *135*, 14462-14472.
[155] P. L. Beatty, O. J. Finn; Preventing cancer by targeting abnormally expressed self-antigens: MUC1 vaccines for prevention of epithelial adenocarcinomas, *Annals of the New York Academy of Sciences*, **2013**, *1284*, 52-56.
[156] C. Mersch, S. Wagner, A. Hoffmann-Röder; Synthesis of Fluorinated Analogues of Tumor-Associated Carbohydrate and Glycopeptide Antigens, *Synlett*, **2009**, *2009*, 2167-2171.
[157] B. Richichi, B. Thomas, M. Fiore, R. Bosco, H. Qureshi, C. Nativi, O. Renaudet, L. BenMohamed; A Cancer Therapeutic Vaccine based on Clustered Tn-Antigen Mimetics Induces Strong Antibody-Mediated Protective Immunity, *Angewandte Chemie*, **2014**, *126*, 12111-12114.
[158] A. Hoffmann-Röder, A. Kaiser, S. Wagner, N. Gaidzik, D. Kowalczyk, U. Westerlind, B. Gerlitzki, E. Schmitt, H. Kunz; Synthetic Antitumor Vaccines from Tetanus Toxoid Conjugates of MUC1 Glycopeptides with the Thomsen–Friedenreich Antigen and a Fluorine-Substituted Analogue, *Angewandte Chemie International Edition*, **2010**, *49*, 8498-8503.
[159] V. J. Somovilla, I. A. Bermejo, I. S. Albuquerque, N. Martinez-Saez, J. Castro-Lopez, F. Garcia-Martin, I. Companon, H. Hinou, S. I. Nishimura, J. Jimenez-Barbero, J. L. Asensio, A. Avenoza, J. H. Busto, R. Hurtado-Guerrero, J. M. Peregrina, G. J. L. Bernardes, F. Corzana; The Use of Fluoroproline in MUC1 Antigen Enables Efficient Detection of Antibodies in Patients with Prostate Cancer, *Journal of the American Chemical Society*, **2017**, *139*, 18255-18261.
[160] C. C. Jansen; Dissertation thesis, Ludwig-Maximilians-Universität München (München), **2020**.
[161] H. Paulsen, J.-P. Hölck; Synthese der glycopeptide O-β-d-galactopyranosyl-(1→3)-O-(2-acetamido-2-desoxy-α-d-galactopyranosyl)-(1→3)-l-serin und -l-threonin, *Carbohydrate Research*, **1982**, *109*, 89-107.
[162] R. Bukowski, Laura M. Morris, Robert J. Woods, T. Weimar; Synthesis and Conformational Analysis of the T-Antigen Disaccharide (β-D-Gal-(1→3)-α-D-GalNAc-OMe), *European Journal of Organic Chemistry*, **2001**, *2001*, 2697-2705.

[163] C. Brocke; Johannes Gutenberg-Universität Mainz **2003**.
[164] C. Plattner, M. Höfener, N. Sewald; One-Pot Azidochlorination of Glycals, *Organic Letters*, **2011**, *13*, 545-547.
[165] H. Cai, Z.-H. Huang, L. Shi, P. Zou, Y.-F. Zhao, H. Kunz, Y.-M. Li; Synthesis of Tn/T Antigen MUC1 Glycopeptide BSA Conjugates and Their Evaluation as Vaccines, *European Journal of Organic Chemistry*, **2011**, *2011*, 3685-3689.
[166] M. J. McKennon, A. I. Meyers, K. Drauz, M. Schwarm; A convenient reduction of amino acids and their derivatives, *The Journal of Organic Chemistry*, **1993**, *58*, 3568-3571.
[167] P. K. Mandal, Z. Ren, X. Chen, C. Xiong, J. S. McMurray; Structure−Affinity Relationships of Glutamine Mimics Incorporated into Phosphopeptides Targeted to the SH2 Domain of Signal Transducer and Activator of Transcription 3, *Journal of Medicinal Chemistry*, **2009**, *52*, 6126-6141.
[168] W. Koenigs, E. Knorr; Ueber einige Derivate des Traubenzuckers und der Galactose, *Berichte der deutschen chemischen Gesellschaft*, **1901**, *34*, 957-981.
[169] N. Martínez-Sáez, J. Castro-López, J. Valero-González, D. Madariaga, I. Compañón, V. J. Somovilla, M. Salvadó, J. L. Asensio, J. Jiménez-Barbero, A. Avenoza, J. H. Busto, G. J. L. Bernardes, J. M. Peregrina, R. Hurtado-Guerrero, F. Corzana; Deciphering the Non-Equivalence of Serine and Threonine O-Glycosylation Points: Implications for Molecular Recognition of the Tn Antigen by an anti-MUC1 Antibody, *Angewandte Chemie International Edition*, **2015**, *54*, 9830-9834.
[170] Y. E. Jad, S. N. Khattab, B. G. de la Torre, T. Govender, H. G. Kruger, A. El-Faham, F. Albericio; Oxyma-B, an excellent racemization suppressor for peptide synthesis, *Organic & Biomolecular Chemistry*, **2014**, *12*, 8379-8385.
[171] B. Bacsa, K. Horváti, S. Bõsze, F. Andreae, C. O. Kappe; Solid-Phase Synthesis of Difficult Peptide Sequences at Elevated Temperatures: A Critical Comparison of Microwave and Conventional Heating Technologies, *The Journal of Organic Chemistry*, **2008**, *73*, 7532-7542.
[172] S. A. Palasek, Z. J. Cox, J. M. Collins; Limiting racemization and aspartimide formation in microwave-enhanced Fmoc solid phase peptide synthesis, *Journal of Peptide Science*, **2007**, *13*, 143-148.
[173] C. S. Bennett, S. M. Dean, R. J. Payne, S. Ficht, A. Brik, C.-H. Wong; Sugar-Assisted Glycopeptide Ligation with Complex Oligosaccharides: Scope and Limitations, *Journal of the American Chemical Society*, **2008**, *130*, 11945-11952.
[174] E. Macho Fernandez, J. Chang, J. Fontaine, E. Bialecki, F. Rodriguez, E. Werkmeister, V. Krieger, C. Ehret, B. Heurtault, S. Fournel, B. Frisch, D. Betbeder, C. Faveeuw, F. Trottein; Activation of invariant Natural Killer T lymphocytes in response to the α-galactosylceramide analogue KRN7000 encapsulated in PLGA-based nanoparticles and microparticles, *International Journal of Pharmaceutics*, **2012**, *423*, 45-54.
[175] F. Broecker, S. Götze, J. Hudon, D. C. K. Rathwell, C. L. Pereira, P. Stallforth, C. Anish, P. H. Seeberger; Synthesis, Liposomal Formulation, and Immunological Evaluation of a Minimalistic Carbohydrate-α-GalCer Vaccine Candidate, *Journal of Medicinal Chemistry*, **2018**, *61*, 4918-4927.
[176] V. Cerundolo, J. D. Silk, S. H. Masri, M. Salio; Harnessing invariant NKT cells in vaccination strategies, *Nature Reviews Immunology*, **2009**, *9*, 28-38.
[177] W. Szymański, J. M. Beierle, H. A. V. Kistemaker, W. A. Velema, B. L. Feringa; Reversible Photocontrol of Biological Systems by the Incorporation of Molecular Photoswitches, *Chemical Reviews*, **2013**, *113*, 6114-6178.
[178] G. Mayer, A. Heckel; Biologically Active Molecules with a "Light Switch", *Angewandte Chemie International Edition*, **2006**, *45*, 4900-4921.
[179] C. Renner, L. Moroder; Azobenzene as conformational switch in model peptides, *Chembiochem*, **2006**, *7*, 868-878.
[180] C. R. Crecca, A. E. Roitberg; Theoretical Study of the Isomerization Mechanism of Azobenzene and Disubstituted Azobenzene Derivatives, *The Journal of Physical Chemistry A*, **2006**, *110*, 8188-8203.

[181] L. Gagliardi, G. Orlandi, F. Bernardi, A. Cembran, M. Garavelli; A theoretical study of the lowest electronic states of azobenzene: the role of torsion coordinate in the cis–trans photoisomerization, *Theoretical Chemistry Accounts*, **2004**, *111*, 363-372.
[182] D. Bléger, J. Schwarz, A. M. Brouwer, S. Hecht; o-Fluoroazobenzenes as Readily Synthesized Photoswitches Offering Nearly Quantitative Two-Way Isomerization with Visible Light, *Journal of the American Chemical Society*, **2012**, *134*, 20597-20600.
[183] Ľ. Vetráková, V. Ladányi, J. Al Anshori, P. Dvořák, J. Wirz, D. Heger; The absorption spectrum of cis-azobenzene, *Photochemical & Photobiological Sciences*, **2017**, *16*, 1749-1756.
[184] H. M. D. Bandara, S. C. Burdette; Photoisomerization in different classes of azobenzene, *Chemical Society Reviews*, **2012**, *41*, 1809-1825.
[185] Z. Yu, S. Hecht; Remote control over folding by light, *Chemical Communications*, **2016**, *52*, 6639-6653.
[186] P. Kobauri, F. J. Dekker, W. Szymanski, B. L. Feringa; Rational Design in Photopharmacology with Molecular Photoswitches, *Angewandte Chemie International Edition*, **2023**, *62*, e202300681.
[187] W. A. Velema, W. Szymanski, B. L. Feringa; Photopharmacology: Beyond Proof of Principle, *Journal of the American Chemical Society*, **2014**, *136*, 2178-2191.
[188] R. J. Mart, R. K. Allemann; Azobenzene photocontrol of peptides and proteins, *Chemical Communications*, **2016**, *52*, 12262-12277.
[189] M. Wegener, M. J. Hansen, A. J. M. Driessen, W. Szymanski, B. L. Feringa; Photocontrol of Antibacterial Activity: Shifting from UV to Red Light Activation, *Journal of the American Chemical Society*, **2017**, *139*, 17979-17986.
[190] L. Albert, J. Xu, R. Wan, V. Srinivasan, Y. Dou, O. Vázquez; Controlled inhibition of methyltransferases using photoswitchable peptidomimetics: towards an epigenetic regulation of leukemia, *Chemical Science*, **2017**, *8*, 4612-4618.
[191] R. J. Mart, R. J. Errington, C. L. Watkins, S. C. Chappell, M. Wiltshire, A. T. Jones, P. J. Smith, R. K. Allemann; BH3 helix-derived biophotonic nanoswitches regulate cytochrome c release in permeabilised cells, *Molecular BioSystems*, **2013**, *9*, 2597-2603.
[192] T. Podewin, J. Broichhagen, C. Frost, D. Groneberg, J. Ast, H. Meyer-Berg, N. H. F. Fine, A. Friebe, M. Zacharias, D. J. Hodson, D. Trauner, A. Hoffmann-Röder; Optical control of a receptor-linked guanylyl cyclase using a photoswitchable peptidic hormone, *Chemical Science*, **2017**, *8*, 4644-4653.
[193] A. Aemissegger, V. Krautler, W. F. van Gunsteren, D. Hilvert; A photoinducible beta-hairpin, *Journal of the American Chemical Society*, **2005**, *127*, 2929-2936.
[194] D. G. Flint, J. R. Kumita, O. S. Smart, G. A. Woolley; Using an Azobenzene Cross-Linker to Either Increase or Decrease Peptide Helix Content upon Trans-to-Cis Photoisomerization, *Chemistry & Biology*, **2002**, *9*, 391-397.
[195] A. Prestel, H. M. Möller; Spatio-temporal control of cellular uptake achieved by photoswitchable cell-penetrating peptides, *Chemical Communications*, **2016**, *52*, 701-704.
[196] R. Denschlag, W. J. Schreier, B. Rieff, T. E. Schrader, F. O. Koller, L. Moroder, W. Zinth, P. Tavan; Relaxation time prediction for a light switchable peptide by molecular dynamics, *Physical Chemistry Chemical Physics*, **2010**, *12*, 6204-6218.
[197] T. M. Doran, E. A. Anderson, S. E. Latchney, L. A. Opanashuk, B. L. Nilsson; An Azobenzene Photoswitch Sheds Light on Turn Nucleation in Amyloid-β Self-Assembly, *ACS Chemical Neuroscience*, **2012**, *3*, 211-220.
[198] L. Guerrero, O. S. Smart, G. A. Woolley, R. K. Allemann; Photocontrol of DNA binding specificity of a miniature engrailed homeodomain, *Journal of the American Chemical Society*, **2005**, *127*, 15624-15629.
[199] L. Guerrero, O. S. Smart, C. J. Weston, D. C. Burns, G. A. Woolley, R. K. Allemann; Photochemical Regulation of DNA-Binding Specificity of MyoD, *Angewandte Chemie International Edition*, **2005**, *44*, 7778-7782.
[200] G. A. Woolley, A. S. I. Jaikaran, M. Berezovski, J. P. Calarco, S. N. Krylov, O. S. Smart, J. R. Kumita; Reversible Photocontrol of DNA Binding by a Designed GCN4-bZIP Protein, *Biochemistry*, **2006**, *45*, 6075-6084.

[201] G. Rydén, I. Sjöholm; Half-Life of Oxytocin in Blood of Pregnant and Non-Pregnant Woman, *Acta Obstetricia et Gynecologica Scandinavica*, **1969**, *48*, 139-140.
[202] R. Ke, X. Ma, L. T. O. Lee; Understanding the functions of kisspeptin and kisspeptin receptor (Kiss1R) from clinical case studies, *Peptides*, **2019**, *120*, 170019.
[203] M. Goodman, A. Kossoy; Conformational Aspects of Polypeptide Structure. XIX. Azoaromatic Side-Chain Effects1,2, *Journal of the American Chemical Society*, **1966**, *88*, 5010-5015.
[204] M. Bose, D. Groff, J. Xie, E. Brustad, P. G. Schultz; The Incorporation of a Photoisomerizable Amino Acid into Proteins in E. coli, *Journal of the American Chemical Society*, **2006**, *128*, 388-389.
[205] C. Hoppmann, V. K. Lacey, G. V. Louie, J. Wei, J. P. Noel, L. Wang; Genetically Encoding Photoswitchable Click Amino Acids in Escherichia coli and Mammalian Cells, *Angewandte Chemie International Edition*, **2014**, *53*, 3932-3936.
[206] M. Goodman, M. L. Falxa; Conformational aspects of polypeptide structure. XXIII. Photoisomerization of azoaromatic polypeptides, *Journal of the American Chemical Society*, **1967**, *89*, 3863-3867.
[207] V. Borisenko, D. C. Burns, Z. Zhang, G. A. Woolley; Optical Switching of Ion−Dipole Interactions in a Gramicidin Channel Analogue, *Journal of the American Chemical Society*, **2000**, *122*, 6364-6370.
[208] W. Li, I.-s. Park, S.-K. Kang, M. Lee; Smart hydrogels from laterally-grafted peptide assembly, *Chemical Communications*, **2012**, *48*, 8796-8798.
[209] J. Li, Z. Chen, M. Zhou, J. Jing, W. Li, Y. Wang, L. Wu, L. Wang, Y. Wang, M. Lee; Polyoxometalate-Driven Self-Assembly of Short Peptides into Multivalent Nanofibers with Enhanced Antibacterial Activity, *Angewandte Chemie International Edition*, **2016**, *55*, 2592-2595.
[210] J. Qiu, B. Xu, Z. Huang, W. Pan, P. Cao, C. Liu, X. Hao, B. Song, G. Liang; Synthesis and biological evaluation of Matijing-Su derivatives as potent anti-HBV agents, *Bioorganic & medicinal chemistry*, **2011**, *19*, 5352-5360.
[211] M. Fukuda, C. M. Beechan, M. Verlander, M. Goodman, M. M. Khan, K. L. Melmon; Conjugates of catecholamines. VII. Synthesis and β-adrenergic activity of peptide catecholamine conjugates†, *International Journal of Peptide and Protein Research*, **1987**, *29*, 300-317.
[212] L. Peura, K. Malmioja, K. Laine, J. Leppänen, M. Gynther, A. Isotalo, J. Rautio; Large Amino Acid Transporter 1 (LAT1) Prodrugs of Valproic Acid: New Prodrug Design Ideas for Central Nervous System Delivery, *Molecular Pharmaceutics*, **2011**, *8*, 1857-1866.
[213] J. Broichhagen, T. Podewin, H. Meyer-Berg, Y. von Ohlen, N. R. Johnston, B. J. Jones, S. R. Bloom, G. A. Rutter, A. Hoffmann-Röder, D. J. Hodson, D. Trauner; Optical Control of Insulin Secretion Using an Incretin Switch, *Angewandte Chemie International Edition*, **2015**, *54*, 15565-15569.
[214] J. Broichhagen, T. Podewin, H. Meyer-Berg, Y. von Ohlen, N. R. Johnston, B. J. Jones, S. R. Bloom, G. A. Rutter, A. Hoffmann-Röder, D. J. Hodson, D. Trauner; Optical control of insulin secretion using an incretin switch, *Angewandte Chemie International Edition*, **2015**, *54*, 15565-15569.
[215] K. Ueno, S. Akiyoshi; Kinetic Study on the Condensation Reaction of Aniline and Nitrosobenzenes, *Journal of the American Chemical Society*, **1954**, *76*, 3670-3672.
[216] E. Merino; Synthesis of azobenzenes: the coloured pieces of molecular materials, *Chemical Society Reviews*, **2011**, *40*, 3835-3853.
[217] S. Trippett; 449. A new synthesis of acetylenes. Part II. The reaction of triphenylphosphine with α-halogeno-carbonyl compounds, *Journal of the Chemical Society (Resumed)*, **1962**, 2337-2340.
[218] A. K. Bose, B. Lal; A facile replacement of hydroxyl by halogen with inversion, *Tetrahedron Letters*, **1973**, *14*, 3937-3940.
[219] C. Hoppmann, I. Maslennikov, S. Choe, L. Wang; In Situ Formation of an Azo Bridge on Proteins Controllable by Visible Light, *Journal of the American Chemical Society*, **2015**, *137*, 11218-11221.

[220] A. M. Spokoyny, Y. Zou, J. J. Ling, H. Yu, Y.-S. Lin, B. L. Pentelute; A Perfluoroaryl-Cysteine SNAr Chemistry Approach to Unprotected Peptide Stapling, *Journal of the American Chemical Society*, **2013**, *135*, 5946-5949.
[221] N. Fillafer, T. Seewald, L. Schmidt-Mende, S. Polarz; Interfacial charge transfer processes in 2D and 3D semiconducting hybrid perovskites: azobenzene as photoswitchable ligand, *Beilstein Journal of Nanotechnology*, **2020**, *11*, 466-479.
[222] G. Leng, M. Ludwig; Neurotransmitters and peptides: whispered secrets and public announcements, *The Journal of Physiology*, **2008**, *586*, 5625-5632.
[223] H. S. Knobloch, A. Charlet, Lena C. Hoffmann, M. Eliava, S. Khrulev, Ali H. Cetin, P. Osten, Martin K. Schwarz, Peter H. Seeburg, R. Stoop, V. Grinevich; Evoked Axonal Oxytocin Release in the Central Amygdala Attenuates Fear Response, *Neuron*, **2012**, *73*, 553-566.
[224] H. Yonekura, I. Kato, Y. Yamamoto, T. Ikeda, H. Higashida, H. Okamoto; Biosynthesis and Function of VIP and Oxytocin: Mechanisms of C-terminal Amidation, Oxytocin Secretion and Transport, *Endocrinology*, **2023**, *164*, bqad121.
[225] M. Busnelli, A. Saulière, M. Manning, M. Bouvier, C. Galés, B. Chini; Functional Selective Oxytocin-derived Agonists Discriminate between Individual G Protein Family Subtypes, *Journal of Biological Chemistry*, **2012**, *287*, 3617-3629.
[226] E. H. van den Burg, I. D. Neumann; Bridging the Gap between GPCR Activation and Behaviour: Oxytocin and Prolactin Signalling in the Hypothalamus, *Journal of Molecular Neuroscience*, **2011**, *43*, 200-208.
[227] M. M. Richert, K. L. Schwertfeger, J. W. Ryder, S. M. Anderson; An Atlas of Mouse Mammary Gland Development, *Journal of Mammary Gland Biology and Neoplasia*, **2000**, *5*, 227-241.
[228] A. Campbell; Oxytocin and Human Social Behavior, *Personality and Social Psychology Review*, **2010**, *14*, 281-295.
[229] D. M. Cochran, D. Fallon, M. Hill, J. A. Frazier; The role of oxytocin in psychiatric disorders: a review of biological and therapeutic research findings, *Harvard review of psychiatry*, **2013**, *21*, 219-247.
[230] I. D. Neumann, R. Maloumby, D. I. Beiderbeck, M. Lukas, R. Landgraf; Increased brain and plasma oxytocin after nasal and peripheral administration in rats and mice, *Psychoneuroendocrinology*, **2013**, *38*, 1985-1993.
[231] K. Wiśniewski, S. Alagarsamy, R. Galyean, H. Tariga, D. Thompson, B. Ly, H. Wiśniewska, S. Qi, G. Croston, R. Laporte, P. J. M. Rivière, C. D. Schteingart; New, Potent, and Selective Peptidic Oxytocin Receptor Agonists, *Journal of Medicinal Chemistry*, **2014**, *57*, 5306-5317.
[232] M. A. Mohammad Nezhady, J. C. Rivera, S. Chemtob; Location Bias as Emerging Paradigm in GPCR Biology and Drug Discovery, *iScience*, **2020**, *23*, 101643.
[233] P. A. Insel, K. Sriram, M. W. Gorr, S. Z. Wiley, A. Michkov, C. Salmerón, A. M. Chinn; GPCRomics: An Approach to Discover GPCR Drug Targets, *Trends in Pharmacological Sciences*, **2019**, *40*, 378-387.
[234] D. Latek, A. Modzelewska, B. Trzaskowski, K. Palczewski, S. Filipek; G protein-coupled receptors--recent advances, *Acta Biochimica Polonica*, **2012**, *59*, 515-529.
[235] E. R. Liman; Use it or lose it: molecular evolution of sensory signaling in primates, *Pflügers Archiv*, **2006**, *453*, 125-131.
[236] H. B. Schiöth, R. Fredriksson; The GRAFS classification system of G-protein coupled receptors in comparative perspective, *General and Comparative Endocrinology*, **2005**, *142*, 94-101.
[237] D. M. Rosenbaum, S. G. F. Rasmussen, B. K. Kobilka; The structure and function of G-protein-coupled receptors, *Nature*, **2009**, *459*, 356-363.
[238] N. R. Latorraca, A. J. Venkatakrishnan, R. O. Dror; GPCR Dynamics: Structures in Motion, *Chemical Reviews*, **2017**, *117*, 139-155.
[239] O. Vögler, J. M. Barceló, C. Ribas, P. V. Escribá; Membrane interactions of G proteins and other related proteins, *Biochimica et Biophysica Acta (BBA) - Biomembranes*, **2008**, *1778*, 1640-1652.
[240] W. I. Weis, B. K. Kobilka; The Molecular Basis of G Protein–Coupled Receptor Activation, *Annual Review of Biochemistry*, **2018**, *87*, 897-919.

[241] D. Kamato, L. Thach, R. Bernard, V. Chan, W. Zheng, H. Kaur, M. Brimble, N. Osman, P. J. Little; Structure, Function, Pharmacology, and Therapeutic Potential of the G Protein, Gα/q,11, *Frontiers in Cardiovascular Medicine*, **2015**, *2*, 14. 10.3389.

[242] C. Y. Ku, A. Qian, Y. Wen, K. Anwer, B. M. Sanborn; Oxytocin stimulates myometrial guanosine triphosphatase and phospholipase-C activities via coupling to G alpha q/11, *Endocrinology*, **1995**, *136*, 1509-1515.

[243] O. Chatterjee, K. Patil, A. Sahu, L. Gopalakrishnan, P. Mol, J. Advani, S. Mukherjee, R. Christopher, T. S. Prasad; An overview of the oxytocin-oxytocin receptor signaling network, *Journal of cell communication and signaling*, **2016**, *10*, 355-360.

[244] M. Busnelli, B. Chini; Molecular Basis of Oxytocin Receptor Signalling in the Brain: What We Know and What We Need to Know, *Current Topics in Behavioral Neurosciences*, **2018**, *35*, 3-29.

[245] B. Jurek, I. D. Neumann; The Oxytocin Receptor: From Intracellular Signaling to Behavior, *Physiological Reviews*, **2018**, *98*, 1805-1908.

[246] C. Cuesta-Marti, F. Uhlig, B. Muguerza, N. Hyland, G. Clarke, H. Schellekens; Microbes, oxytocin and stress: Converging players regulating eating behavior, *Journal of Neuroendocrinology*, **2023**, *35*, e13243.

[247] M. Busnelli, B. Chini; in *Behavioral Pharmacology of Neuropeptides: Oxytocin, Vol. 35*, Springer, **2017**.

[248] K. E. Komolov, Y. Du, N. M. Duc, R. M. Betz, J. P. G. L. M. Rodrigues, R. D. Leib, D. Patra, G. Skiniotis, C. M. Adams, R. O. Dror, K. Y. Chung, B. K. Kobilka, J. L. Benovic; Structural and Functional Analysis of a β_2-Adrenergic Receptor Complex with GRK5, *Cell*, **2017**, *169*, 407-421.e416.

[249] S. K. Shenoy, R. J. Lefkowitz; Seven-Transmembrane Receptor Signaling Through β-Arrestin, *Science's STKE*, **2005**, *2005*, cm10.

[250] A. Hasbi, D. Devost, S. A. Laporte, H. H. Zingg; Real-time detection of interactions between the human oxytocin receptor and G protein-coupled receptor kinase-2, *Molecular Endocrinology*, **2004**, *18*, 1277-1286.

[251] C. A. Grotegut, L. Mao, S. L. Pierce, G. K. Swamy, R. P. Heine, A. P. Murtha; Enhanced Uterine Contractility and Stillbirth in Mice Lacking G Protein-Coupled Receptor Kinase 6 (GRK6): Implications for Oxytocin Receptor Desensitization, *Molecular Endocrinology*, **2016**, *30*, 455-468.

[252] R. H. Oakley, S. A. Laporte, J. A. Holt, L. S. Barak, M. G. Caron; Molecular Determinants Underlying the Formation of Stable Intracellular G Protein-coupled Receptor-β-Arrestin Complexes after Receptor Endocytosis*, *Journal of Biological Chemistry*, **2001**, *276*, 19452-19460.

[253] F. Conti, S. Sertic, A. Reversi, B. Chini; Intracellular trafficking of the human oxytocin receptor: evidence of receptor recycling via a Rab4/Rab5 "short cycle", *American Journal of Physiology-Endocrinology and Metabolism*, **2009**, *296*, E532-E542.

[254] C. V. Carman, J. L. Benovic; G-protein-coupled receptors: turn-ons and turn-offs, *Current Opinion in Neurobiology*, **1998**, *8*, 335-344.

[255] J. G. Krupnick, J. L. Benovic; The role of receptor kinases and arrestins in G protein-coupled receptor regulation, *Annual Review of Pharmacology and Toxicology*, **1998**, *38*, 289-319.

[256] S. Sparapani, C. Millet-Boureima, J. Oliver, K. Mu, P. Hadavi, T. Kalostian, N. Ali, C. M. Avelar, M. Bardies, B. Barrow, M. Benedikt, G. Biancardi, R. Bindra, L. Bui, Z. Chihab, A. Cossitt, J. Costa, T. Daigneault, J. Dault, I. Davidson, J. Dias, E. Dufour, S. El-Khoury, N. Farhangdoost, A. Forget, A. Fox, M. Gebrael, M. C. Gentile, O. Geraci, A. Gnanapragasam, E. Gomah, E. Haber, C. Hamel, T. Iyanker, C. Kalantzis, S. Kamali, E. Kassardjian, H. K. Kontos, T. B. U. Le, D. LoScerbo, Y. F. Low, D. Mac Rae, F. Maurer, S. Mazhar, A. Nguyen, K. Nguyen-Duong, C. Osborne-Laroche, H. W. Park, E. Parolin, K. Paul-Cole, L. S. Peer, M. Philippon, C.-A. Plaisir, J. Porras Marroquin, S. Prasad, R. Ramsarun, S. Razzaq, S. Rhainds, D. Robin, R. Scartozzi, D. Singh, S. S. Fard, M. Soroko, N. Soroori Motlagh, K. Stern, L. Toro, M. W. Toure, S. Tran-Huynh, S. Trépanier-Chicoine, C. Waddingham, A. J. Weekes, A. Wisniewski, C. Gamberi; The Biology of Vasopressin, *Biomedicines*, **2021**, *9*, 89-121.

[257] M. Thibonnier, D. M. Conarty, J. A. Preston; Human vascular endothelial cells express oxytocin receptors, *Endocrinology*, **1999**, *140*, 1301-1309.
[258] T. Sugimoto, M. Saito, S. Mochizuki, Y. Watanabe, S. Hashimoto, H. Kawashima; Molecular cloning and functional expression of a cDNA encoding the human V1b vasopressin receptor, *Journal of Biological Chemistry*, **1994**, *269*, 27088-27092.
[259] G. Gimpl, F. Fahrenholz; The oxytocin receptor system: structure, function, and regulation, *Physiological Reviews*, **2001**, *81*, 629-683.
[260] G. Gimpl, R. Postina, F. Fahrenholz, T. Reinheimer; Binding domains of the oxytocin receptor for the selective oxytocin receptor antagonist barusiban in comparison to the agonists oxytocin and carbetocin, *European Journal of Pharmacology*, **2005**, *510*, 9-16.
[261] R. Acher, J. Chauvet, M. T. Chauvet, G. Michel, Y. Rouillé; Molecular evolution of neurohypophysial hormones in relation to osmoregulation: the two fish options, *Fish Physiology and Biochemistry*, **1997**, *17*, 325-332.
[262] J. Koehbach, T. Stockner, C. Bergmayr, M. Muttenthaler, Christian W. Gruber; Insights into the molecular evolution of oxytocin receptor ligand binding, *Biochemical Society Transactions*, **2013**, *41*, 197-204.
[263] B. Chini, M. Manning; Agonist selectivity in the oxytocin/vasopressin receptor family: new insights and challenges, *Biochemical Society Transactions*, **2007**, *35*, 737-741.
[264] R. Postina, E. Kojro, F. Fahrenholz; Separate agonist and peptide antagonist binding sites of the oxytocin receptor defined by their transfer into the V2 vasopressin receptor, *Journal of Biological Chemistry*, **1996**, *271*, 31593-31601.
[265] C. Breton, H. Chellil, M. Kabbaj-Benmansour, E. Carnazzi, R. Seyer, S. Phalipou, D. Morin, T. Durroux, H. Zingg, C. Barberis, B. Mouillac; Direct identification of human oxytocin receptor-binding domains using a photoactivatable cyclic peptide antagonist: comparison with the human V1a vasopressin receptor, *Journal of Biological Chemistry*, **2001**, *276*, 26931-26941.
[266] F. Fanelli, P. Barbier, D. Zanchetta, P. G. de Benedetti, B. Chini; Activation Mechanism of Human Oxytocin Receptor: A Combined Study of Experimental and Computer-Simulated Mutagenesis, *Molecular Pharmacology*, **1999**, *56*, 214-225.
[267] S. R. Hawtin, H. C. Howard, M. Wheatley; Identification of an extracellular segment of the oxytocin receptor providing agonist-specific binding epitopes, *Biochemical Journal*, **2001**, *354*, 465-472.
[268] T. Engstrom, T. Barth, P. Melin, H. Vilhardt; Oxytocin receptor binding and uterotonic activity of carbetocin and its metabolites following enzymatic degradation, *European Journal of Pharmacology*, **1998**, *355*, 203-210.
[269] V. J. Wesley, S. R. Hawtin, H. C. Howard, M. Wheatley; Agonist-Specific, High-Affinity Binding Epitopes Are Contributed by an Arginine in the N-Terminus of the Human Oxytocin Receptor, *Biochemistry*, **2002**, *41*, 5086-5092.
[270] C. W. Gruber, J. Koehbach, M. Muttenthaler; Exploring bioactive peptides from natural sources for oxytocin and vasopressin drug discovery, *Future Medicinal Chemistry*, **2012**, *4*, 1791-1798.
[271] V J Hruby, a. M S Chow, D. D. Smith; Conformational and Structural Considerations in Oxytocin-Receptor Binding and Biological Activity, *Annual Review of Pharmacology and Toxicology*, **1990**, *30*, 501-534.
[272] P. D. Williams, M. G. Bock, R. D. Tung, V. M. Garsky, D. S. Perlow, J. M. Erb, G. F. Lundell, N. P. Gould, W. L. Whitter, J. B. Hoffman, et al.; Development of a novel class of cyclic hexapeptide oxytocin antagonists based on a natural product, *Journal of Medicinal Chemistry*, **1992**, *35*, 3905-3918.
[273] J. P. Meraldi, V. J. Hruby, A. I. Brewster; Relative conformational rigidity in oxytocin and (1-penicillamine)-oxytocin: a proposal for the relationship of conformational flexibility to peptide hormone agonism and antagonism, *Proceedings of the National Academy of Sciences*, **1977**, *74*, 1373-1377.
[274] R. Walter, J. Rudinger, I. L. Schwartz; Chemistry and structure-activity relations of the antidiuretic hormones, *The American Journal of Medicine*, **1967**, *42*, 653-677.
[275] D. D. Smith, J. Slaninova, V. J. Hruby; Structure-activity studies of a novel bicyclic oxytocin antagonist, *Journal of Medicinal Chemistry*, **1992**, *35*, 1558-1563.

[276] I. A. Karpenko, R. Kreder, C. Valencia, P. Villa, C. Mendre, B. Mouillac, Y. Mély, M. Hibert, D. Bonnet, A. S. Klymchenko; Red Fluorescent Turn-On Ligands for Imaging and Quantifying G Protein-Coupled Receptors in Living Cells, *Chembiochem*, **2014**, *15*, 359-363.
[277] Y. Waltenspühl, J. Ehrenmann, S. Vacca, C. Thom, O. Medalia, A. Plückthun; Structural basis for the activation and ligand recognition of the human oxytocin receptor, *Nature Communications*, **2022**, *13*, 4153.
[278] U. Wirth, K. Raabe, P. Kalaba, E. Keimpema, M. Muttenthaler, B. König; Photoswitchable Probes of Oxytocin and Vasopressin, *Journal of Medicinal Chemistry*, **2023**, *66*, 14853-14865.
[279] M. Gul, K. Bocu, E. C. Serefoglu; Current and emerging treatment options for premature ejaculation, *Nature Reviews Urology*, **2022**, *19*, 659-680.
[280] H. Sun, L. Xu, Y. Li, S. Zhao; Effectiveness and safety of carboxytocin versus oxytocin in preventing postpartum hemorrhage: A systematic review and meta-analysis, *Journal of Obstetrics and Gynaecology Research*, **2022**, *48*, 889-901.
[281] T. A. Katte, M. Kassiou; A patent review of oxytocin receptor antagonists 2013-2017, *Expert Opinion on Therapeutic Patents*, **2017**, *27*, 1287-1290.
[282] G. Gimpl, J. Reitz, S. Brauer, C. Trossen; Oxytocin receptors: ligand binding, signalling and cholesterol dependence, *Progress in Brain Research*, **2008**, *170*, 193-204.
[283] M. Akerlund, T. Bossmar, R. Brouard, A. Kostrzewska, T. Laudanski, A. Lemancewicz, C. Serradeil-Le Gal, M. Steinwall; Receptor binding of oxytocin and vasopressin antagonists and inhibitory effects on isolated myometrium from preterm and term pregnant women, *British Journal of Obstetrics and Gynaecology*, **1999**, *106*, 1047-1053.
[284] L. Nilsson, T. Reinheimer, M. Steinwall, M. Åkerlund; FE 200 440: a selective oxytocin antagonist on the term-pregnant human uterus, *BJOG: An International Journal of Obstetrics & Gynaecology*, **2003**, *110*, 1025-1028.
[285] S. Thornton, T. M. Goodwin, G. Greisen, M. Hedegaard, J. C. Arce; The effect of barusiban, a selective oxytocin antagonist, in threatened preterm labor at late gestational age: a randomized, double-blind, placebo-controlled trial, *American Journal of Obstetrics and Gynecology*, **2009**, *200*, 627.e621-610.
[286] T. Barth, I. Krejčí, J. Vaněčková, K. Jošt, I. Rychlík; Prolonged action of deamino-carba analogues of oxytocin on the rat uterus in vivo, *European Journal of Pharmacology*, **1974**, *25*, 67-70.
[287] N. Cort, S. Einarsson, G. Astrom; Effect of oxytocin and its long-acting analog on milk let-down and intramammary pressure in healthy lactating sows, *American Journal of Veterinary Research*, **1982**, *43*, 1283-1285.
[288] H. Amsalem, C. J. Aldrich, M. Oskamp, R. Windrim, D. Farine; Postpartum uterine response to oxytocin and carbetocin, *The Journal of Reproductive Medicine*, **2014**, *59*, 167-173.
[289] J. Bláha, T. Bartošová; Epidemiology and definition of PPH worldwide, *Best Practice & Research Clinical Anaesthesiology*, **2022**, *36*, 325-339.
[290] D. Feifel, P. D. Shilling, A. M. Belcher; The effects of oxytocin and its analog, carbetocin, on genetic deficits in sensorimotor gating, *European Neuropsychopharmacology*, **2012**, *22*, 374-378.
[291] V. Klenerova, I. Krejci, P. Sida, Z. Hlinak, S. Hynie; Oxytocin and carbetocin ameliorating effects on restraint stress-induced short- and long-term behavioral changes in rats, *Neuroendocrinology Letters*, **2010**, *31*, 622-630.
[292] L. Sikich, A. Kolevzon, B. H. King, C. J. McDougle, K. B. Sanders, S.-J. Kim, M. Spanos, T. Chandrasekhar, M. D. P. Trelles, C. M. Rockhill, M. L. Palumbo, A. Witters Cundiff, A. Montgomery, P. Siper, M. Minjarez, L. A. Nowinski, S. Marler, L. C. Shuffrey, C. Alderman, J. Weissman, B. Zappone, J. E. Mullett, H. Crosson, N. Hong, S. K. Siecinski, S. N. Giamberardino, S. Luo, L. She, M. Bhapkar, R. Dean, A. Scheer, J. L. Johnson, S. G. Gregory, J. Veenstra-VanderWeele; Intranasal Oxytocin in Children and Adolescents with Autism Spectrum Disorder, *New England Journal of Medicine*, **2021**, *385*, 1462-1473.
[293] K. Hüll, J. Morstein, D. Trauner; In Vivo Photopharmacology, *Chemical Reviews*, **2018**, *118*, 10710-10747.
[294] J. M. C. S. K. Singh; Improved coupling method for peptide synthesis at elevated temperatures **2017**, *US 20170342104*,

[295] R. N. Zuckermann, J. M. Kerr, S. B. H. Kent, W. H. Moos; Efficient method for the preparation of peptoids [oligo(N-substituted glycines)] by submonomer solid-phase synthesis, *Journal of the American Chemical Society*, **1992**, *114*, 10646-10647.
[296] D. R. Fuller, M. S. Glover, N. A. Pierson, D. Kim, D. H. Russell, D. E. Clemmer; Cis→Trans Isomerization of Pro(7) in Oxytocin Regulates Zn(2+) Binding, *Journal of the American Society for Mass Spectrometry*, **2016**, *27*, 1376-1382.
[297] G. Egger, G. Liang, A. Aparicio, P. A. Jones; Epigenetics in human disease and prospects for epigenetic therapy, *Nature*, **2004**, *429*, 457-463.
[298] Z. Li, P. Zhao, Q. Xia; Epigenetic Methylations on N6-Adenine and N6-Adenosine with the same Input but Different Output, *International journal of molecular sciences*, **2019**, *20*, 2931.
[299] M. V. C. Greenberg, D. Bourc'his; The diverse roles of DNA methylation in mammalian development and disease, *Nature Reviews Molecular Cell Biology*, **2019**, *20*, 590-607.
[300] K. Hyun, J. Jeon, K. Park, J. Kim; Writing, erasing and reading histone lysine methylations, *Experimental & Molecular Medicine*, **2017**, *49*, e324-e324.
[301] J. Wesche, S. Kühn, B. M. Kessler, M. Salton, A. Wolf; Protein arginine methylation: a prominent modification and its demethylation, *Cellular and Molecular Life Sciences*, **2017**, *74*, 3305-3315.
[302] A. P. Feinberg, B. Tycko; The history of cancer epigenetics, *Nature Reviews Cancer*, **2004**, *4*, 143-153.
[303] R. Finking, M. A. Marahiel; Biosynthesis of Nonribosomal Peptides, *Annual Review of Microbiology*, **2004**, *58*, 453-488.
[304] S. A. Sieber, M. A. Marahiel; Molecular Mechanisms Underlying Nonribosomal Peptide Synthesis: Approaches to New Antibiotics, *Chemical Reviews*, **2005**, *105*, 715-738.
[305] E. Biron, J. Chatterjee, H. Kessler; Optimized selective N-methylation of peptides on solid support, *Journal of Peptide Science*, **2006**, *12*, 213-219.
[306] V. Gogineni, M. T. Hamann; Marine natural product peptides with therapeutic potential: Chemistry, biosynthesis, and pharmacology, *Biochimica et Biophysica Acta (BBA) - General Subjects*, **2018**, *1862*, 81-196.
[307] P. Zhao, Y. Xue, J. Li, X. Li, X. Zu, Z. Zhao, C. Quan, W. Gao, S. Feng; Non-lipopeptide fungi-derived peptide antibiotics developed since 2000, *Biotechnology Letters*, **2019**, *41*, 651-673.
[308] M. Dreyfuss, E. Härri, H. Hofmann, H. Kobel, W. Pache, H. Tscherter; Cyclosporin A and C, *European journal of applied microbiology and biotechnology*, **1976**, *3*, 125-133.
[309] C. A. Lipinski, F. Lombardo, B. W. Dominy, P. J. Feeney; Experimental and computational approaches to estimate solubility and permeability in drug discovery and development settings, *Advanced Drug Delivery Reviews*, **1997**, *23*, 3-25.
[310] C. Mas-Moruno, F. Rechenmacher, H. Kessler; Cilengitide: the first anti-angiogenic small molecule drug candidate design, synthesis and clinical evaluation, *Anti-Cancer Agents in Medicinal Chemistry*, **2010**, *10*, 753-768.
[311] M.-M. Carlos, R. Florian, K. Horst; Cilengitide: The First Anti-Angiogenic Small Molecule Drug Candidate. Design, Synthesis and Clinical Evaluation, *Anti-Cancer Agents in Medicinal Chemistry*, **2010**, *10*, 753-768.
[312] B. K. Handa, A. C. Lane, J. A. H. Lord, B. A. Morgan, M. J. Rance, C. F. C. Smith; Analogues of β-LPH61–64 posessing selective agonist activity at μ-opiate receptors, *European Journal of Pharmacology*, **1981**, *70*, 531-540.
[313] A. Lindqvist, J. Rip, P. J. Gaillard, S. Björkman, M. Hammarlund-Udenaes; Enhanced Brain Delivery of the Opioid Peptide DAMGO in Glutathione PEGylated Liposomes: A Microdialysis Study, *Molecular Pharmaceutics*, **2013**, *10*, 1533-1541.
[314] L. He, J. Fong, M. von Zastrow, J. L. Whistler; Regulation of opioid receptor trafficking and morphine tolerance by receptor oligomerization, *Cell*, **2002**, *108*, 271-282.
[315] S. Patierno, L. Anselmi, I. Jaramillo, D. Scott, R. Garcia, C. Sternini; Morphine Induces μ Opioid Receptor Endocytosis in Guinea Pig Enteric Neurons Following Prolonged Receptor Activation, *Gastroenterology*, **2011**, *140*, 618-626.
[316] J. G. Minnis, S. Patierno, S. E. Kohlmeier, N. C. Brecha, M. Tonini, C. Sternini; Ligand-induced μ opioid receptor endocytosis and recycling in enteric neurons, *Neuroscience*, **2003**, *119*, 33-42.

[317] J. M. J. de Castro, M. Zenz; *Regional Opioid Analgesia: Physiopharmacological Basis, Drugs, Equipment and Clinical Application*, Kluwer Academic Publishers, The Netherlands, **1991**.
[318] S. Allouche, F. Noble, N. Marie; Opioid receptor desensitization: mechanisms and its link to tolerance, *Frontiers in Pharmacology*, **2014**, *5*, 280.
[319] S. G. F. Rasmussen, B. T. DeVree, Y. Zou, A. C. Kruse, K. Y. Chung, T. S. Kobilka, F. S. Thian, P. S. Chae, E. Pardon, D. Calinski, J. M. Mathiesen, S. T. A. Shah, J. A. Lyons, M. Caffrey, S. H. Gellman, J. Steyaert, G. Skiniotis, W. I. Weis, R. K. Sunahara, B. K. Kobilka; Crystal structure of the β2 adrenergic receptor–Gs protein complex, *Nature*, **2011**, *477*, 549-555.
[320] H. Watson; Biological membranes, *Essays in Biochemistry*, **2015**, *59*, 43-69.
[321] W. J. Koch, B. E. Hawes, L. F. Allen, R. J. Lefkowitz; Direct evidence that Gi-coupled receptor stimulation of mitogen-activated protein kinase is mediated by G beta gamma activation of p21ras, *Proceedings of the National Academy of Sciences of the United States of America*, **1994**, *91*, 12706-12710.
[322] A. Manglik, Tae H. Kim, M. Masureel, C. Altenbach, Z. Yang, D. Hilger, Michael T. Lerch, Tong S. Kobilka, Foon S. Thian, Wayne L. Hubbell, R. S. Prosser, Brian K. Kobilka; Structural Insights into the Dynamic Process of β2-Adrenergic Receptor Signaling, *Cell*, **2015**, *161*, 1101-1111.
[323] V. C. Dang, M. J. Christie; Mechanisms of rapid opioid receptor desensitization, resensitization and tolerance in brain neurons, *British Journal of Pharmacology*, **2012**, *165*, 1704-1716.
[324] P. F. W. Leippe; Dissertation thesis, Ludwig-Maximilians-University Munich (Munich), **2018**.
[325] A. Koehl, H. Hu, S. Maeda, Y. Zhang, Q. Qu, J. M. Paggi, N. R. Latorraca, D. Hilger, R. Dawson, H. Matile, G. F. X. Schertler, S. Granier, W. I. Weis, R. O. Dror, A. Manglik, G. Skiniotis, B. K. Kobilka; Structure of the μ-opioid receptor–Gi protein complex, *Nature*, **2018**, *558*, 547-552.
[326] S. C. Miller, T. S. Scanlan; Site-Selective N-Methylation of Peptides on Solid Support, *Journal of the American Chemical Society*, **1997**, *119*, 2301-2302.
[327] A. Porcheddu, G. Giacomelli, I. Piredda, M. Carta, G. Nieddu; A Practical and Efficient Approach to PNA Monomers Compatible with Fmoc-Mediated Solid-Phase Synthesis Protocols, *European Journal of Organic Chemistry*, **2008**, *2008*, 5786-5797.
[328] M. Kotani, M. Detheux, A. Vandenbogaerde, D. Communi, J.-M. Vanderwinden, E. Le Poul, S. Brézillon, R. Tyldesley, N. Suarez-Huerta, F. Vandeput, C. Blanpain, S. N. Schiffmann, G. Vassart, M. Parmentier; The Metastasis Suppressor Gene KiSS-1 Encodes Kisspeptins, the Natural Ligands of the Orphan G Protein-coupled Receptor GPR54, *Journal of Biological Chemistry*, **2001**, *276*, 34631-34636.
[329] T. Ohtaki, Y. Shintani, S. Honda, H. Matsumoto, A. Hori, K. Kanehashi, Y. Terao, S. Kumano, Y. Takatsu, Y. Masuda, Y. Ishibashi, T. Watanabe, M. Asada, T. Yamada, M. Suenaga, C. Kitada, S. Usuki, T. Kurokawa, H. Onda, O. Nishimura, M. Fujino; Metastasis suppressor gene KiSS-1 encodes peptide ligand of a G-protein-coupled receptor, *Nature*, **2001**, *411*, 613-617.
[330] A. I. Muir, L. Chamberlain, N. A. Elshourbagy, D. Michalovich, D. J. Moore, A. Calamari, P. G. Szekeres, H. M. Sarau, J. K. Chambers, P. Murdock, K. Steplewski, U. Shabon, J. E. Miller, S. E. Middleton, J. G. Darker, C. G. C. Larminie, S. Wilson, D. J. Bergsma, P. Emson, R. Faull, K. L. Philpott, D. C. Harrison; AXOR12, a Novel Human G Protein-coupled Receptor, Activated by the Peptide KiSS-1, *Journal of Biological Chemistry*, **2001**, *276*, 28969-28975.
[331] M. K. Clements, T. P. McDonald, R. Wang, G. Xie, B. F. O'Dowd, S. R. George, C. P. Austin, Q. Liu; FMRFamide-Related Neuropeptides Are Agonists of the Orphan G-Protein-Coupled Receptor GPR54, *Biochemical and Biophysical Research Communications*, **2001**, *284*, 1189-1193.
[332] S. Funes, J. A. Hedrick, G. Vassileva, L. Markowitz, S. Abbondanzo, A. Golovko, S. Yang, F. J. Monsma, E. L. Gustafson; The KiSS-1 receptor GPR54 is essential for the development of the murine reproductive system, *Biochemical and Biophysical Research Communications*, **2003**, *312*, 1357-1363.
[333] M. L. Gottsch, D. K. Clifton, R. A. Steiner; From KISS1 to kisspeptins: An historical perspective and suggested nomenclature, *Peptides*, **2009**, *30*, 4-9.

[334] C. M. Trevisan, E. Montagna, R. de Oliveira, D. M. Christofolini, C. P. Barbosa, K. A. Crandall, B. Bianco; Kisspeptin/GPR54 System: What Do We Know About Its Role in Human Reproduction?, *Cellular Physiology and Biochemistry*, **2018**, *49*, 1259-1276.
[335] C. Zhang, T. Roepke, M. J Kelly, O. K Rønnekleiv; Kisspeptin Depolarizes Gonadotropin-Releasing Hormone Neurons through Activation of TRPC-Like Cationic Channels, **2008**, *28*, 4423-4434.
[336] A. E. Oakley, D. K. Clifton, R. A. Steiner; Kisspeptin Signaling in the Brain, *Endocrine Reviews*, **2009**, *30*, 713-743.
[337] J. T. Smith, M. J. Cunningham, E. F. Rissman, D. K. Clifton, R. A. Steiner; Regulation of Kiss1 Gene Expression in the Brain of the Female Mouse, *Endocrinology*, **2005**, *146*, 3686-3692.
[338] J. T. Smith, H. M. Dungan, E. A. Stoll, M. L. Gottsch, R. E. Braun, S. M. Eacker, D. K. Clifton, R. A. Steiner; Differential Regulation of KiSS-1 mRNA Expression by Sex Steroids in the Brain of the Male Mouse, *Endocrinology*, **2005**, *146*, 2976-2984.
[339] A. E. Herbison; Estrogen positive feedback to gonadotropin-releasing hormone (GnRH) neurons in the rodent: The case for the rostral periventricular area of the third ventricle (RP3V), *Brain Research Reviews*, **2008**, *57*, 277-287.
[340] Y. M. Chan, S. Broder-Fingert, S. B. Seminara; Reproductive functions of kisspeptin and Gpr54 across the life cycle of mice and men, *Peptides*, **2009**, *30*, 42-48.
[341] M. M. Grumbach; A Window of Opportunity: The Diagnosis of Gonadotropin Deficiency in the Male Infant1, *The Journal of Clinical Endocrinology & Metabolism*, **2005**, *90*, 3122-3127.
[342] M. Kinoshita, H. Tsukamura, S. Adachi, H. Matsui, Y. Uenoyama, K. Iwata, S. Yamada, K. Inoue, T. Ohtaki, H. Matsumoto, K.-I. Maeda; Involvement of Central Metastin in the Regulation of Preovulatory Luteinizing Hormone Surge and Estrous Cyclicity in Female Rats, *Endocrinology*, **2005**, *146*, 4431-4436.
[343] J. T. Smith, S. M. Popa, D. K. Clifton, G. E. Hoffman, R. A. Steiner; Kiss1 neurons in the forebrain as central processors for generating the preovulatory luteinizing hormone surge, *Journal of Neuroscience*, **2006**, *26*, 6687-6694.
[344] B. Meczekalski, K. Katulski, A. Podfigurna-Stopa, A. Czyzyk, A. D. Genazzani; Spontaneous endogenous pulsatile release of kisspeptin is temporally coupled with luteinizing hormone in healthy women, *Fertil Steril*, **2016**, *105*, 1345-1350.e1342.
[345] Y. Horikoshi, H. Matsumoto, Y. Takatsu, T. Ohtaki, C. Kitada, S. Usuki, M. Fujino; Dramatic elevation of plasma metastin concentrations in human pregnancy: metastin as a novel placenta-derived hormone in humans, *Journal of Clinical Endocrinology and Metabolism*, **2003**, *88*, 914-919.
[346] C. N. Jayasena, A. N. Comninos, S. Narayanaswamy, A. Abbara, G. M. Nijher, M. Cheema, Z. Malik, M. A. Ghatei, S. R. Bloom, W. S. Dhillo; The identification of elevated urinary kisspeptin-immunoreactivity during pregnancy, *Annals of Clinical Biochemistry*, **2015**, *52*, 395-398.
[347] S. Zeydabadi Nejad, F. Ramezani Tehrani, A. Zadeh-Vakili; The Role of Kisspeptin in Female Reproduction, *International journal of endocrinology and metabolism*, **2017**, *15*, e44337-e44337.
[348] S. Oishi, R. Misu, K. Tomita, S. Setsuda, R. Masuda, H. Ohno, Y. Naniwa, N. Ieda, N. Inoue, S. Ohkura, Y. Uenoyama, H. Tsukamura, K.-i. Maeda, A. Hirasawa, G. Tsujimoto, N. Fujii; Activation of Neuropeptide FF Receptors by Kisspeptin Receptor Ligands, *ACS Medicinal Chemistry Letters*, **2011**, *2*, 53-57.
[349] T. Ubuka, K. Tsutsui; Evolution of gonadotropin-inhibitory hormone receptor and its ligand, *General and Comparative Endocrinology*, **2014**, *209*, 148-161.
[350] L. J. Kriegsfeld, E. M. Gibson, W. P. Williams III, S. Zhao, A. O. Mason, G. E. Bentley, K. Tsutsui; The Roles of RFamide-Related Peptide-3 in Mammalian Reproductive Function and Behaviour, *Journal of Neuroendocrinology*, **2010**, *22*, 692-700.
[351] A. E. Curtis, J. H. Cooke, J. E. Baxter, J. R. C. Parkinson, A. Bataveljic, M. A. Ghatei, S. R. Bloom, K. G. Murphy; A kisspeptin-10 analog with greater in vivo bioactivity than kisspeptin-10, *American journal of physiology. Endocrinology and metabolism*, **2010**, *298*, E296-E303.

[352] J. Roa, E. Aguilar, C. Dieguez, L. Pinilla, M. Tena-Sempere; New frontiers in kisspeptin/GPR54 physiology as fundamental gatekeepers of reproductive function, *Frontiers in Neuroendocrinology*, **2008**, *29*, 48-69.

[353] L. Pinilla, E. Aguilar, C. Dieguez, R. P. Millar, M. Tena-Sempere; Kisspeptins and Reproduction: Physiological Roles and Regulatory Mechanisms, *Physiological Reviews*, **2012**, *92*, 1235-1316.

[354] E. Gutiérrez-Pascual, J. Leprince, A. J. Martínez-Fuentes, I. Ségalas-Milazzo, R. Pineda, J. Roa, M. Duran-Prado, L. Guilhaudis, E. Desperrois, A. Lebreton, L. Pinilla, M.-C. Tonon, M. M. Malagón, H. Vaudry, M. Tena-Sempere, J. P. Castaño; In Vivo and in Vitro Structure-Activity Relationships and Structural Conformation of Kisspeptin-10-Related Peptides, *Molecular Pharmacology*, **2009**, *76*, 58-67.

[355] J. Y. Lee, J. S. Moon, Y.-J. Eu, C. W. Lee, S.-T. Yang, S. K. Lee, H. H. Jung, H. H. Kim, H. Rhim, J. Y. Seong, J. I. Kim; Molecular interaction between kisspeptin decapeptide analogs and a lipid membrane, *Archives of Biochemistry and Biophysics*, **2009**, *485*, 109-114.

[356] N. Nishizawa, T. Asami, K. Nishibori, Y. Takatsu, A. Suzuki, K. Ushio, S.-i. Matsumoto, Y. Shimizu, M. Yamaguchi, M. Kusaka, H. Matsui, T. Ohtaki, C. Kitada; A new class of pentapeptide KISS1 receptor agonists with hypothalamic–pituitary–gonadal axis activation, *Bioorganic & Medicinal Chemistry Letters*, **2019**, *29*, 654-658.

[357] T. Asami, N. Nishizawa, H. Matsui, Y. Takatsu, A. Suzuki, A. Kiba, M. Terada, K. Nishibori, M. Nakayama, J. Ban, S.-i. Matsumoto, N. Tarui, Y. Ikeda, M. Yamaguchi, M. Kusaka, T. Ohtaki, C. Kitada; Physicochemically and Pharmacokinetically Stable Nonapeptide KISS1 Receptor Agonists with Highly Potent Testosterone-Suppressive Activity, *Journal of Medicinal Chemistry*, **2014**, *57*, 6105-6115.

[358] A. Januszewki, A. N. Comninos, A. Abbara, C. N. Jayasena, G. M. K. Nijher, K. G. Murphy, L. Sriskandarajah, M. L. Vaal, M. A. Ghatei, W. S. Dhillo, Z. Farzad, S. R. Bloom; The Effects of Kisspeptin-10 on Reproductive Hormone Release Show Sexual Dimorphism in Humans, *The Journal of Clinical Endocrinology & Metabolism*, **2011**, *96*, E1963-E1972.

[359] A. K. Roseweir, R. P. Millar; Kisspeptin antagonists, *Adv Exp Med Biol*, **2013**, *784*, 159-186.

[360] T. Fehrentz, M. Schönberger, D. Trauner; Optochemical Genetics, *Angewandte Chemie International Edition*, **2011**, *50*, 12156-12182.

[361] D. Roccatano, G. Colombo, M. Fioroni, A. E. Mark; Mechanism by which 2,2,2-trifluoroethanol/water mixtures stabilize secondary-structure formation in peptides: A molecular dynamics study, *Proceedings of the National Academy of Sciences*, **2002**, *99*, 12179-12184.

[362] F. D. Sonnichsen, J. E. Van Eyk, R. S. Hodges, B. D. Sykes; Effect of trifluoroethanol on protein secondary structure: an NMR and CD study using a synthetic actin peptide, *Biochemistry*, **1992**, *31*, 8790-8798.

[363] M. Buck; Trifluoroethanol and colleagues: cosolvents come of age. Recent studies with peptides and proteins, *Quarterly Reviews of Biophysics*, **1998**, *31*, 297-355.

[364] V. Saxena, S. Kumar, B. Jha, A. Kumar, D. Kumar, M. Naqvi; Indian journal of experimental biology, **2015**, *53*, 676-680.

[365] A. Savitzky, M. J. E. Golay; Smoothing and Differentiation of Data by Simplified Least Squares Procedures, *Analytical Chemistry*, **1964**, *36*, 1627-1639.

[366] A. Micsonai, F. Wien, L. Kernya, Y.-H. Lee, Y. Goto, M. Réfrégiers, J. Kardos; Accurate secondary structure prediction and fold recognition for circular dichroism spectroscopy, *Proceedings of the National Academy of Sciences*, **2015**, *112*, E3095-E3103.

[367] A. Micsonai, F. Wien, É. Bulyáki, J. Kun, É. Moussong, Y.-H. Lee, Y. Goto, M. Réfrégiers, J. Kardos; BeStSel: a web server for accurate protein secondary structure prediction and fold recognition from the circular dichroism spectra, *Nucleic Acids Research*, **2018**, *46*, W315-W322.

[368] A. Micsonai, É. Bulyáki, J. Kardos; in *Structural Genomics: General Applications* (Eds.: Y. W. Chen, C.-P. B. Yiu), Springer US, New York, NY, **2021**, pp. 175-189.

[369] M. N. Fabian C. Roth, Andreas Draguhn; *Patch-Clamp-Technik*, 2 ed., Springer Spektrum Berlin, Heidelberg, **2023**.

[370] T. D. Yelhekar, M. Druzin, U. Karlsson, E. Blomqvist, S. Johansson; How to Properly Measure a Current-Voltage Relation?—Interpolation vs. Ramp Methods Applied to Studies of GABAA Receptors, *Frontiers in Cellular Neuroscience*, **2016**, 10:10.
[371] S.-K. Han, M. L. Gottsch, K. J. Lee, S. M. Popa, J. T. Smith, S. K. Jakawich, D. K. Clifton, R. A. Steiner, A. E. Herbison; Activation of Gonadotropin-Releasing Hormone Neurons by Kisspeptin as a Neuroendocrine Switch for the Onset of Puberty, *The Journal of Neuroscience*, **2005**, *25*, 11349-11356.
[372] E. Ducret, A. E. Herbison, G. M. Anderson; RFamide-Related Peptide-3, a Mammalian Gonadotropin-Inhibitory Hormone Ortholog, Regulates Gonadotropin-Releasing Hormone Neuron Firing in the Mouse, *Endocrinology*, **2009**, *150*, 2799-2804.
[373] M. Findeisen, D. Rathmann, A. G. Beck-Sickinger; RFamide Peptides: Structure, Function, Mechanisms and Pharmaceutical Potential, *Pharmaceuticals*, **2011**, *4*, 1248-1280.
[374] K.-L. Hu, H.-M. Chang, R. Li, Y. Yu, J. Qiao; Regulation of LH secretion by RFRP-3 – From the hypothalamus to the pituitary, *Frontiers in Neuroendocrinology*, **2019**, *52*, 12-21.
[375] J. Qiu, H. M. Rivera, M. A. Bosch, S. L. Padilla, T. L. Stincic, R. D. Palmiter, M. J. Kelly, O. K. Rønnekleiv; Estrogenic-dependent glutamatergic neurotransmission from kisspeptin neurons governs feeding circuits in females, *Elife*, **2018**, *7*, e35656.